Beyond Plastic Degradation: Microbial Sensing and Response of *Vibrio* sp. to PET Breakdown Products within the Plastisphere

Dissertation

For achieving the degree of

Doctor rerum naturalium (Dr. rer. nat.)

at the Department of Microbiology and Biotechnology

Subdivision at the Faculty of Mathematics, Informatics and Natural Science

of the University of Hamburg

Submitted by

Lena Preuß

Hamburg 2025

Contribution to the quoted articles

The following articles are considered within this thesis:

Polyethylene terephthalate (PET) primary degradation products affect c-di-GMP, cAMP-signaling and quorum sensing (QS) in *Vibrio gazogenes* DSM 21264

Preuss, L., Alawi, M., Dumnitch, A., Trinh, L., Maison, W., Burmeister, N., Poehlein, A., Daniel, R., Vollstedt, C. and Streit, W. R. (2025), Polyethylene terephthalate (PET) primary degradation products affect c-di-GMP-, cAMP-signaling and quorum sensin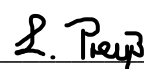g (QS) in *Vibrio gazogenes* DSM 21264, Accepted in Microbiology Spectrum, Temporary DOI: https://doi.org/10.1101/2025.01.28.635239, (Acceptance letter attached in the appendix on page XVII)

> This is the main body of my research. I planned performed and evaluated all the experimental lab work. Further I evaluated and interpreted the transcriptomic data and wrote the main parts of the manuscript.

Prof. Dr. Wolfgang R. Streit (Supervisor)

Hamburg, 20.05.2025, _____

Lena Preuß

Hamburg, 20.05.2025, _____

The Bacteroidetes *Aequorivita* sp. and *Kaistella jeonii* Produce Promiscuous Esterases With PET-Hydrolyzing Activity

Zhang, H., Perez-Garcia, P., Dierkes, R. F., Applegate, V., Schumacher, J., Chibani, C. M., Sternagel, S., **Preuss, L**., Weigert, S., Schmeisser, C., Danso, D., Pleiss, J., Almeida, A., Höcker, B., Hallam, S. J., Schmitz, R. A., Smits, S., Chow, J. and Streit, W. R. (2022). The Bacteroidetes *Aequorivita sp.* and *Kaistella jeonii* Produce Promiscuous Esterases With PET-Hydrolyzing Activity. Frontiers in Microbiology, 12, DOI: https://doi.org/10.3389/fmicb.2021.803896

I contributed to this research paper by performing and evaluating the LSM microscopic images. Further I wrote the method section for my experiments.

Prof. Dr. Wolfgang R. Streit (Supervisor)

Hamburg, 20.05.2025, _____

Lena Preuß

Hamburg, 20.05.2025, _____

Surface Grafted *N*-Oxides have Low-Fouling and Antibacterial Properties

Burmeister, N., Zorn, E., Farooq, A., **Preuss, L.,** Vollstedt, C., Friedrich, T., Mantel, T., Scharnagl, N., Rohnke, M., Ernst, M., Wicha, S. G., Streit, W. R. and Maison W. (2023), Surface Grafted *N*-Oxides have Low-Fouling and Antibacterial Properties, Advanced Material Interfaces, DOI: https://doi.org/10.1002/admi.202300505

I contributed to this research paper by performing and evaluating the LSM microscopic images. Further I wrote the method section for my experiments.

Prof. Dr. Wolfgang R. Streit (Supervisor)

Hamburg, 20.05.2025, _____

Lena Preuß

Hamburg, 20.05.2025, _____

<u>In addition, during the time course of this dissertation, I contributed to the following publications:</u>

Low-Fouling and Antibacterial Polymer Brushes via Surface Initiated Polymerization of a Mixed Zwitterionic and Cationic Monomer

Burmeister, N., Zorn, E., **Preuss, L**., Timm, D., Scharnagl, N., Rohnke, M., Wicha, S. G., Streit, W. R. and Maison, W. (2023), Low-Fouling and Antibacterial Polymer Brushes via Surface-Initiated Polymerization of a Mixed Zwitterionic and Cationic Monomer, ACS Publications, DOI: https://doi.org/10.1021/acs.langmuir.3c02657?urlappend=%3Fref%3DPDF&jav=VoR&rel=cite-as

I contributed to this research paper by performing and evaluating the LSM microscopic images. Further I wrote the method section for my experiments.

Prof. Dr. Wolfgang R. Streit (Supervisor)
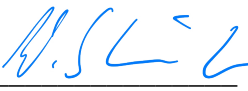
Hamburg, 20.05.2025, _____

Lena Preuß

Hamburg, 20.05.2025, _____

New dienelactone hydrolase from microalgae bacterial community- Antibiofilm activity against fish pathogens and potential applications for aquaculture

Bergmann, L., Balzer Le, S., Hageskal, G., **Preuss, L**., Han, Y., Astafyeva, Y., Loevenich, S., Emmann, S., Perez-Garcia, P., Indenbirken, D., Katzowitsch, E., Thümmler, F., Alawi, M., Wentzel, A., Streit, W. R., & Krohn, I. (2024). New dienelactone hydrolase from microalgae bacterial community-Antibiofilm activity against fish pathogens and potential applications for aquaculture. *Scientific Reports*, *14*(1). https://doi.org/10.1038/s41598-023-50734-9

I contributed to the lab work and enzyme approaches (PCR, purification testing).

Prof. Dr. Wolfgang R. Streit (Supervisor)

Hamburg, 20.05.2025, _____

Lena Preuß

Hamburg, 20.05.2025, _____

Eidesstattliche Versicherung:

Hiermit versichere ich an Eides statt, die vorliegende Dissertationsschrift selbst verfasst und keine anderen als die angegebenen Hilfsmittel und Quellen benutzt zu haben.

Sofern im Zuge der Erstellung der vorliegenden Dissertationsschrift generative Künstliche Intelligenz (gKI) basierte elektronische Hilfsmittel verwendet wurden, versichere ich, dass meine eigene Leistung im Vordergrund stand und dass eine vollständige Dokumentation aller verwendeten Hilfsmittel gemäß der guten wissenschaftlichen Praxis vorliegt. Ich trage die Verantwortung für eventuell durch die gKI generierte fehlerhafte oder verzerrte Inhalte, fehlerhafte Referenzen, Verstöße gegen das Datenschutz- und Urheberrecht oder Plagiate.

Affidavit:

I hereby declare and affirm that this doctoral dissertation is my own work and that I have not used any aids and sources other than those indicated.

If electronic resources based on generative artificial intelligence (gAI) were used in the course of writing this dissertation, I confirm that my own work was the main and value-adding contribution and that complete documentation of all resources used is available in accordance with good scientific practice. I am responsible for any erroneous or distorted content, incorrect references, violations of data protection and copyright law or plagiarism that may have been generated by the gAI.

Hamburg, 20.05.2025

Lena Preuß

Table of Contents

List of Figures

List of figures used in the parts introduction and Results

Abstract

Plastic production and the resulting waste significantly threaten the environment and numerous ecosystems. Due to increasing production rates, global plastic pollution is also rising rapidly. Plastic particles accumulate in a wide range of habitats, and nowadays are found all around the globe. These particles are rapidly colonized by diverse microorganisms. While microbial colonization offers potential advantages, such as contributing to plastic degradation, it also presents risks, particularly due to the accumulation of potentially pathogenic bacteria on plastic surfaces. Another major consequence of microbial colonization is biofouling, where bacteria adhere to plastic materials, used in various industries, leading to surface damage and reduced material durability.

This thesis encompasses three chapters. In chapter one, this study gives for the first time insights into molecular keys, involved in *Vibrio gazogenes* polyethylene terephthalate (PET) colonization and subsequent polymer degradation, using deep transcriptomics, advanced imaging analyses and analytic technologies. The first part of the study focuses on the analysis and transcriptional profiling of the PET6 gene expression. PET6 is a recently discovered PETase in the marine bacterium *Vibrio gazogenes* DSM 21264. Within 24 hours of incubation, degradation products such as *bis*(2-hydroxyethyl) terephthalate (BHET), *mono*(2-hydroxyethyl) terephthalate (MHET) and terephthalic acid (TPA) were detected, when DSM 21264 was incubated with PET foil or powder. For a deep understanding of bacterial response in the presence of PET and its degradation products BHET and TPA, focusing on the transcription of the *pet6* gene, multiple RNAseq approaches were conducted. Further, a number of natural substrates like chitin and cellulose were used, to study the response of DSM 21264 and its gene expression profile. Interestingly, the incubation of DSM 21264 in biofilm condition on PET vs PE surface or planktonic samples with PET powder did not increase the transcription of the *pet6* gene. Highest transcription, however, was detected in planktonic samples, supplemented with BHET. Notably, the intermediate BHET significantly influenced bacterial gene expression on a global level by disrupting key signaling systems like quorum sensing (QS), c-di-GMP and CRP-cAMP signaling pathway. Using these second messenger bacteria adapt to their environment, regulating numerous metabolic pathways. This resulted in failure to form biofilms, altered colony morphology, and inhibited the biosynthesis of the red pigment prodigiosin. These findings imply that microbial and enzyme driven plastic degradation and the generated metabolites, thereby, may not only serve as carbon sources but also as potential signaling molecules.

Furthermore, with this work I provided evidence that UlaG, which has been described as a highly promiscuous esterase, involved in ascorbate metabolism under anaerobic conditions, plays a significant role in BHET degradation. The transcription was 7.9-fold upregulated in the presence of BHET, and biochemical tests using recombinant UlaG verified that the *Vibrio gazogenes* UlaG is involved in BHET metabolism. Further work will have to evaluate its role in the plastisphere.

In the second chapter, the colonization behavior of the Gram-negative bacterium *Kaistella jeonii,* native host of PET 30, was observed on PET surface, using Laser scanning microscopy (LSM). *Kaistella jeonii* is a member of the phylum Bacteroidetes and wide spread in nature. It plays an important role in the plastisphere. Thereby, my imaging analyses contributed to the characterization of the first PET-degrading enzymes from the phylum Bacteroidetes.

In chapter three, *Vibrio campbelli,* a pathogenic member of the plastisphere, was analyzed on treated and untreated polyethylene (PE) foils with the aim to prevent biofouling. A novel surface treatment with poly-*N*-oxides grafted onto PE surface revealed significantly less bacterial colonization.

Altogether, this study investigated for the first the influence of PET degradation products on the microbial community of the plastisphere, and offers solutions towards biodegradation and biofouling

Zusammenfassung

Die Plastikproduktion und die daraus resultierenden Abfälle bedrohen in hohem Maße die Umwelt und zahlreiche Ökosysteme. Mit stetig steigenden Produktionsraten nimmt auch die weltweite Plastikverschmutzung rapide zu. Plastikpartikel reichern sich in einer Vielzahl von Lebensräumen an und sind heute weltweit verbreitet. Diese Partikel werden zeitnah von unterschiedlichsten Mikroorganismen besiedelt. Obwohl die mikrobielle Besiedlung auch potenzielle Vorteile bietet, wie durch den mikrobiellen Plastikabbau, gehen auch Risiken damit einher, insbesondere durch die Anheftung potenziell pathogener Bakterien auf Plastikoberflächen. Eine weitere relevante Folge der mikrobiellen Besiedlung ist das sogenannte Biofouling. Dabei besiedeln Mikroorganismen Plastikoberflächen, die in verschiedenen Industriezweigen verwendet werden, was zu Oberflächenschäden und verringerter Materialhaltbarkeit führen kann.

Diese Arbeit umfasst drei Kapitel. Im ersten Kapitel liefert diese Studie erstmals Einblicke in molekulare Schlüsselmechanismen, die für die Besiedlung von Polyethylenterephthalat- (PET-) Folie durch *Vibrio gazogenes* sowie für den Polymerabbau relevant sind. Dafür wurden tiefgreifende Transkriptomanalysen, fortschrittliche Bildgebungsverfahren und analytische Technologien durchgeführt. Im ersten Teil dieser Arbeit liegt der Fokus auf der Analyse und dem transkriptionellen Profiling der PET6-Genexpression. PET6 ist eine kürzlich entdeckte und charakterisierte PETase des marinen Bakteriums *Vibrio gazogenes* DSM 21264. Bei der Inkubation von DSM 21264 mit PET-Folie oder -Pulver konnten innerhalb von 24 Stunden Abbauprodukte wie *Bis*(2-hydroxyethyl)terephthalat (BHET), *Mono*(2-hydroxyethyl)terephthalat (MHET) und Terephthalsäure (TPA) nachgewiesen werden. Um das bakterielle Verhalten von DSM 21264 in Anwesenheit von PET sowie dessen Abbauprodukten BHET und TPA zu untersuchen, wurden mehrere RNAseq-Analysen durchgeführt. Dabei lag der Fokus auf der Transkription des *pet6*-Gens. Darüber hinaus wurde DSM 21264 mit verschiedenen natürlichen Substraten wie Chitin und Zellulose supplementiert, um die transkriptionelle Reaktion des Organismus und dessen Genexpressionsprofil zu bestimmen. Interessanterweise führte die Inkubation von DSM 21264 im Biofilm auf PET- im Vergleich zu PE-Oberflächen oder in planktonischen Kulturen mit PET-Pulver nicht zu einer erhöhten Transkription von *pet6*. Die höchste Transkription konnte hingegen in planktonischen Kulturen mit Zusatz von BHET detektiert werden. Auffällig war, dass das Zwischenprodukt BHET die bakterielle Genexpression stark beeinflusst, indem es wichtige Signalsysteme wie Quorum Sensing (QS), c-di-GMP sowie den CRP-cAMP-Signalweg stört. Mit der Nutzung dieser sekundären Signalstoffe passen Bakterien ihren Stoffwechsel an die gegeben Umweltbedingungen an.

Dies führte zu einer gestörten Biofilmbildung, veränderter Koloniemorphologie und die Biosynthese des roten Pigments Prodigiosin wurde inhibiert. Diese Ergebnisse deuten darauf hin, dass der mikrobiell und enzymatisch gesteuerte Kunststoffabbau sowie die dabei entstehenden Metabolite nicht nur als Kohlenstoffquelle fungieren, sondern auch als potenzielle Signalmoleküle wirken können.

Darüber hinaus konnte in dieser Arbeit gezeigt werden, dass das Enzym UlaG, das bisher als hoch promiskuitive Esterase im anaeroben Ascorbatstoffwechsel beschrieben wurde, eine bedeutende Rolle beim Abbau von BHET spielt. Die Transkription war unter Einfluss von BHET 7,9-fach hochreguliert, und biochemische Tests mit rekombinantem UlaG bestätigten, dass UlaG aus *Vibrio gazogenes* am BHET-Stoffwechsel beteiligt ist. Weitere Studien sind nötig, um die Rolle von UlaG in der Plastisphäre zu bestimmen.

Im zweiten Kapitel wurde das Kolonisationsverhalten des Gram-negativen Bakteriums *Kaistella jeonii*, dem natürlichen Wirt von PET30, auf PET-Oberflächen mittels Laserscanning-Mikroskopie (LSM) untersucht. *Kaistella jeonii* gehört zum Phylum der Bacteroidota und ist in der Natur weit verbreitet. Darüber hinaus ist es ein wichtiges Mitglied der Plastisphäre. Mit meinen Bildanalysen konnte ich zur Charakterisierung der ersten PET-abbauenden Enzyme aus dem Phylum Bacteroidota beitragen.

In Kapitel drei wurde *Vibrio campbelli,* ein pathogener Vertreter der Plastisphäre, auf behandeltem im Vergleich zu unbehandeltem Polyethylen (PE) untersucht, mit dem Ziel Biofouling vorzubeugen. Durch diese neue Art der Oberflächenbehandlung bei der poly-*N*-Oxide auf PE gebracht werden, konnte die bakterielle Besiedlung signifikant verringert werden.

Zusammenfassend untersucht diese Studie zum ersten Mal den Einfluss von PET Abbauprodukten auf die mikrobielle Gemeinschaft der Plastisphäre und bietet Lösungsansätze im Hinblick auf enzymatischen Plastikabbau sowie Biofouling.

1 Introduction

1.1 Enzymatic plastic degradation as a sustainable solution to pollution?

Global plastic production has increased over the past 70 years, starting at around 2 million tons (Mt) per year in 1950 up to an annual production of over 400 Mt today (Landrigan et al., 2023, Plastics Europe, 2024). The annual growth rate of plastic production is estimated about 8.4%, since it is used in numerous industries such as healthcare, packaging, or construction (Anuar Sharuddin et al., 2016). Along with the rapidly increasing production, also the global plastic waste is increasing annually, leading to an estimation of 12 billion Mt by 2050 (Katnic & Gupta 2025). Especially, materials from the packaging industry have a product lifetime of less than one year, until they are discarded. Only polymers used for industrial machinery or building and construction are used for more than 20 years (Geyer et al., 2017).
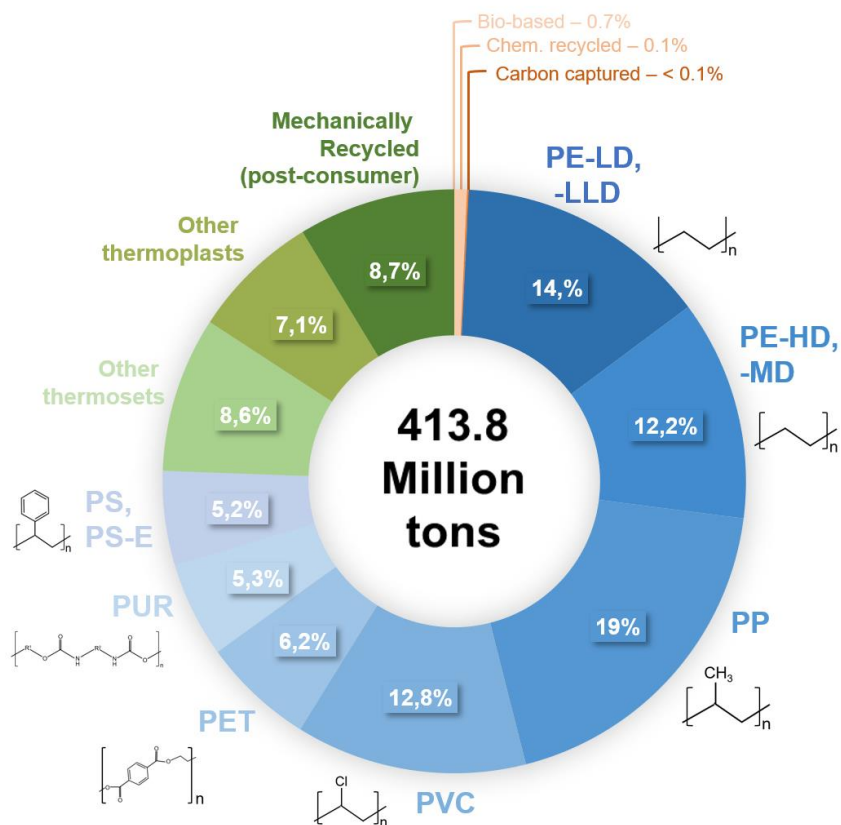
Figure 1: Distribution of the annually produced plastics by the polymer type in Mt Percentage distribution by polymer type of globally produced plastics in 2023. Abbreviations used in this figure: (Expanded) Polystyrene (PS-E), Polyurethane (PUR), Polyethylene terephthalate (PET), Polyvinyl chloride (PVC), Polypropylene (PP), Polyethylene (PE), High density (-HD), Medium density (-MD), Low density (-LD) and Linear low density (-LLD) (adapted from Plastics Europe, 2024).

Since those polymers make a significant lower amount than all other sectors such as packaging, consumer and institutional products or textiles, this results in almost 80% of the plastics produced rapidly becoming waste (Geyer et al., 2017, Yadav & Mantri, 2025). The vast majority of those plastics are based on fuel-fossil resources, giving the advantage of low-cost, high thermostability and durability (Walker & Rothman, 2020). Among the main polymers produced are polyethylene (PE), polypropylene (PP), polyvinylchloride (PVC), polyethylene terephthalate (PET), polyurethanes (PUR) and polystyrene (PS) in descending order (Figure 1, Danso et al., 2019, Plastics Europe, 2024). PE is the most produced plastic polymer, since it is extensively used in the packaging industry (Zhong et al., 2017). PP has a broad range of applications in medical industries for hospital supplies and equipment, as well as bottle caps, straws or automobile parts (Clayman, 1981). PVC is used for packaging materials, too, but also flooring and building materials, toys, and furniture (Ali et al., 2014). The main use of PET in the plastic industry is for PET bottles or foils, but also for textile fibers (Nisticò, 2020). PUR is synthesized for the production of foams, textile coatings or insulation materials (Seymour & Kauffmann, 1992). The use of PS ranges from packing industry to daily use articles such as plastic cutlery or CD cases. (Danso et al., 2019). Due to their high durability, most plastics are not biodegradable and difficult to recycle in large quantities. To date, plastic disposal is extremely inefficient. Among the strategies for disposal are open burning, thermal conversion, but also export from high- to low-income countries, where it is rapidly accumulating in the environment (Landrigan et al., 2023). The lack of knowledge on biodegradation is leading to high costs, lower quality and thereupon inefficient recycling rates of less than 10% of all plastic waste (Zhang et al., 2021). The insufficient waste management regarding disposal strategies and recycling is resulting in 60% of all the plastics ever produced being discarded or exported (Jambeck et al., 2017). As a result, they accumulate in the environment, significantly polluting oceans and increasing the burden on landfills (Su et al., 2019, Alencar et al., 2022). The polymers, enriching in all kinds of ecosystems, pollute air and water, making it a major concern for human health and the environment (Ahmad et al., 2025, Dileepan et al., 2025).

Over the last decades, research has focused on the biodegradation via enzymatic breakdown to enhance recycling processes. Varying chemical structures and composition require specific enzymes for each polymer type (Chow et al., 2022). Synthetic polymers can be divided into two groups: enzymatically hydrolysable and not directly hydrolysable polymers. Among the most commonly produced polymers are PE, PP, PVC, and PS, having a carbon-carbon backbone, which means they lack hydrolysable functional groups (Figure 1). Consequently, no degradation pathways have been identified, for breaking down these polymers. Without prior initial breakdown

it is unlikely that enzymes can access and degrade polymers with chain lengths exceeding 40 units (Wei & Zimmermann, 2017). On the other hand, PET and PUR contain hydrolysable ester bonds, which make them more amenable to enzymatic degradation (Raczyńska et al., 2024, Chen et al., 2025).

Within this study, the polymers that are mainly focused on are PET and PE, since they are the most annually produced plastic substrates from the two distinct enzymatic hydrolysable and not-hydrolysable groups.

Enzymes degrading PET are usually secreted and promiscuous cutinases (EC 3.1.1.74), lipases (EC 3.1.1.3) and esterases (EC 3.1.1), and were first isolated from and investigated in detail in *Fusarium solani, Thermomyces insolens, T. lanuginosus, Aspergillus oryzae, Pseudomonas mendocina*, and *Thermobifida fusca* (Zimmermann & Billig, 2011). Using a metagenomic approach, a cutinase could be isolated from a leaf-branch compost (LCC) showing only 5.4% identity to cutinase from *T. fusca,* but with a much higher PET degradation rate (Sulaiman et al., 2012). This enzyme has been optimized through engineering campaigns, and is the only one being applied in an industrial plant for PET depolymerization (Tournier et a., 2020; Arnal et al., 2023).
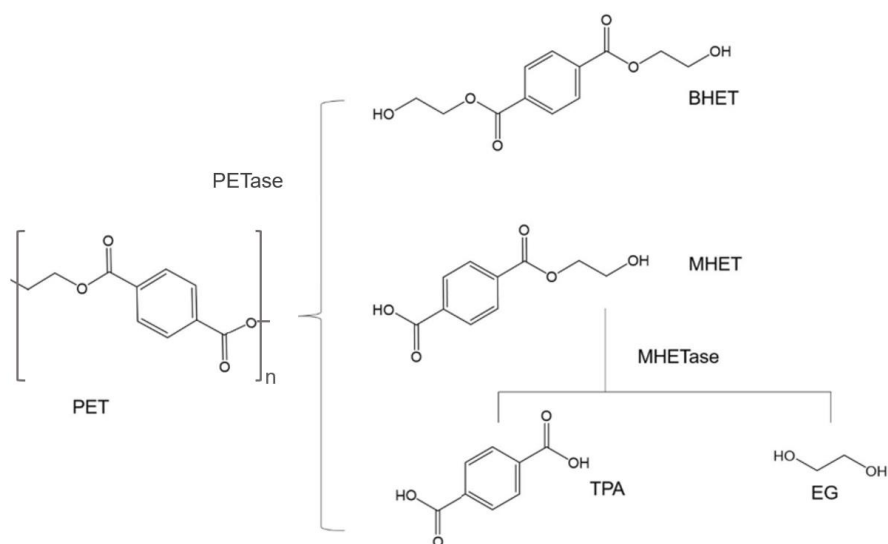
Figure 2: Enzymatic pathway of PET degradation. PETases cleave the polymer into the first intermediates BHET or MHET. An optional MHETase further degrades them into TPA and EG (adapted from Duan et al., 2023).

The intermediates of PET degradation are *bis*(2-hydroxyethyl) terephthalate (BHET) and *mono*(2-hydroxyethyl) terephthalate (MHET). Further, it is degraded into its monomers ethylene glycol (EG) and terephthalic acid (TPA) (Figure 2, Duan et al 2023).

In 2016, Yoshida *et al.* isolated the first microorganism able to use PET as a sole carbon source for growth. *Ideonella sakaiensis* 201-F6 harbors ISF6_4831 protein, which was identified as a PETase, due to its ability to breakdown PET into MHET or BHET. Further, degradation from MHET into TPA and EG was assigned to ISF6_0224 protein, classified as a MHETase (Yoshida et al., 2016). Until now, more than 125 PETases have been characterized, according to the PAZy database. Furthermore, sequence-based screening of publicly available protein databases, using Hidden Markov Models, have identified more than 3,000 homologs of PET-active enzymes (Buchholz et al., 2022).

In contrary, as previously mentioned, biodegradation of PE is highly complex, due to its non-accessible chemical structure. Enzymes acting on carbon chains longer than C_{20} are alkane hydroxylases. The long-chain *n*-alkanes are oxidized to primary corresponding alcohols, which are further oxidized by alcohol and aldehyde dehydrogenases (Ji et al., 2013). The majority of enzymatically accessible *n*-alkanes ranges between 10-30 carbon atoms. In contrary, PE as a native polymer consists of more than 1,000 c-atoms. Several attempts have been made to oxidize the polymer, and thereby weaken its structure, so that it might be more accessible for enzymatic breakdown. Even though some microorganisms (e.g., *Bacillus subtilis* or *Aspergillus flavus)* have been observed to oxidize PE, the specific enzymes responsible for the oxidation have not yet been identified (Ghatge et al., 2020, Yang et al., 2024). Recent studies showed that two cytochrome P450 monooxygenases from *Galleria mellonella* are capable of oxidizing PE (Son et al., 2024). Interestingly, these observations could not be repeated in other studies, indicating that interpretation of potential enzymatic breakdown or weight loss of polyolefins has to be handled carefully (Stepnov et al., 2024). So further work needs to be conducted, to identify truly active enzymes on the respective polymer.

Plastic material in the global biosphere is disrupted through a series of abiotic processes, both chemical and mechanical, the so-called weathering. Weathering includes thermo-oxidative deration, UV-light or hydrolysis through reaction with water (Andrady, 2011). The disrupted plastic particles with a size of < 5 mm are considered microplastics or at diameters of 1 μm nanoplastics (Tirkey & Upadhyay, 2021). Within the term microplastic, it is distinguished between primary microplastic and secondary microplastic. While secondary microplastics refer to breakdown products of larger plastic materials (Ahmad et al., 2020), primary microplastics are originally produced at millimeter sizes. They are mainly used for cosmetic or pharmaceutic products such as skin or hand cleaners, body washes or toothpastes (Gregory, 1996, Conkle et al., 2018, Yadav & Mantri., 2025). Today those microplastics are ubiquitously present in all ecosystems, thereby contaminating food chains for numerous living organisms (Yee et al., 2021).

Several studies already addressed the question, how those microplastics influence human and animal health, leading to the result that more than 117 researches indicate potential risk for mammalian wellbeing, due to the exposure to microplastics (Xu et al., 2022). Numerous systems in the human body can be negatively affected by microplastics, ranging from digestive, respiratory, immune and reproductive system for example (Lee et al., 2023).

1.2 Plastics impact on the marine environment: The Plastisphere

Microorganisms are known for their ability to adapt to new or changing habitats. Thus, it is not surprising that also artificially formed ecological niches such as micro- and nanoplastics are rapidly colonized by a wide array of microorganisms (Oberbeckmann et al., 2014, Roager & Sonnenschein, 2019). The first evidence of microorganisms attaching to plastic particles was reported in the 1970s (Carpenter and Smith, 1972). Nevertheless, it was not until 2013 when Zettler *et al.* performed first next generation sequencing studies, using plastic particles collected in the North Atlantic Ocean, for the determination of the microbial communities forming biofilms on the surfaces. Within this work, the term "plastisphere" was coined for the newly formed micro-habitat (Zettler et al., 2013). Once the particles enter the ocean, both, prokaryotes and eukaryotes begin to adhere to the surfaces, and initiate the development of biofilms. Main bacterial phyla associated with the plastisphere are Pseudomonadota, Vibrionales, Bacteroidetes, Bacillota, and Cyanobacteriota (Roager and Sonnenschein, 2019, Zhai et al., 2023). Especially, Pseudomonadota show a high abundance within the plastisphere, and along with Bacteroidetes and Planctomycetes are more often found on plastic than on non-plastic surfaces (Ogonowski et al., 2018). Yet, it should be mentioned that until now no microorganisms were found exclusively on plastic surfaces (Amaral-Zettler et al., 2020).

The process of biofilm formation on plastic debris can be divided into various stages, including the initial colonization, the early plastisphere and the mature plastisphere (Figure 3, Dey et al., 2022). The formation of the plastisphere is initiated by the attachment of the first microorganisms. (Wright et al., 2020). Pioneer organisms, characterized by their ability to adhere to surfaces and initiate biofilm development, attach very quickly after particles enter their habitat, occurring within a time frame of approximately 15 minutes to 4 hours (Latva et al., 2022, Dey et al., 2022). Alpha- and Gammaproteobacteria are amongst the primary colonizers, but also phototrophic microbes such as Cyanobacteria, diatoms, and green algae have been described (Quero & Luna, 2017). Initially, Gammaproteobacteria are predominant, and some of these microorganisms are believed to degrade plastic, forming the early plastisphere. However, this process would occur only at low

rates, meaning it doesn't result in the complete breakdown of the polymers (Wright et al., 2020). As biofilm development progresses the community succession stage is reached, characterized by a rather stable microbial community. Gammaproteobacteria are outcompeted by Bacteroidetes, particularly from the Flavobacteriaceae family (Dey et al., 2022).
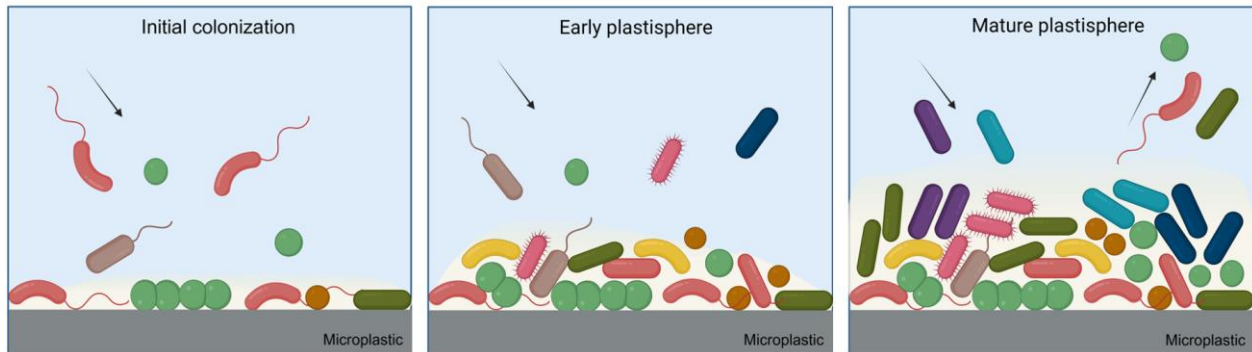
Figure 3: Formation of the plastisphere. The process is initiated by the pioneer microorganisms, develops in the early plastisphere and is fully established within the mature plastisphere, forming a stable micro-habitat (Created with Biorender, adapted from Zhai et al., 2023).

Once the mature plastisphere is established, the biofilm becomes dominated by microbes that metabolize polymer additives and organic substrates released by the pioneer organisms, such as metabolites produced by photosynthetic organisms (Figure 3, Andrady, 2011, Wright et al., 2020, Amaral-Zettler et al., 2020, Zhang et al., 2022). Those organisms mainly compose of members of the Alphaproteobacteria, Gammaproteobacteria and Bacteroidetes (Gulizia et al., 2025).

1.3   Factors influencing the establishment of the marine plastisphere

Many studies have investigated the formation and microbial distribution within the plastisphere, especially in marine environments (Amaral Zettler et al., 2013, Wright et al., 2022, Davidov et al., 2022). Contrary to expectations, observations reveal that the type of polymer is not the primary factor determining the composition of the microbial community found on the plastic surface (Amaral-Zettler et al., 2015, Yu et al., 2023). The largest impact on the microbial composition in the plastisphere have the aquatic environmental conditions. Most decisive factors for the formation of the plastisphere are the geographical location and physicochemical conditions. This includes on the macroscale temperature, pH, light availability, hydrodynamics, nutrient levels or salinity, determining, which organisms appear in the respective habitat (Figure 4, Wright et al., 2021, Yu et al., 2023).
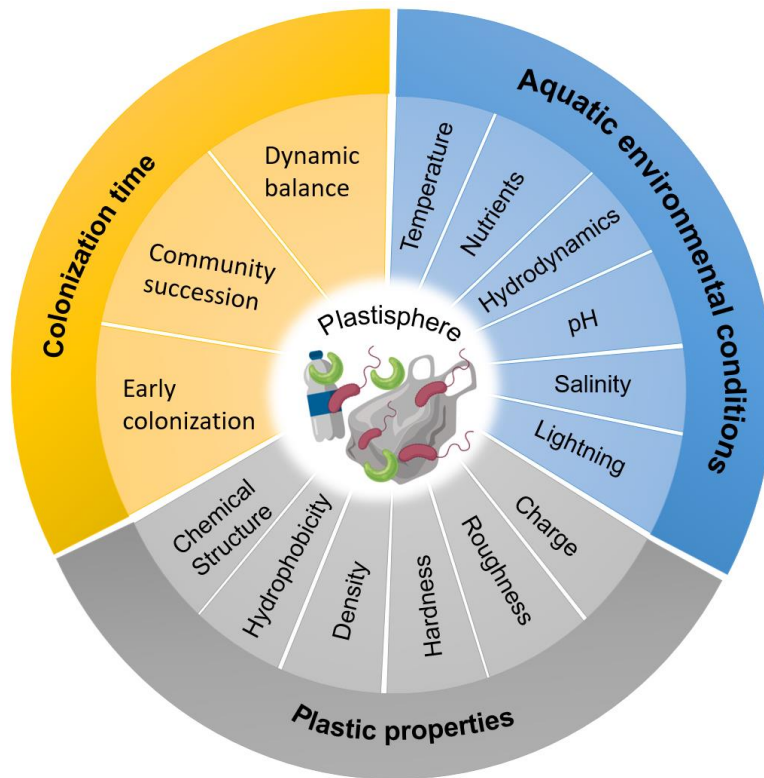
Figure 4: Most decisive factors influencing the colonization of the marine plastisphere. Aquatic environmental conditions determine the contribution of the seawater community. Plastic properties and colonization time are relevant for the distribution of attaching bacteria (adapted from Yu et al., 2023).

Free-living bacterial seawater communities vary highly compared to the attaching bacteria. While the seawater community is heavily influenced by seasonal changes, the microplastic communities form a relatively stable micro-habitat (Davidov et al., 2024) Colonizing microbiota are characterized by their capability of metabolic adaption, and harbor mechanisms for attachment, motility, secretion, biofilm formation, and quorum sensing (Roager and Sonnenschein, 2019).

On the microscale, colonization time and plastic properties determine the microbial distribution (Figure 4, Yu et al., 2023). Plastic polymers provide different surface characteristics, regarding their roughness, hardness, charge, or hydrophobicity. Therefore, also the polymer type influences the microbial distribution found within the aquatic plastisphere as well (Kirstein et al., 2018). In both short- and long-term experiments, conducted under the same incubation conditions, it was found that a greater number of bacteria adhered to PE and PVC compared to PP and PET. In this context, the substrates showed significant variation in surface hardness. PET and PP, which supported lower numbers of colonizing bacteria, are hard materials. In contrast, PE and PVC, which had higher bacterial adhesion, exhibited lower surface hardness. This suggests that surface hardness is a major factor influencing bacterial attachment (Cai et al., 2019).

Differences in colonization patterns are also due to varying hydrophobicity and chemical structure of the polymers. This suggests that strain-specific characteristics, such as their nutritional status, cell hydrophobicity, and the ratio of intra- to extracellular nutrients, also play a role in their ability of attaching to surfaces. Nevertheless, only few studies have addressed the impact of the chemical properties of the plastic substrates in relation to the number of bacteria attaching to them (Hansen et al., 2021).

Another important factor is the distribution of the polymers within the aquatic system. PET, PVC, or polyamide (PA) are mainly found in the bottom sediments, whereas PP or PE can persist in upper water columns. This results in a shift in colonization, since different microorganisms are enriched in the respective habitats (Andrady, 2011). But the buoyancy can also be changed due to microbial colonization on the plastic debris. Biofouling terms the biofilm formation on plastic surfaces, and is the reason for polymers to sink instead of floating on the surface, additionally affecting the microbial community (Sugathapala et al., 2025).

1.4   Biotechnological perspectives and advantages of the plastisphere

Several studies have already addressed the question, to what extend the plastic-associated communities are capable of degrading the respective polymers. As previously mentioned, it is assumed that during the formation of the plastisphere bacteria accumulate that are, theoretically, to some extent, capable of degrading the polymer (Wright et al., 2021). Some hydrocarbon-degrading bacteria, associated with *Oceanospirillalles, Alteromonadales* or *Halomonadaceae,* were more enriched on plastic surfaces than on non-plastic control biofilms (Prince et al., 2010, Wright et al., 2021).

In 2019, Roager and Sonnenschein collected and summarized most of the published research on microorganisms degrading plastics (Roager & Sonnenschein, 2019). Interestingly, most of the existent work focuses on the determination of weight loss over time, rarely exceeding 10% after several months (Sudhakar et al., 2008, Auta et al., 2017). LDPE incubated with *Alcanivorax borkumensis* over 80 days showed only 3.5% weight loss (Dellacuvellerie et al., 2019). *Bacillus cereus* and *B. gottheii* isolated from mangrove sediment partially degraded PE, PET, and PS after 40 days of incubation. Nevertheless, this resulted in weight losses ranging from 1.6% to 7.4% (Auta et al., 2017). A consortium consisting of *Vibrio alginolyticus* and *V. parahaemolyticus* have shown biodegradation of polyvinyl alcohol-linear low-density polyethylene (PVA-LLDPE) (Raghul et al., 2014).

Still, it remains unclear to what extend the colonizing organisms contribute to the measured biodegradation, or if other abiotic and biotic factors are involved, and what enzymes might be responsible for the potential breakdown (Roager & Sonnenschein, 2019). For the finding of such degrading organisms it is assumed that they are closely attached to the respective polymer, but not found in the upper layers of a mature biofilm (Figure 3; Wright et al., 2021). However, biodegradation remains uncertain, particularly for the previously mentioned carbon-carbon-backbone polymers. Even if bacteria possess plastic-degrading enzymes, it has not been proven that these enzymes are expressed in natural environments.

1.5   Emerging risks of plastic colonization

Despite the potential advantages that the plastisphere offers, numerous threats also emerge from this newly formed ecological niche.

Another, negative, aspect of the above-mentioned biofouling is the colonization of all artificial objects, including also plastic surfaces within the marine environment (Qian et al., 2022). Highly threatened by biofouling are for example the shipping industry or membranes used for desalting water, which are made of polyamide (Khan et al., 2015, Pan et al., 2022). This leads to high economic losses, and the damages significantly reduce the lifespan of those materials, which thereupon increases plastic pollution (Hong et al., 2024). Various approaches have already aimed to reduce biofouling by antifouling coatings or chemical adaptions of the surface (Burmeister et al., 2023[3], Weber and Esmaeili, 2023). The drift of plastic debris or by biofouling contaminated ships, along with the enrichment of its associated communities, has been identified as a pathway for the invasion of alien species, which can have unpredictable and significant consequences for the marine environment. This invasion could harm local community structures, affecting water quality and its associated aquaculture (Derraik et al., 2002, Shen et al., 2019).

The novel niche created by microplastics may promote enrichment of certain microorganisms, which can result in an increased gene exchange through horizontal transfer. This exchange can encompass antibiotic resistance genes and virulence factors (Shen et al., 2019). Studies have shown that antibiotic resistance genes are more abundant within the plastic community compared to surface water (Wang et al., 2024, Malla et al., 2025). Since microplastics also act as carriers of pollutants like heavy metals, the horizontal gene transfer of bacteria might further be increased (Zhang et al., 2022). For the spread of antibiotic resistance genes also heavy metals play a not negligible role, promoting horizontal gene transfer (Lin et al., 2024).

Additionally, the accumulation of potentially pathogenic bacteria on plastic surfaces has been recognized as an emerging risk factor, as these polymers may serve as vectors for the dispersal of human or animal pathogens (Wang et al., 2021, Oliver et al., 2024, Mphasa et al., 2025). Among the identified potential pathogens, enriched on plastics from marine environments, are *Tenacibaculum, Pirellulaceae, Clostridiales, Vibrionaceae, Thalassospira* and *Chlamydiae*, respectively (Wright et al., 2021).

Plastic debris from a river in Chicago harbored possible human-infecting pathogens like *Aeromonas, Aquabacterium, Arcobacter,* and *Pseudomonas* (McCormick et al., 2014). In coastal lagoons, at least 15 species have been identified as potentially pathogenic towards humans or fish, such as *Shewanella, Enterobacter, Klebsiella, Serratia, Pseudomonas, Vibrio* and *Stenotrophomonas* (Garcés-Ordónez et al., 2024). Overall, the most abundant potentially harmful bacteria found in the aquatic plastisphere, including marine and fresh water, in descending order, are *Vibrio, Pseudomonas, Acinetobacter, Arcobacter, Bacillus, Aquabacterium, Mycobacterium, Aeromonas, Tenacibaculum, Escherichia, Klebsiella* and *Legionella* (Junaid et al., 2022).

Yet, it is important to note that most of the studies use sequencing methods to identify bacteria at the genus level, which is insufficient to determine the pathogenesis of the organisms accurately. The ability of bacteria to cause diseases is determined by their expression of virulence factors. Thus, deeper analyses are required to verify if the identified bacteria are indeed pathogenic, rather than merely potential pathogens (Wright et al., 2021).

In the context of pathogen accumulation within the plastisphere, particular attention should be given to *Vibrio* spp, representing a significant group of concern. The genus is associated with at least 12 human pathogens such as *V. parahaemolyticus, V. vulnificus,* and *V. cholerae*, which are able to cause life-threatening septicemia and cholera, as well as additional plant and animal pathogens like *V. campbelli, V. alginolyticus*, and *V. anguillarum.* They naturally occur in marine habitats (Defoirdt et al., 2007, Baker-Austin et al., 2018, Li et al., 2025, Sathiyamoorthi et al., 2025, Che et al., 2025). In 2016, *V. parahaemolyticus* was identified to colonize PE, PP, and PS (Kirstein et al., 2016). Under artificial environmental conditions, *V. cholerae* was able to persist up to 14 days on plastic particles at concentrations sufficient for potential human infection (Ormsby et al., 2023). It is suggested that non-pathogenic *Vibrio* spp. are capable of resuscitating toxigenic *V. cholerae* O1 through quorum sensing, potentially enabling seasonal cholera outbreaks (Naser et al., 2021). This underscores the need for a better understanding of gene expression in plastic biofilms concerning the production of autoinducers and virulence factors.

1.6   *Vibrio* sp. is dominating the plastisphere

Numerous studies identified *Vibrio* sp. among the most abundant genera within the plastisphere (Figure 5, Amaral-Zettler et al., 2013, Zhai et al., 2023). Figure 5 outlines its global presence on plastic substrates, which is independent form the polymer type, according to several researches. Numerous studies using metagenomic approaches predominantly found *Vibrio* sp. within their samples (Figure 5).
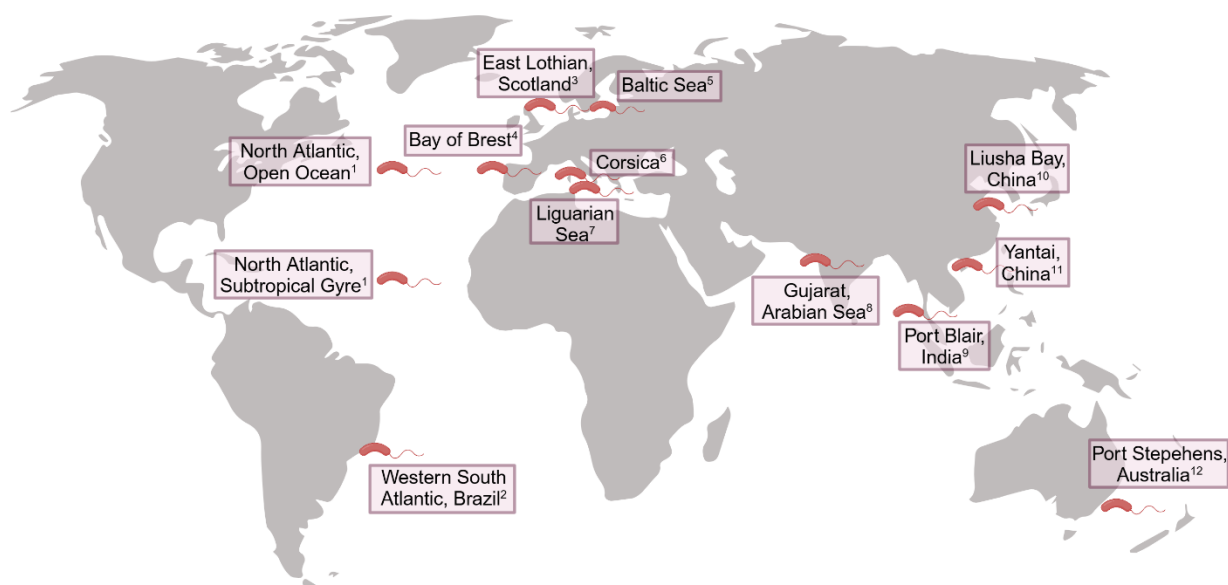
Figure 5: Global distribution of *Vibrio sp.* in the marine habitat. The Figure outlines studies that sampled numerous types of plastic substrates (PP, PE, PVC, PET, PA, PUR) from the shown habitats and all of them found *Vibrio sp.* among the most abundant genera within their samples. This strongly outlines the relevance of *Vibrio* sp. in the plastisphere (Zettler et al., 2013[1]; Lacerda et al., 2021[2]; Rodrigues et al., 2019[3]; Frere et al., 2018[4]; Kirstein et al., 2016[5]; Delacuvellerie et al., 2021[6]; Delacuvellerie et al., 2022[7]; Kumar et al., 2022[8]; Joshi et al., 2021[9]; Wang et al., 2024[10]; Zhang et al., 2020[11]; Bhagwat et al., 2021[12], created with Biorender).

Generally, *Vibrio* spp. occur ubiquitously in aquatic habitats, due to their ability to adapt to different ecological and metabolic lifestyles (Frère et al., 2018). Regarding the surface distribution in marine habitats, they were found to be more abundant in plastic-based biofilms than in control samples on other surfaces (Wright et al., 2020). Therefore, it is not surprising that the genus is described to belong to the first colonizers, especially within the marine plastisphere (Zhai et al., 2023). Due to climate change, leading to increasing water temperature, *Vibrio* sp. are more often found in higher numbers in aquatic environments, and are further enriched during diatom blooms.

Especially during the summer months, they are capable of dominating the plastisphere, independently of polymer type and geographical location (Figure 5; Amaral-Zettler et al., 2020).

An important factor for the high abundance of *Vibrio* spp. on surfaces is their capability to form strong biofilms. Depending on the species, they possess two or even three quorum sensing systems (Baker-Austin et al., 2018). These include the autoinducer system 1 (AI-1) and 2 (AI-2) and the cholera autoinducer system (CAI). They are required for cell-cell communication, controlling extracellular polymeric substances (EPS) production, expression of virulence genes and the secretion of hydrolases, possibly involved in degradation processes (Hammer and Bassler, 2003, Zhai et al., 2023).

Summarizing, *Vibrio* sp. are highly relevant in terms of plastic colonization as they are partially dominating the plastisphere. Interestingly, the genus is associated with members potentially capable of degrading plastic polymers (Auta et al., 2017, Weigert et al., 2022, Buhari et al., 2025), but also with numerous human and animal pathogens (e.g., *Vibrio cholerae*) (Van Kessel & Camilli, 2024).

1.7 *Vibrio gazogenes* DSM 21264 as a model organism for this work

For this thesis, *Vibrio gazogenes* DSM 21264 was chosen as a model organism. It was first isolated in 1978 from a saltwater marsh mud in Massachusetts (USA; Harwood, 1978). Initially classified as *Beneckea gazogenes*, it was reclassified in 1981 after sequence homology analyses (Baumann et al., 1981). The organism is a rod-shaped, Gram-negative, facultative anaerobe Gammaproteobacterium (Allen et al., 1982). *V. gazogenes* produces a red, prodiginine-like pigment, called prodigiosin, which was first isolated in 1946 from *Chromobacterium prodigiosum* (*Serratia marcescens*). The compound has been studied since then for its antimicrobial and anticancer properties (Lichstein and Vam de Sand, 1946, Castro, 1967, Vijay et al., 2022). Interestingly, *V. gazogenes* carries a putative PET-degrading hydrolase, named PET6, which has been well characterized *in vitro* (Weigert et al., 2022). Additionally, homologs of this PETase were found in *V. ruber*, *V. spartinae*, *V. palustris*, and *V. zhugei*. The amino acid sequences of all PET6 homologs share 90-95% identity and full coverage. While these homologs have just been identified, it has yet to be shown whether they also degrade PET, although it is most likely. Intriguingly, average nucleotide identity (ANI) and pangenome analysis showed that *V. palustris* and *V. zhugei* form a different cluster to the other three species, suggesting the occurrence of horizontal gene transfer of the gene coding for the PETase (Weigert et al., 2022).

Regarding all the above-mentioned interesting characteristics of *V. gazogenes* DSM 21264, it was chosen as a model organism for this work, to gain deeper understanding of its role in the plastisphere. This species is a representative of the predominant genus and theoretically has the ability to degrade PET. Consequently, we aimed to address, whether organisms with the enzymatical potential to hydrolyze artificial polymers actually contribute to their degradation *in vivo*.

1.8   Intention of this work

After summarizing the obtained information on plastic pollution and the increase of the new formed micro-habitat, the plastisphere, it is outstanding that besides the comprehensive knowledge, that has been generated, still significant gaps are occurring. Within this framework steps towards the closing of those knowledge gaps should be made, addressing three main research questions.
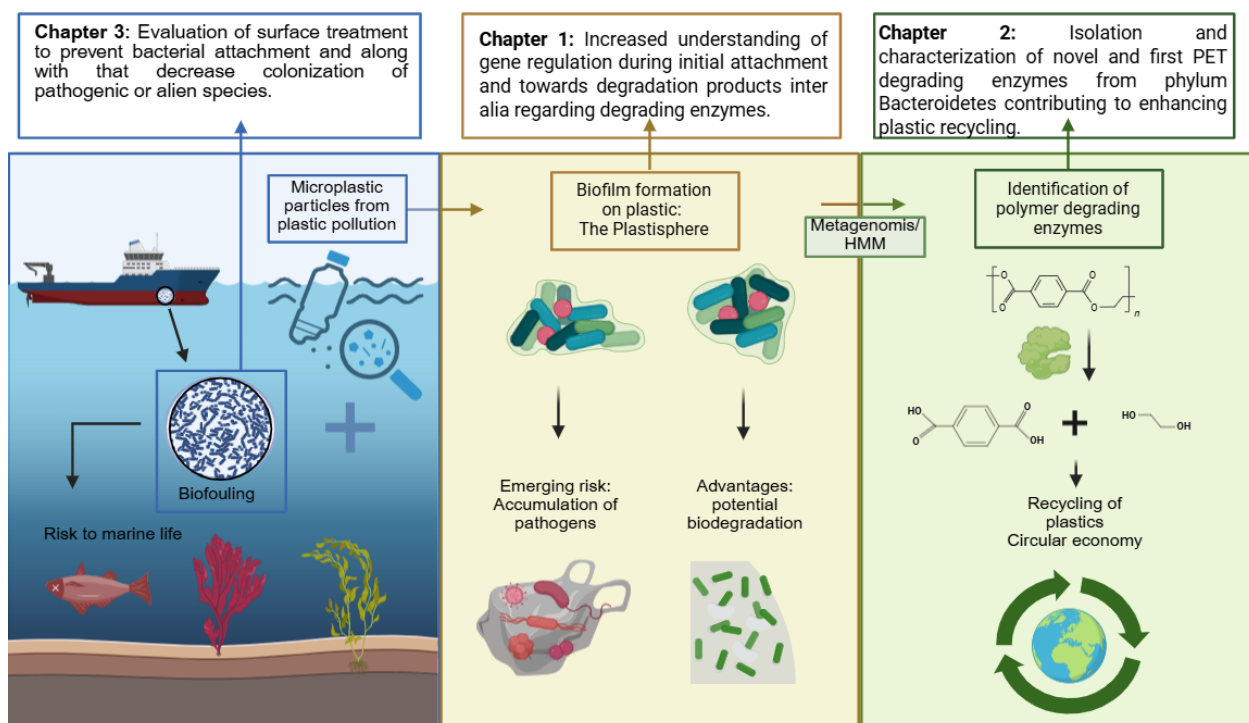
Figure 6: Lifecycle of plastic debris in the sea and possible solutions. The figure has been adapted from Katnic & Gupta, 2025 to point out the potential support by this work for obtaining the goal of plastic recycling and less harm to marine life and human (created with Biorender).

Figure 6 (adapted from Katnic & Gupta, 2025) briefly summarizes the lifecycle of plastic waste, pointing out the best possible outcome in biodegradation and recycling of the polymers. The figure

has been evaluated outlining, the contribution of the following chapters to the achievement of the addressed goal.

Since *Vibrio* spp. are not only ubiquitously found in aquatic environments but also are partially dominating the plastisphere, representative *Vibrio gazogenes* DSM 21264 was chosen, to get detailed information about gene response during first colonization on plastic polymers. The previously described controversy of the chemical structures of PE and PET and along with that the different possibilities of enzymatic breakdown, make the polymers interesting for the investigation of the question, if and to what extend bacteria distinguish in their gene transcription during attachment to different surfaces.

Even though the toxicity of some polymers is described already, little is known about the influence of the breakdown products of the different plastic types. In Chapter 1 the influence of the primary degradation products of PET, BHET and TPA is studied in detail, using various RNAseq approaches (Preuss et al., 2025).

Plastic recycling rates remain insufficient, and due to increasing plastic production its pollution keeps threatening the environment. Until now, already numerous PETases have been discovered, but their role in nature remains unknown. The phylum Bacteroidetes is among the main colonizers of plastics surfaces, making it an important factor for the understanding of the plastisphere and the degradation possibilities. Chapter 2 aims to increase the understanding of PETases. PET27 and PET30 are the first PETases from the phylum Bacteroidetes, which were studied for their potential role in plastic degradation *in vitro* and colonization behavior of its native host (Zhang et al., 2022).

Once exposed to biotic environment, almost all materials are colonized by microorganisms, potentially harming the surface or enhance the accumulation of pathogenic bacteria, posing a potential threat for human and the environment. To reduce biofouling, surface adaption on PE were generated in Chapter 3, to obtain low-fouling surfaces, with the aim to prevent bacterial colonization. Marine fish pathogen *Vibrio campelli* was used, to evaluate, if grafted polymeric *N*-oxides can be used for low-fowling coating and the determination of changes in adherence and biofilm formation.

2 Polyethylene terephthalate (PET) primary degradation products affect c-di-GMP-, cAMP-signaling and quorum sensing (QS) in *Vibrio gazogenes* DSM 21264

Lena Preuss[1*], Malik Alawi[2], Albert Dumnitch[1], Ly Trinh[1], Wolfgang Maison[3], Nils Burmeister[3], Anja Poehlein[4], Rolf Daniel[4], Christel Vollstedt[1], and Wolfgang R. Streit[1*]

[1]Department of Microbiology and Biotechnology, University of Hamburg, Ohnhorststr.18, D-22609 Hamburg. Germany.
[2]Bioinformatics Core, UKE Hamburg, Martinitstr. 52. D-20246 Hamburg, Germany
[3]Department of Chemistry, University of Hamburg, Bundesstr. 45, D-20146 Hamburg. Germany
[4]Department of Genomic and Applied Microbiology, Georg-August University of Göttingen, Grisebachstr. 8, D-37077 Göttingen, Germany

The authors declare no conflict of interest.

ABSTRACT

Global plastic pollution in oceans and estuaries is increasing rapidly and it's well known that bacteria colonize plastic particles of all sizes. *Vibrio* spp. are frequently found as part of the plastisphere. We recently showed that *Vibrio gazogenes* DSM 21264 harbors a promiscuous esterase designated PET6. We now provide evidence that the *pet6* gene is expressed under a wide range of environmental conditions in its native host. However, in PET- and PE-grown biofilms the *pet6* gene expression was not affected by the type of surface. The *pet6* transcription was sufficient to allow enzyme production and release of µM amounts of mono(2-hydroxyethyl) terephthalate (MHET) and terephthalic acid (TPA) already after 24 hours of incubation on PET foil. Notably, the highest *pet6* gene transcription was observed in planktonic lifestyle in the presence of bis(2-hydroxyethyl) terephthalate (BHET) one of the primary degradation products of PET. BHET was further hydrolyzed by PET6 and UlaG, a lactonase that had not been known to be involved in BHET degradation. Elevated concentrations of BHET affected the major signaling circuits involved in bacterial quorum sensing (QS), c-di-GMP and cAMP-CRP signaling. This resulted in failure to form biofilms, synthesis of the red pigment prodigiosin and altered colony morphologies. While BHET had a very wide impact, TPA interfered mainly with the bacterial QS by attenuating the expression of the CAI-I autoinducer synthase gene. These observations imply a potential role of BHET and TPA as nutritional signals in *Vibrio gazogenes* and that may affect its growth and survival in the plastisphere.

IMPORTANCE

This study provides first evidence that *Vibrio gazogenes* DSM 21264 secretes an active PET hydrolase and degrades the polymer using PET6 when growing in biofilms on foils and microplastic particles. The study further provides evidence that the primary PET degradation products BHET and TPA may have a profound impact on the global QS, c-di-GMP and cAMP-CRP signaling of *V. gazogenes* and its capability to colonize plastic particles in the marine environment.

INTRODUCTION

Global plastic pollution has reached an alarming and unprecedented level in the recent decade. Recently, it was estimated that a minimum of 8-10 million tons of plastic is entering the oceans annually [1], [2], [3], [4], [5]. While most of the plastic enters the environment as larger floating fragments, weathering results in the production of smaller particles (micro-, nano- and pico-plastics) with sizes less than 5 mm in diameter [6], [7]. These particles and the additives contained in them are believed to have negative impact on all ecological niches and their biodiversity [8], [9]. Ultimately, they will also affect human health and wellbeing [10].

The majority of the fossil-fuel based and synthetic polymers which end up in the environment are polyethylene (PE), polypropylene (PP), polyvinylchloride (PVC), polyethylene terephthalate (PET), polyurethane (PUR), polystyrene (PS) and polyamide (PA) only being produced at lower quantities [11]. While for most of these polymers no enzymes and microorganisms are known to degrade them the degradation of PET is well understood (www.PAZy.eu) [12]. PET is degraded by promiscuous and secreted esterases, lipases or cutinases that all have a wide substrate specificity and are members of the E.C classes 3.1.1.- [11], [13], [14]. In addition to these studies recently much effort has been made to analyze and characterize the phylogenetic makeup of microbial communities associated with plastic particles found in the marine environment. The microorganisms colonizing plastic particles (i.e. the plastic microbiota) have been termed 'plastisphere' [15], [16], [17], [18]. These studies indicate that growth on and the initial colonization of plastic surfaces depends on the chemical and the physical properties of the various polymers. Thereby, the surface charge, roughness and the different chemical compositions of additives play key roles during the attachment and growth of the plastic colonizing microbiota [19], [16].

Notably, the simple colonization does not imply any biodegradation [6]. The microbial communities observed are highly diverse in their phylogeny and bacteria affiliated with the genus *Vibrio* are often observed on plastic particles [20] [18] [21] [22] [23] [24]. *Vibrio* species are ubiquitously occurring gram-negative bacteria that are mainly found in marine environments where they are

considered to be key players in carbon and nitrogen cycling [25] [26]. There are more than 100 known *Vibrio* species of which few are either human or fish pathogens (e.g. *Vibrio cholerae*, *Vibrio parahaemolyticus, Vibrio alginolyticus, Vibrio vulnificus* and others) [27] [28] [29].

Recently, we have shown that the marine organism *V. gazogenes* DSM 21264 (from here on DSM 21264) harbors a gene encoding a promiscuous esterase designated PET6 in its 4.6 Mbp genome [30] [31]. DSM 21264 (synonym PB1, AATCC 29988) is a gram-negative and non-pathogenic bacterium. It was isolated from sulfide-containing mud collected from a saltwater marsh and produces a red pigment, prodigiosin [32]. The species is globally occurring and typically found in estuaries. The *pet6* gene is encoded by ORF AAC977_05355. The heterologous expressed protein hydrolyzes amorphous PET and other substrates including short chain fatty acid esters [30] [31] and its activity is salt- dependent. PET hydrolysis catalyzed by recombinant PET6 is, however, rather low compared to other known enzymes used in industrial processes like the well-characterized IsPETase or LCC [31]. While much information was gathered on the enzyme structure and biochemical function of PETases, only few studies focused on the expression of the enzyme within the native host. *Ideonella sakaiensis* is among the only organisms for which the PET-metabolism is well understood [33]. With respect to DSM21264 it was not known under which conditions the *pet6* gene is transcribed in its native host and if the native enzyme would result in PET degradation in the environment. Within this manuscript we provide first evidence that the *pet6* gene is transcribed at low levels under various environmental conditions. The *pet6* gene expression is, however, not affected by the presence of PET, PE foil or PET powder.

Instead, BHET, a primary PET degradation product, affects *pet6* transcription at mM concentrations. Further, our data imply that BHET is a nutritional signal affecting the c-di-GMP, the cAMP-CRP and QS-dependent signaling pathways in DSM 21264. These three signaling pathways are essential to lifestyle transitions from motility, attaching to a surface and forming biofilms in the plastisphere.

RESULTS

DSM 21264 forms patchy biofilms on PE and PET independent from the surface and releases µM amounts of MHET and TPA.

Since we had earlier shown that DSM 21264 produces a PET-active hydrolase, designated PET6 [31] [30], we wanted to know if the organism forms biofilms on PET foil and actively degrades PET. Further, we asked if the *pet6* gene is expressed at significant levels. Therefore, we inoculated DSM 21264 in artificial seawater medium (ASWM) with PET or PE foil for biofilm formation and potential degradation. Since no PE-degradative genes have been reported in gram-negative bacteria PE-foil was used as a control. In these biofilm experiments cells attached in general at very low frequencies and only thin single cell layer biofilms were formed after 10 and 180 days (FIGURE 1 & S1).
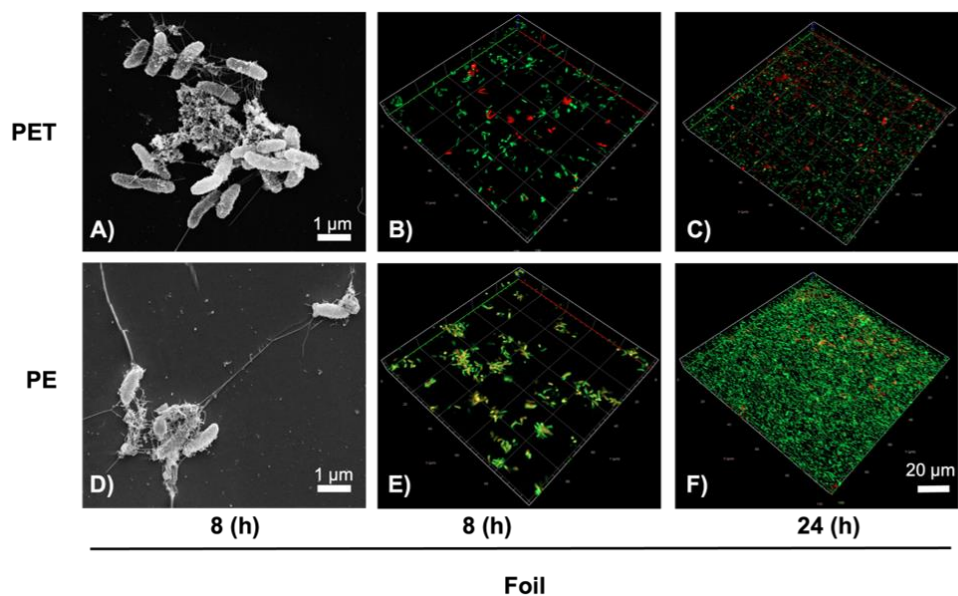
FIGURE 1: Scanning electron microscope (SEM) **(A, D)** and confocal laser scanning microscope (CLSM) images **(B, C, E, F)** of *V. gazogenes* DSM 21246 biofilms grown on PET and PE foil. SEM images and CLSM images **A), B) & D), E)** show first attachment of cells after 8 hours of incubation in ASW medium at 22 °C of incubation on PET foil **A) & B)** and PE foil **D) & E)**. CLSM images **C) & F)** show biofilm formation of DSM 21264 on PET foil **C)** and PE foil **F)** after 24 hours of incubation. Cells were stained using LIVE/DEAD stain.

Therefore, we used ASWM supplemented with tryptone and yeast extract 1% (w/v) in further tests to promote growth and biofilm formation. Under these conditions DSM 21264 attached within few hours and formed patchy biofilms on both plastic surfaces, whereby the biofilms formed on PE were less patchy than those on PET (FIGURE 1). Biofilms formed on PE and PET had an average thickness of 2-3 μm equaling one cell layer (FIGURE 1).

SEM images showed that the cells on PET and PE were interconnected by fiber- and net-like structures with a length of 4-10 μm. However, the net-like structures were more prominent on PE surfaces (FIGURE 1). Additional tests with air plasma-treated PET and PE foil were conducted [34]. Air plasma treatment leads to the formation of oxygen-functionalities and thus an increase in surface polarity. It typically gives a potential degradative enzyme better access to the polymer fibers [35]. However, in these tests only minor differences were observed with respect to biofilm formation (FIGURES 1 & S1). Notably, when we grew DSM 21264 on PET foil or powder, we detected µM amounts of BHET, MHET and TPA in the biofilm and culture supernatants already after 24 hours (FIGURE 2).
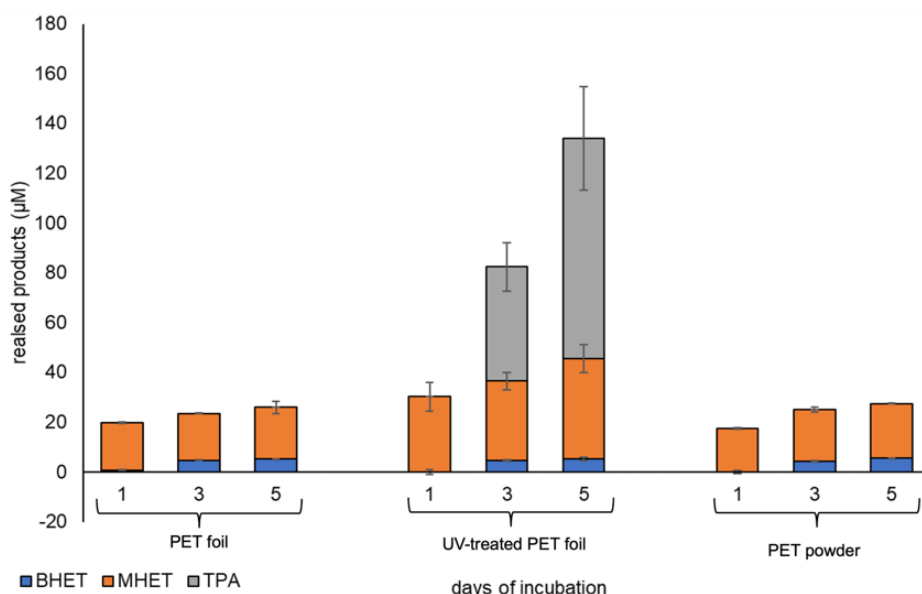
FIGURE 2: PET degradation products observed in supernatants of *V. gazogenes* DSM 21264 biofilms grown on PET foil (non-treated), UV-treated foil and PET powder. *V. gazogenes* DSM 21264 was grown in ASWM medium with reduced carbon source. Supernatants were collected after 1, 3 and 5 days and the degradation products were measured using UHPLC and as described in the Material and Methods section.

Data were normalized and corrected to *E. coli* DH5α growing on PET foil and powder. Data are mean values of three independent replications and bars represent the standard deviations.

Transcriptome analysis identifies keys to PET6 gene expression.

Based on the above-made observations, we further asked if the *pet6* gene (AAC977_05355) was expressed and if surface attachment to PET or PE resulted in major transcriptional changes. To address these questions, we mainly used transcriptome studies with the goal to obtain an insight into the overall gene expression pattern of DSM 21264 in response to PET or other substrates during life in biofilms and planktonic cultures. In total we analyzed 14 different environmental parameters and/or carbon sources. Each experiment was repeated 3 times resulting in 42 RNAseq data sets which have been submitted to the European Nucleotide Archive (ENA). They are publicly available under accession PRJEB80907. Obtained reads were mapped against the genome of DSM 21264. For this purpose, we established a high-quality genome sequence of DSM 21264 that encompasses two chromosomes coding for 4,159 genes. Chromosome 1 (CP151640) codes for 3,121 genes and chromosome 2 (CP151641) for 1,038 genes. The newly established genome sequence is available under accession numbers CP151640 and CP151641 at NCBI/GenBank. An overview of the data sets reads obtained, the percentage of reads mapped to the genome and other parameters together with the level of *pet6* gene expression is given in TABLE S2 and FIGURE 3.
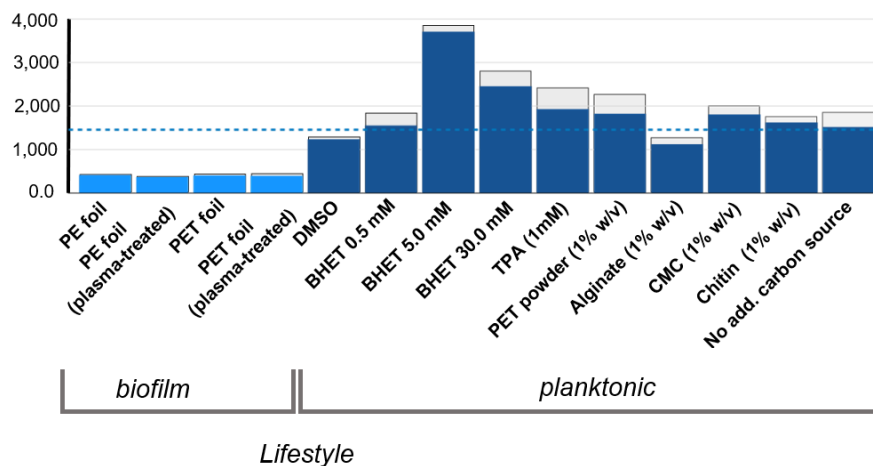
FIGURE 3: Transcription level of the *pet6* gene in relation to all 4,117 genes transcribed in DSM 21264. Blue bars indicate ranking of *pet6* depending on all genes transcribed.

Each data set represents the mean data from three independent biological replicates. Standard deviations are indicated as light grey bars on top of the colored bars. The blue dotted line indicates the mean transcription level of all 4,117 genes in all 42 experiments.

PET6 is weakly expressed in biofilms grown on PET and PE foils.

When we compared PET-grown biofilms versus PE-grown biofilms, the expression *of pet6* was low and ranked around 25% of the weakest transcribed genes. FIGURE 3 summarizes the level of expression of *pet6* under the biofilm conditions tested and in relation to the genome-wide expression of all genes. Plasma-treatment of the PET or PE foil had no significant impact on the low level of *pet6* gene expression (TABLE S1 and FIGURE 3). This observation is in line with the slow degradation of the polymer in biofilm cultures as described above (FIGURE 2). In addition, we noticed, that in all biofilm experiments the transcription of *ompU* was among the highest transcribed genes. OmpU is an outer membrane protein which has for *V. cholerae* been described to be important for biofilm formation [40], implying that OmpU possibly is involved in surface colonization. Furthermore, only four genes were differentially expressed in all biofilm studies (TABLE S1 and S3). Highest log2-foldchanges were detected for a glutathione peroxidase and an alkyl hydroxide peroxidase, both involved in hydrogen peroxide scavenging [36]. In addition, the *adhE* gene, which is involved in ethylene glycol (EG) metabolism was significantly upregulated in PET biofilms but not in PE-grown biofilms (TABLE S1). To further verify the increased expression of *adhE,* a reporter fusion was constructed fusing the promoter with the amcyan gene in pBBR1-MCS-1 and mobilized into DSM 21264 (TABLE 1). Using the *P_adhE::amcyan* transcriptional reporter gene fusion in DSM 21264 we were able to verify that *adhE* was 2-fold upregulated in the presence of 5 mM EG (FIGURE S5).

Since PET and PE are no natural substrate for bacteria, we further asked if other natural polymers would stimulate *pet6* gene expression. Therefore, we added alginate, chitin and carboxymethyl cellulose (CMC) (1% w/v) to planktonic cultures and assayed the transcriptomes after 24 hours of aerobic growth. As expected in the planktonic cultures a largely different pattern of gene transcription was observed compared to the biofilm conditions (Table S1, FIGURES 4-6 & FIGURE S2).

Since under all tested conditions a number of reads was mapped to the *pet6* gene, it appears to be constitutively expressed (FIGURE 3). In general, the transcription level of *pet6* was low and close to 0.4% of the transcription observed for *rpoD* (TABLE S2). In summary, the data imply that *pet6* gene expression is not strongly activated by any of the added natural polymers or by PET powder (1% w/v) containing cultures. However, the expression was significantly higher in the planktonic cultures compared to the biofilm cultures (FIGURE 3).

Pet6 and *ulaG* transcription are induced by BHET in DSM 21264.

Since PET6 hydrolyzes PET, we further asked if DSM 21264 would be able to metabolize BHET and use it as sole carbon and energy source, and if it would affect *pet6* gene expression. To address these questions additional experiments in liquid media were performed challenging DSM 21264 with BHET at concentrations of 0.5, 5.0 and 30 mM. The growth of the strain was not affected by lower BHET concentrations (0.5 mM and 5.0 mM) after 24 h of incubation (FIGURE S8). Since higher concentrations of BHET precipitate, measurement of OD_{600} was not valid. Testing 30 mM of BHET on agar plates determined less colony formation than other tested concentration implying reduced growth (FIRGURE S6). The overall gene expression profile using RNAseq was tested for the respective BHET concentrations. As controls we incubated DSM 21264 in the presence of 1.0 mM TPA, DMSO (0.5% v/v) and PET powder (1% w/v) in liquid cultures. TABLE S2 summarizes the data obtained for all RNAseq experiments. The volcano plots highlight major changes in gene expression (FIGURE S2). A detailed analysis identified a large

number of genes and operons differentially regulated (>log2-foldchange of 2) in the presence of the different BHET concentrations clearly indicating that DSM 21264 senses and adapts its metabolism to the presence of BHET (TABLE S1 and FIGURES 4-6). High concentrations (5.0 and 30 mM) of BHET had the most pronounced effects on the overall gene expression levels in DSM 21264 with >230 upregulated and >100 downregulated genes in the presence of 5.0 mM and >830 upregulated and >550 downregulated genes in the presence of 30 mM BHET compared to the DMSO or the TPA controls (FIGURE S7). Our data imply that BHET is most likely initially metabolized by PET6 releasing MHET as the primary degradation product of BHET. This is in line with an almost 5-fold (log2-foldchange) increased transcription level of *pet6* (AAC977_05355) at 5 mM BHET and 1.8-fold increase at 30 mM. Surprisingly, the RNAseq data indicated that UlaG, a predicted metallo-ß-lactamase, is also involved in BHET metabolism. In the presence of 30 mM BHET *ulaG* was most strongly transcribed with a 7.9-fold upregulation compared to the control. To further verify this novel role of UlaG, we expressed it in *E. coli* T7 SHuffle and used the recombinant protein to hydrolyze BHET. In these tests the promiscuous enzyme was able to cleave BHET at slow but significant rates (FIGURE S3). Further UHPLC measurement confirmed that MHET is the main and initial degradation product of DSM 21264 cells grown on BHET (FIGURE S4). While MHET is converted to EG and TPA, DSM 21264 was neither able to grow on TPA and EG as sole carbon and energy source nor on BHET. It does not encode any mono- and dioxygenases involved in aromatic ring cleavage.

BHET and TPA affect the central circuits involved in c-di-GMP, cAMP-CRP and QS signaling in DSM 21264.

During the above-described growth experiments using BHET as a substrate, we noticed major phenotypic changes in DSM 21264 affecting colony morphology, biofilm formation, prodigiosin biosynthesis and others (FIGURE S6).

BHET altered colony morphology already at rather low concentrations (0.5 mM). Colonies were less structured and had smooth edges. Higher concentrations of BHET resulted in the disappearance of the red pigment prodigiosin. Biofilm formation was disturbed at 0.5 mM and no solid biofilms were formed at 10 mM BHET present in the medium (FIGURE S6).

These phenotypic observations implied a larger impact of BHET on the metabolism and main regulatory circuits of DSM 21264 in planktonic cultures. To further elucidate these effects, we analyzed our transcriptome data with respect to the influence of BHET on regulatory pathways linked to QS, cAMP-CRP signaling and c-di-GMP signaling. These pathways were chosen, as they are known to have a wider impact on biofilm formation, motility, secretion, secondary metabolite production and others.

Most notably, 30 mM BHET strongly affected the transcription of genes essential for c-di-GMP biosynthesis. The signal c-di-GMP is synthesized by diguanylate cyclases degraded by phosphodiesterases. DSM 21264 harbors at least 16 possible c-di-GMP cyclases/ phosphodiesterases in its genome. The majority of the diguanylate cyclases were strongly downregulated in their transcription in the presence of high concentrations of BHET, while they were strongly upregulated in the presence of low concentrations of BHET or other carbon sources (FIGURE 4). The most strongly attenuated genes coding for diguanylate cyclases were *cdgB, C, I, J* and *M* (log2-foldchange < –4.5). On the contrary, *cdgG* and *acgB* were strongly upregulated in the presence of increased BHET concentrations (log2-foldchange 3.5 and 5) (FIGURE 4).
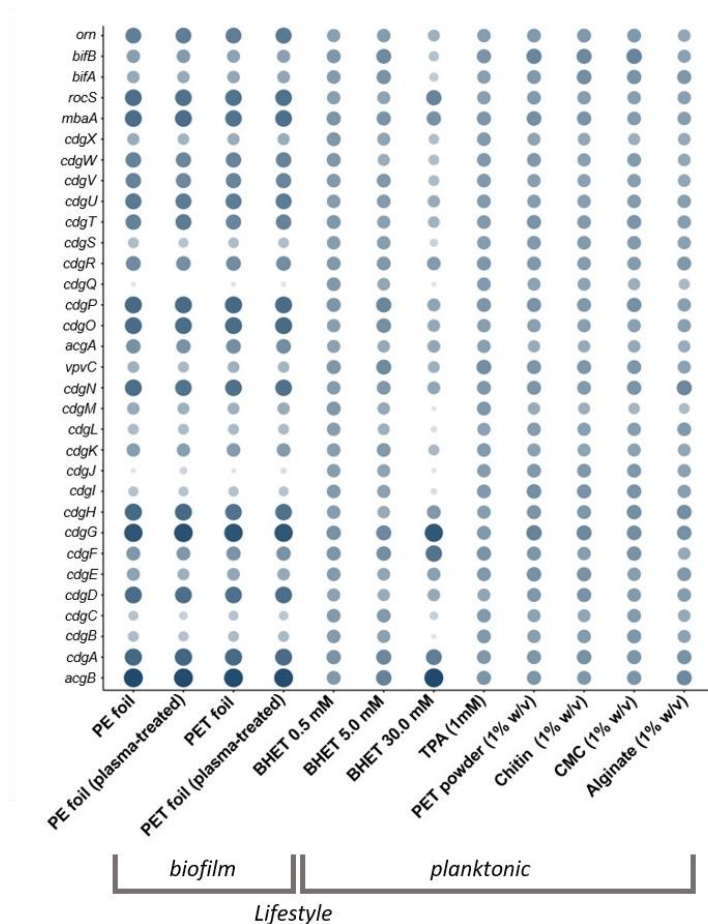
FIGURE 4: Relative transcription level of *c*-di-GMP-signaling related genes in DSM 21264. The circles size and color correlate with the normalized transcription level. The color intensity and size of the circles is adjusted to logarithmized values (log_value) ranging from -2 to 4 and according to the mapped reads. CdgA-CdgN are diguanylate cyclases (DGC) and CdgO-CdgX are phosphodiesterases (PDE), *bifA* and *bifB* code for bifunctional genes and Orn is an oligoribonuclease. Each data point is a mean value of three independent experiments for each of the 12 conditions shown.

Further, we observed that BHET affected quorum sensing (QS) processes. In this context, transcription of the master QS regulator *aphA* was almost not detectable at 30 mM BHET, while it was well expressed at 0.5 and 5.0 mM BHET or in the presence of TPA in planktonic cultures (FIGURE 5). HapR was also only weakly transcribed in the presence of 30 mM BHET. While it is well known that AphA and HapR are usually transcribed at opposite levels, no differences in transcription levels were visible neither in the presence of lower concentrations of BHET nor in the presence of TPA. These differences in expression were, however, clearly visible in all the biofilm experiments and in the planktonic cultures supplemented with natural polymers (FIGURE 5).

Furthermore, TPA negatively affected the transcription of the autoinducer synthase gene *cqsA,* which is involved in the cholera autoinducer I biosynthesis (CAI-I) (TABLE S1 and FIGURE 5). Further our data showed that the DSM 21264 autoinducer (AI) -I synthase, LuxM*,* and the cognate

sensor LuxN as well as the genes coding for the AI-2 synthase, *luxS*, the periplasmatic binding protein, LuxP, and the sensor kinase LuxQ were significantly affected in their transcription levels at 30 mM BHET (FIGURE 5).
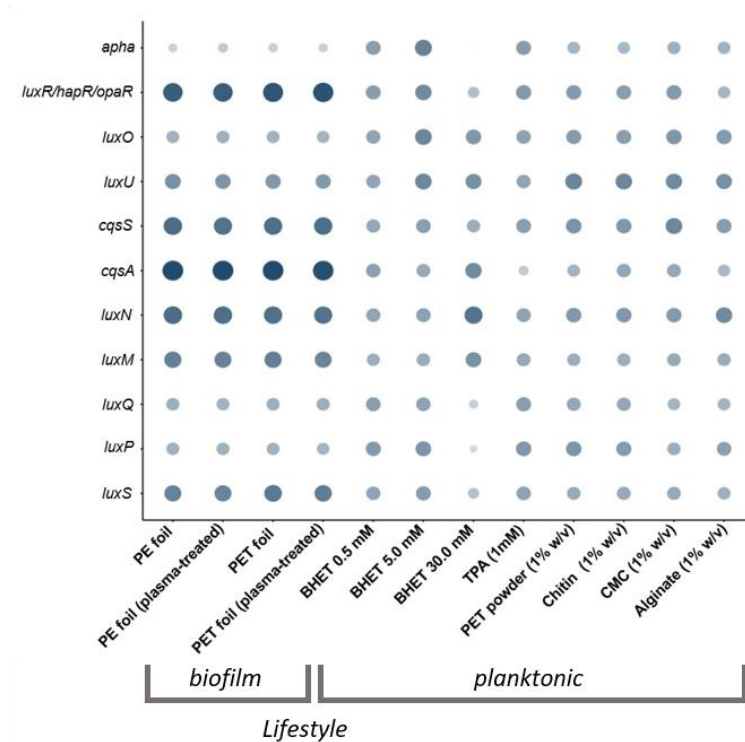
FIGURE 5: Relative transcription level of essential quorum sensing (QS)-related and differentially regulated genes in DSM 21264. The circles size and color correlate with the normalized transcription level. The color intensity and size of the circles is adjusted to logarithmized values (log_value) ranging from -2 to 4 and according to the mapped reads. *luxS*, *luxM* and *cqsA* code for autoinducer synthases, LuxP is annotated as periplasmatic binding protein and LuxQ, LuxN and CqsS are autoinducer sensor kinases. Apha is the low cell density regulator and LuxR high cell density regulator. Each data point is a mean value of three independent experiments for each of the 12 conditions shown.

Finally, our data implied that BHET interfered with the cAMP-CRP signaling. The catabolite activator protein transcription was almost completely turned off in the presence of 30 mM BHET (FIGURE 6).
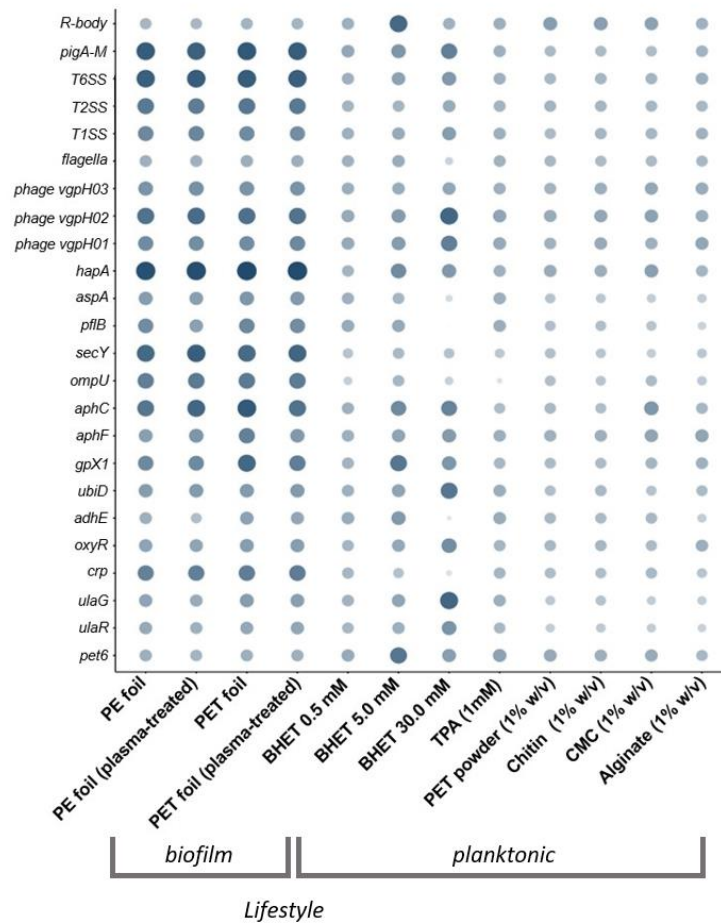
FIGURE 6: Relative transcription level and changes of differentially regulated major genes and gene clusters in DSM 21264. The circles size and color correlate with the normalized transcription level. The color intensity and size of the circles is adjusted to logarithmized values (log_value) ranging from -2 to 4 and according to the mapped reads. R bodies belong to the Rebb family gene cluster, pig gene cluster is responsible for synthesis of prodigiosin, hapA is M4 metallopeptidase annotated as vibriolysin, *aspA* encodes an aspartate ammonia-lyase, *pflB* codes for a formate C-acetyltransferase. Each data point is a mean value of three independent experiments for each of the 12 conditions shown.

Besides the direct impact of 30 mM BHET on the above-mentioned regulatory circuits, 30 mM BHET strongly attenuated transcription of motility genes, *hap*A, *aspE, ompU*. In the contrary, *ulaG, ulaR*, *aphC*, *aphF* and the prodigiosin operon were strongly upregulated (FIGURE 6).

Interestingly, among the highest upregulated genes in the samples supplemented with 30 mM BHET several phage related genes were observed. In total, DSM 21264 codes for three

prophages (Phage 1, designated VGPH01, AAC977_19445 – AAC977_19700; Phage 2, designated VGPH02, AAC977_20360 – AAC977_20490 and Phage 3, designated VGPH03, AAC977_09080 – AAC977_09210) which can be grouped into the class of Caudoviricetes. VGPH01 and VGPH02 are encoded on the smaller chromosome CP151641 whereas VGPH03 is part of the larger chromosome CP151640. All three phages were transcribed under biofilm conditions. In contrast, their transcription was generally low in planktonic cultures. However, in planktonic cultures, 30 mM BHET resulted in strong transcription of the gene clusters coding for VGPH01 and VGPH02 (TABLE S4 and FIGURE 6).

In summary our data imply that BHET and TPA may have a wider effect on the metabolism of DSM 21264 and interfere with the interconnected pathways involved in c-di-GMP, QS and cAMP-CRP signaling.

DISCUSSION

Today 124 PET-active enzymes are known and most of these enzymes have been characterized very well with respect to their structures, functions and catalytic activities on the synthetic polymer. These enzymes are generally secreted and promiscuous hydrolases belonging to the E.C. 3.1.-. [12] [11] [13] [14] [6]. However, only very few studies have analyzed growth of bacteria on PET foil using global RNAseq approaches [37] [38] [39]. Despite these first studies, it is not clear if bacteria differentiate between the different types of synthetic polymers either as a surface to attach to or as a potential substrate for breakdown.

Our data suggest that only very few genes are differentially regulated when DSM 21264 is grown on PET versus the non-biodegradable PE, implying that most likely DSM21264 is not able to differentiate between these two polymers. Also, the treatment with plasma did not affect this response. Interestingly, our data identified *ompU* as one of the most strongly transcribed genes when grown in biofilms (TABLE 2). OmpU is an outer membrane protein known to be an important adherence factor in *Vibrio cholerae* and an essential biofilm matrix assembly protein [40]. Based

on these earlier findings it is likely that the DSM 21264 OmpU plays a major role in biofilm formation on plastic surfaces and life in the plastisphere.

Only a few *Vibrio* species harbor PET6 homologues but all of them share a very conserved core genome and have common regulatory networks [31] [41] [42]. Within this setting our data imply that *pet6* is expressed at low levels under most environmental conditions (FIGURE 3) and increasing BHET concentrations affected transcription of the gene.

Besides these observations our study has further revealed that UlaG is involved in BHET metabolism. Previous work has already demonstrated that UlaG is a promiscuous metallo-beta-lactamase with a wide range of functions in bacteria and archaea [43] [44]. We observed a strongly increased transcription of *ulaG* in the presence of high BHET concentrations. Additional BHET degradation assays confirmed this novel functional role of UlaG (FIGURE S3, FIGURE 7).
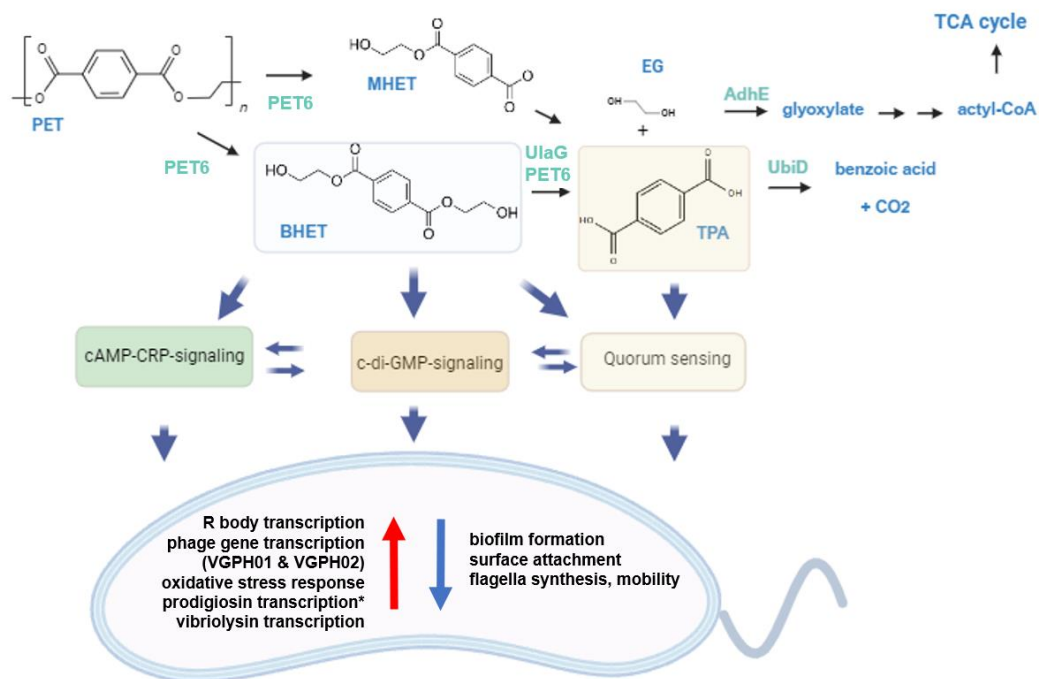
FIGURE 7: Possible PET degradation pathway in DSM 21264 and regulatory model affecting QS, cAMP-CRP and c-di-GMP signaling through BHET and TPA. Proteins involved in enzymatic PET breakdown are in cyan color. PET and degradation products released are labeled in blue. Blue arrows indicate regulatory

pathways affected by BHET and /or TPA in DSM 21264. Red and blue arrows inside the cell model indicate up- and downregulated pathways.

*Transcription of prodigiosin operon is strongly upregulated (log2-foldchange >3) in the presence of high BHET concentrations, but synthesis of the pigment is inhibited.

Ideonella sakaiensis is the only organism for which the whole degradation pathway of PET is mostly understood. PET is degraded into MHET and EG and further transformed by the IsMHETase into TPA and EG. EG is then oxidized by an alcohol dehydrogenase to glycolaldehyde (GAD) and further metabolized by the aldehyde dehydrogenase to glycolic acid (GA) [45]. Similar to the EG metabolism of *I. sakaiensis*, our data support the notion that *adhE* in DSM 21264 is involved in the metabolism of EG. This observation was supported by both RNAseq and experimental data (FIGURE S5). Since *adhE* is transcribed at higher levels in PET biofilms it is likely that this increase is caused already by the degradation of the polymer and the parallel BHET release (FIGURE 7)

Additionally, the data from our study suggest that BHET and TPA are nutritional signals affecting QS, c-di-GMP and cAMP signaling at mM concentrations (TABLE S1 and FIGURE 4-6). This hypothesis is based on 42 transcriptome datasets of DSM 21264 that have given us insight into the response of this bacterium when challenged with PET, other natural polymers, BHET and TPA. Because of the important role of *Vibrio* spp. in pathogenicity, regulatory networks have been well studied in this genus [46] [47] [48]. These networks are known to be involved in surface attachment, biofilm formation, infection, toxin and secondary metabolite production, phage assembly and others. Biofilm formation in *Vibrio* spp. is controlled by quorum sensing (QS), an integrated and highly complex network of multiple transcriptional regulators (e.g. VpsR, VpsT, HapR, H-NS and AphA). The c-di-GMP signaling influences the planktonic-to-biofilm transition. In addition, cAMP-CRP-signaling represses biofilm formation in *Vibrio* spp. [49] [47] [50].

In this study, we showed that many of the above-mentioned regulatory circuits and their key regulators in DSM 21264 were affected by BHET and in part by TPA in planktonic cultures

(FIGURES 4-6). For instance, essential components of the QS signaling like the low cell density regulator, AphA, and the regulator for high cell density, HapR, were strongly attenuated by high concentrations of BHET. Like AphA and HapR, the autoinducer-I and 2 synthase genes (*luxM, luxS*), the cognate sensor genes (*luxN, luxQ*) and the transcription of the periplasmic binding protein (LuxP) were significantly affected in their transcription levels by 30 mM BHET (FIGURE 5). QS thereupon regulates the c-di-GMP level in the cell. The major signal c-di-GMP is produced by diguanylate cyclases and degraded by specific phosphodiesterases which are directly regulated by HapR [51] [50]. DSM 21264 has a very similar set of c-di-GMP cyclases and phosphodiesterases compared to *V. cholerae* or other well studied *Vibrio* species. Many of the cyclase genes were differentially regulated at higher concentrations of BHET (TABLE S1 and FIGURE 4). The lack of sufficient cyclase transcription will most likely result in low intracellular levels of c-di-GMP that would not be sufficient to allow biofilm formation. This observation is in line with the failure to form biofilms in medium supplemented with >10 mM BHET (FIGURE S6).

Within this framework, cAMP-CRP signaling is well known to be involved in the expression of inducible catabolic operons. Besides this function cAMP-CRP signaling is also involved in processes related to infection and biofilm formation. Thereby, a specific adenylate cyclase catalyzes the formation of cAMP from ATP, whereas cAMP phosphodiesterases catalyze its breakdown [52] [53]. The DSM 21264 cAMP-CRP signaling pathway is conserved as well and its main regulatory protein is the CRP regulator. While CRP was highly transcribed under biofilm conditions, its transcription was in general much lower in planktonic lifestyle. Notably, 5.0 and 30 mM BHET downregulated the CRP transcription even further, implying that BHET is interfering with this signaling cycle as well (FIGURE 6). Overall, the interference with key regulatory networks implies that the degradation products of PET strongly induce stress responses in DSM 21264. This results in rapid changes of several metabolic pathways and linked to different survival strategies.

Based on the above made observations we were able to establish a putative first model outlining the main genes and enzymes involved in PET degradation and metabolism and the regulatory circuits involved (FIGURE 7). This preliminary model and our experimental data provide a foundation for future research on bacterial metabolism and nutritional signaling during life in the plastisphere. Since *Vibrio* spp. is found with high frequencies in the plastisphere data from this study will help to identify key factors involved in enriching for pathogens in this man-made habitat. Finally, this study will be useful for the design of bacterial strains for efficient plastics removal in the marine environment.

DATA AVAILABILITY

Sequence data reported in this publication have been submitted to NCBI/ENA. The raw reads of the 42 sequencing runs are publicly available under accession PRJEB80907 at European Nucleotide Archive (ENA). The newly established genome sequence of *Vibrio gazogenes* DSM 21264 is available under accession numbers CP151640 and CP151641 at NCBI/GenBank.

MATERIAL AND METHODS

<u>Bacterial strains and growth conditions</u>

Bacterial strains and plasmids used in this study are summarized in TABLE 1. *Vibrio* sp. was cultured either at 22 °C or 28 °C in artificial seawater medium (28.13 g/L NaCl, 0.77 g/L KCl, 1.6 g/L $CaCl_2$ x $2H_2O$, 4.8 g/L $MgCl_2$ x 6 H_2O, 0.11 g/L $NaHCO_3$, 3.5 g/L $MgSO_4$ x 7 H_2O, 10 g/L yeast extract, 10 g/L tryptone) or in AS medium 1:10 diluted (1 g/L tryptone, 1 g/L yeast extract) and either CMC (1% w/v), chitin (1% w/v), alginate (1% w/v), PET powder (1% w/v), TPA (1mM) or BHET (0.5, 5 and 30 mM) was added. Additional growth experiments were implemented in M9 medium (Na_2HPO_4 33.7 mM, KH_2PO_2 22 mM, NaCl 51.3 mM, NH_4Cl 9.35 mM, $MgSO_4$ 1 mM, biotin 1 µg, thiamin 1 µg, EDTA 0.134 mM, $FeCl_3$-$6H_2O$ 0.031 mM, $ZnCl_2$ 0.0062 mM, $CuCl_2$ $2H_2O$ 0.76 µM, $CoCl_2$ 2 H_2O 0.42 µM, H_3BO_3 1.62 µM, $MnCl_2$ $4H_2O$ 0.081 µM).

E. coli was grown at 37°C aerobically in LB medium (10 g/L tryptone, 5 g/L yeast, 5 g/L NaCl) and supplemented with the appropriate antibiotics.

For the observation of the phenotypical reaction and halo formation of DSM 21264 to various concentrations of BHET LB agar plates (10 g/L tryptone, 5 g/L yeast, 5 g/L NaCl, 15 g/L agar) were prepared. After autoclaving, the respective amount of BHET was added to reach final concentrations of 0.5 mM, 5.0 mM, 10 mM and 30 mM in the respective plate. 5 µl of DSM 21264 OD_{600} = 1 were added and incubated 24 h at 28 °C.

<u>Fluorescence imaging analysis of biofilms</u>

To observe biofilm formation of DSM 21264 on plastics surfaces, cells were inoculated at OD_{600} = 0.05 in ASW medium and incubated in 6 -well cell culture plates (Nunc cell culture plate, catalog no. 130184; Thermo Fisher Scientific, Waltham, MA) at 22 °C or 28 °C at 80 rpm shaking. After incubation foil was washed in PBS buffer and placed into µ-slide eight-well (ibiTreat. catalog no. 80826, ibidi USA, Inc., Fitchburg, Wisconsin). Cells were stained using LIVE/DEAD BacLight bacterial viability kit (Thermo Fisher Scientific, Waltham, MA, USA).

Cells were visualized using confocal laser scanning microscope (CLSM) Axio Observer.Z1/7 LSM 800 with airyscan (Carl Zeiss Microscopy GmbH, Jena, Germany) and a C-Apochromat 63x/1.20W Korr UV VisIR objective. Settings for the microscope are presented in Table S5. For the analysis of the CLSM images the ZEN software was used (version 2.3. Carl Zeiss Microscopy GmbH, Jena, Germany). For each sample at least three different positions were observed and one representative CLSM image was chosen.

Preparation for scanning electron microscopy

Strains and polymers were incubated as described above and after incubation fixed overnight in 1% PFA in 50 mM Cacodylate buffer, pH 7. The following day samples were incubated in 0.25% GA in 50 mM Cacodylate buffer, pH 7 overnight. For drainage samples were incubated in 30%, 50% and 70% of ethanol in the following order each for 20 min. An additional incubation in 70% ethanol was performed overnight. Drainage continued with sample incubation in 80%, 96% and 100% of ethanol for 20 min and 100% of ethanol for 30 min. Critical point drying was performed using Leica EM CPD300 thereby washed 18 x with $CO_2.$ Next, coated in a thin carbon layer using Sputter Coater LEICA EM ACE600. Microscopy was performed at the scanning electron microscope LEO 1525 using Software SmartSEM V06.00.

Sample preparation for RNA seq and analysis

Precultures of DSM 21264 were inoculated at $OD_{600} = 0.05$ in ASW medium (4 mL/well) in 6 -well cell culture plates (Nunc cell culture plate, catalog no. 130184; Thermo Fisher Scientific, Waltham, MA). To each well either PE or PET foil (35 mm diameter) was added and incubated for 8 hours at 22 °C shaking at 80 rpm. Foil was washed in PBS buffer to get rid of planktonic cells, then cells were scratched off the surface. 2 ml of 20% stop mix consisting of 95% ethanol and 5% phenol was added to the cells and the mixture was centrifuged for 20 minutes at 4 °C. Supernatant was

discarded, the pellet was washed three times in PBS buffer and afterwards immediately frozen in liquid nitrogen and stored at -70 °C.

The liquid cultures were inoculated at OD_{600} = 0.05 in diluted artificial seawater. Respective C-source (CMC, PET powder (particle size 300 µm max; >50% crystallinity, product no. ES30-PD-000132), chitin and alginate (1% w/v) and BHET concentrations ranging from 0.5 mM, 5 mM and 30 mM as well as 1 mM TPA) was added and incubated shaking at 28 °C at 130 rpm for 24 hours. As negative controls no additional carbon source and DMSO controls were prepared. Cells were harvested and cell pelleted.

Harvested cells were re-suspended in 800µl RLT buffer (RNeasy Mini Kit, Qiagen) with β-mercaptoethanol (10µl ml^{-1}) and cell lysis was performed using a laboratory ball mill. Subsequently, 400µl RLT buffer (RNeasy Mini Kit Qiagen) with β-mercaptoethanol (10µl ml^{-1}) and 1200 µl 96% (vol./vol.) ethanol were added. For RNA isolation, the RNeasy Mini Kit (Qiagen) was used as recommended by the manufacturer, but instead of RW1 buffer RWT buffer (Qiagen) was used in order to isolate RNAs smaller than 200 nucleotides also. To determine the RNA integrity number the isolated RNA was run on an Agilent Bioanalyzer 2100 using an Agilent RNA 6000 Nano Kit as recommended by the manufacturer (Agilent Technologies, Waldbronn, Germany). Remaining genomic DNA was removed by digesting with TURBO DNase (Invitrogen, Thermo Fischer Scientific, Paisley, UK). The Illumina Ribo-Zero plus rRNA Depletion Kit ((Illumina Inc., San Diego, CA, USA) was used to reduce the amount of rRNA-derived sequences. For sequencing, the strand-specific cDNA libraries were constructed with a NEB Next Ultra II Directional RNA library preparation kit for Illumina and the NEB Next Multiplex Oligos for Illumina (96) (New England BioLabs, Frankfurt am Main, Germany). To assess quality and size of the libraries samples were run on an Agilent Bioanalyzer 2100 using an Agilent High Sensitivity DNA Kit as recommended by the manufacturer (Agilent Technologies). Concentration of the libraries was determined using the Qubit® dsDNA HS Assay Kit as recommended by the manufacturer (Life Technologies GmbH, Darmstadt, Germany). Sequencing was performed on the NovaSeq

6000 instrument (Illumina Inc., San Diego, CA, USA) using NovaSeq 6000 SP Reagent Kit (100 cycles) and the NovaSeq XP 2-Lane Kit v1.5 for sequencing in the paired-end mode and running 2x 61 cycles. For quality filtering and removing of remaining adaptor sequences, Trimmomatic-0.39 (Bolger et al., 2014) and a cutoff phred-33 score of 15 were used. The mapping against the reference genome of *V. gazogenes* DSM 21264[T] was performed with Salmon (v 1.10.2) [54]. As mapping back-bone a file that contains all annotated transcripts excluding rRNA genes and the whole genome of the reference as decoy was prepared with a k-mer size of 11. Decoy-aware mapping was done in selective-alignment mode with '–mimicBT2', '–disableChainingHeuristic'and'–recoverOrphans'flags as well as sequence and position bias correction and 10 000 bootstraps. For–fldMean and–fldSD, values of 325 and 25 were used respectively. The quant.sf files produced by Salmon were subsequently loaded into R (v 4.3.2) [55] using the tximport package (v 1.28.0) [56]. DeSeq2 (v 1.40.1) was used for normalization of the reads and fold change shrinkages were also calculated with DeSeq2 [57] and the apeglm package (v 1.22.0) [58]. Genes with a log2-foldchange of +2/-2 and ap-adjust value <0.05 were considered differentially expressed.

Fastp [59] was used to remove sequences originating from sequencing adapters and sequences of low-quality sequences. Reads were then aligned to the *V. gazogenes* DSM 21264 reference assembly [60] using BWA mem. Differential expression analysis was carried out with DESeq2 [57]. A gene was considered significantly differentially expressed in a comparison if the corresponding false discovery rate (FDR) was smaller or equal to 0.05 and the absolute log2-foldchange (|log2FC|) was larger than 2. All software was used with standard parameters.

Sequence data reported in this publication have been submitted to the European Nucleotide Archive (ENA). They are publicly available under accession PRJEB80907.

Key genes presented in Figures 4-6. The size of the circles and color intensity were calculated based on the transcriptome hits per gene (absolute values) and scaled using log-10-fold changes to allow better scaling.

Cloning and expression of *V. gazogenes* UlaG

UlaG (NCBI Ref. Seq. WP_072962133.1) was cloned into pET21a(+) vector (Novagen/Merck) using restriction sites *Nde*I and *Xho*I in front of C-terminal 6x HisTag. Primers were designed using SnapGene (GSL Biotech LLC, San Diego CA, United States) and PCR was performed using parameters indicated by design tool. After PCR cleanup, 7 µl DNA (≈30 ng/µl) were mixed with 1 µl of T4 Ligase Buffer (10x), 1 µl of T4 Ligase (400 U/µl) and 1 µl of purified pET21a(+) plasmid and incubated over night at 6 °C. Ligation construct was transformed into competent *E. coli* DH5α cells, positive clones were identified via DNA sequencing (Microsynth seqlab). Positive sequenced plasmids were isolated and transformed into competent *E. coli* T7 Shuffle cells.

Protein production and purification

For protein production cells were overexpressed by growing inoculated cultures with T7 SHuffle harboring pET21a(+):*UlaG* or BL21(DE3) harboring pET28a(+):*pet6* at 37 °C to OD_{600} = 0.8. Cells were induced with IPTG to final concentrations of 0.4 mM and incubated at 22 °C over night until cells were harvested by centrifugation at 5.000 g.

For protein purification cell pellet was resuspended in lysis buffer (50 mM NaH_2PO_4, 300 mM NaCl, 10 mM imidazole, pH 8.0) and sonicated for cell disruption with Ultrasonic Processor UP200S by *Hielscher* with amplitude 70% and cycle 0.5. Afterwards, the proteins harboring a sixfold C-terminal histidine tag were purified with nickel-ion affinity chromatography using Ni-NTA agarose (Qiagen, Hilden, Germany). The elution buffer was exchanged against 0.1 mM potassium phosphate buffer pH 8.0 in a 30 kDa Amicon Tube (GE Health Care, Solingen, Germany).

Measurement of PET and BHET degradation

Precultures of DSM 21264 were inoculated at OD_{600} = 0.05 in 20 mL M9 medium supplemented with 5 mM of glucose and additional 5 mM of BHET. Flasks were incubated shaking at 28 °C and 130 rpm for six days. Each day 1 mL of each sample was taken and measured at the UHPLC. As

negative control medium was incubated under same conditions with *E. coli* Dh5α and samples were taken at same timepoints.

For detection of PET powder and foil degradation DSM 21264 was incubated as described above in 6 well plates and also 0.5 mL of sample was taken each day and prepared for UHPLC measurements.

For enzymatic BHET degradation purified enzyme in ranging concentrations was incubated with 300 µM of BHET for 24 h and samples were prepared for UHPLC.

Respective supernatants were prepared and measured at the UHPLC following protocols described previously [61] [62].

<u>Cloning promoter fusion of *adhE*</u>

Promoter of *adhE* (AAC977_10260) was identified using the software tool published at softberry.com (<u>BPROM - Prediction of bacterial promoters</u>) and cloned into pBBR1-MCS-1 vector [63] carrying amCyan in the multiple cloning site using restriction enzymes *Sac*l and *Xba*l.

Primer design, PCR, ligation and transformation into competent *E. coli* DH5α cells were performed as described above. Positive constructs were transformed into competent *E. coli* WM3064 cells. Since electroporation didn't result in sufficient colony amount, the plasmid was conjugated via biparental conjugation into DSM 21264. Cells were grown in overnight cultures. 1 mL of donor strain (*E. coli* WM3064 carrying the respective plasmid) and receptor strain (DSM 21264) were mixed at ratio 1:1 and centrifuged at 5,000 rpm for 8 min. Cells were washed three times in LB medium, resuspended after final centrifugation step in 150 µl of LB medium and spot was given onto LB agar plate supplemented with 300 µM DAP. The plate was incubated overnight at 28 °C and spot was washed off. Dilutions ranging from 1:1 to 1:5 were prepared and plated onto ASWM agar plates supplemented with 25 µg chloramphenicol and 25 µg kanamycin. Colonies were detectable after 2 to 3 days of incubation and inoculated in liquid medium.

Promoter fusion measurements

For the identification of the influence of ethylene glycol on the expression of *adhE,* DSM 21264 carrying promoter fusion construct pBBR1MCS-1_*adhE_amcyan* as well as wild type strain were inoculated at $OD_{600} = 0.05$ in M9 medium with 5 mM glucose. Cells were incubated in 48 well-plates (1 mL/well) (Nunc cell culture plate, catalog no. 150687; Thermo Fisher Scientific, Waltham, MA, USA) for 48 h at 130 rpm shaking. For the detection of the influence of ethylene glycol 5 mM were added and strains were grown in the presence with and without EG. After incubation optical density and fluorescence of cyan (450;496) was measured at Synergy HT plate reader using Gen5 software (Biotek, Winooski, USA). Average was evaluated and fluorescence was divided by optical density to detect fluorescence units.

Plasma activation of PE and PET foil

For plasma activation, an atmospheric air plasma system from Plasmatreat GmbH (Steinhagen, Germany) was used. The atmospheric-pressure plasma was produced by a generator FG5001 with an applied working frequency of 21 kHz, generating a non-equilibrium discharge in a rotating jet nozzle RD1004 in combination with the stainless-steel tip No. 22826 for an expanded treatment width of approximately 22 mm. Additionally, the jet nozzle was connected to a Janome desktop robot type 2300N for repetitious accuracy regarding treatment conditions. The process gas was dry and oil-free air at an input pressure of 5 bar in all experiments.

TABLES

TABLE 1: Bacterial strains and plasmids used in this study.

Strain or plasmid	Relevant trait(s)[a]	Source or reference
Strains		
E. coli DH5α	F⁻ φ80d*lacZ*ΔM15 Δ(*argF-lacZYA*) U169 *endA1 hsdR17* (r_K^-. m_K^-) *supE44 thi-1 recA1 gyrA96 relA1*	[64]
E. coli WM3064	*thrB1004 pro thi rpsL hsdS lacZ*ΔM15 RP4–1360 Δ(*araBAD*)*567* Δ*dapA1341*::[*erm pir*(wt)]	W. Metcalf, University of Illinois, Urbana-Champaign, USA
E. coli SHuffle® T7	*huA2 lacZ::T7 gene1 [lon] ompT ahpC gal λatt::pNEB3-r1-cDsbC (SpecR. lacIq) ΔtrxB sulA11 R(mcr-73::miniTn10--TetS)2 [dcm] R(zgb-210::Tn10 --TetS) endA1 Δgor Δ(mcrC-mrr)114::IS10*	NEB, Frankfurt am Main, Germany
E. coli BL21 (DE3)	*F−. ompT. hsdS B (rB− m B−) gal. dcm. λDE3*	Novagen/Merck, Darmstadt, Germany
V. gazogenes DSM 21264	Wild-type strain	DSMZ, Braunschweig, Germany
Plasmids		
pBBR1MCS-1	Broad host range vector. low copy no.; Cm^r	[63]
pBBR1-MCS-1::*amcyan*	*pBBR1MCS-5 carrying the amcyan gene in the* MCS *between Xba*I *and Bam*HI *restriction site*	This work
pBBR1-MCS-1::a*dh*E*::amcyan*	*pet6*::*amcyan* reporter fusion *in pBBR1MCS-5 between SacI and XbaI restriction site in front of amcyan*	This work
pET21a(+)	Expression vector. *lacI.* Amp^R T7-*lac*-promoter. C-terminal His-tag coding sequence	Novagen/Merck (Darmstadt, Germany)
pET21a(+)::*ulaG*	1056 bp insert in pET21a(+) coding for UlaG	This work
pET28a(+)	Expression vector. *lacI.* Kana^R T7-*lac*-promoter. C-terminal His-tag coding sequence	Novagen/Merck (Darmstadt, Germany)
pET28a(+)::*pet6*	894 bp insert in pET28a(+) coding for PET6	[31]

TABLE 2: The 25 genes with the highest normalized counts in DSM 21264 grown in biofilms on PET and PE

	8-hour biofilms			
#	PET foil		PE foil	
	Predicted Function	Locus tag	Predicted Function	Locus tag
1	*ompU*. porin	AAC977_02740	*ompU*, porin	AAC977_02740
2	*secY*, translocase	AAC977_01575	*secY*, translocase	AAC977_01575
3	*pflB,* acetyltransferase	AAC977_06195	*pflB*, acetyltransferase	AAC977_06195
4	r*poA*, RNA polymerase	AAC977_01600	*rpoA,* RNA polymerase	AAC977_01600
5	dehydrogenase	AAC977_05600	elongation factor	AAC977_11845
6	*fusA,* elongation factor	AAC977_11845	*rpoB,* RNA polymerase	AAC977_14125
7	*rpoB*, RNA polymerase	AAC977_14125	*rpoC*. RNA polymerase	AAC977_14120
8	peptide synthetase	AAC977_13870	peptide synthetase	AAC977_13870
9	*rpoC*. RNA polymerase	AAC977_14120	cold-shock protein	AAC977_16695
10	*aspA,* ammonia-lyase	AAC977_00985	dehydrogenase	AAC977_05600
11	*metallopeptidase	AAC977_18400	*aspA*, ammonia-lyase	AAC977_00985
12	cold-shock protein	AAC977_16695	methyltransferase	AAC977_01345
13	methyltransferase	AAC977_01345	dehydrogenase	AAC977_02520
14	*tuf,* elongation factor	AAC977_13935	elongation factor	AAC977_13935
15	ATP synthase	AAC977_15540	acyl carrier protein	AAC977_10205
16	*tuf,* elongation factor	AAC977_14160	ATP synthase	AAC977_15540
17	l*uxR*, regulator	AAC977_02535	elongation factor	AAC977_14160
18	chaperone	AAC977_04160	*metallopeptidase	AAC977_18400
19	fumarate reductase	AAC977_01180	chaperone	AAC977_04160
20	chaperonin	AAC977_01145	quinone reductase	AAC977_11710
21	quinone reductase	AAC977_11710	elongation factor	AAC977_13940
22	ATP synthase	AAC977_15530	ATP synthase	AAC977_15530
23	acyl carrier protein	AAC977_10205	dehydrogenase	AAC977_02525
24	aldolase	AAC977_13010	ACP synthase	AAC977_10200

| 25 | pyruvate dehydrogenase | AAC977_02520 | nucleotidyltransferase | AAC977_02820 |

*vibriolysin

References

1. Nayanathara Thathsarani Pilapitiya, P.G.C. and A.S. Ratnayake, *The world of plastic waste: A review.* Cleaner Materials, 2024. **11**.
2. OECD, *Global Plastics Outlook.* 2022.
3. Jambeck, J., et al., *Plastic waste inputs from land into the ocean.* 2015.
4. Eriksen, M., et al., *Plastic Pollution in the World's Oceans: More than 5 Trillion Plastic Pieces Weighing over 250,000 Tons Afloat at Sea.* Plos One, 2014. **9**(12).
5. Wilcox, C., E. Van Sebille, and B.D. Hardesty, *Threat of plastic pollution to seabirds is global, pervasive, and increasing.* Proceedings of the national academy of sciences, 2015. **112**(38): p. 11899-11904.
6. Chow, J., et al., *Microbial enzymes will offer limited solutions to the global plastic pollution crisis.* Microbial Biotechnology, 2022.
7. Kaandorp, M.L.A., et al., *Global mass of buoyant marine plastics dominated by large long-lived debris.* Nature Geoscience, 2023. **16**(8): p. 689-694.
8. Wright, R.J., et al., *Plasticizer Degradation by Marine Bacterial Isolates: A Proteogenomic and Metabolomic Characterization.* Environmental Science & Technology, 2020. **54**(4): p. 2244-2256.
9. Osman, A.I., et al., *Microplastic sources, formation, toxicity and remediation: a review.* Environ Chem Lett, 2023: p. 1-41.
10. Li, Y., et al., *Potential Health Impact of Microplastics: A Review of Environmental Distribution, Human Exposure, and Toxic Effects.* Environ Health (Wash), 2023. **1**(4): p. 249-257.
11. Danso, D., J. Chow, and W.R. Streit, *Plastics: Microbial Degradation, Environmental and Biotechnological Perspectives.* Appl Environ Microbiol, 2019.
12. Buchholz, P.C.F., et al., *Plastics degradation by hydrolytic enzymes: The plastics-active enzymes database-PAZy.* Proteins, 2022. **90**(7): p. 1443-1456.
13. Wei, R. and W. Zimmermann, *Microbial enzymes for the recycling of recalcitrant petroleum-based plastics: how far are we?* Microbial biotechnology, 2017. **10**(6): p. 1308-1322.
14. Tournier, V., et al., *Enzymes' Power for Plastics Degradation.* Chemical Reviews, 2023. **123**(9): p. 5612-5701.
15. Amaral-Zettler, L.A., E.R. Zettler, and T.J. Mincer, *Ecology of the plastisphere.* Nature Reviews Microbiology, 2020. **18**(3): p. 139-151.
16. Yang, Y., et al., *Microplastics provide new microbial niches in aquatic environments.* Applied Microbiology and Biotechnology, 2020. **104**(15): p. 6501-6511.
17. Zettler, E.R., T.J. Mincer, and L.A. Amaral-Zettler, *Life in the "plastisphere": microbial communities on plastic marine debris.* Environmental science & technology, 2013. **47**(13): p. 7137-7146.
18. Kirstein, I.V., et al., *The Plastisphere – Uncovering tightly attached plastic "specific" microorganisms.* PLOS ONE, 2019. **14**(4): p. e0215859.
19. Wright, R.J., et al., *Marine Plastic Debris: A New Surface for Microbial Colonization.* Environmental Science & Technology, 2020. **54**(19): p. 11657-11672.
20. Kirstein, I.V., et al., *Dangerous hitchhikers? Evidence for potentially pathogenic Vibrio spp. on microplastic particles.* Marine environmental research, 2016. **120**: p. 1-8.
21. Du, Y., et al., *A review on marine plastisphere: biodiversity, formation, and role in degradation.* Comput Struct Biotechnol J, 2022. **20**: p. 975-988.
22. Kimura, Y., et al., *A lesson from polybutylene succinate plastisphere to the discovery of novel plastic degrading enzyme genes in marine vibrios.* Environ Microbiol, 2023. **25**(12): p. 2834-2850.

23. Dey, S., et al., *Plastisphere community assemblage of aquatic environment: plastic-microbe interaction, role in degradation and characterization technologies.* Environ Microbiome, 2022. **17**(1): p. 32.

24. Zhai, X., X.H. Zhang, and M. Yu, *Microbial colonization and degradation of marine microplastics in the plastisphere: A review.* Front Microbiol, 2023. **14**: p. 1127308.

25. Zhang, X., et al., *Significance of Vibrio species in the marine organic carbon cycle—A review.* Science China Earth Sciences, 2018. **61**(10): p. 1357-1368.

26. Grimes, D.J., *The Vibrios: Scavengers, Symbionts, and Pathogens from the Sea.* Microb Ecol, 2020. **80**(3): p. 501-506.

27. Baker-Austin, C., et al., *Vibrio spp. infections.* Nat Rev Dis Primers, 2018. **4**(1): p. 8.

28. Sampaio, A., et al., *Vibrio spp.: Life Strategies, Ecology, and Risks in a Changing Environment.* Diversity, 2022. **14**(2).

29. Marques, P.H., et al., *Insights into the Vibrio Genus: A One Health Perspective from Host Adaptability and Antibiotic Resistance to In Silico Identification of Drug Targets.* Antibiotics (Basel), 2022. **11**(10).

30. Danso, D., et al., *New Insights into the Function and Global Distribution of Polyethylene Terephthalate (PET)-Degrading Bacteria and Enzymes in Marine and Terrestrial Metagenomes.* Appl Environ Microbiol, 2018. **84**(8).

31. Weigert, S., et al., *Investigation of the halophilic PET hydrolase PET6 from Vibrio gazogenes.* Protein Science, 2022. **31**(12): p. e4500.

32. Harwood, C.S., *Beneckea gazogenes sp. nov., a Red, Facultatively Anaerobic, Marine Bacterium.* Current Microbiology, 1978. **1**: p. 233-238.

33. Yoshida, S., et al., *A bacterium that degrades and assimilates poly(ethylene terephthalate).* Science, 2016. **351**(6278): p. 1196-9.

34. Burmeister, N., et al., *Surface Grafted N-Oxides have Low-Fouling and Antibacterial Properties.* Advanced Materials Interfaces, 2023. **10**(35): p. 2300505.

35. Maliszewska, I., et al., *On the Effect of Non-Thermal Atmospheric Pressure Plasma Treatment on the Properties of PET Film.* Polymers (Basel), 2023. **15**(21).

36. Seaver, L.C. and J.A. Imlay, *Alkyl hydroperoxide reductase is the primary scavenger of endogenous hydrogen peroxide in Escherichia coli.* J Bacteriol, 2001. **183**(24): p. 7173-81.

37. Kumari, A., et al., *Transcriptome-Guided Insights Into Plastic Degradation by the Marine Bacterium.* Front Microbiol, 2021. **12**: p. 751571.

38. Wright, R.J., et al., *A multi-OMIC characterisation of biodegradation and microbial community succession within the PET plastisphere.* Microbiome, 2021. **9**(1): p. 141.

39. Guo, W., et al., *Biodegradation of PET by the membrane-anchored PET esterase from the marine bacterium Rhodococcus pyridinivorans P23.* Commun Biol, 2023. **6**(1): p. 1090.

40. Potapova, A., et al., *Outer membrane vesicles and the outer membrane protein OmpU govern Vibrio cholerae biofilm matrix assembly.* mBio, 2024. **15**(2): p. e0330423.

41. Nathamuni, S., et al., *Insights on genomic diversity of Vibrio spp. through Pan-genome analysis.* Annals of Microbiology, 2019. **69**(13): p. 1547-1555.

42. Bosi, E., et al., *Pan-Genome Provides Insights into Vibrio Evolution and Adaptation to Deep-Sea Hydrothermal Vents.* Genome Biol Evol, 2024. **16**(7).

43. Fernandez, F.J., et al., *The UlaG protein family defines novel structural and functional motifs grafted on an ancient RNase fold.* BMC Evol Biol, 2011. **11**: p. 273.

44. Perez-Garcia, P., et al., *A promiscuous ancestral enzyme´s structure unveils protein variable regions of the highly diverse metallo-β-lactamase family.* Communications biology, 2021. **4**(1): p. 1-12.

45. Hachisuka, S.I., et al., *Ethylene glycol metabolism in the poly(ethylene terephthalate)-degrading bacterium Ideonella sakaiensis.* Appl Microbiol Biotechnol, 2022. **106**(23): p. 7867-7878.

46. Butler, S.M. and A. Camilli, *Going against the grain: chemotaxis and infection in Vibrio cholerae.* Nat Rev Microbiol, 2005. **3**(8): p. 611-20.

47. Teschler, J.K., et al., *Living in the matrix: assembly and control of Vibrio cholerae biofilms.* Nat Rev Microbiol, 2015. **13**(5): p. 255-68.

48. Conner, J.G., et al., *The ins and outs of cyclic di-GMP signaling in Vibrio cholerae.* Curr Opin Microbiol, 2017. **36**: p. 20-29.

49. Liu, J., et al., *Biodegradation and up-cycling of polyurethanes: Progress, challenges, and prospects.* Biotechnol Adv, 2021. **48**: p. 107730.

50. Conner, J.G., et al., *The ins and outs of cyclic di-GMP signaling in Vibrio cholerae.* Curr Opin Microbiol, 2017. **36**: p. 20-29.

51. Liu, J. and Y. Hu, *Discovery and evolution of [4 + 2] cyclases.* Curr Opin Chem Biol, 2024. **81**: p. 102504.

52. Botsford, J.L. and J.G. Harman, *Cyclic AMP in Prokaryotes.* Microbiological Reviews, 1992. **56**: p. 100-122.

53. Matange, N., *Revisiting bacterial cyclic nucleotide phosphodiesterases: cyclic AMP hydrolysis and beyond.* FEMS Microbiol Lett, 2015. **362**(22).

54. Patro, R., et al., *Salmon provides fast and bias-aware quantification of transcript expression.* Nat Methods, 2017. **14**(4): p. 417-419.

55. Team, R.C., *R: A Language and Environment for Statistical Computing.* R Foundation for Statistical Computing, Vienna, Austria, 2020: p. http://www.r-project.org/.

56. Soneson, C., M.I. Love, and M.D. Robinson, *Differential analyses for RNA-seq: transcript-level estimates improve gene-level inferences.* F1000Res, 2015. **4**: p. 1521.

57. Love, M.I., W. Huber, and S. Anders, *Moderated estimation of fold change and dispersion for RNA-seq data with DESeq2.* Genome Biol, 2014. **15**(12): p. 550.

58. Zhu, A., J.G. Ibrahim, and M.I. Love, *Heavy-tailed prior distributions for sequence count data: removing the noise and preserving large differences.* Bioinformatics, 2019. **35**(12): p. 2084-2092.

59. Chen, S., et al., *fastp: an ultra-fast all-in-one FASTQ preprocessor.* Bioinformatics, 2018. **34**(17): p. i884-i890.

60. Li, H. and R. Durbin, *Fast and accurate short read alignment with Burrows-Wheeler transform.* Bioinformatics, 2009. **25**(14): p. 1754-60.

61. Zhang, H., R.F. Dierkes, and W.R. Streit, *Microbial Degradation of Plastics*, in *Characterization and Failure Analysis of Plastics* J. Menna, Editor. 2022, ASM International: ASM Handbooks online.

62. Dierkes Robert, F., et al., *An Ultra-Sensitive Comamonas thiooxidans Biosensor for the Rapid Detection of Enzymatic Polyethylene Terephthalate (PET) Degradation.* Applied and Environmental Microbiology, 2022. **89**(1): p. e01603-22.

63. Kovach, M.E., et al., *Four new derivatives of the broad-host-range cloning vector pBBR1MCS, carrying different antibiotic-resistance cassettes.* Gene, 1995. **166**(1): p. 175-6.

64. Hanahan, D., *Studies on transformation of Escherichia coli with plasmids.* J Mol Biol, 1983. **166**(4): p. 557-80.

3 The Bacteroidetes *Aequorivita* sp. and *Kaistella jeonii* Produce Promiscuous Esterases With PET-Hydrolyzing Activity

Hongli Zhang[1], Pablo Perez-Garcia[1,2], Robert F. Dierkes[1], Violetta Applegate[3], Julia Schumacher[3], Cynthia Maria Chibani[2], Stefanie Sternagel[4], **Lena Preuss[1]**, Sebastian Weigert[5], Christel Schmeisser[1], Dominik Danso[1], Juergen Pleiss[6], Alexandre Almeida[7,8], Birte Höcker[5], Steven J. Hallam[4,9,10,11,12], Ruth A. Schmitz[2], Sander H. J. Smits[3,13], Jennifer Chow[1] and Wolfgang R. Streit[1*]

1   Department of Microbiology and Biotechnology, University of Hamburg, Hamburg, Germany

2   Molecular Microbiology, Institute for General Microbiology, Kiel University, Kiel, Germany

3   Center for Structural Studies, Heinrich-Heine-University, Düsseldorf, Germany

4   Department of Microbiology and Immunology, University of British Columbia, Vancouver, BC, Canada

5   Department of Biochemistry, University of Bayreuth, Bayreuth, Germany

6   Institute of Biochemistry and Technical Biochemistry, University of Stuttgart, Stuttgart, Germany

7   European Bioinformatics Institute (EMBL-EBI), Hinxton, United Kingdom

8   Wellcome Sanger Institute, Hinxton, United Kingdom

9   Graduate Program in Bioinformatics, University of British Columbia, Vancouver, BC, Canada

10   Genome Science and Technology Program, University of British Columbia, Vancouver, BC, Canada

11   Life Sciences Institute, University of British Columbia, Vancouver, BC, Canada

12   ECOSCOPE Training Program, University of British Columbia, Vancouver, BC, Canada

13   Institute of Biochemistry, Heinrich-Heine-University, Düsseldorf, Germany

frontiers
in Microbiology

The Bacteroidetes *Aequorivita* sp. and *Kaistella jeonii* Produce Promiscuous Esterases With PET-Hydrolyzing Activity

Hongli Zhang[1], Pablo Perez-Garcia[1,2], Robert F. Dierkes[1], Violetta Applegate[3], Julia Schumacher[3], Cynthia Maria Chibani[2], Stefanie Sternagel[4], Lena Preuss[1], Sebastian Weigert[5], Christel Schmeisser[1], Dominik Danso[1], Juergen Pleiss[6], Alexandre Almeida[7,8], Birte Höcker[5], Steven J. Hallam[4,9,10,11,12], Ruth A. Schmitz[2], Sander H. J. Smits[3,13], Jennifer Chow[1] and Wolfgang R. Streit[1]*

[1] Department of Microbiology and Biotechnology, University of Hamburg, Hamburg, Germany, [2] Molecular Microbiology, Institute for General Microbiology, Kiel University, Kiel, Germany, [3] Center for Structural Studies, Heinrich-Heine-University, Düsseldorf, Germany, [4] Department of Microbiology and Immunology, University of British Columbia, Vancouver, BC, Canada, [5] Department of Biochemistry, University of Bayreuth, Bayreuth, Germany, [6] Institute of Biochemistry and Technical Biochemistry, University of Stuttgart, Stuttgart, Germany, [7] European Bioinformatics Institute (EMBL-EBI), Hinxton, United Kingdom, [8] Wellcome Sanger Institute, Hinxton, United Kingdom, [9] Graduate Program in Bioinformatics, University of British Columbia, Vancouver, BC, Canada, [10] Genome Science and Technology Program, University of British Columbia, Vancouver, BC, Canada, [11] Life Sciences Institute, University of British Columbia, Vancouver, BC, Canada, [12] ECOSCOPE Training Program, University of British Columbia, Vancouver, BC, Canada, [13] Institute of Biochemistry, Heinrich-Heine-University, Düsseldorf, Germany

Certain members of the Actinobacteria and Proteobacteria are known to degrade polyethylene terephthalate (PET). Here, we describe the first functional PET-active enzymes from the Bacteroidetes phylum. Using a PETase-specific Hidden-Markov-Model- (HMM-) based search algorithm, we identified several PETase candidates from Flavobacteriaceae and Porphyromonadaceae. Among them, two promiscuous and cold-active esterases derived from *Aequorivita* sp. (PET27) and *Kaistella jeonii* (PET30) showed depolymerizing activity on polycaprolactone (PCL), amorphous PET foil and on the polyester polyurethane Impranil®DLN. PET27 is a 37.8 kDa enzyme that released an average of 174.4 nmol terephthalic acid (TPA) after 120 h at 30°C from a 7 mg PET foil platelet in a 200 µl reaction volume, 38-times more than PET30 (37.4 kDa) released under the same conditions. The crystal structure of PET30 without its C-terminal Por-domain (PET30ΔPorC) was solved at 2.1 Å and displays high structural similarity to the *Is*PETase. PET30 shows a Phe-Met-Tyr substrate binding motif, which seems to be a unique feature, as *Is*PETase, LCC and PET2 all contain Tyr-Met-Trp binding residues, while PET27 possesses a Phe-Met-Trp motif that is identical to Cut190. Microscopic analyses showed that *K. jeonii* cells are indeed able to bind on and colonize PET surfaces after a few days of incubation. Homologs of PET27 and PET30 were detected in metagenomes, predominantly aquatic habitats, encompassing a wide range of different global climate zones and suggesting a hitherto unknown influence of this bacterial phylum on man-made polymer degradation.

Keywords: metagenomics, metagenomic screening, PET degradation, polyethylene terephthalate (PET), PETase, Bacteroidetes, Flavobacteriaceae

48

INTRODUCTION

PET is one of the major plastic pollutants found in landfills, oceans and other environments (Jambeck et al., 2015; Geyer et al., 2017). Our knowledge of microbial degradation of most plastics is rather limited, but recent research has demonstrated that some bacteria are able to degrade PET (Yoshida et al., 2016). Although it is unclear if larger crystalline fibers are degraded by bacteria, it is well known that some cutinases (EC 3.1.1.74), lipases (EC 3.1.1.3) and carboxylesterases (EC 3.1.1.1) can act on amorphous and low crystalline PET. These enzymes, often referred to as "PETases," cleave the ester bond of the polymer to either produce bis-(2-hydroxyethyl) terephthalate (BHET), mono-hydroxyethyl terephthalate (MHET) or they complete degradation to terephthalic acid (TPA) and ethylene glycol (EG). TPA monomers can be further degraded via cleavage of the aromatic ring structure using known aryl pathways and can then enter the β-ketoadipate pathway (Wei and Zimmermann, 2017; Danso et al., 2019; Wright et al., 2021).

To date, only a limited number of bacterial and fungal species have been identified that are capable of breaking down PET to either its oligomers or monomers, TPA and EG. Most bacterial isolates with verified enzymatic PET-degrading activity are affiliated with the Gram-positive phylum Actinobacteria (Acero et al., 2011). The best characterized examples belong to the genera *Thermobifida* or *Thermomonospora* (Kleeberg et al., 1998; Chen et al., 2008; Hu et al., 2010; Acero et al., 2011; Ribitsch et al., 2012; Wei et al., 2014). Further, the leaf compost-derived cutinase LCC is closely related to Actinobacterial enzymes and is currently one of the best described and most active PETases (Sulaiman et al., 2012, 2014). Regarding Proteobacteria, the Gram-negative Betaproteobacterium *Ideonella sakaiensis* 201-F6 is capable of using amorphous PET as a major energy and carbon source (Yoshida et al., 2016). *I. sakaiensis'* genome also encodes a tannase which is designated MHETase as it is capable of degrading MHET. Besides, a number of other PETases affiliated with the Proteobacteria have been identified originating from e.g., *Pseudomonas aestusnigri* and *Vibrio gazogenes* (Ronkvist et al., 2009; Haernvall et al., 2017; Danso et al., 2018; Bollinger et al., 2020).

In a previous study, we identified potential PET esterases affiliated with the Bacteroidetes phylum using HMM profile database searches (Danso et al., 2018, 2019). These enzyme hits mainly occurred in metagenomes and genomes from marine environments and were annotated solely on the basis of homology. However, their enzymatic function and environmental distributions have not been studied within that framework, and we target these questions in the present study. Bacteroidetes representatives can be found in nearly all ecological niches including soils, oceans and fresh water and are part of the microbiome of many animals, especially as inhabitants of the intestinal tract (Wexler, 2007; Krieg et al., 2015; Hahnke et al., 2016; Munoz et al., 2016). The Bacteroidetes phylum, however, is highly heterogeneous and contains at least four classes of bacteria (e.g., Bacteroidia, Flavobacteria, Sphingobacteria, and Cytophagia), with each class having several thousand described species. The phylum contains non-spore forming and rod shaped microorganisms, some aerobic, but often anaerobic, with an enormous metabolic diversity (Krieg et al., 2015). The global distribution of Bacteroidetes representatives is likely due to their ability to decompose a very wide variety of bio-based polymers such as cellulose, chitin or algal cell walls. In particular, the decomposition of polysaccharides (cellulose and hemicellulose) by Bacteroidetes inhabiting the intestinal tract of humans and animals has been well-studied in gut microbiome research (Thomas et al., 2011).

Here, we provide the first experimental evidence that different Bacteroidetes representatives have evolved promiscuous esterases that degrade the PET polymer. We show that at least two Bacteroidetes genera, *Aequorivita* and *Kaistella* (formerly *Chryseobacterium*), harbor PET-active enzymes and elucidated the crystal structure of PET30. These enzymes have relatively low turnover rates, indicating that PET hydrolysis may be a side reaction. Still, given their abundance and diversity, we speculate that the described bacteroidetal PET-active enzymes could have considerable impact on long-term degradation of PET in the marine environment.

MATERIALS AND METHODS

Bacterial Strains, Plasmids, and Primers

Bacterial strains, plasmids and primers used in this study are listed in **Supplementary Tables 1, 2**. If not mentioned otherwise, *Escherichia coli* clones were grown in LB medium (1% tryptone/peptone, 0.5% yeast extract, 1% NaCl) supplemented with appropriate antibiotics (25 μg/ml kanamycin, or 100 μg/ml ampicillin) at 37°C for 18 h.

Databases Used in This Study and Bioinformatic Analyses

Nucleotide and amino acid sequences of putative and confirmed PETases were acquired from databases integrated into the NCBI[1], UniProt[2] and IMG (JGI)[3] servers (Markowitz et al., 2012; NCBI Resource Coordinators, 2017; The UniProt Consortium, 2017). Human gut sequences were retrieved from the Unified Human Gastrointestinal Protein (UHGP) catalog (PMID: 32690973). Sequences were compared to others deposited in the NCBI databases using BLAST alignment tools (Agarwala et al., 2016). Amino acid sequence HMM search was carried out using the HMMER[4] webpage or a local version of the software (v3.1b2) (Mistry et al., 2013) with downloaded datasets. Structural information on the enzymes was retrieved from the RCSB-PDB (Berman et al., 2000) database.

Sequence data were processed and analyzed using ChromasPro 2.1.8 (Technelysium, Brisbaine Australia) or SnapGene (GSL Biotech LLC, San Diego CA, United States). Amino acid alignment was constructed using structural alignments with T-Coffee (Notredame et al., 2000) and was

---

[1] https://www.ncbi.nlm.nih.gov/
[2] http://www.uniprot.org/
[3] http://jgi.doe.gov/
[4] http://hmmer.org

49

Zhang et al.

PET-Hydrolyzing Esterases From Bacteroidetes

TABLE 1 | Key traits of predicted bacteroidetal PET esterases.

Predicted PETase	GenBank entry/MGY identifier	Phylogenetic Affiliation	aa/MW (kDa)	Derived from	Expression level/solubility	Active on						
						*p*NP-C6/-C10	TBT	Impranil® DLN	PCL	BHET	PET-foil	PET particles
PET27	WP_111881932	*Aequorivita* sp. CIP111184	364/37.8	Antarctic source (Li et al., 2017)	High/majority in inclusion bodies	+	+	+	+	+	+	+
PET28	WP_073216622	*Aequorivita viscosa*	365/38.3	Seaweed (Li et al., 2017)	High/majority in inclusion bodies	+	+	+	+	+	-	-
PET29	WP_052671284	*Aequorivita vladivostokensis*	365/39.3	Troitsa bay, Sea of Japan (Li et al., 2017)	High/majority in inclusion bodies	+	+	+	+	+	-	-
PET30	WP_039353427	*Kaistella jeonii*	366/37.4	Antarctic moss (Li et al., 2017)	High/majority soluble	+	+	+	+	+	+	+
PET38	WP_083800582.1/GCA_000194605.1	*Fluviicola taffensis*	447/40.4	River, United Kingdom (Woyke et al., 2011)	Low	-	-	N.D.	-	-	-	-
PET53	k99_709705_13	*Aequorivita* sp.	294/37.8	Marine aquaculture fish tank metagenome/ unpublished data University of Hamburg	Low	-	-	N.D.	-	N.D.	N.D.	N.D.
PET57	GUT_GENOME137663_00143	*Porphyromonas* sp.	323/36.3	Human gut (Mitchell et al., 2019; Almeida et al., 2021)	High/majority soluble	-	-	+	+	N.D.	N.D.	N.D.
PET58	GUT_GENOME065712_01381	*Porphyromonas bennonis*	338/37.6	Human gut (Mitchell et al., 2019; Almeida et al., 2021)	High/majority in inclusion bodies	-	-	-	+	N.D.	N.D.	N.D.
PET59	GUT_GENOME243617_00165	*Porphyromonas* sp.	345/38.4	Human gut (Mitchell et al., 2019; Almeida et al., 2021)	High/majority soluble	-		-	+	N.D.	N.D.	N.D.

TBT, tributyrin; BHET, bis-(2-hydroxyethyl) terephthalate; PCL, polycaprolactonate; pNP-C6/C10, para-nitrophenyl esters with chain length C6 or C10; aa, amino acids; MW, molecular weight. N.D. not determined. +, active; -, not active.

PET57-59 were extracted from the gut genomes available at: https://www.ebi.ac.uk/metagenomics/genomes/MGYG-HGUT-01059 (PET57); https://www.ebi.ac.uk/metagenomics/genomes/MGYG-HGUT-01060 (PET58) and https://www.ebi.ac.uk/metagenomics/genomes/MGYG-HGUT-00764 (PET59).

50

further visualized with Bioedit (Hall, 1999). The model structures of bacteroidetal PETase-candidates were modeled with the Robetta server (Kim et al., 2004) using the *Is*PETase crystal structure (6EQE) as a backbone. A phylogenetic tree was constructed using the RAxML-NG autoMRE algorithm (Kozlov et al., 2019) with the treesapp create command implemented in TreeSAPP (Morgan-Lang et al., 2020) with maximum bootstraps set at 1,000. RAxML-MG has recently been shown to return the best scoring tree for highest number of datasets when compared against other fast maximum likelihood (ML) methods (Kozlov et al., 2019), allowing a large number of maximum bootstraps to be used to produce as conservative a tree as possible. Sequences were assigned NCBI lineages according to source organisms listed in **Table 1** and **Supplementary Table 3**, and colors were assigned to the tree at the phylum level using the treesapp color command. The tree was visualized in iTOL (Letunic and Bork, 2019).

Scanning IMG/M was completed on 19/November/2020 for PET30 and on 14/January/2021 for PET27. Geo locations were used as provided whenever available. In case no Geo location was available, whenever possible, information about isolation source/location/city/country were used to look up Geo coordinates on GeoHack.[5] The map representing the frequency and geographical distribution of PET hydrolases in metagenomes (**Figure 1**) was constructed using QGis Desktop 2.18.5[6].

Heterologous Expression of Putative Polyethylene Terephthalate Esterase Genes in *Escherichia coli* BL21 (DE3)

The putative PETases were extracted from metagenomic datasets (**Table 1**), therefore the gene sequences were optimized for expression in *E. coli* and synthesized into pET21a(+) vector at Biomatik (Wilmington, United States). The obtained constructs were sequenced at Microsynth Seqlab GmbH (Goettingen, Germany) and checked for correctness by comparing to the original sequences. *E. coli* T7-Shuffle or *E. coli* BL21 (DE3) cells were used for heterologous expression of possible PETases. The *Is*PETase gene in pMAL-p4x was expressed in *E. coli* BL21 and purified by its maltose-binding tag. The cultures were grown aerobically in auto-induction medium (ZYM-5052) (Studier, 2005) containing 100 μg/ml ampicillin at 37°C until they reached an OD_{600} of 1.0. The proteins were expressed afterward at 22°C for 16–20 h. The cells were harvested and lysed with pressure using a French press. Afterward, the proteins harboring a sixfold C-terminal histidine tag were purified with nickel-ion affinity chromatography using Ni-NTA agarose (Qiagen, Hilden, Germany) and analyzed by SDS-PAGE. The elution buffer was exchanged against 0.1 mM potassium phosphate buffer pH 8.0 in a 10 kDa Amicon Tube (GE Health Care, Solingen, Germany).

Biochemical Characterization of PET27 and PET30

For activity tests, both enzymes were assayed using purified recombinant protein. bis-(2-hydroxyethyl) terephthalate (BHET)

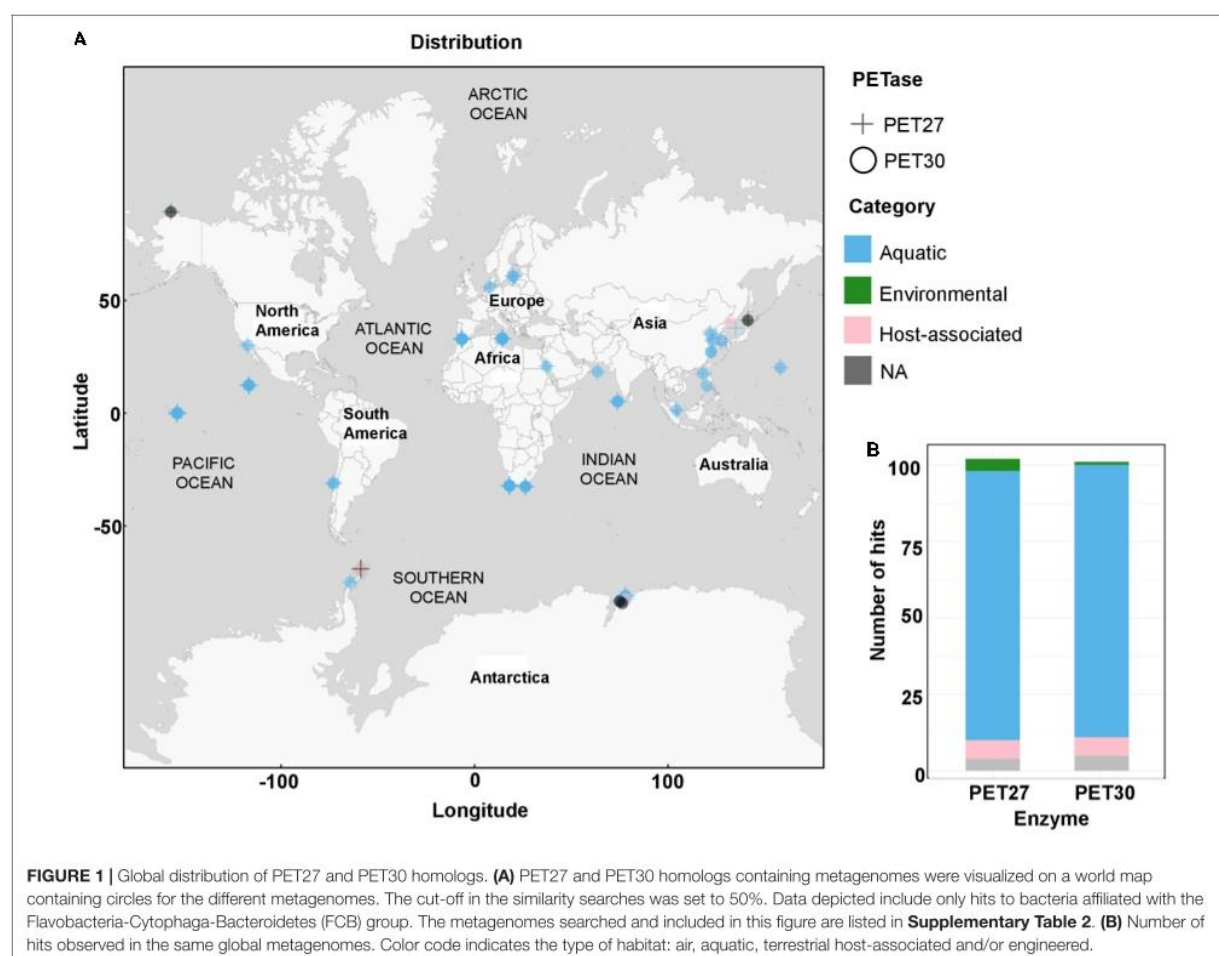[5]https://geohack.toolforge.org
[6]http://www.qgis.org

and polycaprolactone (PCL) agar plates were prepared as described elsewhere (Pérez-García et al., 2021). The polyester polyurethane Impranil DLN containing LB agar plates were prepared according to Molitor et al. (2020) with LB medium. For the *p*NP-assay, unless otherwise indicated, a total amount of 0.1–1 μg of the enzymes were added to a substrate solution containing 190 μl of either 0.2 M sodium phosphate buffer or 0.1 M potassium phosphate with a defined pH between 7 and 8 and 10 μl of 0.1 mM *p*NP-substrate dissolved in isopropanol. After incubating the samples for 10 min, the assay was stopped by adding 200 mM of Na_2CO_3. Afterward, the samples were centrifuged at 4°C, 13,000 rpm for 3 min. As substrates, *p*NP-esters with chain lengths of C4, C6, C8, C10, C12, C14, C16 and C18 were tested. After incubation at defined temperatures, the color change from colorless to yellow was measured at 405 nm in a plate reader (Biotek, Winooski, United States). All samples were measured in triplicate. To determine the optimal temperature, samples were incubated between 10 and 90°C for 10 min. The influence of pH conditions on the activity of each enzyme was measured in citrate phosphate (pH 3.0, 4.0, and 5.0), potassium phosphate (pH 6.0, 7.0, and 8.0) and carbonate bicarbonate buffer (pH 9.2 and 10.2). The impact of cofactors, solvents, detergents, and inhibitors was assayed at different concentration levels. The possible cofactors Ca^{2+}, Co^{2+}, Cu^{2+}, Fe^{3+}, Mg^{2+}, Mn^{2+}, Rb^{2+}, and Zn^{2+} with a final concentration of 1 and 10 mM were used. Detergent stability was assayed with sodium dodecyl sulfate (SDS), Triton X-100 and Tween 80 at 1 and 5% (w/v, v/v) concentration. The inhibitory effect of ethylenediaminetetraacetic acid (EDTA), dithiothreitol (DTT) and phenylmethanesulfonyl fluoride (PMSF) was tested at 1 and 10 mM concentration. After 1 h incubation in the presence of these substances, the residual activity was determined after 10 min incubation at the optimal temperature with *para*-nitrophenol- (*p*NP-) C6 and at the optimal pH.

For the verification of enzymatic PET hydrolysis, a 7 mg platelet (Ø 5 mm) of low-crystallinity PET film (Goodfellow GmbH, Bad Nauheim, Germany), which corresponds to 36.4 μmol of the terephthalic acid-ethylene glycol (TPA-EG) unit, was folded in half and used as substrate together with 200 μg of enzyme in 200 μl of 100 mM potassium phosphate buffer at pH 8.0. Incubation was carried out under continuous shaking at 400 rpm in 1.5 ml microcentrifuge tubes at 30°C, if not stated otherwise.

Analysis of breakdown products was performed with an UltiMate[TM] 3000 UHPLC system from Thermo Fisher Scientific (Waltham, MA, United States) using a Triart C18 column (YMC Europe GmbH, Dinslaken, Germany) with a dimension of 100 × 2.0 mm containing particles with 1.9 μm diameter. Isocratic elution was performed using a mobile phase consisting of 20:80 (v/v) acetonitrile and water (acidified with 0.1% vol trifluoroacetic acid) at a flowrate of 0.4 ml min^{-1}. UHPLC samples were prepared by mixing 50 μl of incubation supernatant with 200 μl acetonitrile (acidified with 1% vol trifluoroacetic acid), followed by centrifugation at 10,000 × g for 3 min and transferring 200 μl of the supernatant into 600 μl water. Fifteen microliter of sample were injected per measurement and detection was performed at 254 nm with a VWD-3400

51

FIGURE 1 | Global distribution of PET27 and PET30 homologs. **(A)** PET27 and PET30 homologs containing metagenomes were visualized on a world map containing circles for the different metagenomes. The cut-off in the similarity searches was set to 50%. Data depicted include only hits to bacteria affiliated with the Flavobacteria-Cytophaga-Bacteroidetes (FCB) group. The metagenomes searched and included in this figure are listed in **Supplementary Table 2**. **(B)** Number of hits observed in the same global metagenomes. Color code indicates the type of habitat: air, aquatic, terrestrial host-associated and/or engineered.

detector from Thermo Scientific (Waltham, MA, United States). The UHPLC profiles were plotted and edited using the software MATLAB version R2020b [The MathWorks, Inc., Natick, MA, United States (Matlab, 2012)]. Quantification of peak areas was performed using data analysis software supplied with the Compass HyStar software package from Bruker (Billerica, MA, United States).

Crystallization and Data Collection

Crystallization of PET30ΔPorC was achieved by sitting-drop vapor-diffusion at 12°C. 0.2 µl of 10.2 mg/ml PET30ΔPorC in 100 mM phosphate buffer pH 8.0 and 0.1 µl reservoir solution consisting of 0.1 M sodium aetate pH 4.6 and 25% (w/v) PEG 4000 were mixed. This drop was equilibrated against reservoir solution and crystals formed after several weeks. Crystallization drops were overlayed with mineral oil and the crystals were dragged through it for cryoprotection, flash frozen and diffraction data were collected at beamline P13 (DESY, Hamburg, Germany). The PET30ΔPorC crystals had the space group P 43 21 2 and diffracted to 2.1 Å resolution.

Structure Determination

A complete data set of the PET30ΔPorC was collected at beamline P13 (DESY, EMBL, Hamburg, Germany) at 100 K and wavelength 0.9795 Å up to 2.1 Å resolution. All data were processed using the automated pipeline at the EMBL HAMBURG and reprocessed afterward using XDS (Kabsch, 2014). The above obtained model for PET30ΔPorC by TOPMODEL was successfully used to phase the 2.1 Å data set of PET30ΔPorC using the PHASER program from the PHENIX program suite (Afonine et al., 2012; Mulnaes et al., 2020). The structure was then refined in iterative cycles of manual building and refinement in coot followed by software-based refinements using the program suite Phenix (Emsley and Cowtan, 2004; Liebschner et al., 2019). All residues were in the preferred and additionally allowed regions of the Ramachandran plot. The data collection and refinement statistics are listed in **Supplementary Table 4**. The images of the models were prepared using PyMOL (DeLano, 2002) and UCSF Chimera X.[7] The structure was deposited at the worldwide protein data bank under the accession code 7PZJ.

---

[7]www.cgl.ucsf.edu/chimera

52

Confocal Laser Scanning Microscopy of Polyethylene Terephthalate Foil Platelets

The starter culture of *K. jeonii* was grown in R2A medium at 22°C and 130 rpm to a cell density of 0.2. 1% of the starter culture was inoculated into 30 ml fresh R2A medium and PET foil platelets were put into the cultures. PET platelets were removed after 5-7 days, washed three times with PBS and subsequently given into μ-Slide 8 wells plates from ibidi GmbH (Martinsried, Germany). Cells were stained using 100 μl of LIVE/DEAD stain BacLight Viability Kit (Thermo Fisher Scientific). The stain is composed of propidium iodide (PI) dying dead cells with a damaged membrane and causing red fluorescence and green fluorescence SYTO 9[TM] dying all bacterial membranes of living cells. Therefore, 10 μl PI and 10 μl SYTO 9[TM] were mixed. 15 μl of the nucleic acid-binding stains were pipetted into 5 ml PBS. The PET platelets were incubated for 1 h in the dark at room temperature. Afterward, the samples were investigated under the microscope Axio Observer Z1/7, LSM 800 using objective C-Apochromat 63x/1.20 W Korr UV VisIR (both Carl Zeiss Microscopy GmbH, Jena, Germany) using the Channels Syto 09 (528/20 nm emission wavelength) and PI (645/20 nm emission wavelength).

RESULTS

Profile Hidden Markov Model Searches Identify Potential Bacteroidetal PETases

Protein sequences from both genomes and metagenomes were screened using the previously described Hidden Markov Model (HMM) (Danso et al., 2018) to enrich the diversity of PET-active enzymes from Bacteroidetes. The global searches were performed in publicly available datasets of NCBI GenBank and additionally in several private datasets harboring human-associated and environmental Bacteroidetes sequences (**Table 1**). Searches were conducted from January until March 2019. This global search initially resulted in the identification of 37 potential PETase sequences from Bacteroidetes with a bit score above 298.7. After sequence comparison, nine distinct hits were chosen. These candidates belonged to bacteroidetal genomes originating from either Seaweed (Li et al., 2017), Antarctic moss (Li et al., 2017), river sediment (Woyke et al., 2011), an aquaculture (own unpublished dataset) or human gut microbiomes (Mitchell et al., 2019; Almeida et al., 2021; **Table 1**). Most of these candidates were affiliated with the Flavobacteriaceae genus *Aequorivita* sp. (PET27-29, PET31 and PET53). PET29 and PET31 were highly similar on amino acid level (< 98% identity) but differed in the length of their sequence by 10 amino acids (aa). PET30, annotated as a potential lipase, was derived from the published genome sequence of *Kaistella jeonii* NCTC 13459. The predicted PETases PET57-59 were derived from bacteria affiliated with the genus *Porphyromonas* sp. (Porphyromonadaceae), while the predicted enzyme PET38 was derived from the species *Fluviicola taffensis* (Cryomorphaceae).

Recombinant PET27 and PET30 Hydrolyze Polycaprolactone, Impranil®-DLN and Polyethylene Terephthalate Foil

The nine candidate genes of the predicted PETases were synthesized, cloned into the expression vector pET21a(+) (Biomatik, Wilmington, DA, United States) and transformed in *E. coli* BL21 and T7-Shuffle cells (**Supplementary Table 1**). Initial tests using recombinant purified proteins and tributyrin (TBT)-containing agar plates indicated that the genes PET27-30 coded for active esterases. The remaining enzymes PET38, PET53, PET57, and PET58 were inactive and were either produced as insoluble proteins and/or only at very low amounts (**Table 1**). Because of these obvious difficulties facing their expression, these four predicted enzymes were not further characterized. Additional tests with PET27-PET30 indicated that these enzymes hydrolyzed the esters *p*NP-hexanoate (C6), and *p*NP-decanoate (C10, **Table 1**). All four recombinant enzymes were able to hydrolyze the polymeric polycaprolactone (PCL), the PET-constituent BHET, and the polyester polyurethane Impranil®DLN (Covestro AG, Leverkusen, Germany) (**Table 1** and **Figure 2A**). The enzymes produced clear halos on agar plates containing these substrates after overnight incubation at 30°C (**Figure 2A** and **Table 1**). PET-hydrolyzing activities were confirmed for the enzymes PET27 and PET30 on amorphous PET foil as substrate in a 200 μl reaction volume by UHPLC analyses. In these tests, 1 mg ml^{-1} PET27 released 871.8 ± 200.4 μM (corresponds to 174.4 ± 40.0 nmol in 200 μl reaction volume) of TPA in 120 h at 30°C from a 7 mg PET platelet. PET foil (7 mg) corresponds to 36.4 μmol of a TPA-EG monomer unit (**Figure 2B** and **Table 2**). Surprisingly, under the same conditions, PET30 released only 15.9 ± 9.5 μM TPA (corresponds to 3.2 ± 1.9 nmol; **Figure 2C** and **Table 2**). These results were directly benchmarked with recombinant *Is*PETase, of which 1 mg ml^{-1} released under the same conditions $4,055.7 \pm 516.9$ μM of TPA (corresponds to 811.1 ± 103.4 nmol). Thus, *Is*PETase is 4.7-fold more active compared to PET27 and approximately 253-fold more active compared to PET30. Because of the relatively low turnover rates observed for PET27 and PET30 on PET foil, it can be assumed that PET is not the preferred substrate of both enzymes.

Biochemical Characterization and Activity of PET27 and PET30 on Esterase Substrates

Both recombinant enzymes were characterized in more detail with *p*NP-esters. A substrate spectrum was recorded with *p*NP-esters, which had acyl chain lengths of 4–18 C-atoms. PET27 and PET30 revealed a relatively narrow spectrum of substrates they could hydrolyze. The highest activities were observed with *p*NP-hexanoate (-C6) for PET30 and *p*NP-octanoate (-C8) for PET27 (**Figure 3A**). The optimal temperature of PET30 is 30°C, but 80% activity was observed at 20°C and between 40 and 50°C (**Figure 3B**). In contrast to that, PET27 shows a better activity at higher temperatures with an optimum at 40°C and even 45% activity at 90°C. Surprisingly, at 10°C, both enzymes still showed

FIGURE 2 | Hydrolytic activities of PET27-PET30 on PCL, BHET, Impranil®DLN and PET foil. Activities on PCL, BHET and Impranil®DLN were visible by halo-formation on agar plates **(A)**. 10 μl of purified enzyme (10-100 μg) were applied to agar plates containing either 500 mg/l PCL, 5 mM BHET or 1% Impranil®DLN. Clearing zones were observed after 12 h at 30°C. Control indicates plates without enzymes but treated with 10 μl buffer. UHPLC profiles of PET27 **(B)** and PET30 **(C)** after incubation on PET foil for 120 h. Two hundred microliter of recombinant and purified enzymes (1 mg/ml) were applied to amorphous foil and incubated over 120 h at 30°C. The *Is*PETase was included for reasons of benchmarking in **(B)** at 1 mg/assay (upper right corner). Graphs shown are representative graphs and were repeated at least three times.
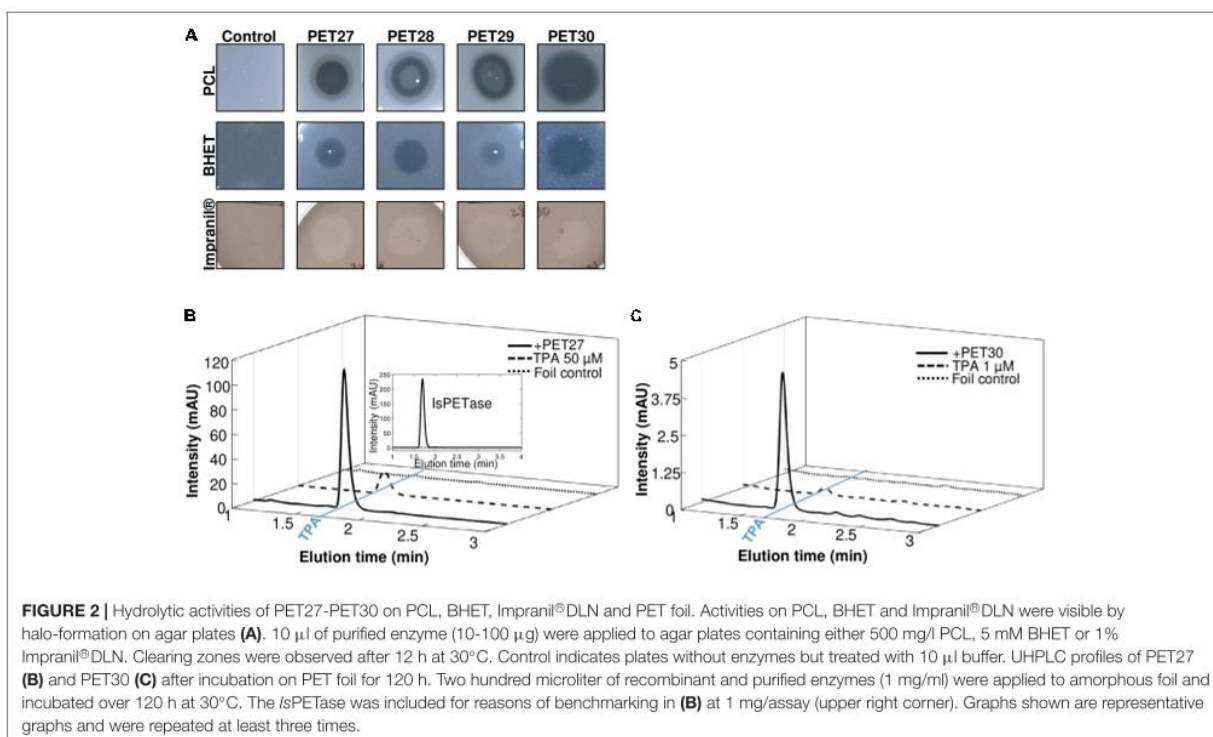
TABLE 2 | Amount of TPA released by different PET active enzymes.

Enzyme	Released TPA-EG unit			Av. weight loss of PET foil [%]
	[μM]	[nmol]	[μg]	
PET27	871.8 ± 200.4	174.4 ± 40.0	33.5 ± 7.7	0.45
PET30	15.9 ± 9.5	3.2 ± 1.9	0.6 ± 0.3	0.01
PET30ΔPorC	23.3 ± 9.2	4.7 ± 1.8	0.9 ± 0.3	0.01
*Is*PETase	4,055.7 ± 516.9	811.1 ± 103.4	155.8 ± 19.9	2.23

The different recombinant and purified enzymes were incubated at a concentration of 1 mg ml^{-1} for a time period of 120 h at 30°C. For the tests a circular piece of 7 mg PET foil which corresponds to 36.4 μmol of the TPA-EG unit (Ø 5 mm, and as specified in section "Materials and Methods") was employed and folded once in the middle. Incubations were carried out in a reaction volume of 200 μl. Data are mean values with standard deviations of a minimum of 3 and up to 6 measurements per sample.

a relative activity of 65% (PET30) and 73% (PET27). PET30 remained active at 4°C showing a relative activity of 42% on *p*NP-C6. Concerning the optimal pH, PET27 was most active between pH 7–8 and PET30 between pH 6-8 when tested in 0.1 M potassium phosphate (**Figure 3C**).

To further characterize the effects of metal ions, different ions (Ca^{2+}, Co^{2+}, Cu^{2+}, Fe^{3+}, Mg^{2+}, Mn^{2+}, Ni^{2+}, and Zn^{2+}) were added to the assays at 1 and 10 mM final concentrations. Metal ions have a minor influence on PET27. Addition of Ca^{2+} resulted in a 1.4-fold increase of the activity (**Supplementary Figure 1A**). In case of PET30, addition of Zn^{2+}, Ni^{2+}, and Co^{2+} resulted in an up to threefold increase of activity.

The kinetic parameters for PET27 and PET30 were determined with *p*NP-C6 at 30°C and pH 8 according to Michaelis-Menten. Thereby, PET27 revealed a v_{max} of 4.9 nmol min^{-1}, a k_{cat} of 19.08 s^{-1}, a K_m of 1.37 mM and a k_{cat}/K_m value

of 13,859.27 M^{-1} s^{-1}. For PET30, we calculated a v_{max} of 2.3 nmol min^{-1}, a k_{cat} of 8.9 s^{-1}, a K_m of 0.3 mM and a k_{cat}/K_m value of 26,136.11 M^{-1} s^{-1}.

Further, PET30 was investigated in more detail. To assess thermostability, the enzyme was incubated at 50 and 60°C for 3 h, after which the enzyme retained only 23 and 5% of its original activity, respectively (**Supplementary Figure 1B**). As inhibiting substances, EDTA, DTT and PMSF were applied in final concentrations of 1 and 10 mM (**Supplementary Figure 1C**). The presence of DTT and PMSF (1 and 10 mM) inactivated PET30 almost completely, whereas EDTA at 1 and 10 mM had no large impact on the enzyme's activity. A concentration of 1 and 5 % of the detergents Triton X-100, Tween 80 and SDS decreased PET30's activities (**Supplementary Figure 1D**).

As both enzymes were active at lower temperatures, PET foil degradation was assayed at 4°C. Over a time of 30 days in

54

a 200 µl reaction volume, TPA release was measured. Under these conditions, 1 mg ml^{-1} of PET30 released an average of 6.1 µM of TPA (corresponds to 1.2 nmol). Interestingly, *Is*PETase released under the same conditions a similar amount (5.9 µM TPA corresponds to 1.2 nmol). Notably, under these conditions, no detectable amounts of TPA were released with PET27 after 30 days.

Amino Acid Sequence and Structural Analyses Identify Unique Traits of Bacteroidetal Polyethylene Terephthalate-Hydrolyzing Enzymes

While all four enzymes PET27-PET30 were able to hydrolyze PCL, BHET and Impranil®DLN, only PET27 and PET30 were able to depolymerize PET. To identify the key differences that confer this activity on PET, all predicted PETases were studied on sequence and structural level. With an average of 330 aa, the predicted molecular weights of the enzymes ranged from 36 to 48 kDa. Each candidate contained a C-terminal signal domain for protein transport to the periplasm as predicted with SignalP 5.0 (Almagro Armenteros et al., 2019), supporting the notion that these are secreted proteins (**Table 3**). Remarkably, the predicted PETases PET27-PET30 and PET38 showed a type IX secretion system (T9SS)/PorC-type sorting domain-containing part at the C-terminus. It has been described earlier by a profile HMM from the TIGRFAM database (TIGR04183). T9SS sorting domains are involved in protein transport across the bacterial outer membrane and have so far been described as a Bacteroidetes-specific secretion system (Sato et al., 2010; Shoji et al., 2011; de Diego et al., 2016). The predicted domain encompassed 62–64 aa in the cases of PET27-PET30 and PET38. PET57 and 58 carried truncated sorting domains of 42 and 55 aa in length. This observation also implies that these enzymes are most likely exoenzymes (**Table 3** and **Supplementary Figures 3, 4**). To ensure that this C-terminus does not affect catalytic activity, a deletion mutant designated PET30ΔPorC was created that lacked the sorting sequence between the amino acids 300–366. Activity tests confirmed that it was not affected in its activities using *p*NP-C6 or PET foil (**Supplementary Figure 1E** and **Table 2**). The enzyme released similar amounts of TPA as it was observed for the native PET30 (**Table 2**).

Further analyses of the amino acid sequences identified a G-x-S-x-G motif which is typical for α/β serine hydrolases (Ollis et al., 1992) and a catalytic triad that consists of the residues Asp-His-Ser (**Figure 4** and **Supplementary Figure 4**). Potential substrate binding sites in all bacteroidetal enzymes were identified containing the aa Phe-Met-(Trp/Tyr/Ala). The latter differed from the known *Is*PETase, the LCC and PET2 binding sites, in which a Tyr-Met-Trp motif is present (**Table 3**). PET57 is the only exception with a Trp-Met-Tyr binding site. PET27, however, has the Tyr replaced with a Phe that is identical to Cut190, while PET30 has in addition the Trp in position 3 replaced with a Tyr (**Table 3**). This single amino acid substitution in the predicted substrate binding pocket of PET30, however, is not solely responsible for PET-degrading activity. The mutants PET30_F80Y and PET30_Y178W as well as a version containing
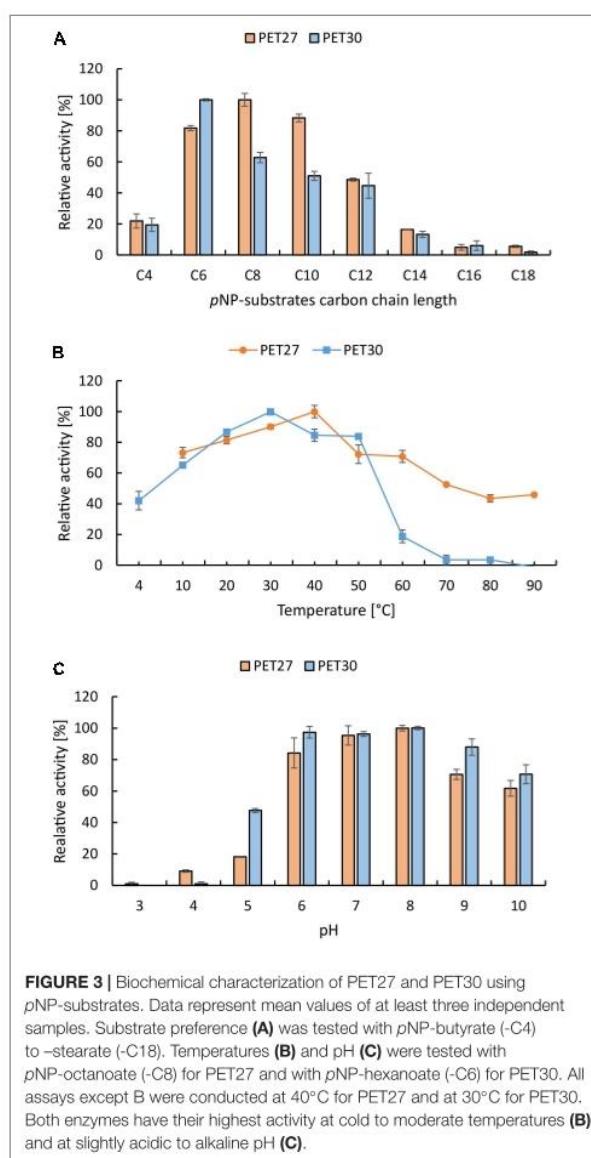
FIGURE 3 | Biochemical characterization of PET27 and PET30 using *p*NP-substrates. Data represent mean values of at least three independent samples. Substrate preference **(A)** was tested with *p*NP-butyrate (-C4) to –stearate (-C18). Temperatures **(B)** and pH **(C)** were tested with *p*NP-octanoate (-C8) for PET27 and with *p*NP-hexanoate (-C6) for PET30. All assays except B were conducted at 40°C for PET27 and at 30°C for PET30. Both enzymes have their highest activity at cold to moderate temperatures **(B)** and at slightly acidic to alkaline pH **(C)**.

both of these point mutations even lost BHET- and PET-degrading activity (data can be shown upon request).

Structure Determination of PET30 and Structural Modeling of the Other Putative PETases

For structural insights into the mechanism of polymer degradation, the structures of all predicted PETases, except PET30, were modeled using the *Is*PETase (PDB code 6EQE) as template. Crystallization was conducted with purified PET30ΔPorC and X-ray structure determination using a model of PET30 for molecular replacement. The structure was solved at 2.1 Å resolution, containing one monomer in the asymmetric

55

unit, with 16.2% for R_{work} and 21.9% for R_{free}. Data collection and structure refinement statistics are given in **Supplementary Table 4**. Coordinates of PET30ΔPorC were deposited under the PDB accession code 7PZJ. The PET30ΔPorC protein shows a canonical α/β-fold consisting of a central twisted β-sheet composed of 9 β-strands flanked by 7 α-helices on both sides (**Figure 4A**), as already reported for homologous structures, i.e., PETases and cutinases (Han et al., 2017; Numoto et al., 2018). The structure of PET30ΔPorC revealed an extra β-sheet (β10) which is located at the C-terminus and connects the PorC domain which has been deleted in this construct. PET30ΔPorC represents the overall fold of several PETases as revealed by a similarity search performed by PDBeFold.[8] Here, especially the known structures of the PETase from *Ideonella sakaiensis* (for example PDB code 5XH3; Han et al., 2017), show high consistency indicated by the rmsd of 1.3-1.5 Å. Also, high structural similarity can be seen with the structure of PE-H from *Pseudomonas aestusnigri* (PDB code 6SCD rmsd 1.3) and the cutinase from a member of the Burkhoderiales bacteria family (PDB code 7CWQ, rmsd of 1.32 (Bollinger et al., 2020; Chen et al., 2021). One disulfide bond is present in PET30ΔPorC (C262-C285), a common feature for Type II PET-degrading enzymes (Joo et al., 2018). In the PETase from *I. sakaiensis* (PDB code 5YNS), a second disulfide bond is present which is located closely to the active site. Mutational analysis revealed that this disulfide bond plays a crucial role in activity since mutation of the involved cysteine to serine completely abolished activity, likely due to a destabilizing effect on the active site. The sequence in PET30ΔPorC at this position deviates, and here, G195 and V232 are present. In the PE-H structure, also no disulfide bridge can be found, although one cysteine residue remained (G195 and C251). From the many structures of the PETase from *I. sakaiensis*, one was solved in complex with 2-hydroxyethyl methyl terephthalate (HEMT; PDB code 5XH3). Here, HEMT is bound via interactions with W156, I179, H208, A131, W130, Y58, and M132. We looked into the active site and overlaid the HEMT molecule with our PET30ΔPorC structure (**Supplementary Figure 2**). Here similar interactions of the HEMT molecule by the PET30ΔPorC protein can be deduced mediated by Y178, T200, H230, W152, F80, and M154 (**Figure 4B**).

The largest differences can be seen in the C-terminal part affiliated with the T9SS-domain. It differed largely from the *Is*PETase and consisted of up to seven predicted β-sheets and, occasionally, a few α-helices (**Supplementary Figure 3A and Table 3**). Another difference between PET27, PET30, *Is*PETase and LCC is the surface hydrophobicity of the region channeling the substrates to the active site (**Figure 4C**). PET30 shows a less hydrophobic surrounding of the catalytic pocket when compared to the structures of Type I and Type II PET-degrading enzymes (Joo et al., 2018). PET27 contains a bulkier hydrophobic domain on one of the sides of the channel. This feature might influence accommodation of the substrate and activity on the polymers. A similar catalytic pocket was predicted for PET28 and PET29 (**Supplementary Figure 3**). Although active on BHET and PCL, these enzymes showed no measurable activity on PET.

---

[8]www.ebi.ac.uk/msd-srv/ssm/

The enzymes derived from the human gut present a larger hydrophobic surface around the catalytic site, especially PET58 and PET59 (**Supplementary Figure 3B**).

Bacteroidetal Polyethylene Terephthalate-Degrading Esterases Forming Two Phylogenetic Subclusters Are Globally Occurring Enzymes

Using the amino acid sequences of published and functionally verified PETases and employing the RAxML-NG autoMRE algorithm via TreeSAPP (Morgan-Lang et al., 2020), aphylogenetic analysis was performed. Multiple phylogenetic clusters formed that roughly corresponded to Actinobacteria, Proteobacteria, Firmicutes and Ascomycota (**Figure 5A**). While the putative and now confirmed Bacteroidetal PET-degrading hydrolases appear to be polyphyletic when added into the tree, distinct subclusters were formed. Notably, the two enzymes PET27 and PET30, shown to be active on PET foil, were grouped as part of subcluster that consisted of predicted and functional enzymes affiliated with genera *Aequorivita* and *Kaistella*. Furthermore, the predicted but functionally not verified enzymes from the genus *Porphyromonas* (PET57-PET59) formed a separate subcluster. Interestingly, these two subclusters harbored only sequences of aquatic and environmental origin orgut-affiliated sequences, respectively. Overall, sequences derived from Bacteroidetes seem to group by both taxonomy and environment, though low bootstrap values do not show a high degree of confidence. However, the interleaving of Bacteroidetal sequences from both a Firmicute, *B. subtilis*, and the eukaryotic Ascomycota sequences may suggest that PET-active enzymes are widely distributed phylogenetically, and further characterization studies resulting in additions to the tree are likely to provide better phylogenetic resolution. Additionally, the pairwise distance on the level computed in MEGAX with the p-distance model (**Figure 5B**) confirmed these groupings, with the highest similarity, as indicated by low pairwise distanced, occurring within the subclusters described. This analysis also indicated rather low similarity between the putative bacteroidetal PETases and the known PETases (*Is*PETase, LCC, PE-H, and PET2), mounting further evidence for the wide phylogenetic distribution of these enzymes.

The diversity of bacteroidetal enzymes acting on PET raised the question to what extent these enzymes could impact plastic degradation in the environment. To address this question in part, we analyzed the global distribution of PET27 and PET30 and their homologs. The protein sequences of PET27 and PET30 were analyzed for their occurrence and frequency in global databases available in IMG/M ER (Woyke et al., 2011; Mukherjee et al., 2020). Using both enzymes for a BLASTp-based search (cutoffs 50% identity; 80% coverage), we were initially able to identify very few (<10) possible homologs in the global databases analyzed and affiliated with the genera *Aequorivita* and *Kaistella* (**Figure 1A**). Interestingly, when we extended our search to the Flavobacterium-Cytophaga-Bacteroidetes (FCB), we were able to identify 98 possible homologs in our global searches including single-cell amplified genomes (SAGs) from the Baltic Sea

56

TABLE 3 | Conserved motifs and structural features identified in the predicted bacteroidetal PET-hydrolyzing esterases.

Enzyme	N-terminus			Catalytic triad	Substrate binding site	Disulf. bridge*	C-terminus			
	Aln 1st aa	Length [N]	SP cleavage site				Aln last aa	Length [N]	Secondary structure	CD
*Is*PETase	A47	47	27–28	D-H-S	Y-M-W	2x	C273	18	N/A	N/A
LCC	D53	53	21–22	D-H-S	Y-M-W	1x	L274	19	N/A	N/A
Cut190	R64	64	N/A	D-H-S	F-M-W	2x	L278	29	N/A	N/A
PET27	P36	36	23–24	D-H-S	F-M-W	1x	L265	99	7xβ	PorC
PET28	P36	36	23–24	D-H-S	F-M-W	1x	L265	100	6xβ	PorC
PET29	P36	36	23–24	D-H-S	F-M-W	1x	L265	100	α, 4xβ, α, 2xβ	PorC
PET30	P36	36	23–24	D-H-S	F-M-Y	1x	A266	100	7xβ	PorC
PET38	S7	7	19–20	D-H-S	F-M-A	1x	I279	168	5xβ, α, 2xβ	PorC
PET53	T36	36	22–23	D-H-S	F-M-W	1x	V268	86	4xβ	N/A
PET57	N35	35	25–26	D-H-S	W-M-Y	N/A	F289	34	α + loops	N/A
PET58	I34	34	24–25	D-H-S	F-M-Y	N/A	F293	45	loops + α	N/A
PET59	Y48	48	24–25	D-H-S	F-M-Y	N/A	Y294	51	α + semi-α	N/A

The Ideonella sakaiensis PETase (IsPETase, PDB: 6EQE; Yoshida et al., 2016; Austin et al., 2018), the LCC (4EB0; Sulaiman et al., 2014) and the Cut190 (4WFI; Miyakawa et al., 2015) were included for benchmarking purposes.
*Aln: Alignment; SP: Signal Peptide; α, α -helix; ß, ß-sheet; N/A, not identified; *, verified and predicted disulfide bonds; CD: Conserved Domain; PorC, Por secretion system C-terminal sorting domain.*

(**Supplementary Table 5**). 47 hits were affiliated with the genus of the *Marinimicrobia* (candidate phylum of the FCB group), indicating a potential role for these ubiquitous and abundant marine microorganisms in PET-degradation. Others were more closely associated with Bacteroidetes (Austin et al., 2018). As expected, the majority of these homologs were associated with marine and aquatic samples (**Figure 1B**).

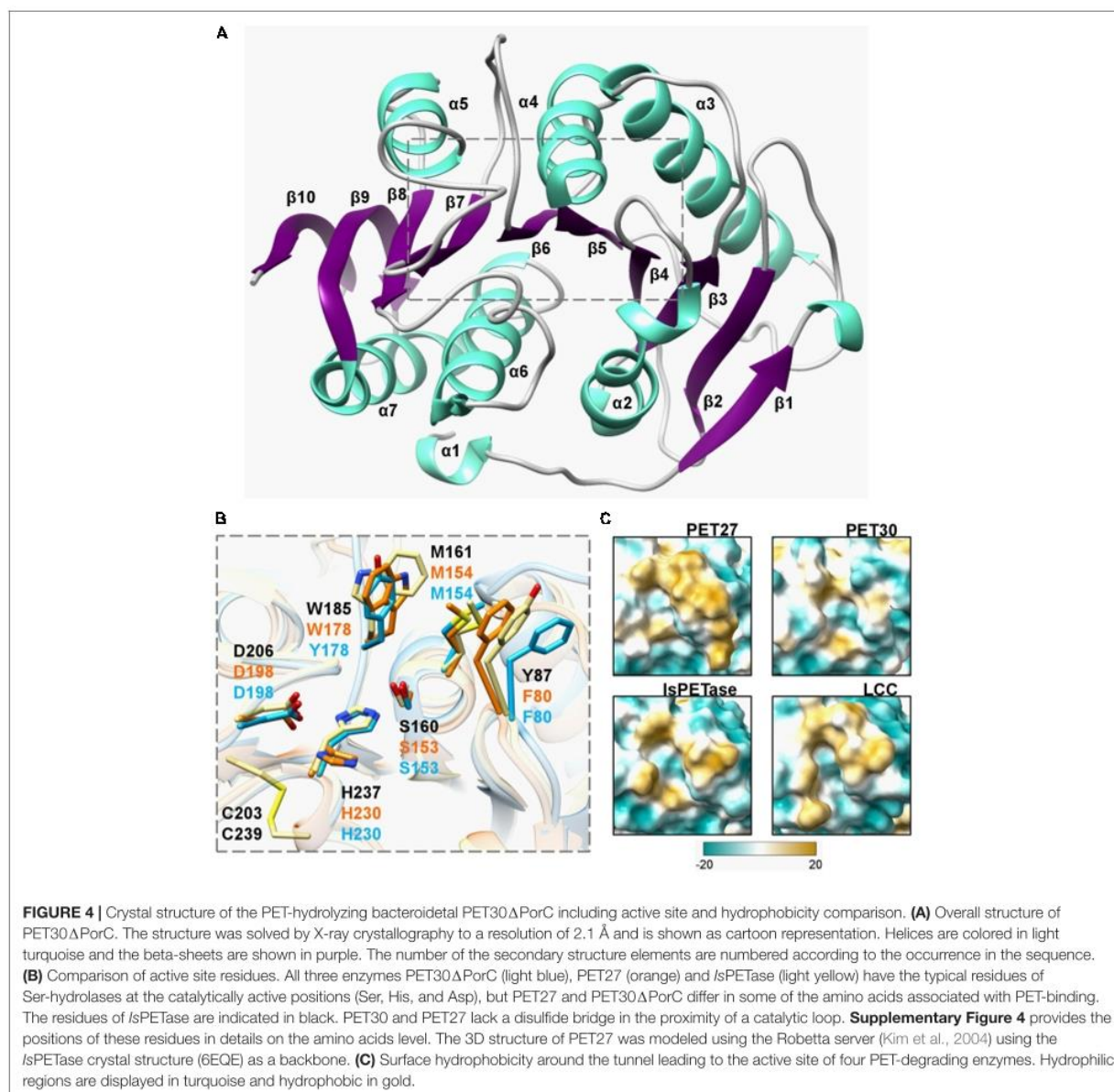## *Kaistella jeonii* Is Able to Colonize Polyethylene Terephthalate Surfaces

These metagenomic analyses showed that *K. jeonii*, the organism from which PET30 originates, exists primarily in aquatic habitats. To illustrate that it not only exists there, but is also able to actively colonize PET surfaces, a culture of this organism was incubated with PET foil platelets. The foil sections were incubated for up to 1 week in R2A medium with *K. jeonii*, removed from the culture, and washed three times with buffer before staining with LIVE/DEAD staining solution. Samples were investigated under the confocal laser scanning microscope Axio Observer Z1/7, LSM 800 by Carl Zeiss Microscopy GmbH (Jena, Germany). Cells visible in **Supplementary Figure 5** resisted repeated washing, indicating that they adhere under these laboratory conditions to the surface and an increasing number of cells was visible on the amorphous PET-foil after 5–7 days. The exact mechanism of attachment is not known. Nonetheless, it can be speculated that SusD binding modules, which are crucial for sugar polymer binding, could be involved. They can be found in both genomes of *K. jeonii* (GenBank acc. no. WP_039349586.1; RagB/SusD family nutrient uptake outer membrane protein) and *Aequorivita* sp. CIP111184 (GenBank acc. no. WP_111879847.1; SusD/RagB family nutrient-binding outer membrane lipoprotein).

DISCUSSION

Currently, only a handful of known bacterial phyla are known to produce active PET-esterases (**Figure 5** and **Supplementary Table 3**). Here, we have identified and partially characterized two novel functional PET-hydrolyzing enzymes affiliated with the *Kaistella* and *Aequorivita* genera within the Bacteroidetes phylum. Bacteria belonging to the genus *Kaistella* are globally occurring aerobic organisms colonizing a wide range of different habitats including plants, soil, fish, the human gut, and sea water. Within the genus *Kaistella*, over one hundred species have been described of which few are pathogens, but many are beneficial and host-associated (Bernardet et al., 2005; Loch and Faisal, 2015). Only a few species have been identified within the genus *Aequorivita*, mainly belonging to marine or fresh-water organisms that are mostly psychrotolerant and aerobic (Bowman and Nichols, 2002). Notably, Bacteroidetes have been described as very potent degraders of polymers, and they harbor a multitude of hydrolases and binding modules (Dodd et al., 2011; Thomas et al., 2011; Foley et al., 2016).

The enzymes PET27 and PET30 characterized here are both typical esterases (i.e., serine hydrolases) belonging to the EC 3.1. Both appear to be secreted enzymes as they carry an C-terminal secretion signal linked to the transport into the periplasm (Desvaux et al., 2009) and one secretion PorC-like motif which is related to the type IX secretion system (T9SS) (Sato et al., 2010; de Diego et al., 2016). The T9SS is composed of several outer membrane, periplasmic and inner membrane proteins, whereby it is responsible for the secretion of pathogenicity factors, hydrolases and also for gliding motility in the Bacteroidetes phylum (Sato et al., 2010; de Diego et al., 2016).

PET27 and PET30 were active on PET foil, but differed strongly in their overall activities. PET27 contains a Phe-Met-Trp

57

FIGURE 4 | Crystal structure of the PET-hydrolyzing bacteroidetal PET30ΔPorC including active site and hydrophobicity comparison. **(A)** Overall structure of PET30ΔPorC. The structure was solved by X-ray crystallography to a resolution of 2.1 Å and is shown as cartoon representation. Helices are colored in light turquoise and the beta-sheets are shown in purple. The number of the secondary structure elements are numbered according to the occurrence in the sequence. **(B)** Comparison of active site residues. All three enzymes PET30ΔPorC (light blue), PET27 (orange) and *Is*PETase (light yellow) have the typical residues of Ser-hydrolases at the catalytically active positions (Ser, His, and Asp), but PET27 and PET30ΔPorC differ in some of the amino acids associated with PET-binding. The residues of *Is*PETase are indicated in black. PET30 and PET27 lack a disulfide bridge in the proximity of a catalytic loop. **Supplementary Figure 4** provides the positions of these residues in details on the amino acids level. The 3D structure of PET27 was modeled using the Robetta server (Kim et al., 2004) using the *Is*PETase crystal structure (6EQE) as a backbone. **(C)** Surface hydrophobicity around the tunnel leading to the active site of four PET-degrading enzymes. Hydrophilic regions are displayed in turquoise and hydrophobic in gold.

motif and PET30 a Phe-Met-Tyr. The most active enzymes such as LCC and *Is*PETase both carry a Tyr-Met-Trp consensus binding motif while the non-active enzymes PET38, PET53, PET57 PET58 and PET59 revealed either a Phe-Met-Ala, a Phe-Met-Trp or a Trp-Met-Tyr substrate binding motif. PET30 mutants, in which the amino acids were adjusted according to the active PETases, did not show the expected increase in activity. Therefore, we assume that not only individual amino acids are decisive, but rather that an interplay of hydrophobicity, location and accessibility of the catalytic triad is crucial for whether polymers can be degraded (**Figure 4**).

Benchmarking activities of polymer active enzymes with literature values is not trivial since most studies use different types of foils with different degrees of crystallinity and distinct assay conditions. To partially overcome this challenge, we produced our own recombinant wildtype enzymes of the *Is*PETase and compared its activities with PET27 and PET30. As expected, *Is*PETase was 4.7-fold more active at 30°C than PET27 and up to 253-fold more active than PET30. With respect to the overall activity of the *Is*PETase, however, our data are in line with published data for this enzyme (Son et al., 2019). The observation here that the activities of the PET27 and PET30 enzymes are relatively low compared to the *Is*PETase and certainly with

FIGURE 5 | Phylogenetic tree and pairwise comparison of known PETases and bacteroidetal PET-hydrolyzing enzymes. **(A)** The tree was constructed using the RAxML-NG autoMRE algorithm (Kozlov et al., 2019) with the treesapp create command implemented in TreeSAPP (Morgan-Lang et al., 2020) with maximum bootstraps set at 1,000. GenBank entries of the putative and verified PET-active enzymes affiliated with the Bacteroidetes phylum are listed in **Table 1**; the entries of all other PETases included in the tree are indicated in **Supplementary Table 3**. The term "uncultured bacterium" refers to a not further specified microorganism derived from a metagenome or a mixed microbial consortium. **(B)** Heatmap representation of pairwise similarities between all enzymes affiliated with the Bacteroidetes phylum in comparison with four known PETases (*Is*PETase, LCC, PE-H, and PET2). The pairwise comparison was performed in MEGAX with the p-distance model. High values indicating low similarity are colored in red, low values indicating high similarity are colored in green.

respect to the published values of the even more active LCC imply that PET27 and PET30 are not PET esterases *in sensu strictu*. However, our data imply that both are short-chain fatty acid acting esterases revealing promiscuity in their substrate profile (**Table 3** and **Figure 3**).

Intriguingly, the observation that both enzymes were catalytically active on PET foil could imply a wider role in the degradation of PET and especially PET nanoparticles. Because of the significant activities even at 4°C, these enzymes may in fact play a yet unknown role in long-term degradation of

PET microparticles in cold environments. This hypothesis is supported by our observations that homologs of both enzymes can be found on a global level covering a wide range of climate zones (**Figure 1**) and that at least the cultivable *K. jeonii* is able to attach to PET surfaces.

In summary, our biochemical results significantly extend the knowledge of PET-degrading enzymes and provide promising candidates for biotechnological applications at low temperatures. Furthermore, the data presented here will help to advance our knowledge on the ecological role of the

Bacteroidetes in the decomposition of marine PET litter and enable the development of an expanded phylogenetic framework for identifying the diversity of putative PETases in diverse marine microbial groups throughout the global ocean.

DATA AVAILABILITY STATEMENT

The original contributions presented in the study are included in the article/**Supplementary Material**, further inquiries can be directed to the corresponding author/s.

AUTHOR CONTRIBUTIONS

FUNDING

ACKNOWLEDGMENTS

SUPPLEMENTARY MATERIAL

The Supplementary Material for this article can be found online at: https://www.frontiersin.org/articles/10.3389/fmicb.2021.803896/full#supplementary-material

Supplementary Figure 1 | Further biochemical characterization of PET27 and PET30 using *p*NP-substrates. Cofactor requirements were tested for PET27 with *p*NP-C8 at 40°C and for PET30 with *p*NP-C6 at 30°C **(A)**. For PET30, all other tests were carried out with *p*NP-C6 and all assays except **(B)** were conducted at 30°C. Thermostability of PET30 was assessed at 50 and 60°C over 3 h with *p*NP-C6 **(B)**. Inhibitors **(C)** and detergents **(D)** generally decrease the activity of PET30, particularly with higher concentrations. Activity of PET30 and PET30∆PorC were compared under the same conditions using *p*NP-C6 **(E)**. Data represent mean values of at least three independent measurements.

Supplementary Figure 2 | Zoom into the active site of PET30∆PorC. Overlaid are the structures of PET30∆PorC (blue) with the PETase from *I. sakaiensis* (light yellow, black labeling) in complex with HEMT (purple; PDB code 5XH3). The residues involved in binding are highlighted and numbered according to their structure. *The structure 5XH3 is a mutant where the catalytic Serine was mutated to an Alanine.

Supplementary Figure 3 | Structure prediction models of verified and predicted PETases affiliated with the phylum of the Bacteroidetes. **(A)** 3D structures were modeled using the Robetta server using the *Is*PETase crystal structure (light yellow, 6EQE) as a backbone. For PET30, the crystal structure was shown. **(B)** Surface hydrophobicity around the tunnel leading to the active site of putative bacteroidetal PETases and functionally verified PET-degrading enzymes. Hydrophilic regions are displayed in turquoise and hydrophobic in gold.

Supplementary Figure 4 | Amino acid alignment of 9 potential PETases affiliated with the Bacteroidetes phylum. The original sequences were used for the structural alignment and the alignment was constructed with T-Coffee. Alignment was visualized with Bioedit version 7.0.5. The *Is*PETase was included for reasons of benchmarking. Blue arrows indicate the start and the end of the active PET27 and PET30 clones. We introduced a methionine as the first aa of the protein sequences. The signal peptide deleted version of the enzymes was functionally verified. The red arrow labeled with CS indicates the predicted cleavage site of C-terminal PorC domain (Lasica et al., 2017). The gray arrow indicates the C-terminus of the truncated version of PET30 (PET30∆300-366), number indicates the position of amino acid). PET30∆300-366 was active on PCL and BHET.

Supplementary Figure 5 | Confocal microscopic pictures of *K. jeonii* colonizing PET foil. The pictures were taken after 5–7 days of incubation of *K. jeonii* in R2A medium. Cells are dyed with LIVE/DEAD™ stain. Green fluorescence shows living cells, red fluorescence indicates dead cells. 2D front pictures were taken with Axio Observer Z1/7, LSM 800 (Carl Zeiss, Jena, Germany) of a 3D Z-stack image.

REFERENCES

Acero, E. H., Ribitsch, D., Steinkellner, G., Gruber, K., Greimel, K., Eiteljoerg, I., et al. (2011). Enzymatic surface hydrolysis of PET: effect of structural diversity on kinetic properties of cutinases from

Thermobifida. *Macromolecules* 44, 4632–4640. doi: 10.1021/ma200 949p

Afonine, P. V., Grosse-Kunstleve, R. W., Echols, N., Headd, J. J., Moriarty, N. W., Mustyakimov, M., et al. (2012). Towards automated crystallographic structure refinement with phenix. refine. *Acta*

Crystallogr. D Biol. Crystallogr. 68, 352–367. doi: 10.1107/S090744491200 1308

Agarwala, R., Barrett, T., Beck, J., Benson, D. A., Bollin, C., Bolton, E., et al. (2016). Database resources of the national center for biotechnology information. *Nucleic Acids Res.* 44, D7–D19.

Almagro Armenteros, J. J., Tsirigos, K. D., Sønderby, C. K., Petersen, T. N., Winther, O., Brunak, S., et al. (2019). SignalP 5.0 improves signal peptide predictions using deep neural networks. *Nat. Biotechnol.* 37, 420–423. doi: 10.1038/s41587-019-0036-z

Almeida, A., Nayfach, S., Boland, M., Strozzi, F., Beracochea, M., Shi, Z. J., et al. (2021). A unified catalog of 204,938 reference genomes from the human gut microbiome. *Nat. Biotechnol.* 39, 105–114. doi: 10.1038/s41587-020-0603-3

Austin, H. P., Allen, M. D., Donohoe, B. S., Rorrer, N. A., Kearns, F. L., Silveira, R. L., et al. (2018). Characterization and engineering of a plastic-degrading aromatic polyesterase. *Proc. Natl. Acad. Sci. U.S.A.* 115, E4350–E4357. doi: 10.1073/pnas.1718804115

Berman, H. M., Westbrook, J., Feng, Z., Gilliland, G., Bhat, T. N., Weissig, H. I, et al. (2000). The protein data bank. *Nucleic Acids Res.* 28, 235–242.

Bernardet, J. F., Vancanneyt, M., Matte-Tailliez, O., Grisez, L., Tailliez, P., Bizet, C., et al. (2005). Polyphasic study of *Chryseobacterium* strains isolated from diseased aquatic animals. *Syst. Appl. Microbiol.* 28, 640–660. doi: 10.1016/j.syapm.2005.03.016

Bollinger, A., Thies, S., Knieps-Grunhagen, E., Gertzen, C., Kobus, S., Hoppner, A., et al. (2020). A novel polyester hydrolase from the marine bacterium *Pseudomonas aestusnigri*–structural and functional insights. *Front. Microbiol.* 11:114. doi: 10.3389/fmicb.2020.00114

Bowman, J. P., and Nichols, D. S. (2002). *Aequorivita* gen. nov., a member of the family Flavobacteriaceae isolated from terrestrial and marine Antarctic habitats. *Int. J. Syst. Evol. Microbiol.* 52, 1533–1541. doi: 10.1099/00207713-52-5-1533

Chen, C.-C., Han, X., Li, X., Jiang, P., Niu, D., Ma, L., et al. (2021). General features to enhance enzymatic activity of poly (ethylene terephthalate) hydrolysis. *Nat. Catal.* 4, 425–430. doi: 10.1038/s41929-021-00616-y

Chen, S., Tong, X., Woodard, R. W., Du, G., Wu, J., and Chen, J. (2008). Identification and characterization of bacterial cutinase. *J. Biol. Chem.* 283, 25854–25862. doi: 10.1074/jbc.m800848200

NCBI Resource Coordinators (2017). Database resources of the national center for biotechnology information. *Nucleic Acids Res.* 45, D12–D17.

Danso, D., Chow, J., and Streit, W. R. (2019). Plastics: microbial degradation, environmental and biotechnological perspectives. *Appl. Environ. Microbiol.* 85, 1–14. doi: 10.1007/978-3-030-48973-1_1

Danso, D., Schmeisser, C., Chow, J., Zimmermann, W., Wei, R., Leggewie, C., et al. (2018). New insights into the function and global distribution of polyethylene terephthalate (PET)-degrading bacteria and enzymes in marine and terrestrial metagenomes. *Appl. Environ. Microbiol.* 84:e02773-17. doi: 10.1128/AEM.02773-17

de Diego, I., Ksiazek, M., Mizgalska, D., Koneru, L., Golik, P., Szmigielski, B., et al. (2016). The outer-membrane export signal of *Porphyromonas gingivalis* type IX secretion system (T9SS) is a conserved C-terminal β-sandwich domain. *Sci. Rep.* 6:23123. doi: 10.1038/srep23123

DeLano, W. L. (2002). Pymol: an open-source molecular graphics tool. *CCP4 Newslett. Protein Crystallogr.* 40, 82–92.

Desvaux, M., Hébraud, M., Talon, R., and Henderson, I. R. (2009). Outer membrane translocation: numerical protein secretion nomenclature in question in mycobacteria. *Trends Microbiol.* 17, 338–340. doi: 10.1016/j.tim.2009.05.008

Dodd, D., Mackie, R. I., and Cann, I. K. O. (2011). Xylan degradation, a metabolic property shared by rumen and human colonic Bacteroidetes. *Mol. Microbiol.* 79, 292–304. doi: 10.1111/j.1365-2958.2010.07473.x

Emsley, P., and Cowtan, K. (2004). Coot: model-building tools for molecular graphics. *Acta Crystallogr. D Biol. Crystallogr.* 60, 2126–2132. doi: 10.1107/s0907444904019158

Foley, M. H., Cockburn, D. W., and Koropatkin, N. M. (2016). The Sus operon: a model system for starch uptake by the human gut Bacteroidetes. *Cell. Mol. Life Sci.* 73, 2603–2617. doi: 10.1007/s00018-016-2242-x

Geyer, R., Jambeck, J. R., and Law, K. L. (2017). Production, use, and fate of all plastics ever made. *Sci. Adv.* 3:e1700782. doi: 10.1126/sciadv.1700782

Haernvall, K., Zitzenbacher, S., Amer, H., Zumstein, M. T., Sander, M., McNeill, K., et al. (2017). Polyol structure influences enzymatic hydrolysis of bio-based

2,5-furandicarboxylic acid (FDCA) polyesters. *Biotechnol. J.* 12:1600741. doi: 10.1002/biot.201600741

Hahnke, R. L., Meier-Kolthoff, J. P., García-López, M., Mukherjee, S., Huntemann, M., Ivanova, N. N., et al. (2016). Genome-based taxonomic classification of bacteroidetes. *Front. Microbiol.* 7:2003. doi: 10.3389/fmicb.2016.02003

Hall, T. A. (1999). *BioEdit: A User-Friendly Biological Sequence Alignment Editor and Analysis Program for Windows 95/98/NT. Nucleic Acids Symposium Series.* London: Information Retrieval Ltd., c1979–c2000.

Han, X., Liu, W., Huang, J. W., Ma, J., Zheng, Y., Ko, T. P., et al. (2017). Structural insight into catalytic mechanism of PET hydrolase. *Nat. Commun.* 8:2106.

Hu, X., Thumarat, U., Zhang, X., Tang, M., and Kawai, F. (2010). Diversity of polyester-degrading bacteria in compost and molecular analysis of a thermoactive esterase from *Thermobifida alba* AHK119. *Appl. Microbiol. Biotechnol.* 87, 771–779. doi: 10.1007/s00253-010-2555-x

Jambeck, J. R., Geyer, R., Wilcox, C., Siegler, T. R., Perryman, M., Andrady, A., et al. (2015). Plastic waste inputs from land into the ocean. *Science* 347, 768–771. doi: 10.1126/science.1260352

Joo, S., Cho, I. J., Seo, H., Son, H. F., Sagong, H. Y., Shin, T. J., et al. (2018). Structural insight into molecular mechanism of poly(ethylene terephthalate) degradation. *Nat. Commun.* 9:382.

Kabsch, W. (2014). Processing of X-ray snapshots from crystals in random orientations. *Acta Crystallogr. D Biol. Crystallogr.* 70, 2204–2216. doi: 10.1107/S1399004714013534

Kim, D. E., Chivian, D., and Baker, D. (2004). Protein structure prediction and analysis using the Robetta server. *Nucleic Acids Res.* 32, W526–W531.

Kleeberg, I., Hetz, C., Kroppenstedt, R. M., Muller, R. J., and Deckwer, W. D. (1998). Biodegradation of aliphatic-aromatic copolyesters by *Thermomonospora fusca* and other thermophilic compost isolates. *Appl. Environ. Microbiol.* 64, 1731–1735. doi: 10.1128/AEM.64.5.1731-1735.1998

Kozlov, A. M., Darriba, D., Flouri, T., Morel, B., and Stamatakis, A. (2019). RAxML-NG: a fast, scalable and user-friendly tool for maximum likelihood phylogenetic inference. *Bioinformatics* 35, 4453–4455. doi: 10.1093/bioinformatics/btz305

Krieg, N., Ludwig, W., Euzéby, J., and Whitman, W. (2015). "Bacteroidetes phyl. nov.," in *Bergey's Manual of Systematics of Archaea and Bacteria*, eds M. E. Trujillo, S. Dedysh, P. DeVos, et al. (Hoboken, NJ: John Wiley & Sons, Inc.), 1–2. doi: 10.1002/9781118960608.pbm00004

Lasica, A. M., Ksiazek, M., Madej, M., and Potempa, J. (2017). The type IX secretion system (T9SS): highlights and recent insights into its structure and function. *Front. Cell. Infect. Microbiol.* 7:215. doi: 10.3389/fcimb.2017.00215

Letunic, I., and Bork, P. (2019). Interactive tree of life (iTOL) v4: recent updates and new developments. *Nucleic Acids Res.* 47, W256–W259. doi: 10.1093/nar/gkz239

Li, N., Zhu, Y., LaFrentz, B. R., Evenhuis, J. P., Hunnicutt, D. W., Conrad, R. A., et al. (2017). The type IX secretion system is required for virulence of the fish pathogen *Flavobacterium columnare*. *Appl. Environ. Microbiol.* 83:e01769-17.

Liebschner, D., Afonine, P. V., Baker, M. L., Bunkóczi, G., Chen, V. B., Croll, T. I., et al. (2019). Macromolecular structure determination using X-rays, neutrons and electrons: recent developments in Phenix. *Acta Crystallogr. D Struct. Biol.* 75, 861–877. doi: 10.1107/S2059798319011471

Loch, T. P., and Faisal, M. (2015). Emerging flavobacterial infections in fish: a review. *J. Adv. Res.* 6, 283–300. doi: 10.1016/j.jare.2014.10.009

Markowitz, V. M., Chen, I. M., Palaniappan, K., Chu, K., Szeto, E., Grechkin, Y., et al. (2012). IMG: the integrated microbial genomes database and comparative analysis system. *Nucleic Acids Res.* 40, D115–D122.

Matlab, S. (2012). *Matlab*. Natick, MA: The MathWorks.

Mistry, J., Finn, R. D., Eddy, S. R., Bateman, A., and Punta, M. (2013). Challenges in homology search: HMMER3 and convergent evolution of coiled-coil regions. *Nucleic Acids Res.* 41:e121. doi: 10.1093/nar/gkt263

Mitchell, A. L., Almeida, A., Beracochea, M., Boland, M., Burgin, J., Cochrane, G., et al. (2019). MGnify: the microbiome analysis resource in 2020. *Nucleic Acids Res.* 48, D570–D578. doi: 10.1093/nar/gkz1035

Miyakawa, T., Mizushima, H., Ohtsuka, J., Oda, M., Kawai, F., and Tanokura, M. (2015). Structural basis for the Ca^{2+}-enhanced thermostability and activity of PET-degrading cutinase-like enzyme from *Saccharomonospora viridis* AHK190. *Appl. Microbiol. Biotechnol.* 99, 4297–4307. doi: 10.1007/s00253-014-6272-8

61

Molitor, R., Bollinger, A., Kubicki, S., Loeschcke, A., Jaeger, K. E., and Thies, S. (2020). Agar plate-based screening methods for the identification of polyester hydrolysis by *Pseudomonas* species. *Microb. Biotechnol.* 13, 274–284. doi: 10.1111/1751-7915.13418

Morgan-Lang, C., McLaughlin, R., Armstrong, Z., Zhang, G., Chan, K., and Hallam, S. J. (2020). TreeSAPP: the tree-based sensitive and accurate phylogenetic profiler. *Bioinformatics* 36, 4706–4713. doi: 10.1093/bioinformatics/btaa588

Mukherjee, S., Stamatis, D., Bertsch, J., Ovchinnikova, G., Sundaramurthi, J. C., Lee, J., et al. (2020). Genomes OnLine Database (GOLD) v.8: overview and updates. *Nucleic Acids Res.* 49, D723–D733. doi: 10.1093/nar/gkaa983

Mulnaes, D., Porta, N., Clemens, R., Apanasenko, I., Reiners, J., Gremer, L., et al. (2020). TopModel: template-based protein structure prediction at low sequence identity using top-down consensus and deep neural networks. *J. Chem. Theory Comput.* 16, 1953–1967. doi: 10.1021/acs.jctc.9b00825

Munoz, R., Rosselló-Móra, R., and Amann, R. (2016). Revised phylogeny of Bacteroidetes and proposal of sixteen new taxa and two new combinations including Rhodothermaeota phyl. nov. *Syst. Appl. Microbiol.* 39, 281–296. doi: 10.1016/j.syapm.2016.04.004

Notredame, C., Higgins, D. G., and Heringa, J. (2000). T-Coffee: a novel method for fast and accurate multiple sequence alignment. *J. Mol. Biol.* 302, 205–217.

Numoto, N., Kamiya, N., Bekker, G.-J., Yamagami, Y., Inaba, S., Ishii, K., et al. (2018). Structural dynamics of the PET-degrading cutinase-like enzyme from *Saccharomonospora viridis* AHK190 in substrate-bound states elucidates the Ca^{2+}-driven catalytic cycle. *Biochemistry* 57, 5289–5300. doi: 10.1021/acs.biochem.8b00624

Ollis, D. L., Cheah, E., Cygler, M., Dijkstra, B., Frolow, F., Franken, S. M., et al. (1992). The alpha/beta hydrolase fold. *Protein Eng.* 5, 197–211.

Pérez-García, P., Danso, D., Zhang, H., Chow, J., and Streit, W. R. (2021). Exploring the global metagenome for plastic-degrading enzymes. *Methods Enzymol.* 648, 137–157. doi: 10.1016/bs.mie.2020.12.022

Ribitsch, D., Herrero Acero, E., Greimel, K., Dellacher, A., Zitzenbacher, S., Marold, A., et al. (2012). A new esterase from *Thermobifida halotolerans* hydrolyses polyethylene terephthalate (PET) and polylactic acid (PLA). *Polymers* 4, 617–629. doi: 10.3390/polym4010617

Ronkvist, ÅM., Xie, W., Lu, W., and Gross, R. A. (2009). Cutinase-catalyzed hydrolysis of poly(ethylene terephthalate). *Macromolecules* 42, 5128–5138.

Sato, K., Naito, M., Yukitake, H., Hirakawa, H., Shoji, M., McBride, M. J., et al. (2010). A protein secretion system linked to bacteroidete gliding motility and pathogenesis. *Proc. Natl. Acad. Sci. U.S.A.* 107, 276–281. doi: 10.1073/pnas.0912010107

Shoji, M., Sato, K., Yukitake, H., Kondo, Y., Narita, Y., Kadowaki, T., et al. (2011). Por secretion system-dependent secretion and glycosylation of *Porphyromonas gingivalis* hemin-binding protein 35. *PLoS One* 6:e21372. doi: 10.1371/journal.pone.0021372

Son, H. F., Cho, I. J., Joo, S., Seo, H., Sagong, H.-Y., Choi, S. Y., et al. (2019). Rational protein engineering of thermo-stable PETase from *Ideonella sakaiensis* for highly efficient PET degradation. *ACS Catal.* 9, 3519–3526.

Studier, F. W. (2005). Protein production by auto-induction in high-density shaking cultures. *Protein Exp. Purif.* 41, 207–234.

Sulaiman, S., Yamato, S., Kanaya, E., Kim, J. J., Koga, Y., Takano, K., et al. (2012). Isolation of a novel cutinase homolog with polyethylene terephthalate-degrading activity from leaf-branch compost by using a metagenomic

approach. *Appl. Environ. Microbiol.* 78, 1556–1562. doi: 10.1128/AEM.067 25-11

Sulaiman, S., You, D. J., Kanaya, E., Koga, Y., and Kanaya, S. (2014). Crystal structure and thermodynamic and kinetic stability of metagenome-derived LC-cutinase. *Biochemistry* 53, 1858–1869. doi: 10.1021/bi40 1561p

The UniProt Consortium (2017). UniProt: the universal protein knowledgebase. *Nucleic Acids Res.* 45, D158–D169.

Thomas, F., Hehemann, J. H., Rebuffet, E., Czjzek, M., and Michel, G. (2011). Environmental and gut Bacteroidetes: the food connection. *Front. Microbiol.* 2:16. doi: 10.3389/fmicb.2011.00093

Wei, R., Oeser, T., and Zimmermann, W. (2014). Synthetic polyester-hydrolyzing enzymes from thermophilic actinomycetes. *Adv. Appl. Microbiol.* 89, 267–305. doi: 10.1016/B978-0-12-800259-9.00007-X

Wei, R., and Zimmermann, W. (2017). Microbial enzymes for the recycling of recalcitrant petroleum-based plastics: how far are we? *Microb. Biotechnol.* 10, 1308–1322. doi: 10.1111/1751-7915.12710

Wexler, H. M. (2007). *Bacteroides*: the good, the bad, and the nitty-gritty. *Clin. Microbiol. Rev.* 20, 593–621. doi: 10.1128/CMR.00008-07

Woyke, T., Chertkov, O., Lapidus, A., Nolan, M., Lucas, S., Del Rio, T. G., et al. (2011). Complete genome sequence of the gliding freshwater bacterium *Fluviicola taffensis* type strain (RW262). *Stand. Genomic Sci.* 5, 21–29. doi: 10.4056/sigs.2124912

Wright, R. J., Bosch, R., Langille, M. G., Gibson, M. I., and Christie-Oleza, J. A. (2021). A multi-OMIC characterisation of biodegradation and microbial community succession within the PET plastisphere. *Microbiome* 9, 1–22. doi: 10.1155/2021/6620574

Yoshida, S., Hiraga, K., Takehana, T., Taniguchi, I., Yamaji, H., Maeda, Y., et al. (2016). A bacterium that degrades and assimilates poly(ethylene terephthalate). *Science* 351, 1196–1199. doi: 10.1126/science.aad6359

62

4   Surface Grafted N-Oxides have Low-Fouling and Antibacterial Properties

Nils Burmeister[1], Eilika Zorn[1], Aneeq Farooq[1], **Lena Preuss[2]**, Christel Vollstedt[2], Timo Friedrich[1], Tomi Mantel[3], Nico Scharnagl[4], Marcus Rohnke[5], Mathias Ernst[3], Sebastian G. Wicha[1], Wolfgang R. Streit[2], and Wolfgang Maison[1]*

1   Department of Chemistry Universität Hamburg Bundesstrasse 45, 20146 Hamburg, Germany

2   Department of Microbiology and Biotechnology Universität Hamburg Ohnhorststrasse 18, 22609 Hamburg, Germany

3   Institute of Water Resources and Water Supply Technische Universität Hamburg Denickestraße 17, 21073 Hamburg, Germany

4   Institute of Surface Science Helmholtz-Zentrum Hereon GmbH Max-Planck-Strasse 1, 21502 Geesthacht, Germany

5   Institute of Physical Chemistry and Center for Materials Research Justus-Liebig-University Giessen Heinrich-Buff-Ring 17, 35392 Giessen, Germany

Check for updates

RESEARCH ARTICLE

Surface Grafted *N*-Oxides have Low-Fouling and Antibacterial Properties

Nils Burmeister, Eilika Zorn, Aneeq Farooq, Lena Preuss, Christel Vollstedt, Timo Friedrich, Tomi Mantel, Nico Scharnagl, Marcus Rohnke, Mathias Ernst, Sebastian G. Wicha, Wolfgang R. Streit, and Wolfgang Maison*

Low-fouling materials are often generated by surface zwitterionization with polymers. In this context, poly-*N*-oxides have recently attracted considerable attention as biomimetic stealth coatings with low protein adsorption. Herein, this study reports that poly-*N*-oxides can be grafted from plasma-activated plastic base materials. The resulting hydrophilic surfaces have low-fouling properties in bacterial suspensions and suppress the formation of biofilms. Moreover, efficient antibacterial activity against Gram-negative and Gram-positive bacteria caused by release of reactive oxygen species is observed. The latter effect is specific for polymeric *N*-oxides and is most likely triggered by a reductive activation of the *N*-oxide functionality in the presence of bacteria. In contrast to other zwitterionic polymers, *N*-oxides combine thus low-fouling (stealth) properties with antibacterial activity. The bioactive *N*-oxide groups can be regenerated after use by common oxidative disinfectants. Poly-*N*-oxides are thus attractive antibacterial coatings for many base materials with a unique combined mechanism of action.

1. Introduction

Almost all materials are rapidly covered by biomolecules and microorganisms when exposed to biological media. This so-called biofilm formation is of fundamental importance in nature and has implications for many industrial processes and the health sector.[1] For in vivo applications, the adhesion of biomolecules to surfaces contributes to immunogenicity and low blood compatibility.[2] Microbial biofilms enhance the development of resistance and increased pathogenicity of microbes[3]

causing unwanted spread and/or infections in hospitals, implants, food packaging, the distribution of drinking water and other areas.[4] Low-fouling (also antifouling or stealth) surfaces are designed to prevent the attachment of biomolecules and microorganisms.[5] Low-fouling surface properties come typically with good biocompatibility of materials. This allows in vivo applications without platelet activation or the initiation of the foreign body recognition system.[6] Biocompatibility is thus often linked to low-fouling, although the two concepts are not synonymous. However, there is a strong overlap in the technology used to implement them. Surface zwitterionization, often achieved by grafting polymeric zwitterions, is a particularly successful method in this context.[7] The resulting polymer layers are strongly hydrated and they install a protective water layer at the material/solution interface.[8] Zwitterions fit therefore the requirements defined by Whitesides for low-fouling applications.[9]

Three major classes of zwitterions have been used frequently for low-fouling applications: phosphobetaines $-OPO_3^-(CH_2)_nN^+Me_3$,[10] carboxybetaines $-N^+(CH_2)_nCO_2^-$[11] and sulfobetaines $-N^+(CH_2)_nSO_3^-$.[12] It has been demonstrated that the hydration properties of these polymers depend on the alkyl spacer $-(CH_2)_n-$ between the anionic (acidic) and the

N. Burmeister, E. Zorn, A. Farooq, T. Friedrich, S. G. Wicha, W. Maison
Department of Chemistry
Universität Hamburg
Bundesstrasse 45, 20146 Hamburg, Germany
E-mail: wolfgang.maison@uni-hamburg.de

L. Preuss, C. Vollstedt, W. R. Streit
Department of Microbiology and Biotechnology
Universität Hamburg
Ohnhorststrasse 18, 22609 Hamburg, Germany

T. Mantel, M. Ernst
Institute of Water Resources and Water Supply
Technische Universität Hamburg
Denickestraße 17, 21073 Hamburg, Germany

N. Scharnagl
Institute of Surface Science
Helmholtz-Zentrum Hereon GmbH
Max-Planck-Strasse 1, 21502 Geesthacht, Germany

M. Rohnke
Institute of Physical Chemistry and Center for Materials Research
Justus-Liebig-University Giessen
Heinrich-Buff-Ring 17, 35392 Giessen, Germany

Surface grafted *N*-Oxides have low fouling and antibacterial properties

**ADVANCED
SCIENCE NEWS**
www.advancedsciencenews.com

**ADVANCED
MATERIALS
INTERFACES**
Open Access
www.advmatinterfaces.de

cationic ammonium group (other cations besides ammonium groups have also been used but are less common). A short alkyl spacer was found to be advantageous for optimal low-fouling properties in most studies.[13] Recently, Jiang et al. introduced consequently polymeric *N*-oxides –N$^+$—O$^-$ as low-fouling and biocompatible polymers.[14] With only one sigma bond, *N*-oxides contain the smallest possible spacer to separate the charges in a zwitterion. In addition, *N*-oxides have several desirable properties for low-fouling applications. They are easy to prepare by oxidation of tertiary amines[15] and they have a dative N$^+$–O$^-$ bond with extremely high charge separation compared to homologue P$^+$–O$^-$ or S$^+$–O$^-$ bonds. Consequently, *N*-oxides have high dipole moments of 4-5 D[16] and form strong hydrogen bonds with water.[17] This makes *N*-oxides powerful kosmotropes,[18] a property used technically, for example as kinetic hydrate inhibitors to avoid the formation of gas clathrates in gas or oil production.[19] The same properties are also used in nature for example with trimethylammoniumoxide (TMAO), a natural *N*-oxide found in seawater fish (and also in humans).[20,21] TMAO stabilizes proteins by counteracting protein-denaturing compounds (eg. chaotropes like urea) or denaturing forces like heat and pressure. It is also notable that *N*-oxides of alkaloids are non-toxic derivatives of their toxic membrane-permeable parent amines used for vesicle storage in plants and insects.[22] With the transfer of these properties to a polymeric *N*-oxide (PTMAO), Jiang et al. demonstrated that zwitterionization of surfaces with PTMAO leads to extremely low levels of blood protein adsorption and reduced fibroblast adhesion. It was also shown that protein conjugates of PTMAO were invisible to immune recognition in mice. These interesting findings trigger the question: Are polymeric *N*-oxides also efficient low-fouling reagents to prevent the formation of microbial biofilms on surfaces? Several other questions come to mind, when considering the fundamental differences of *N*-oxides compared to other zwitterions. In addition to the (favorable) properties mentioned above, *N*-oxides contain a weak N—O bond and are chemically reactive compounds.[23] This is reflected by their common use as oxidants and intermediates in organic synthesis[24] as well as biosynthesis.[25] Several *N*-oxides of low molecular weight are biologically active and have been explored as drugs.[22c,26] Reductive metabolism by microorganisms or in hypoxic tissue triggers their biological activity as antibiotics or cytotoxic compounds for chemotherapy.[27] Polymeric *N*-oxides are used as oxidants in organic synthesis,[24c] as cathode interlayer materials in organic solar cells[28] and have been found to be active against silicosis.[29] The chemical reactivity as well as the antibacterial and cytotoxic properties of many *N*-oxides raises questions about additional biological activities of polymeric *N*-oxides beyond their stealth properties.[30]

The most important questions addressed by this study are thus: 1. Do polymeric *N*-oxides on surfaces have antifouling properties for microorganisms? 2. How durable are their effects given their relatively high chemical reactivity? 3. Do polymeric *N*-oxides have other biological effects besides their stealth properties? 4. Are the biological effects of polymeric *N*-oxides different from those of their small molecule analogues? In this report, we use grafted polymeric *N*-oxides on polyethylene (PE) as a base material to address the questions above.

2. Results

2.1. Surface Grafting of Poly-*N*-Oxides to Polyethylene

Covalent zwitterionization of PE with polymeric *N*-Oxides was performed via a three-step procedure (**Figure 1**). Briefly, the chemically unreactive PE surface was activated through an atmospheric plasma treatment. The resulting reactive functionalities serve as anchor points for heat-induced graft polymerization of a suitable precursor of the methacrylate- or vinylbenzyl-type (either VBDMA, MADMA or MAADMA) to form the corresponding polymer brushes (poly-VBDMA, poly-MADMA or poly-MAADMA). These two initial steps followed an established procedure for surface modification of PE from our lab.[31] Final zwitterionization of the polymer brushes was achieved by post-grafting oxidation with H$_2$O$_2$. An alternative direct polymerization of monomeric *N*-oxides of the methacrylate- or vinylbenzyl-type (as described for the syntheses of other polymeric *N*-oxides)[14] was not an option here because the *N*-oxide moieties were found to be not compatible with the heat-induced polymerization protocol employed. Successful grafting and subsequent oxidation were reflected by extremely low static contact angles θ = 10–30° with water for the resulting materials PE-poly-(VBNOx), PE-poly-(MAANOx) an PE-poly-(MANOx) (**Table 1**). In addition, the presence of poly-*N*-oxides was confirmed by combined 3D mass spectrometric and scanning probe microscopy (SPM) analysis by a variety of characteristic nitrogen and oxygen-containing organic mass fragments such as CN$^-$ and CNO$^-$ (**Figure 2**). SPM images taken before and after depth profiling with a time-of-flight secondary ion mass spectrometer (ToF-SIMS) revealed a surface roughness R_a of 1–2.5 µm and a brushlayer thickness of $\approx$50–100 nm.

The successful immobilization of polymeric *N*-oxides on PE was also verified by ATR-FTIR spectroscopy and X-ray photoelectron spectroscopy (XPS) analysis. Exemplary data is depicted in **Figure 3** (see Figure S1, Supporting Information for IR-spectra of other materials). The FTIR-spectra of PE-poly-(VBNOx) in Figure 3a reveal the characteristic N-O vibration at 933 cm^{-1}, which is also visible in the monomer (VBNOx) spectrum. These characteristic N—O bands are also observed for the other zwitterionic materials PE-poly-(MANOx) and PE-poly-(MAANOx), along with carbonyl bands from the polymethacrylate and polymethacrylamide backbones (spectra not shown, see Figure S1, Supporting Information). For full characterization of the grafting process, we performed XPS measurements of pristine PE, plasma activated PE and modified poly-(*N*-oxide)-PE (see SI for additional spectra). The spectra revealed the presence of peroxides on the PE surface after plasma activation with a dominant peak at 532.4 eV in the O1s spectra (Figures S3 and S4, Supporting Information). The atomic ratios of N/C was 0.07 which is similar to the theoretical value of 0.09 and indicates successful radical polymerization and subsequent oxidation to PE-poly-(VBNOx) (Figure S5, Supporting Information). Slight deviation of the theoretical atomic ratios of N/O and O/C can be explained by impurities, probably associated to polymer entrapped carbon monoxide and/or water. The deconvoluted peak at 402.6 eV in the N1s spectra was assigned to the quaternary ammonium group in the N—O bond which is also reflected by a peak at 531.0 eV in the O1s spectra (Figure 3b). Both, N1s and
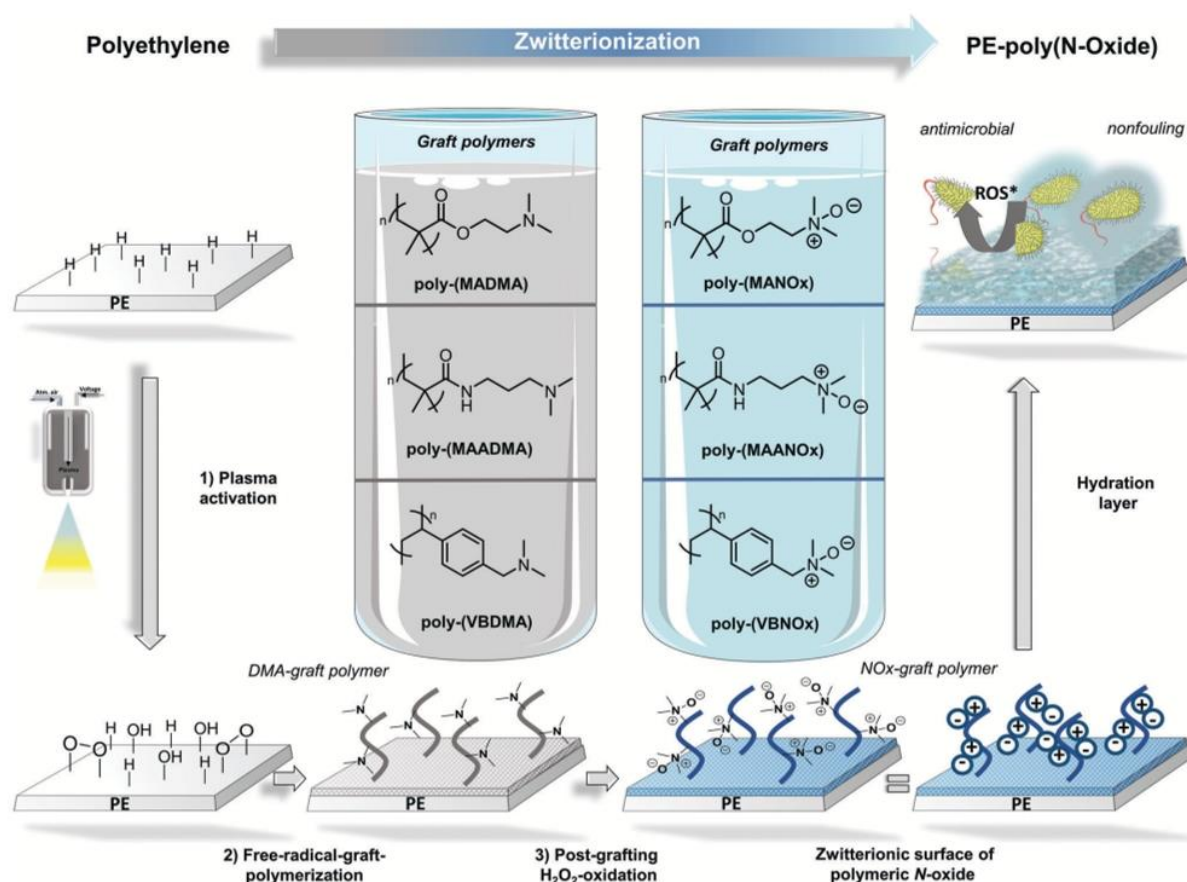
Figure 1. Surface grafting of *N*-oxides to PE foils. 1) Plasma activation of otherwise inert PE, 2) heat-induced radical polymerization, 3) post-grafting zwitterionization of the polymer brushes by oxidation of tertiary amines to *N*-oxides with H_2O_2.

O1s binding energies are consistent with previous reports on polymeric *N*-oxides. N1s spectra indicate good conversion of tertiary amines to the corresponding *N*-oxides by H_2O_2-treatment for 72 h. However, the signal at 399.3 eV can be assigned to residual tertiary amines. Furthermore, a detailed deconvolution of N1s spectra reveals an additional small signal at 400.3 eV, which is also detectable in the survey spectra of pristine PE (Figures S2,S5, and S6, Supporting Information). These minor impurifications are due to non-identified nitrogen species on the surface.

2.2. Microbiological Assessment of Low-Fouling Activity

The low-fouling activity of PE with three different grafted *N*-oxides was tested with a bacterial adhesion assay and a LIVE/DEAD staining.[31b,32] *Staphylococcus aureus* (Gram-positive, strain ATCC29213) was used as a model pathogen. It is a clinically relevant pathogen responsible for many health care related infections.[33] In addition, *Vibrio campbellii* (previously classified as *Vibrio harveyi*) (Gram-negative, strain BB120 was used as a second model organism because it is a major

Table 1. Polymerization conditions and water contact angles (WCA) for grafted polymers on PE.

Entry	Monomer [wt%]	AIBN [wt%]	PE-poly-(XXDMA), WCA [°] [a]	PE-poly-(XXNOx), WCA [°] [a]
1	–	–	–	pristine PE, 95.2 ± 1.6
2	VBDMA, 40	1.0	PE-poly-(VBDMA), 9.9 ± 1.4	PE-poly-(VBNOx), 9.9 ± 1.4
3	MADMA, 20	0.1	PE-poly-(MADMA), 19.8 ± 2.	PE-poly-(MANOx), 19.8 ± 2.3
4	MAADMA, 40	0.1	PE-poly-(MAADMA) 29.4 ± 1.9	PE-poly-(MAANOx) 29.4 ± 1.9

[a] Advancing WCA were measured with deionized water using the static sessile drop method and are given as mean value ± SD of at least three independent samples.
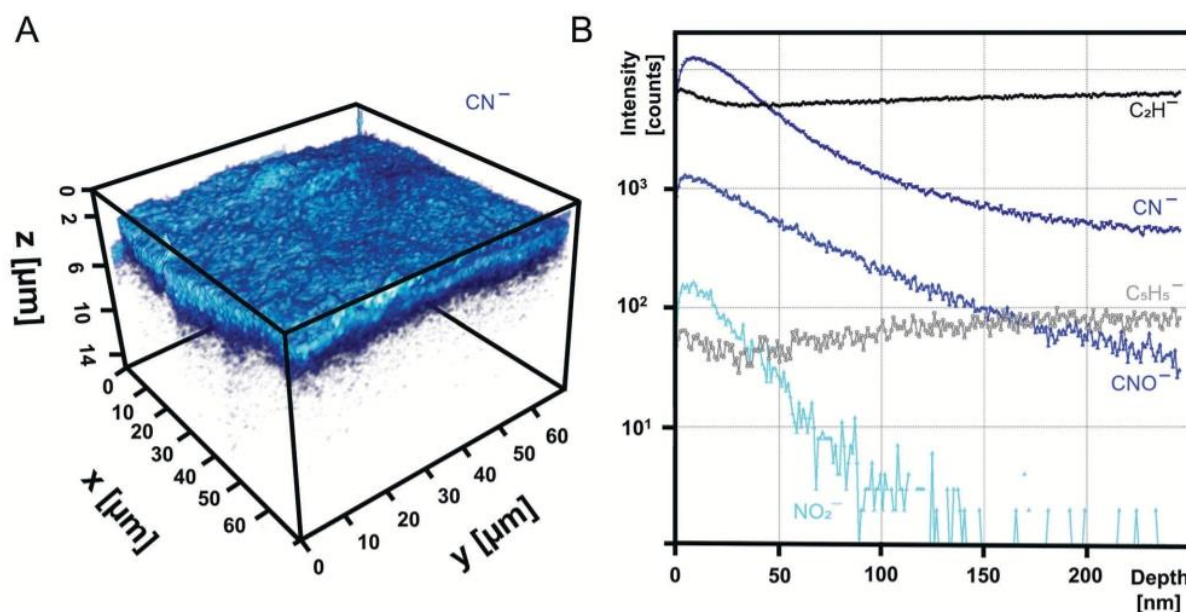
Figure 2. Combined 3D ToF-SIMS and SPM imaging analysis of PE-poly-(VBNOx). A) Correlative SPM/SIMS-3D image of the poly-(VBNOx) coating layer with the spatial distribution of CN^- as the most intensive ion on top of the substrate. Shades of blue correspond to signal intensity of CN^-. B) ToF-SIMS depth profile of PE-poly-(VBNOx) with poly-(VBNOx)-specific nitrogen containing mass fragments CN^-, CNO^-, and NO_2^- and characteristic PE fragments C_2H^- and $C_5H_5^-$. SIMS analysis was performed in negative ion mode with Bi_3^{++} ions. Depth profiling was carried out using Ar^+_{2000} cluster ions for sputtering.
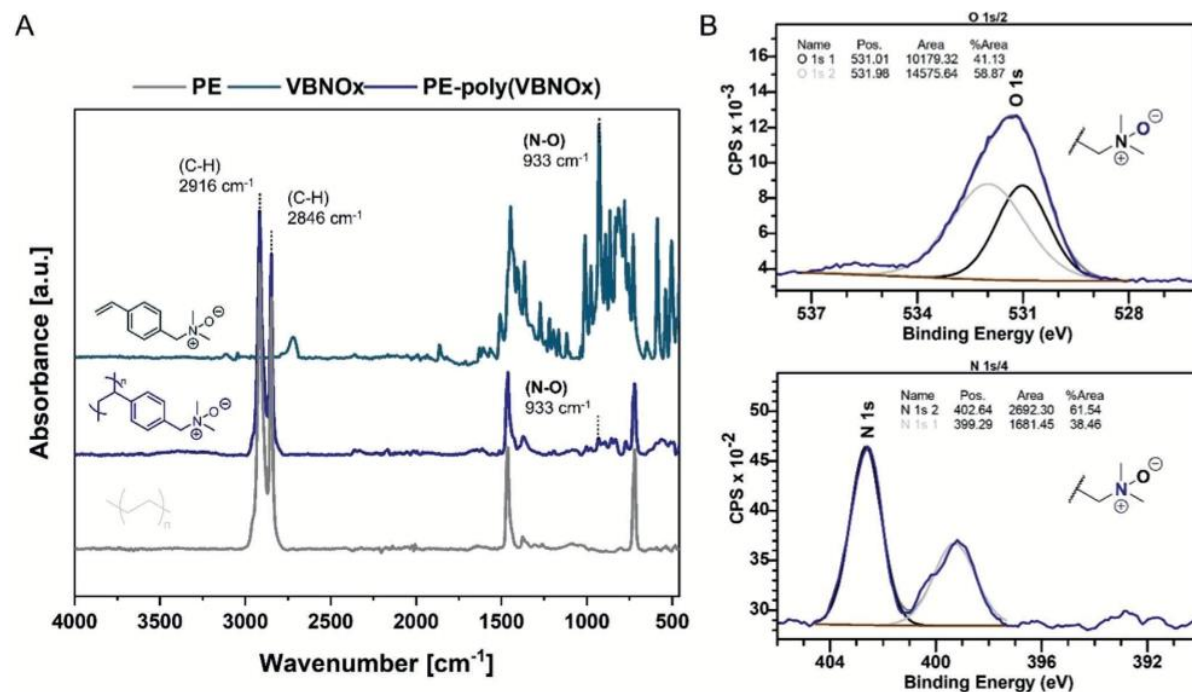
Figure 3. Characterization of PE-poly-(VBNOx) by ATR-FTIR and XPS. A) ATR-FTIR spectra in absorbance mode of pristine PE, PE-poly-(VBNOx), and VBNOx monomer for comparison. B) Deconvoluted regions of O1s and N1s XPS spectra of PE-poly-(VBNOx). Survey spectra of pristine PE, plasma activated PE and PE-poly-(VBNOx) are available in the supporting material.
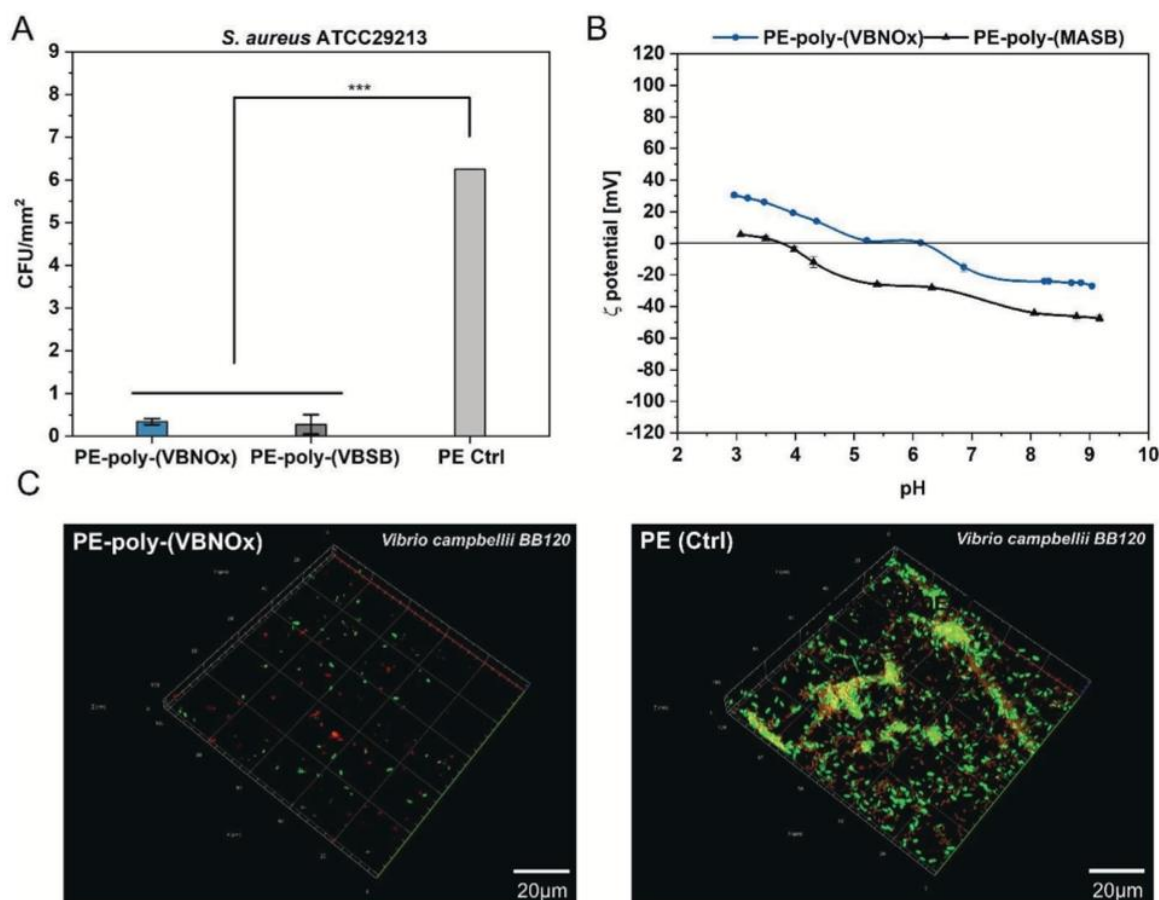
Figure 4. Microbiological assessment of low-fouling surfaces. A) Bacterial adhesion assay with *S. aureus* (strain ATCC29213): Colony counts after incubation of PE-poly-(VBNOx), PE-poly-(VBSB) and pristine PE as control (Ctrl) with *S. aureus* (initial concentration: 10^5 CFU mL^{-1} in MHB) for 24 h. Statistical significance was determined via pairwise comparison (Tukey test) $p \leq 0.001$ (***). B) Zeta potential measurement of PE-poly-(VBNOx) and PE-poly-(MASB) at pH 3–9. C) Biofilm adhesion: confocal microscopy of PE-poly-(VBNOx) (left) and PE (right) after 24 h incubation with *V. campbellii* (strain BB120) in artificial seawater, followed by LIVE/DEAD^{TM} staining. Live bacteria appear light green, dead bacteria red. The images indicate representative areas within static biofilms.

contributor to the marine microbiome and has also been identified as a potential pathogen in coastal water. Moreover, *V. campbellii* forms rapidly biofilms on plastic substrates (particularly on PE) accompanied with high antibiotic resistance.[34] Briefly, sterilized test specimens (size: 1.0 cm^2) were fully immersed in a bacterial suspension (10^2–10^5 CFU mL^{-1}) and stored with gentle shaking ensuring complete contact of the materials with the inoculum. After 24 h, samples were transferred into a sterile saline solution to desorb loosely attached microbes. Growth controls of each media were collected at this point to verify presence and concentration of living bacteria. Finally, test specimens were printed carefully onto an agar plate (Columbia Agar) and were subsequently incubated at 37 °C for 20 h before colony counting. Pristine PE specimens were used as controls. In addition, a poly-sulfobetaine grafted zwitterionic PE sample (PE-poly-(VBSB)) with known excellent low-fouling properties was used for comparison.[31b] The results shown in **Figure 4**a reveal a low-fouling effect of the grafted polymeric *N*-oxide on

PE (PE-poly-(VBNOx)), comparable to the corresponding polymeric sulfobetaine control material (PE-poly-(VBSB)). A second adhesion assay was performed with the marine organism *V. campbellii* in artificial seawater, followed by confocal microscopy after a LIVE/DEAD staining (LIVE/-DEAD BacLight Viability Kit). The resulting images after incubation confirmed the low-fouling activity of PE-poly-(VBNOx) and show almost no adhering live bacteria (green fluorescence) on PE-poly-(VBNOx) after 24 h immersion in seawater whereas pristine PE was rapidly colonized by bacteria (Figure 4C). Polymeric *N*-oxides like poly-(VBNOx) have thus excellent low-fouling activity against the here tested Gram-negative and Gram-positive bacteria and are competitive with established zwitterionic materials such as polysulfobetaines. *N*-oxides (pKa $\approx$4–5) have significantly higher pKa values than sulfonic acids in sulfobetaines (pKa $\approx$1–2). The zeta potential of zwitterionic materials bearing sulfobetaines is thus strongly negative in a broad pH range.[35] In contrast, the analysis of poly-*N*-oxide materials like PE-poly-(VBNOx) revealed

only slightly negative to neutral zeta potentials at biologically most relevant pH values of 5–8.[36] Neutral surface zeta potentials were previously found to be ideal for optimal low-fouling performance.[35]

2.3. Antibacterial Activity of Poly-(*N*-Oxides)

The observed low-fouling activity of polymeric *N*-oxides against bacteria has not been described before. However, it is not surprising, given the reported low protein fouling of these materials.[14,36] It was notable though, that a dramatic antimicrobial effect was observed in the growth controls of the adhesion assays. When bacterial solutions were exposed to PE-poly-(VBNOx) almost all bacteria were immediately killed. This was a striking contrast to growth controls of pristine PE and also sulfobetaine PE-poly-(VBSB). Both did not reveal any antibacterial effect. The antimicrobial activity of three different *N*-oxides was therefore confirmed by a quantitative analysis according to ASTM E2149-13a, a common assay to evaluate antimicrobial materials.[37] We selected *S. aureus* (Gram-positive, strain ATCC29213) and *E. coli* (Gram-negative, strain ATCC25922) for the assay. Briefly, sterilized PE test specimens were immersed with bacterial solutions of 10^5 CFU mL^{-1} at 37 °C. After incubation for 2 h, the resulting solutions were aliquoted in *log* levels ranging from 10^5–10^2 CFU mL^{-1} onto Columbia agar and were subsequently incubated for 17 h before colony counting. Results are depicted in **Figure 5** and reveal a remarkable antimicrobial effect of the poly-*N*-oxide-grafted materials for both Gram-positive *S. aureus* and Gram-negative *E. coli*.

The antimicrobial effect was confirmed for all three polymeric *N*-oxides tested and is thus not dependent of the polymer backbone structure. However, the methacrylamide-derivative PE-poly-(MAANOx) showed a lower antimicrobial effect than both other *N*-oxides. This might indicate an effect of the alkyl-spacer length or the linking functionality (amide vs ester) of the polymerizable group on antibacterial activity. Either a release of antimicrobial compounds from the material or a contact-active mechanism might explain the observed antibacterial effect. The latter would be principally possible due to the high pK$_a$ value of *N*-oxides. This might cause protonation under slightly acidic conditions created by colonizing bacteria. Significant protonation of PE-poly-(VBNOx) starts at pH values lower than 4, leaving a positively charged and thus possibly contact-active surface, as evident from the zeta potential measurements in Figure 4B. However, such low pH values have only been reported locally in biofilms.[38] We have not detected any biofilm formation or adhesion of bacteria to the *N*-oxide test specimens in our adhesion assays making contact activity unlikely. Further evidence for a release mechanism came from an agar plate diffusion test (DIN EN ISO 20645:2002-02) with *S. aureus* and *E. coli*. An inhibition zone around the poly-*N*-oxide test specimen was clearly visible supporting leaching of antimicrobial compounds (Figure S7, Supporting Information). Release of residual H$_2$O$_2$ from the oxidative preparation of *N*-oxide polymer brushes was excluded through inspection of the XPS spectra and via a horseradish peroxidase assay (Figure S10, Supporting Information)[39] This assay is sensitive to H$_2$O$_2$-concentrations in the micromolar range which is or-

ders of magnitudes lower than the MIC of H$_2$O$_2$ for *S. aureus* (MIC = 0.27-0.66 mM) and *E. coli* (MIC = 1.33-2.66 mM).[40]

As mentioned in the introduction, some *N*-oxides have been reported to have antimicrobial or cytotoxic properties. These compounds are typically benzotriazine dioxides or phenazine dioxides of low molecular weight. A prototype is tirapazamine (TPZ, MW = 178 g mol^{-1}), an experimental anticancer drug and antibiotic. The mode of action of TPZ involves most likely a reductive activation leading to the formation of cytotoxic hydroxyl radicals by cleavage of a N—O bond.[27] The latter homolytic bond cleavage is not surprising because the bond dissociation energies of *N*-oxides are known to be relatively low.[23] However, the formation of reactive oxygen species from *N*-oxides under physiological conditions has been reported for a limited set of compounds only but not for polymeric *N*-oxides.[27] The formation of radical species from grafted polymeric *N*-oxides was tested with DPPH*, a stable radical commonly used as a radical scavenger. The DPPH*-radical has an absorption maximum at 520 nm and the loss of absorption intensity at this wavelength can be correlated to the formation of radical adducts.[41] Treatment of PE-poly-(VBNOx) with DPPH* at 37 °C lead to significant scavenging of DPPH* after 2 h and almost complete DPPH* consumption after 24 h (**Figure 6**a). In contrast, the corresponding monomeric *N*-oxide VBNOx leads to only minor consumption of DPPH* after 24 h suggesting that only polymeric *N*-oxides generate potentially antibacterial radical species under physiological conditions. The identity of the generated radicals was analyzed by electron paramagnetic resonance (EPR)-spectroscopy after treatment of PE-poly-(VBNOx) with DMPO as a spin trap. The resulting EPR spectra show the presence of a radical trapped by DMPO (Figure 6b). The analysis of respective hyperfine coupling constants (a_N = 15.9 G and a^β_H = 4.1 G) revealed an oxygen-centered radical, either a hydroxyl-radical (OH*) or a superoxide-radical (O^{2-}*)[42] and is a clear indication of released reactive oxygen species (ROS-formation). Again, generation of ROS species was found to be specific for the grafted polymeric *N*-oxides but was not observed for the monomeric *N*-oxide (VBNOx) (Figure 6). In consequence, no antibacterial activity of VBNOx was detected and we determined minimal inhibitory concentrations (MIC) of VBNOx > 1024 µg mL^{-1} for *E. coli* and *S. aureus* (Table S1, Supporting Information).

The release of ROS from polymeric *N*-oxides triggered questions regarding the fate of the material and the durability of the observed antibacterial effect. Specimens of PE-poly-(VBNOx) were therefore repeatedly exposed to bacteria according to ASTM E2149-13a. **Figure 7** shows the results of these experiments. They reveal a retained activity of the material after repeated use with no measurable loss in function. The antibacterial activity after repeated use is not dependent on intermediate purification and treatment of the test specimens before the next incubation experiment. Intermediate treatment of PE-poly-(VBNOx) with three different disinfection reagents (NaOCl, H$_2$O$_2$ and *i*PrOH/PrOH/EtOH (BacillolAF)) lead to identical antibacterial activity of the material. Activity is also retained if no disinfection is performed between incubations. However, the transfer of residual bacteria leads to a significantly higher (>10^5 CFU mL^{-1}) initial concentration of bacteria in the test solutions after repeated incubation. The resulting high inoculum leads to a slight
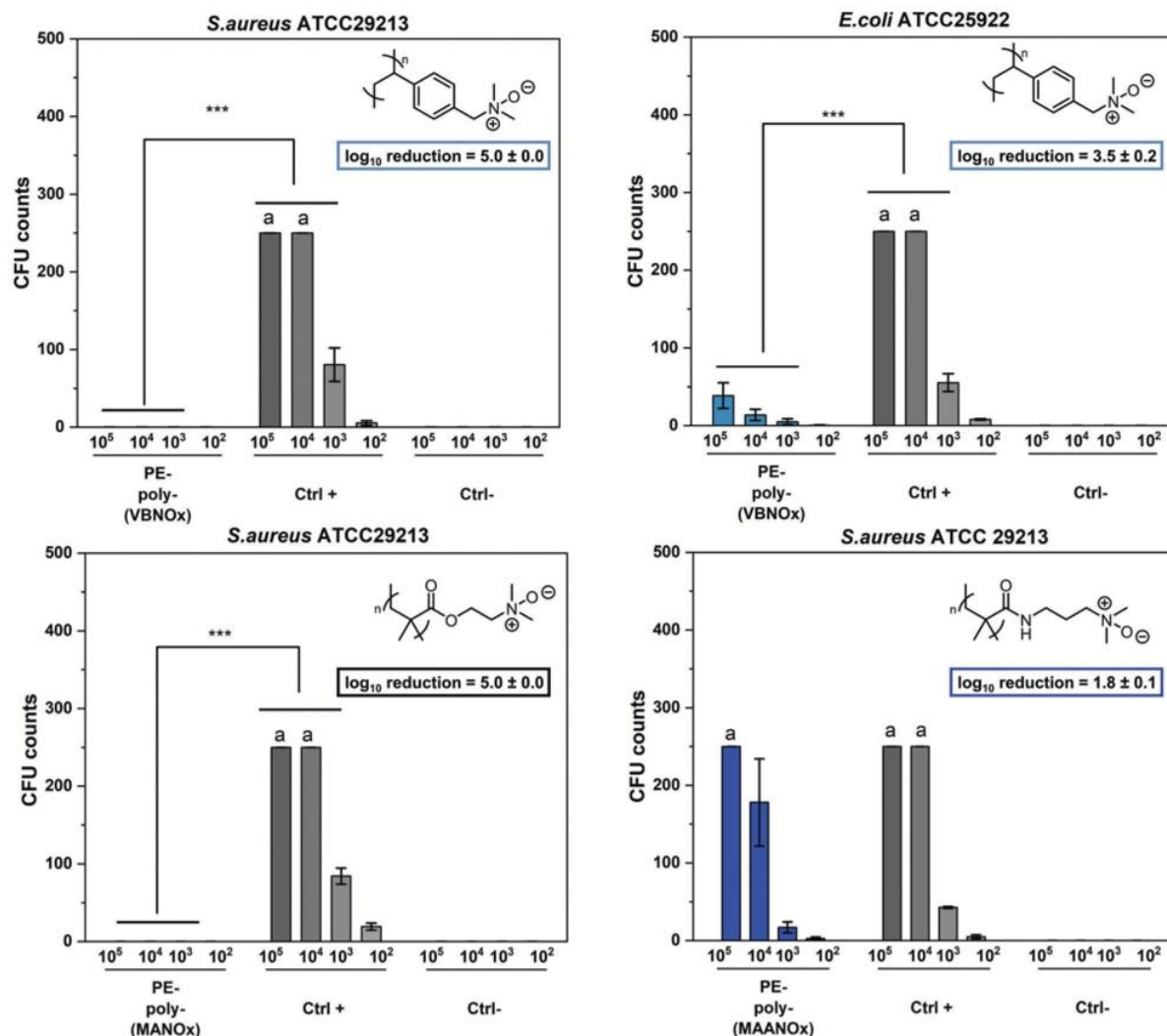
Figure 5. Antibacterial activity of three different grafted polymeric *N*-oxides on PE measured by ASTM E2149-13a. Colony counts after incubation of PE test specimens with bacterial suspensions at different dilutions (10^5–10^2 CFU mL^{-1}) for 2 h. Each experiment was performed in triplicate, pristine PE (Ctrl +) and pure saline (Ctrl -) were used in control experiments. Colony counts above 250 were set as "too numerous to count" (TNTC) (a). Log10 reduction was calculated as described in the experimental. Statistical significance was determined via pairwise comparison (Tukey test) $p \leq 0.001$ (***), $p \leq 0.01$ (**).

increase of surviving bacteria after the repeated 2 h exposure to the PE-poly-(VBNOx) specimen. Analysis of the test specimens after repeated exposure to microorganisms revealed identical chemical and physical properties of the material. It is notable that we observed no degradation of the grafted polymeric *N*-oxides. Chemical degradation processes of *N*-oxides can lead to the formation of hydroxylamines and carbonyl groups, although these conversions are typically observed at higher temperatures than our test conditions.[15,24a] We did not find any evidence for these functional groups and in addition, the contact angle and the zeta potential of the materials remained constant after threefold use (Figure S13, Supporting Information). The release of ROS

from polymeric *N*-oxides at room temperature is most likely a consequence of a reductive activation of the *N*-oxide in the presence of microorganisms. It might thus follow the same mechanisms reported for cytotoxic activation of some *N*-oxides in hypoxic tumor tissue.[26a,b,27,43]

3. Discussion

Three different polymeric *N*-oxides were successfully grafted to PE as a base material. We have used an established two-step protocol involving atmospheric plasma activation of PE and subsequent heat-induced graft polymerization of methacrylate,

70
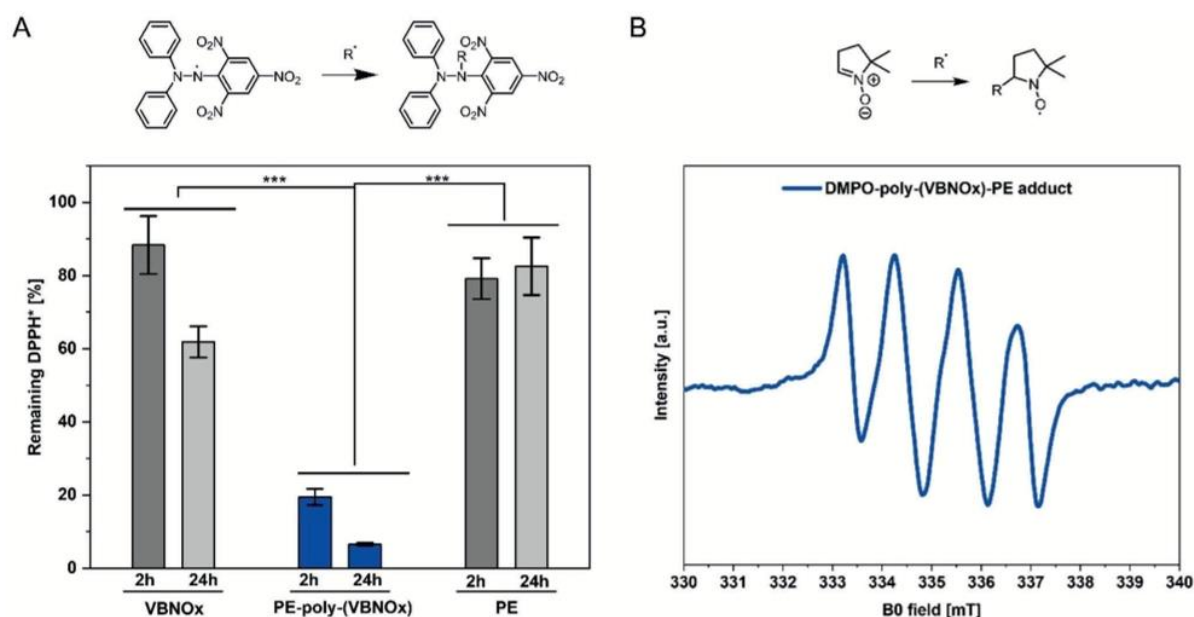
Figure 6. Evaluation of ROS formation from PE-poly-(VBNOx). A) DPPH radical scavenging and remaining DPPH-radical after exposure to VBNOx (1024 µg mL^{-1}), PE-poly-(VBNOx) (surface area: 1 cm^2), and pristine PE (surface area: 1 cm^2) at 37 °C in MeOH. B) EPR spectra after treatment of DMPO with a PE-poly-(VBNOx) specimen (surface area: 1 cm^2). Control experiments were performed with pristine PE + DMPO and PE-poly-(VBNOx) without DMPO, data available in the supplementary material (Figure S12, Supporting Information). Statistical significance was determined via pairwise comparison (Tukey test) $p \leq 0.001$ (***).
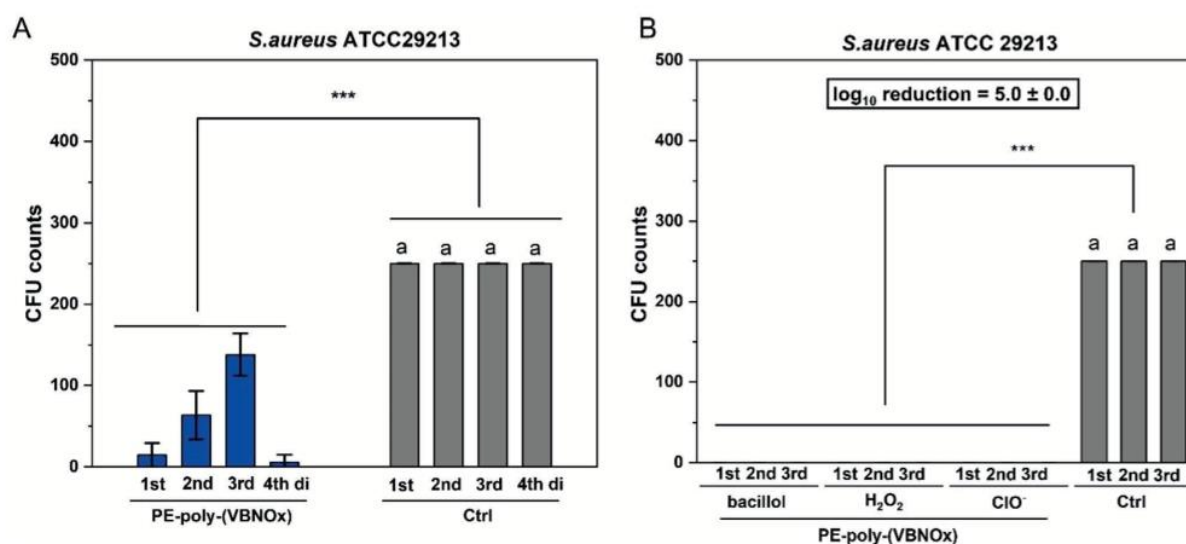
Figure 7. A) Repeated use of pristine PE (Ctrl) and PE-poly-(VBNOx) specimens (surface area: each 1.0 cm^2) in an antibacterial assay following ASTM E2149-13a. The test specimens were exposed to the incubation solutions without intermediate disinfection three times (1st, 2nd, 3rd). An additional fourth exposure was performed after H$_2$O$_2$ disinfection (4th di). B) Repeated antibacterial assay (ASTM E2149-13a with *S. aureus*) for pristine PE and PE-poly-(VBNOx) specimens (surface area: each 1.0 cm^2). The test specimens were exposed to new incubation solutions (10^5 CFU mL^{-1}) after intermediate disinfection (BacillolAF: *i*PrOH/PrOH/EtOH, aqueous H$_2$O$_2$ (30% v/v) and aqueous NaOCl (12% v/v)) three times (1st, 2nd, 3rd). Bars represent mean values ± SD of three independent measurements. Colony counts above 250 were set as "too numerous to count" (TNTC) (a). Statistical significance was determined via pairwise comparison (Tukey test) $p \leq 0.001$ (***).

71

methacrylamide and vinylbenzene monomers. The process generates covalently linked dense polymer brushes of polymeric tertiary amines. These were oxidized with H_2O_2 to the target polymeric *N*-oxides in a final step. The resulting materials were characterized by IR, XPS and ToF-SIMS confirming the complete conversion of tertiary amine groups to the corresponding *N*-oxides. We found a brush layer thickness of $\approx$50–100 nm for the grafted polymeric *N*-oxides. The surfaces are characterized by extremely low static contact angles $\theta = 10$–$30°$ with water and almost neutral zeta potentials in the pH range from 5–7 for PE-poly-(VBNOx), PE-poly-(MAANOx) and PE-poly-(MANOx). The latter parameter distinguishes grafted poly-*N*-oxides from other poly-zwitterions such as sulfobetaines which have negative zeta potentials at pH values as low as 4, reflecting the higher acidity of sulfonic acids ($pk_a \approx 1$–2) compared to *N*-oxides ($pk_a \approx 4$–5).

The whole process of *N*-oxide grafting described herein is scalable and uses readily available starting materials. It should also be applicable to many other plastics besides PE as a base material. However, the heat-induced graft polymerization is not compatible with monomers containing *N*-oxides because these are intrinsically unstable at higher temperatures. This is a notable difference to other grafting procedures such as copper catalyzed surface-initiated atom transfer radical polymerization (SI-ATRP), which has been shown to be compatible with *N*-oxide monomers.[14] The low water contact angles and the almost neutral zeta potentials of all three grafted poly-*N*-oxides (PE-poly-(VBNOx), PE-poly-(MAANOx) an PE-poly-(MANOx)) are ideal parameters for low-fouling surfaces. These stealth properties of poly-*N*-oxides have been shown to prevent protein adhesion before.[14,36,44] It was therefore not surprising that we also observed good low-fouling properties in bacterial adhesion tests against *S. aureus*, an important pathogen for health care related infections and *V. campbellii*, a marine microorganism.

However, beside the confirmation of a low-fouling effect for poly-*N*-oxides, the growth controls of these adhesion experiments revealed clear antibacterial properties. These were confirmed in standard ASTM assays with Gram-negative and Gram-positive bacteria. We attribute these antibacterial properties to the generation and release of radicals, which we confirmed at 37 °C via DPPH as a radical scavenger. The resulting EPR spectra of DMPO-radical adducts revealed the generation of ROS from poly-*N*-oxide surfaces. Other possible reasons for the antibacterial properties of poly-*N*-oxides such as contact-activity through protonation of *N*-oxides or release of residual (antibacterial) H_2O_2 are unlikely. A release mechanism is clearly supported by an inhibition zone around the PE-poly-*N*-oxide specimens which would not be observed for a contact-active material. Release of residual H_2O_2 was excluded via a sensitive HRP-assay. The generation of ROS from *N*-oxides under physiological conditions has been reported for a limited set of aromatic *N*-oxides of low molecular weight only. It has been reported that the release of ROS from drugs containing *N*-oxide groups (e.g., tirapazamine) is triggered in hypoxic tumor tissue or in the presence of bacteria by reductive activation. In this context it is remarkable that we found the generation of ROS to be an exclusive feature of poly-*N*-oxides (PE-poly-(VBNOx), PE-poly-(MAANOx) and PE-poly-(MANOx)) and it was not observed in close analogues of low molecular weight such as VBNOx, MANOx or MAANOx. The latter compounds did not show any ROS formation and did also not have appreciable levels of antibacterial activity (MICs > 1024 µg mL^{-1} against *E. coli* and *S. aureus*).

We propose that the formation of ROS from poly-*N*-oxides follows a similar mechanism as tirapazamine and derivatives. Further evidence for this hypothesis comes from a recent report of Gao and coworkers.[43a] In this study, polymeric *N*-oxides were used as selective drug carriers for hypoxic tumor tissue (see also[45]) due to their bioreduction by CYP450-enzymes. We suspect that a similar reductive conversion of poly-*N*-oxides occurs in the presence of microorganisms leading to ROS release and thus antibacterial activity. In contrast to the most common chemical *N*-oxide degradation mechanisms mentioned above, this bioreductive pathway reduces PE-poly-(VBNOx), PE-poly-(MAANOx) an PE-poly-(MANOx) back to the corresponding polymeric tertiary amines PE-poly-(VBDMA), PE-poly-(MAADMA) and PE-poly-(MADMA). The *N*-oxides could then be regenerated from these polyamines explaining the constant antibacterial effects of polymeric *N*-oxides even after repeated exposure to bacteria. This reoxidation step might be mediated by oxidative disinfectants like NaOCl and H_2O_2. Remarkably, we noted no loss of antibacterial activity for repeated use of poly-*N*-oxides even without oxidative intermediate treatment (disinfection with BacillolAF) or even without intermediate disinfection. These latter findings might suggest self-replenishing properties of poly-*N*-oxides, presumably mediated by molecular oxygen either in solution or in air. Both the release of ROS (and thus antibacterial activity) and the reoxidation of the material are clearly special properties of the polymeric *N*-oxide because neither significant ROS production nor antibacterial activity was observed with the corresponding monomeric *N*-oxides of low molecular weight. These special properties might be caused by the close assembly of multiple *N*-oxide functionalities and thus a neighbor group effect in the polymer. Similar effects have been proposed to operate in charge transfer from polymeric *N*-oxides used in intermolecular n- or p-doping processes in optoelectronic devices.[28a,46] Neighbor group effects of polar groups have also been proposed to accelerate oxidations of tertiary amines of low molecular weight.[47]

4. Conclusion

Our studies reveal that grafted polymeric *N*-oxides are attractive low-fouling coatings for plastic base materials and might thus find application in many fields related to bacterial biofilm formation. In contrast to other zwitterionic polymers poly-*N*-oxides do not only generate stealth surfaces upon grafting but have unique antibacterial properties caused by the release of ROS. Poly-*N*-oxides combine thus low-fouling properties with the release of antibacterial compounds in a rather simple polymer. In addition, the biologically active *N*-oxide functionality can easily be regenerated upon oxidation with common disinfectants. Even without added oxidants, we noted antibacterial activity of poly-*N*-oxides upon repeated challenge of our materials with bacteria. However, whether this effect is caused by *N*-oxide regeneration or the large reservoir of *N*-oxide functionalities on the surface needs to be confirmed in future studies. The combined low-fouling and antibacterial mode of action enables applications requiring the eradication of bacteria. If ROS formation limits in vivo applications of poly-*N*-oxides needs to be determined in future studies. However, current in vivo data do not support toxic effects of poly-*N*-

Surface grafted *N*-Oxides have low fouling and antibacterial properties

**ADVANCED
SCIENCE NEWS**

www.advancedsciencenews.com

**ADVANCED
MATERIALS
INTERFACES**
Open Access

www.advmatinterfaces.de

oxides,[14,43a,b,45,48] which is plausible assuming that ROS release is only triggered in hypoxic tumor tissue or in the presence of bacteria.

5. Experimental Section

Chemicals and Materials: Polyethylene (LD-PE) with a thickness of 750 µm was purchased from Goodfellow and were used as received. Vinylbenzylchloride (90 %), dimethylamine solution (33 % in ethanol), azo-bis-(isobutylonitrile) (AIBN) (98 %), hydrogen-peroxide solution (30 % v/v in water), (2-dimethylaminoethyl) methacrylate (99 %), *N*-[3-diemthylamino)-propyl]-methacrylamide (99 %), 2,2-diphenyl-1-pikryl-hydrazyl (DPPH), 5,5-dimethyl-1-pyrrolin-*N*-oxide (DMPO), horseradish peroxidase (250 units per mg), pyrogallol (99 %) were purchased from Sigma-Aldrich. Microorganisms *S.aureus* (strain ATCC29213), *E.coli* (strain ATCC29522) and *Vibrio campbellii* (strain BB120 also known as strain ATCC-BAA-1116) were purchased from American Type Culture Collection. All reagents were used without further purification. Crimp neck vials (N20, 10 mL volume) and crimp caps (N20, PTFE septum) for degassing were purchased from Macherey-Nagel GmbH (Düren, Germany).

Atmospheric Air Plasma: For plasma activation, an atmospheric air plasma system from Plasmatreat GmbH (Steinhagen, Germany) was used. The atmospheric-pressure plasma was produced by a generator FG5001 with an applied working frequency of 21 kHz, generating a non-equilibrium discharge in a rotating jet nozzle RD1004 in combination with the stainless-steel tip No. 22826 for an expanded treatment width of ≈22 mm. Additionally, the jet nozzle was connected to a Janome desktop robot type 2300N for repetitious accuracy regarding treatment conditions. The process gas was dry and oil-free air at an input pressure of 5 bar in all experiments.

IR- and UV/Vis Spectroscopy: Infrared spectra were recorded with an attenuated total reflectance Fourier Transform infrared system (ATR-FTIR), model "IRAffinity-1S" from Shimadzu (Kyoto, Japan) using a "Quest" ATR accessory from Specac. The spectral range was set at 4000 cm^{-1}–400 cm^{-1} with a resolution of 0.5 cm^{-1} in absorbance mode and spectra were processed with OriginPro 9 (2021) software. UV/vis spectra were obtained on a Genesys 10S spectrophotometer from Thermo Scientific (Waltham, USA) using Visionlite software for analysis.

Contact Angle Measurements: Contact angles were acquired with an OCA 20 goniometer from DataPhysics (Filderstadt, Germany) equipped with two automated dispensing units for different liquid probes, a high-speed video system with CCD-camera, measuring stage and halogen-lighting for static and dynamic contact angle measurements. For evaluation, independent triplicate measurements at three different points of the surface were done. Advancing contact angles were measured with deionized water using the static sessile drop method with a dispensing volume of 5 µL. The dispensing rate of the automatic syringe was set at 1 µL min^{-1}. The obtained angle was calculated with the OCA software.

Electrokinetic ζ-Potential Measurements: The surface zeta potential (ζ-potential) was determined as streaming potential using an electrokinetic analyzer Surpass (Anton Paar, Graz, Austria). The measurements were carried out using an adjustable gap cell in which two samples with a rectangular size of 1 cm x 2 cm were clamped vis-á-vis with a micro slit of 110 µm in between. For each measurement, the starting conductivity was set to 17 µS m^{-1} with KCl as electrolyte. The pH was adjusted from 9.5–2.5 stepwise with automatic pH titration by adding 0.05 M HCl. Presented values of z potentials were determined as mean value of four measurements for each pH step.

Nuclear Magnetic Resonance (NMR) Spectroscopy: The measurements were performed in 5 mm o.d. sample tubes using either a Bruker Avance 600, 500, or 400 MHz (AV600, AV500 and AV400, Bruker, Ettlingen, Germany). The obtained spectra were processed with MestReNova x64 software. ^{13}C-spectra were recorded with ^{1}H-decoupling. Peak assignments were supported by 2D NMR experiments like ^{1}H,^{1}H-COSY, ^{1}H,^{13}C-HSQC and ^{1}H,^{13}C-HMBC.

Time of Flight Secondary Ion Mass Spectrometry (Tof-SIMS) and Scanning Probe Microscopy (SPM): The analysis was carried out with an M6 Plus machine (IONTOF Company, Münster, Germany). Here a scanning probe microscope is included in the main vacuum chamber of the ToF-SIMS, which offers the possibility for correlation of topographic and mass spectrometric imaging data. For SIMS analysis 60 keV Bi$_3$$^{++}$ primary ions were used (*I* = 0.05 pA at 200 µs cycle time). The Bi gun (nanoprobe 50) was operated in high-current bunched mode with a beam-defining aperture of 700 µm. For depth profiling, the machine was operated in a non-interlaced mode in combination with a 5 keV Ar$_{2000}$$^+$ sputter beam (*I* = 1.328 nA). Low energetic electrons were used for charge compensation during the pause time of 1 s. An analysis area of 70×70 µm^2 (128×128 pixels) was chosen in the centre of the 200×200 µm^2 sputter area. Depth profiling was stopped at the interface between coating and substrate. Before and after the measurement a scanning probe microscopy image of the analysis area was recorded in intermitted mode with 2048×128 pixels resolution as well as line scans in *x* and *y* directions with a scan length of 600 µm each. Data evaluation was carried out with Surface Lab software version 7.3 (IONTOF Company). Negative mass spectra were recorded and the achieved mass resolution was *m*/D*m* >7.500 (FWHM) at *m/z* = 65.04 (C$_5$H$_5$$^-$).

X-Ray Photoelectron Spectroscopy (XPS): XPS measurements were performed using a KRATOS AXIS Ultra DLD (Kratos Analytical, Manchester, United Kingdom) equipped with a monochromatic Al K$_\alpha$ anode working at 15 kV (225 W). For the survey spectra, a pass energy of 160 eV was used while for the region spectra, the pass energy was 20 eV. The investigated area was 700×300 µm^2. For all of the PE samples, charge neutralization was necessary. The evaluation and validation of the data were carried out with the software CASA-XPS version 2.3.24. The spectra were calibrated by adjusting the C1s signal to 284.5 eV. For deconvolution of the region files, background subtraction (U 2 Tougaard or Shirley) was performed before calculation.

Electron Paramagnetic Resonance (EPR) Spectroscopy: EPR spectroscopy was performed on a Magnettech Miniscope MS400 X-band benchtop spectrometer (9.30–9.55 GHz). The samples were measured in 4 mm quartz glass EPR tubes at RT and 77K. 5,5-Dimethyl-1-pyrrolin-*N*-oxide (DMPO, 100 mm in either MeOH or benzene) was used as a spin trap to detect short-living radicals. Data evaluation was performed using "ESR-MPlot & Analyze" software. The final examination of recorded EPR spectra was carried out using OriginPro 9.0 software.

DPPH-Radical Detection Assay: The assay was performed according to a modified literature procedure.[49] A 2,2-diphenyl-1-pikryl-hydrazyl (DPPH, 10^{-4} m) stock solution in MeOH and benzene was prepared. A volume of 2 mL DPPH stock solution was added to each test sample. Reactions were carried out for 2 and 24 h at 37 °C (and 70 °C) without stirring. For determination of remaining DPPH-radical, absorptions (A$_{520nm}$) of sample solutions and DPPH* stock solution were measured via UV/vis spectroscopy at 520 nm. Background absorption of the pure solvent was subtracted. The concentration of remaining DPPH-radical after sample exposition was determined according to Equation 1:

$$\text{Remaining [DPPH}^*\text{] (\%)} = \frac{A_{520nm}\,(\text{sample}) - A_{520nm}\,(\text{solvent})}{A_{520nm}\,(\text{DPPH stock}) - A_{520nm}\,(\text{solvent})} \times 100 \quad (1)$$

Horseradish Peroxidase (HRP) Assay for Hydrogen Peroxide Detection: Horseradish-peroxidase (0.2 mg mL^{-1}) and pyrogallol (2.5 mg mL^{-1}) were dissolved in a PBS solution (pH adjusted to 8.0). Grafted-poly-*N*-oxide samples were added and incubated for 5 min at 25 °C under gentle shaking. For validation, a positive control with added hydrogen peroxide (0.1 mm) and a negative control without hydrogen peroxide were evaluated under the same conditions. Absorptions (A$_{420nm}$) of test samples were measured via UV/vis spectroscopy at 420 nm. A blank value of PBS solution was subtracted. Residual enzymatic activity was determined relatively to the H$_2$O$_2$-containing positive control using equation 2:

$$\text{Relative HRP activity (\%)} = \frac{A_{420nm}\,(\text{sample}) - A_{420nm}\,(\text{solvent})}{A_{420nm}\,(\text{positive control}) - A_{420nm}\,(\text{solvent})} \times 100 \quad (2)$$

Determination of Antibacterial Activity (ASTM E2149-13a): A modified ASTM assay E2149-13a was performed for evaluation of antimicrobial activity. All test samples were sterilized with iPrOH/water mixture (90 vol %)

and subsequently dried under laminar airflow (LAF) prior to testing. The bacterial strains *Staphylococcus aureus* (strain ATCC 29213) and *Escherichia coli* (strain ATCC 25922) were cultured on Columbia agar overnight. The overnight culture was suspended and diluted in sterile saline solution (0.9 %) to preserve a cell density of 1.5×10^8 (OD = 0.5) and diluted to a final concentration of 10^5 colony-forming units per milliliter (CFU mL^{-1}). Zwitterionized and pristine PE test specimens (surface area: 1.0 cm^2) were placed in a 24-well plate (one specimen per well) and covered with 2.0 mL of the respective bacterial suspension (10^5 CFU mL^{-1}). The incubation was carried out at 37 °C under air for 2 h. Afterwards, the incubated solutions and three subsequent dilutions were incubated on Columbia Agar (100 µL of 10^5, 10^4, 10^3 and 10^2 CFU mL^{-1}) for 17 h at 37 °C, prior to cell counting. Colony counts above 250 CFU were set as "too numerous to count" (TNTC). Each experiment was performed as a triplicate. The log10 reduction for each assay was calculated using following equation 3:

$$\log 10 \text{ reduction} = \log \left(\frac{\text{colony forming units (CFU) before exposure}}{\text{colony forming units (CFU) after exposure}} \right) \quad (3)$$

Determination of Low-Fouling Activity (Adhesion Test): All test samples were treated with 90-vol % iPrOH and dried under laminar airflow (LAF) before testing. The strain *Staphylococcus aureus* (strain ATCC 29213) was cultured on Columbia agar overnight. The overnight culture was suspended and diluted in sterile saline solution (0.9 %) to preserve a cell density of 10^4 colony-forming units per milliliter (CFU mL^{-1}). Zwitterionized and pristine PE test specimens (surface area: 1.0 cm^2) were placed in a 24-well plate (one specimen per well) and covered with each 1980 µL of Mueller Hinton Broth (MHB). 20 µL of the bacterial suspension was added to each well to obtain a starting cell density of 10^2 CFU mL^{-1}. The samples were incubated in bacterial solution for 24 h at 37 °C and were subsequently transferred into 3 mL of sterile saline solution without stirring or shaking for 10 min to remove loosely attached bacteria. Each foil was slightly pressed with the modified side onto an agar plate (Columbia agar) and removed after 30 s. Transferred cells were incubated for 20 h at 37 °C prior to cell counting. An aliquot of 100 µL supernatant was taken from each incubation experiment and analyzed with respect to bacterial growth in comparison to a positive control of MHB containing the initial bacterial suspension without added test specimens.

LIVE/DEAD Staining and Confocal Microscopy: Modified poly-*N*-oxide-PE and pristine PE specimens with a surface area of 0.8 cm^2 were immersed in a 6 well plate into 4 mL of *Vibrio campbellii* (strain BB120, OD600nm 0.05) in artificial seawater. The samples were incubated 24 h at 28 °C under gentle shaking (100 rpm) to simulate natural growth conditions. After 24 h test specimens were rinsed with PBS buffer shortly to detach loosely attached planktonic cells. Fluorescence imaging to examine biofilm formation on the test samples was carried out using the LIVE/DEAD *Bac*Light Viability Kit. Images were visualized via confocal laser scanning microscope LSM 800 with AiryScan from Zeiss (Jena, Germany) and edited with ZEN 2 (Blue Edition) software.

Agar Diffusion Plate Test: DIN EN ISO 20645: Leaching of antibacterial components from the poly-*N*-oxide-specimens was evaluated following DIN EN ISO 20645:2002-02 (agar-diffusion assay). Briefly, test specimens were placed with the poly-*N*-oxide-grafted surface facing downwards in a two-layer agar plate (Columbia agar). The top agar layer was previously covered with 200 µL of 1.5×10^8 CFU mL^{-1} of either *S. aureus* (strain ATCC29213) or *E. coli* (strain ATCC25922) suspension. Plates were incubated for 20 h at 37 °C. The plates were then assessed for the development of an inhibition zone surrounding the test specimen.

Determination of Minimum Inhibitory Concentration (MIC): The minimum inhibitory concentration (MIC) of VBNOx, MANOx and MAANOx against *S. aureus* (strain ATCC29213) and *E. coli* (strain ATCC25922) was determined by the microdilution method (Methods for Dilution Antimicrobial Susceptibility Tests for Bacteria That Grow Aerobically; Approved Standard—Ninth Edition. CLSI document M07-A9. Wayne, PA: Clinical and Laboratory Standards Institute; 2012) and compared to the MICs of (vinyl benzyl-)-trimethylammonium chloride (VBTAC) and benzalkoniumchloride (BAC). Tests were performed under air at 37 °C for 20 h. The MIC was defined as the minimum concentration to achieve transparent solu-

tions in the wells. As an upper limit, a concentration of 1024 µg mL^{-1} of the test compounds was used.

Zwitterionization of PE-Foils with Grafted Poly-N-Oxides: PE foils with a thickness of 0.75 mm were rinsed with an isopropanol/water mixture of 70% (v/v) and dried for 15 min at 50 °C prior to use. Plasma treatment of the PE foils was performed at a distance of 6 mm between the plasma jet nozzle and the surface. The speed of the plasma jet nozzle was set at 110 mm s^{-1}. Samples were stored at room temperature under air for 8 min after plasma treatment. In a typical experiment, a solution of the appropriate polymerizable tertiary amine (VBDMA, MADMA or MAADMA) (20 or 40 wt%) and 2,2'-Azobis(isobutyronitrile) (AIBN) as a free radical initiator (0.1 wt% or 1.0 wt%) in EtOAc was purged with nitrogen for 10 min. Plasma-treated PE foils were placed in the degassed solution containing the appropriate polymerizable tertiary amine and AIBN. The resulting reaction mixtures were purged with nitrogen for another 15 min and were subsequently polymerized for 2 h at 85 °C. After polymerization, the materials were treated with a EtOH/water mixture (70vol%) for 15 min with ultrasonication three times and dried for 30 min at room temperature. The resulting specimens were subsequently treated with an aqueous solution of hydrogen peroxide (30% w/w) for 72 h at room temperature under rapid shaking (150 min). Residual hydrogen peroxide was destroyed by immersion of the specimens into NaOH solution (1.0 mol L^{-1}) for 24 h at room temperature under gentle shaking. The resulting specimens were washed three times with EtOH/water mixture (70vol%) for each 15 min in an ultrasonic bath and dried for 30 min in a nitrogen stream and were stored before use at room temperature under nitrogen atmosphere.

Statistical Analysis: Statistics were performed using OriginPro 9 (2021) software. Data are reported as mean value ± standard deviation for continuous variables, or as a selective frequency for categorical variables, unless otherwise described. A pairwise comparison with the Tukey test was performed to determine statistical significance. A *p*-value of less than 0.05 (*) was considered significant.

Supporting Information

Supporting Information is available from the Wiley Online Library or from the author.

Conflict of Interest

The authors declare no conflict of interest.

Data Availability Statement

The data that support the findings of this study are available in the supplementary material of this article.

[1] L. Hall-Stoodley, J. W. Costerton, P. Stoodley, *Nat. Rev. Microbiol.* **2004**, *2*, 95.

[2] Y. X. Wang, J. L. Robertson, W. B. Spillman, R. O. Claus, *Pharm. Res.* **2004**, *21*, 1362.

[3] H. C. Flemming, J. Wingender, U. Szewzyk, P. Steinberg, S. A. Rice, S. Kjelleberg, *Nat. Rev. Microbiol.* **2016**, *14*, 563.

[4] a) S. Galie, C. Garcia-Gutierrez, E. M. Miguelez, C. J. Villar, F. Lombo, *Front. Microbiol.* **2018**, *9*, 898; b) S. L. Percival, L. Suleman, C. Vuotto, G. Donelli, *J. Med. Microbiol.* **2015**, *64*, 323; c) W. Zhou, W. Li, J. Chen, Y. Zhou, Z. Wei, L. Gong, *RSC Adv.* **2021**, *11*, 25484.

[5] a) I. Banerjee, R. C. Pangule, R. S. Kane, *Adv. Mater.* **2011**, *23*, 690; b) D. Rana, T. Matsuura, *Chem. Rev.* **2010**, *110*, 2448; c) A. M. C. Maan, A. H. Hofman, W. M. Vos, M. Kamperman, *Adv. Funct. Mater.* **2020**, *30*, 2000936; d) S. Zheng, M. Bawazir, A. Dhall, H. E. Kim, L. He, J. Heo, G. Hwang, *Front Bioeng Biotechnol* **2021**, *9*, 643722.

[6] M.-C. Sin, S.-H. Chen, Y. Chang, *Polym. J.* **2014**, *46*, 436.

[7] a) A. Venault, Y. Chang, *Langmuir* **2019**, *35*, 1714; b) J. B. Schlenoff, *Langmuir* **2014**, *30*, 9625; c) Y. Chang, *J. Polym. Res.* **2022**, *29*, 286; d) Q. Li, C. Wen, J. Yang, X. Zhou, Y. Zhu, J. Zheng, G. Cheng, J. Bai, T. Xu, J. Ji, S. Jiang, L. Zhang, P. Zhang, *Chem. Rev.* **2022**, *122*, 17073; e) S. Paschke, K. Lienkamp, *ACS Applied Polymer Materials* **2020**, *2*, 129.

[8] Q. Shao, S. Jiang, *J. Phys. Chem. B* **2014**, *118*, 7630.

[9] R. G. Chapman, E. Ostuni, S. Takayama, R. E. Holmlin, L. Yan, G. M. Whitesides, *J. Am. Chem. Soc.* **2000**, *122*, 8303.

[10] a) S. Hiranphinyophat, Y. Iwasaki, *Sci. Technol. Adv. Mater.* **2021**, *22*, 301; b) K. Ishihara, N. P. Ziats, B. P. Tierney, N. Nakabayashi, J. M. Anderson, *J. Biomed. Mater. Res.* **1991**, *25*, 1397.

[11] B. Cao, Q. Tang, G. Cheng, *J. Biomater. Sci., Polym. Ed.* **2014**, *25*, 1502.

[12] a) A. B. Lowe, M. Vamvakaki, M. A. Wassall, L. Wong, N. C. Billingham, S. P. Armes, A. W. Lloyd, *J Biomed Mater Res* **2000**, *52*, 88; b) C. Viklund, K. Irgum, *Macromolecules* **2000**, *33*, 2539; c) Y. Zhang, Y. Liu, B. Ren, D. Zhang, S. Xie, Y. Chang, J. Yang, J. Wu, L. Xu, J. Zheng, *J. Phys. D: Appl. Phys.* **2019**, *52*, 403001.

[13] a) Q. Shao, S. Jiang, *J. Phys. Chem. B* **2013**, *117*, 1357; b) H. Du, X. Qian, *J. Comput. Chem.* **2016**, *37*, 877; c) C. Y. Chiu, Y. Chang, T. H. Liu, Y. N. Chou, T. J. Yen, *J. Mater. Chem. B* **2021**, *9*, 8437; d) S. Abraham, A. So, L. D. Unsworth, *Biomacromolecules* **2011**, *12*, 3567; e) Y. Higaki, J. Nishida, A. Takenaka, R. Yoshimatsu, M. Kobayashi, A. Takahara, *Polym. J.* **2015**, *47*, 811; f) J. F. Karthäuser, J. Koc, E. Schönemann, R. Wanka, N. Aldred, A. S. Clare, A. Rosenhahn, A. Laschewsky, *Advanced Materials Interfaces* **2022**, *9*, 2200677.

[14] B. Li, P. Jain, J. Ma, J. K. Smith, Z. Yuan, H. C. Hung, Y. He, X. Lin, K. Wu, J. Pfaendtner, S. Jiang, *Sci. Adv.* **2019**, *5*, 9562.

[15] I. O'Neil, *Sci. Synth.* **2009**, *40*, 860.

[16] E. P. Linton, *J. Am. Chem. Soc.* **1940**, *62*, 1945.

[17] J. Hunger, N. Ottosson, K. Mazur, M. Bonn, H. J. Bakker, *Phys. Chem. Chem. Phys.* **2015**, *17*, 298.

[18] Q. Zou, B. J. Bennion, V. Daggett, K. P. Murphy, *J. Am. Chem. Soc.* **2002**, *124*, 1192.

[19] Q. Zhang, M. A. Kelland, H. Frey, J. Blankenburg, L. Limmer, *Energy Fuels* **2020**, *34*, 6298.

[20] J. Zhen, Z. Zhou, M. He, H. X. Han, E. H. Lv, P. B. Wen, X. Liu, Y. T. Wang, X. C. Cai, J. Q. Tian, M. Y. Zhang, L. Xiao, X. X. Kang, *Front. Endocrinol. (Lausanne)* **2023**, *14*, 1085041.

[21] a) A. Rani, A. Jayaraj, B. Jayaram, V. Pannuru, *Sci. Rep.* **2016**, *6*, 23656; b) Y. T. Liao, A. C. Manson, M. R. DeLyser, W. G. Noid, P. S. Cremer, *Proc. Natl. Acad. Sci. USA* **2017**, *114*, 2479; c) T. C. Gluick, S. Yadav, *J. Am. Chem. Soc.* **2003**, *125*, 4418.

[22] a) R. Lindigkeit, A. Biller, M. Buch, H. M. Schiebel, M. Boppre, T. Hartmann, *Eur. J. Biochem.* **1997**, *245*, 626; b) T. Hartmann, G. Toppel,

Phytochemistry **1987**, *26*, 1639; c) V. M. Dembitsky, T. A. Gloriozova, V. V. Poroikov, *Phytomedicine* **2015**, *22*, 183.

[23] R. D. Bach, H. B. Schlegel, *J. Phys. Chem. A* **2021**, *125*, 5014.

[24] a) D. Bernier, U. K. Wefelscheid, S. Woodward, *Org. Prep. Proced. Int.* **2009**, *41*, 173; b) A. Petrosyan, R. Hauptmann, J. Pospech, *Eur. J. Org. Chem.* **2018**, *2018*, 5237; c) A. M. Bauer, E. E. Ramey, K. G. Oberle, G. A. Fata, C. D. Hutchison, C. R. Turlington, *Tetrahedron Lett.* **2019**, *60*, 151193.

[25] D. Yan, K. Wang, S. Bai, B. Liu, J. Bai, X. Qi, Y. Hu, *J. Am. Chem. Soc.* **2022**, *144*, 4269.

[26] a) G. Cheng, B. Li, C. Wang, H. Zhang, G. Liang, Z. Weng, H. Hao, X. Wang, Z. Liu, M. Dai, Y. Wang, Z. Yuan, *PLoS One* **2015**, *10*, 0136450; b) Z. Shah, R. Mahbuba, B. Turcotte, *FEMS Microbiol. Lett.* **2013**, *347*, 61; c) C. Avendaño, J. C. Menéndez, in *Medicinal Chemistry of Anticancer Drugs*, (Eds.: C. Avendaño, J. C. Menéndez), Elsevier, Amsterdam **2008**, p. 93; d) S. E. Walsh, J. Y. Maillard, A. D. Russell, C. E. Catrenich, D. L. Charbonneau, R. G. Bartolo, *J. Appl. Microbiol.* **2003**, *94*, 240; e) P. Wardman, K. I. Priyadarsini, M. F. Dennis, S. A. Everett, M. A. Naylor, K. B. Patel, I. J. Stratford, M. R. L. Stratford, M. Tracy, *Br. J. Cancer* **1996**, *74*, 70.

[27] X. Shen, K. S. Gates, *Chem. Res. Toxicol.* **2019**, *32*, 348.

[28] a) M. Lv, Y. Li, X. Wei, Y. Xu, Z. Ge, X. Chen, *ACS Appl. Energy Mater.* **2019**, *2*, 2238; b) A. C. Griffin, A. M. Bhatti, G. A. Howell, *MRS Online Proc. Libr.* **1987**, *109*, 115.

[29] a) H. W. Schlipköter, A. Brockhaus, *Klin. Wochenschr.* **1961**, *39*, 1182; b) N. G. Puchkova, A. V. Nekrasov, Y. F. Razvodovskii, B. S. El'tsefon, *Polymer Science U.S.S.R* **1980**, *22*, 1407.

[30] N. Zhang, K. Cheng, J. Zhang, N. Li, X. Yang, Z. Wang, *J. Membr. Sci.* **2022**, *660*, 120829.

[31] a) S. Kliewer, S. G. Wicha, A. Broker, T. Naundorf, T. Catmadim, E. K. Oellingrath, M. Rohnke, W. R. Streit, C. Vollstedt, H. Kipphardt, W. Maison, *Colloids Surf., B* **2020**, *186*, 110679; b) N. Burmeister, C. Vollstedt, C. Kröger, T. Friedrich, N. Scharnagl, M. Rohnke, E. Zorn, S. G. Wicha, W. R. Streit, W. Maison, *Colloids Surf., B* **2023**, *224*, 113195.

[32] F. Khalil, E. Franzmann, J. Ramcke, O. Dakischew, K. S. Lips, A. Reinhardt, P. Heisig, W. Maison, *Colloids Surf., B* **2014**, *117*, 185.

[33] G. L. Archer, *Clin. Infect. Dis.* **1998**, *26*, 1179.

[34] a) I. Karunasagar, S. K. Otta, I. Karunasagar, *Aquaculture* **1996**, *140*, 241; b) C. M. Waters, B. L. Bassler, *Genes Dev.* **2006**, *20*, 2754.

[35] S. Guo, D. Jańczewski, X. Zhu, R. Quintana, T. He, K. G. Neoh, *J. Colloid Interface Sci.* **2015**, *452*, 43.

[36] C. Zhang, J. Zhou, X. Ye, Z. Li, Y. Wang, *Macromolecules* **2021**, *54*, 4236.

[37] M. van de Lagemaat, A. Grotenhuis, B. van de Belt-Gritter, S. Roest, T. J. A. Loontjens, H. J. Busscher, H. C. van der Mei, Y. Ren, *Acta Biomater.* **2017**, *59*, 139.

[38] H.-C. Flemming, J. Wingender, *Nat. Rev. Microbiol.* **2010**, *8*, 623.

[39] Z. Temoçin, M. Yiğitoğlu, *Bioprocess Biosyst. Eng.* **2009**, *32*, 467.

[40] Y. S. Raval, L. Flurin, A. Mohamed, K. E. Greenwood-Quaintance, H. Beyenal, R. Patel, *Antimicrob. Agents Chemother.* **2021**, *65*, 01966.

[41] O. P. Sharma, T. K. Bhat, *Food Chem.* **2009**, *113*, 1202.

[42] J. P. Gotham, R. Li, T. E. Tipple, J. R. Lancaster, T. Liu, Q. Li, *Free Radical Biology and Medicine* **2020**, *154*, 84.

[43] a) L. Zhang, J. Sun, W. Huang, S. Zhang, X. Deng, W. Gao, *J. Am. Chem. Soc.* **2023**, *145*, 1707; b) J. Jin, P. Yuan, W. Yu, J. Lin, A. Xu, X. Xu, J. Lou, T. Yu, C. Qian, B. Liu, J. Song, L. Li, Y. Piao, Y. Xie, Y. Shen, H. Tao, J. Tang, *ACS Nano* **2022**, *16*, 10327; c) H. Zhang, C.-H. Huang, *Environ. Sci. Technol.* **2005**, *39*, 593.

[44] H. Huang, C. Zhang, R. Crisci, T. Lu, H. C. Hung, M. S. J. Sajib, P. Sarker, J. Ma, T. Wei, S. Jiang, Z. Chen, *J. Am. Chem. Soc.* **2021**, *143*, 16786.

[45] W. Fan, Q. Wei, J. Xiang, Y. Tang, Q. Zhou, Y. Geng, Y. Liu, R. Sun, L. Xu, G. Wang, Y. Piao, S. Shao, Z. Zhou, J. Tang, T. Xie, Z. Li, Y. Shen, *Adv. Mater.* **2022**, *34*, 2109189.

[46] X. Guan, K. Zhang, F. Huang, G. C. Bazan, Y. Cao, *Adv. Funct. Mater.* **2012**, *22*, 2846.

[47] A. L. J. Beckwith, P. H. Eichinger, B. A. Mooney, R. H. Prager, *Aust. J. Chem.* **1983**, *36*, 719.

[48] P. F. Holt, *Br. J. Ind. Med.* **1971**, *28*, 72.

[49] M. Suzuki, A. Kishida, H. Iwata, Y. Ikada, *Macromolecules* **1986**, *19*, 1804.

2300505 (13 of 13)

5   Discussion

Increasing plastic production and the concomitant plastic pollution challenge the environment and human health in multiple ways. In Figure 6, the lifecycle of plastic is pictured, pointing out potential risks and advantages of plastic colonization. In recent years, research has intensively studied the plastisphere and searched for plastic degrading bacteria and enzymes. Yet, several knowledge gaps occur. Gene regulation within the plastisphere and the role of degradation products gained insufficient attention. Recycling rates still remain rather low and the actual biodegradation in nature is not determined. Additionally, biofouling contaminates surfaces, reducing the material durability. In Chapter 1-3, this study aimed to provide steps towards closing those gaps (Figure 6). This thesis contributes to a detailed understanding of the initial attachment of bacteria to plastic surfaces and additionally the influence of plastic degradation products towards the plastisphere community (Chapter 1), the characterization of PET degrading enzymes for potential industrial approaches, but also for the understanding of their role in nature (Chapter 2) and the prevention of biofouling by changing the polymer surfaces, and characterizing bacterial behavior towards adapted PE foil (Chapter 3).

5.1   DSM 21264 highly transcribes virulence factors during initial attachment on plastic surfaces

Many studies have already explored the formation of the plastisphere, the processes involved, and the major phyla associated (Quero & Luna, 2017, Pinto et al., 2019, Latva et al., 2022, Dey et al., 2022, Gulizia et al., 2025) However, there remains a lack in our knowledge regarding the gene transcription and expression, relevant for the development of the plastisphere (Amaral-Zettler et al., 2020). Within this study, the gene regulation of *V. gazogenes* DSM 21264 during the initial attachment after 8 hours of incubation on PET and PE, both untreated and plasma-activated, was detected. RNAseq revealed that DSM 21264 doesn't distinguish significantly between the different surfaces, and only four genes were differentially upregulated when DSM 21264 was colonizing PET compared to PE (Preuss et al., 2025, TABLE S3). Interestingly, among the highest transcribed genes on all tested surfaces were the outer membrane protein OmpU and the translocase SecY. In *V. cholera*, OmpU is described to be involved in cell-surface adhesion and biofilm formation (Potapova et al., 2024). Additionally, the protein is involved in its pathogenesis, and its adaptions have contributed to increased antimicrobial resistance (Grant et al., 2023). On the other hand, translocases transport polypeptides from the *cis* to the *trans* side of the membrane, suggesting that SecY could be responsible for the transport of OmpU (Economou, 1998).

Moreover, among the most highly expressed genes in biofilm state was the C-acetyltransferase, also referred to as pyruvate-formiate-lyase (*pfl*), which is involved in anaerobic and mixed acidic fermentation in enteric bacteria. This suggests that partial anaerobic metabolism could be taking place within our single-layer biofilms (Hanževački *et al.,* 2022). This observation is in line with the strong expression of the aspartate ammonium lyase (*asp*), cleaving aspartate into ammonia and fumarate to use the latter as electron acceptor (Yoo et al., 2024).

Another notable finding is the strongly transcribed M4 metallopeptidase, commonly referred to as vibriolysin. Vibriolysin like proteases (VLPs) are key pathogenesis factors in *Vibrio* species (Huang et al., 2018). During infection, vibriolysin is believed to facilitate host colonization and dissemination, and to contribute to tissue degradation and hemolysis (Iqbal et al., 2011). Although, only few studies have addressed the expression of virulence factors within the plastisphere, their findings are in line with our RNAseq results, indicating significant expression of virulence factors within the plastisphere community (Wang et al., 2024, Messer et al., 2024). Since quorum sensing plays a crucial role in bacterial surface colonization, it is not surprising that HapR- the master QS regulator in *Vibrio* species- was highly transcribed under all tested biofilm conditions. HapR regulates more than 300 genes, including previously mentioned vibriolysin production, biofilm formation, and type VI secretion system (T6SS) (Lydick et al., 2025) (Preuss et al., 2025, TABLE 2). In *V. cholerae,* T6SS is responsible for the delivery of virulence factors (Shao & Bassler, 2014). This is in line with the results of the RNAseq data of DSM 21264 on plastic surfaces. Like HapR, the T6SS was highly transcribed and the strongest expressed among the secretion systems encoded in DSM 21264. (Preuss et al., 2025, FIGURE 5). Secretion systems in bacteria are used for the delivery of toxins, virulence, or enzymes into their environment (Hay et al., 2017). The upregulation of several virulence-associated genes in strain DSM21264 suggests that other potential pathogens in the plastisphere may also strongly transcribe these genes.

5.2 PET-degrading enzymes are secreted outside the cell

Proteins, which degrade polymers outside the cell, have to be transported through the cell membrane mainly via secretion systems. PET6 carries a signal peptide (SP). SPs are short peptides which are located in the N-terminal of the respective enzyme, determining the transport pathway as well as the destination of the protein (Owji et al., 2018). This suggests that PET6 is most likely transported outside the cell. This is in line with the findings that PET degradation was observed when DSM 21264 was incubated with PET foil and powder (Preuss et al., 2025, FIGURE 2). BLAST-results of the sequence of PET6 in SignalP (SignalP 6.0 - DTU Health Tech - Bioinformatic Services) showed that the SP belongs to the Sec-dependent

pathway, which is characterized by post-translational translocation (Owji et al., 2018). For the release of the respective protein from the membrane, signal peptidases (SPases)are required to cleave the SP (Musik et al., 2019). It is distinguished between two types of SPases, Type I and Type II, respectively, While SPases II are mainly associated with lipoproteins, SPase I cleaves off the signal peptides of several bacterial proteins. The signal peptidase from DSM 21264 for PET6 cleavage refers to Type I SPase, which is the most commonly utilized signal peptidase in many bacteria (Paetzel, 2019).

For the secretion outside the cell, it is likely that the organism uses secretion systems, to carry PET6 outside the cell, enabling the degradation of PET and BHET in its environment. The genome of DSM 21264 codes for three secretion systems, Type I (T1SS), Type II (T2SS) and Type VI (T6SS). T1SS occurs in Gram-negative bacteria and transports proteins in one-step process across both bacterial membranes. Mainly, it exports enzymes of different sizes and functions like proteases or lipases. In *Vibrio* it also mediates the secretion of hemolysin (Pena et al., 2019). In many Gram-negative bacteria, the T2SS is used for the transport of folded proteins across the membrane into the extracellular milieu (Korotkov et al., 2012). For *P. aeruginosa* it has been characterized to be amongst others especially involved in the secretion of hydrolases, indicating that also the transport of PET6 might be affiliated with the T2SS (Hay et al., 2017). It consists usually of 12 to 15 proteins, forming a multiprotein machinery. The enzymes are located in one operon, which is also encoded in the genome of DSM 21264. The enzymes are transported over the inner membrane by the SecYEG translocases, which was also strongly regulated in biofilm samples like the T2SS (Korotkov et al., 2012). Those results indicate that DSM 21264 uses T2SS for the transport of PET6 through the membranes.

5.3   Potential PET -degradation pathway in DSM 21264

DSM 21264 harbors a well characterized PET-degrading enzyme, designated PET6 (Weigert et al., 2022). Nevertheless, the regulation of *pet6* in the native host, as well as the associated metabolic pathways, have not been identified before this thesis. Using various RNAseq approaches within this study, we characterized the transcriptional behavior of DSM 21264 in the presence of PET and its degradation products, providing a more detailed understanding of the potential gene regulation within the plastisphere.

PET can be metabolized as sole carbon source by *Ideonella sakaiensis.* It is among the only organisms. for which the whole hydrolysis process is well understood (Yoshida et al., 2016, Maity et al., 2021). Regarding PET degradation products, also for *P. putida* KT2440 detailed information in EG uptake and metabolism were generated (Franden et al., 2018). TPA uptake and metabolization on the other hand is well characterized in *Comamonas testosteroni,* which

is able to grow with TPA as a sole carbon source (Vural & Ettadili, 2024). Based on those previously identified pathways and comparing them to the findings made for DSM 21264, using the data obtained from RNAseq results, we were able to develop a potential degradation pathway of PET (Preuss et al., 2025 FIGURE 7). Initial breakdown of PET and BHET is assumed to be catalyzed by PET6, as this gene was strongly upregulated in the presence of 5 mM BHET (log2-foldchange 5) and 30 mM BHET (log2-foldchange 1.5). Additionally, we were able to identify Utilization of L-ascorbate protein G (UlaG) as a novel BHETase, which was upregulated in the presence of 5 mM BHET and was one of the most strongly upregulated genes at 30 mM BHET (log2-foldchange 7.8) (Preuss et al., 2025, FIGURE 6, 7). UHPLC measurements using the purified enzyme also revealed slow but significant BHET degradation rates (Figure 7, Preuss et al., 2025).
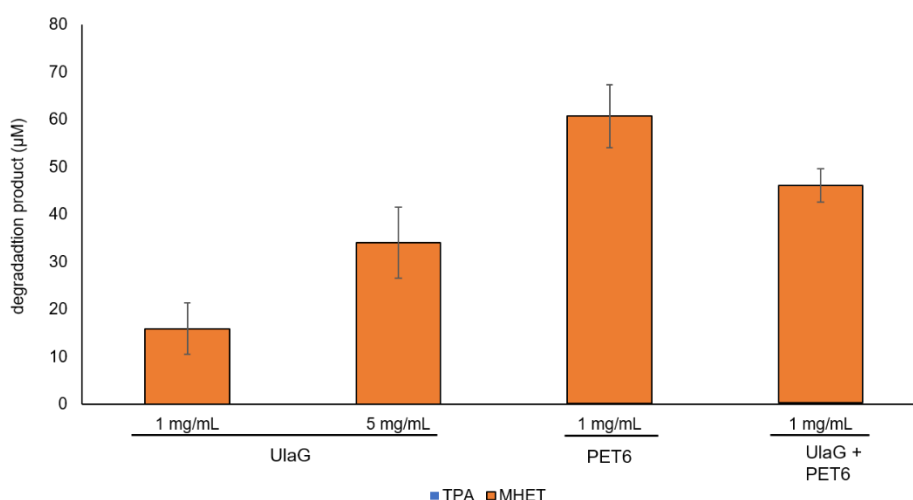

Figure 7 (Preuss et al., 2025, FIGURE S3): **BHET degradation assay of recombinant and purified UlaG and PET6**. Samples were measured using UHPLC ad as outlined in the Materials and Methods section. For detection of degradation products MHET and TPA. BHET was added at 300 µM. Bars indicate production of MHET. Data are mean values of three measurements and the simple SD is given. Data were recorded after 24 hours of incubation.

UlaG, a member of the E.C. 3.1.1.-, has first been characterized in *E. coli,* responsible under anaerobic conditions for the metabolization of L-ascorbate, when it is the sole carbon source. It is annotated as L-ascorbate-6-phosphate lactonase, catalyzing the first step in 6-phosphate degradation (Garces et al., 2008). It is believed that UlaG's ancestral function could have been related to hydrolysis and maturation of RNA substrates, but it would have adapted its substrates specify to novel substrates during evolution (Garces et al., 2010). Even though the function of UlaG as a BHETase has not been shown before, it is discussed that UlaG also catalyzes side activities, which might evolve to enzyme specialists within a novel pathway (Perez-Garcia et al., 2021). UlaG could therefore play a role in the plastisphere that has not been sufficiently characterized, yet.

BHET is cleaved outside the cell into MHET and EG and further into EG and TPA, which can be taken up by specific transporters. *C. thiooxidans,* metabolizing TPA as a sole carbon source, uses a specific tripartite tricarboxylate transporter for the TPA uptake (Dierkes et al., 2022). The genome of DSM 21264 encodes 6 tripartite tricarboxylate transporters. Interestingly, the transcriptomic data have also shown that one transporter (AAC977_10445) and its corresponding permease (AAC977_10440) were upregulated in the presence of 1 mM TPA (log2-foldchange > 0.5). The data might imply that DSM 21264 utilizes a transportation mechanism comparable to that of *C. thiooxidans*. Supplementing the strain with higher concentrations of TPA could provide further insight into this hypothesis. According to UHPLC measurements, DSM 21264 cleaved all BHET into MHET within three days, when supplemented with 5 mM of BHET. TPA concentration thereupon increased at that timepoint indicating that further degradation of MHET is only initiated when no BHET is in the medium. (Preuss et al., 2025, FIGURE S4).

This is in line with the finding that after 24 h of incubation of DSM 21264 in the presence of 5 mM BHET, the respective TPA transporter was not regulated yet, but it can be assumed that the transcription increases at rising TPA concentrations in the medium. We hypotesize that TPA is furhter degraded by Ubiquinone biosynthesis gene D (UbiD). UbiD is a member of the UbiD decarboxylase family, which are known to catalyze the decarboxylation of aromatic substrates (Khusnutdinova et al., 2024). The product of the single decarboxylation would be benzoic acid (Figure 8). UbiD (AAC977_13085) was strongly upregulated in the presence of 30 mM BHET (log2-foldchange of 6). In the presence of TPA a slight increase in transcription was detected (log2-foldchange of 0.4).

Besides MHET, the degradation of BHET leads to the release of EG (Figure 8, Preuss et al., 2025, FIGURE 7). In both, *P. putida* KT2440 and *I. sakaiensis* the oxidation of EG to Glycolaldehyde (GAD) is initialized by alcohol dehydrogenases (Franden et al., 2018, Hachisuka et al., 2022). In DSM 21264, we identified one putative bifunctional acetaldehyde - CoA/ alcohol dehydrogenase, referred to as *adhE,* which was upregulated in the presence of 5 mM BHET (log2-foldchange of 2), and interestingly, also when DSM 21264 is grown on PET surface compared to PE foil in biofilm condition (log2-foldchange of 1). Glycolaldehyde is further catabolized to glycolic acid (GA) by aldehdyde dehydrogenases. Blasting *adhE* from DSM 21264 against the proteins characterized for its role in EG catabolism from *P. putida* and *I. sakaiensis,* percent identity of 23.28% and 22.78% for aldehdyde dehydrogenases PedI and IsPedI was detected. IsPedI was also upregulated in the presence of PET and EG in *I. sakaiensis* (Hachisuka et al., 2022). In order to further investigate the role of *adhE,* a promoter fusion construct was cloned and analyzed, using fluorescence measurements. Results showed a significant induction of the *adhE* promoter in the presence of 5 mM EG (Preuss et al., 2025, FIGURE S5). For *Thermotoga neapolitana,* it has already been shown that a bifunctional

aldehdyde/alcohol dehydrogenase is capable of catalyzing two consecutive reactions (Wang et al., 2021), indicating that *adhE* could also be involved in the reaction from EG to GAD and its further conversion to GA. To verify the role of *adhE* in the EG metabolism, further biochemical analysis have to be conducted (Figure 8).
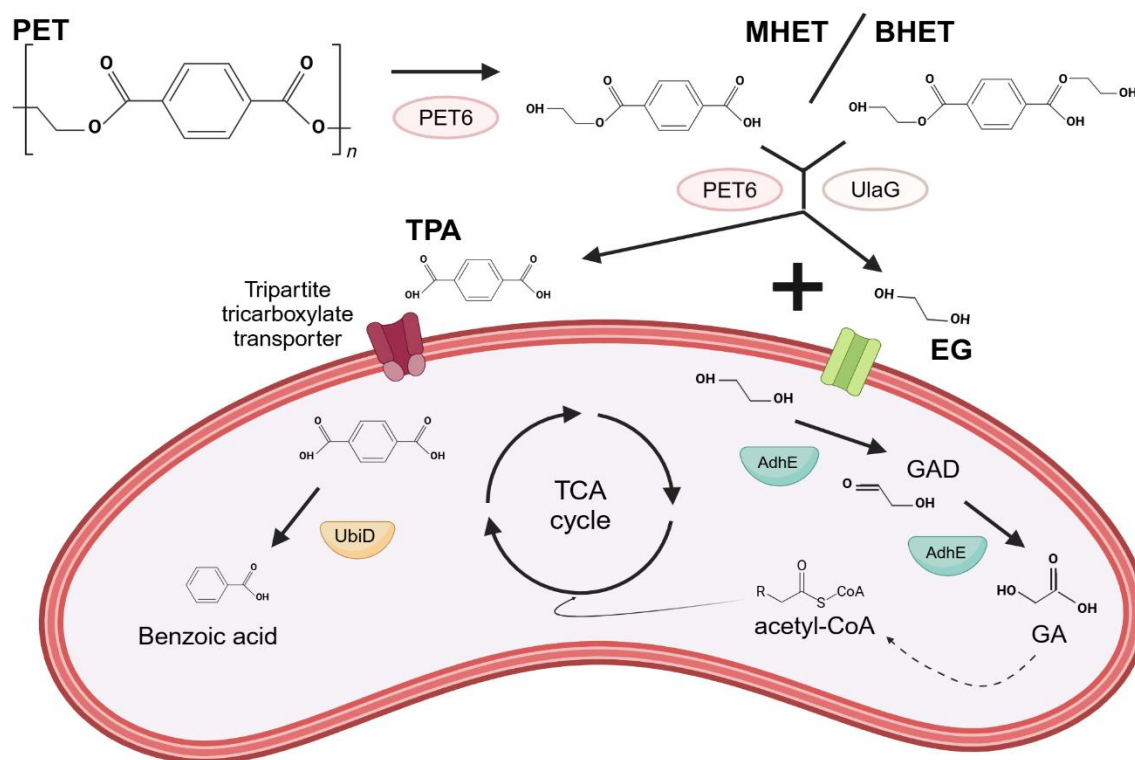

Figure 8: Potential PET degradation pathway and metabolism of PET-degradation products in DSM 21264. PET is degraded by PET6 into BHET or MHET. The intermediates are further degraded by PET6 and UlaG into EG and TPA. TPA is transported through tripartite tricarboxylate transporter into the cell and potentially decarboxylated by UbiD into benzoic acid. EG is oxidized by AdhE into GAD and further metabolized also by AdhE into GA. GA is then potentially converted into acetyl-CoA and inserted into the TCA cycle (Created with Biorender).

Until now, most studies focused either on the characterization of the purified PETase or the bacterial degradation, determining the product release, but ignore the transcriptomic changes induced by the polymer or degradation products (Liu et al., 2024). Within this study, we were able to develop a model of the potential degradation pathway, and identify genes that might play important roles in the metabolism (Figure 8). Additionally, this is the first study that gives insight in to changes in gene expression due to different substrates and concentrations related to PET. The study revealed that gene transcription strongly relies on the concentration supplemented within the medium.

5.4   Identification and characterization of PETases and their hosts

Since PET is one of the few plastic polymers, for which the full degradation pathway is well understood, this offers the ability, to search for effective enzymes for PET biodegradation. Different approaches are applied for the finding of novel PETases, and recently, methods have been conducted for the improvement of the degradation rates of those enzymes (Buchholtz et al., 2022, Fritzsche et al., 2024, de Oliveira et al., 2025). The approaches for the detection of PET degrading enzymes vary from basic laboratory screening methods, using agar plates supplemented with PET (Urbeliene et al., 2025) to the establishment of complex sequence-based screening motifs (Danso et al., 2018, Buchholtz et al., 2022, Jahanshahi et al., 2025). Using a profile Hidden Markov Model (HMM) search, PET6 derived from *Vibrio gazogenes* DSM 21264, intensively studied in Chapter 1, as well as PET27 and PET30 characterized in Chapter 2, were, inter alia, identified (Danso et al., 2018, Zhang et al., 2022, Preuss et al., 2025). The field of PET degrading enzymes expanded rapidly, and a more detailed knowledge of conserved motifs and key amino acid sequences was obtained (Jahanshahi et al., 2025). Despite the deep understanding of the well characterized PETases, the expression within their native hosts only received insufficient attention. However, for *Kaistella jeonii*, the native host of PET30, it was observed that the cells attach to PET surface, indicating a potential degradation also in nature. Additionally, enzyme activity could be detected at 4 °C making PET degradations at low temperatures in the oceans by Bacteroidetes very likely (Zhang et al., 2022, FIGURE S5). The phylum Bacteroidetes encodes a distinct secretion system than the previously named. The Type IX secretion system (T9SS), previously referred to Por Secretion System, is widely found within the phylum Bacteroidetes and is not encoded within the genomes of other phyla (McBride & Zhu, 2013). It has been predominantly studied in pathogenic bacteria for its role in infection, due to the release of virulence factors (Mizgalska et al., 2024). The T9SS allows the transport across the membranes with the aid of the Sec system for enzymes carrying a secretion tag. Since PET27 and PET30 harbor a PorC-motif, it is assumed that they are secreted via the T9SS (Pena et al., 2019, Zhang et al., 2022). Our findings regarding DSM 21264 and *K. jeonii* imply that signal peptides and the associated secretion of the enzymes via secretion systems are essential for plastic degradation in the environment. Despite the deep characterization of the purified PETases from the phylum Bacteroidetes, about other genes involved in the PET-degradation pathway within *K. jeonii* can only be speculated.

5.5 Influence of BHET and natural substrates towards the metabolism of DSM 21264

Regarding the expression of PET6, which is potentially involved in biodegradation of PET, no differentially regulation on the distinct polymers like PET foil and powder could be observed. Even tough after the incubation of DSM 21246 with PET foil and powder MHET release was detected, indicating that the constitutively expressed enzyme is sufficient for low degradation rates, the substrate is not inducing the gene expression (Preuss et al., 2025). Until now more than 125 PET-active hydrolases have been detected, but the majority have been heterologous expressed and characterized under laboratory conditions in expression strains such as *E. coli* and not their native hosts (Almeida et al., 2019; Zurier & Goddard, 2022, Carter et al., 2024). The results of Chapter 1 indicate that organisms, in theory capable of degrading plastic substrates, not necessarily enhance biodegradation in the environment at high levels.

To get a deeper insight on the transcriptional regulation of PET6 further RNAseq experiments were conducted, using natural occurring substrates as additional carbon sources such as CMC, chitin and alginate, several BHET concentrations, and TPA. Numerous *Vibrio* species harbor chitinases involved in chitin degradation (Deng et al., 2025) and also alginate lyases, degrading alginate (He et al., 2022). Thus, we hypothesized that PET6 might also be involved in either of those metabolisms. Even though there was no differentially expression of PET6 observable, when DSM 21264 was supplemented with those natural substrates, we detected a significant increase in transcription of *pet6,* when 5 mM and 30 mM BHET were added to the medium.

Our data reveal that not only the PETase transcription was induced, but increasing BHET concentrations significantly affected the overall bacterial metabolism of DSM 21264. In total, 250 genes were upregulated and >100 genes were downregulated in the presence of 5 mM BHET. At 30 mM concentration, >850 genes were upregulated and >600 genes were downregulated (Preuss et al., 2025, FIGURE S2, S7). Among those differentially regulated genes and pathways were Quorum sensing systems (QS), Bis-(3'-5')-cyclic dimeric guanosine monophosphate (cyclic-di GMP) and cyclic adenosine monophosphate (cAMP) signaling, the prodigiosin cluster, prophages and genes involved in oxidative stress (Preuss et al., 2025, FIGURE 4-6). It has already been determined that plastic substrates can negatively influence metabolic pathways of the aquaculture regarding oxidative stress, inflammations or fertility (Hodkovicova et al., 2022). In general, only 9% of all the studies, referring to microplastics, focus on PET and even less are concerned with its degradation products (Hodkovicova et al., 2022). As a result, the metabolic changes, they may induce, have not been determined, yet.

Already 0.5 mM of BHET altered biofilm morphology in DSM 21264. In the presence of 10 mM, the red pigment prodigiosin was not detectable anymore, but gained back when inoculated in BHET-free fresh medium (Figure 9, Preuss et al., 2025).
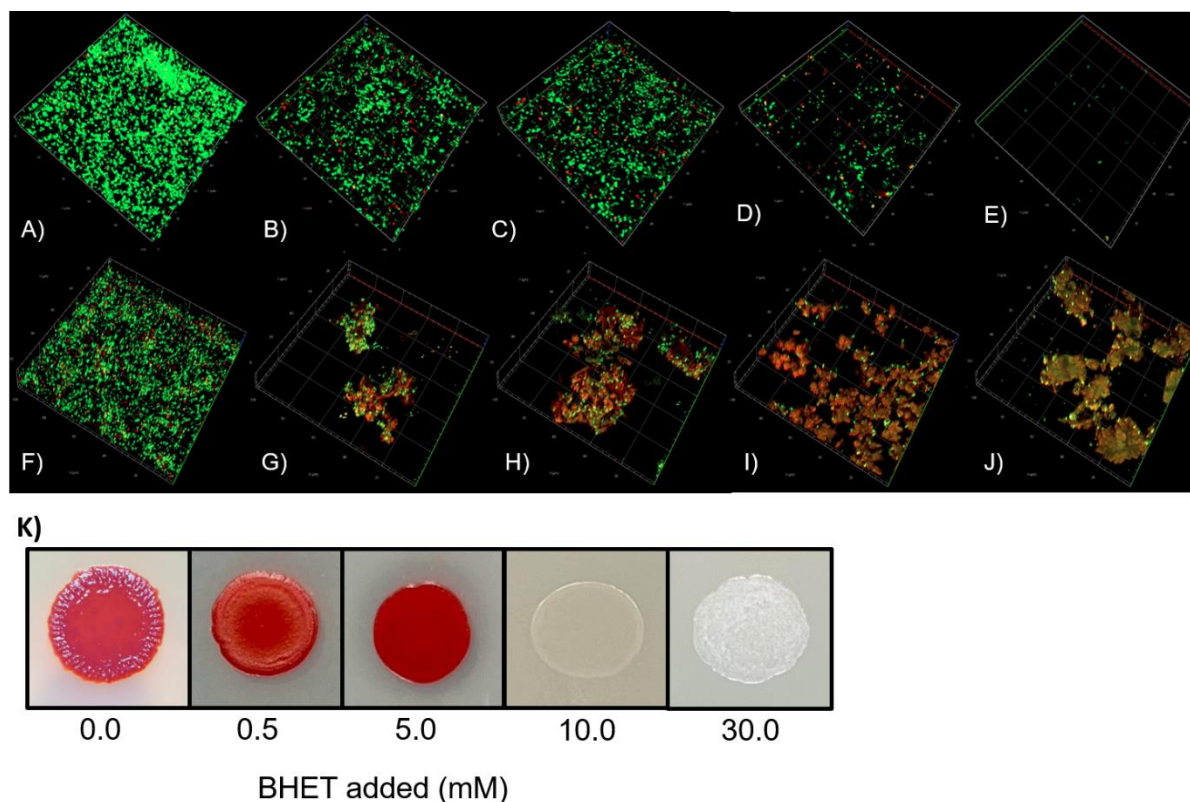

Figure 9 (Preuss et al., 2025, FIGURE S6): Phenotypical changes of DSM 21264 influenced by BHET and TPA Confocal laser scanning microscope (CLSM) images **(A-J)** of V. gazogenes DSM 21246 biofilms grown in the presence of increasing concentrations of BHET **(B-E)** and TPA **(G-J)** for 24 h of incubation at 28 °C. BHET concentrations ranged from 0.5 mM **B)**, 5 mM **C)**, 10 mM **D)**, 30 mM **E)**. Used TPA concentrations were 1 mM**(G)**, 5 mM **H)**, 10 mM **I)** and 20 mM **J)**. As controls DSM 21264 was inoculated with DMSO **F)** and also without any added substrates **A)**. Cells were stained using LIVE/DEAD stain.

K) Changing colony morphology of DSM 21246 in the presence of increasing BHET concentrations in LB agar plates at 28 °C after 24h of incubation.

As previously mentioned, prodigiosin is deeper characterized in *Serratia marcescens,* for which the prodigiosin synthase genes, such as *pigA* or *pigC,* are categorized as virulence factors (Liu et al., 2023). For the prodigiosin synthesis, numerous transcriptional regulators have been determined Among them are LuxS as part of AI-2, but also the two-component-systems EnvZ/OmpR, RssB/RssA and PigQ/W (Xiang et al., 2022). The transcription of the two-component-system EnvZ/OmpR decreased at rising BHET concentrations, indicating a connection to the failure of prodigiosin synthesis in DSM 21264, according to our RNAseq analysis. Since in the presence of higher BHET concentrations no prodigiosin was observable,

it is likely that the downregulation of EnvZ/OmpR contributed to the absence of red pigmentation (Figure 9, Preuss et al., 2025, FIGURE 6). Another interesting finding was the strong upregulation of genes from Reb family protein, involved in R-body synthesis, in the presence of 5 mM BHET. R-bodies, also called "killer trait", were first characterized in *Caedibacter* sp., which are endosymbionts of paramecia (Schrallhammer et al., 2011). Genes responsible for R-body production belong to the *reb* operon, and have also been found in the phylum Proteobacteria. R-bodies are believed to be involved in bacterial pathogenesis in species that carry the *reb* operon (Matsuoka et al 2017). For *Vibrio,* the R-body synthesis has not been described yet, thus the role in DSM 21264 can only be assumed. Since BHET seems to trigger stress responses, it is likely that DSM 21264 tries to use R-body synthesis as a protection mechanism.

5.6   BHET interferes with main regulatory circuits

For the deeper understanding of the role of PET and as well its degradation products towards the gene regulation of DSM 21264, main regulatory circuits influencing the metabolism and lifestyle, such as Quorum sensing (QS), cyclic-di-GMP synthesis and cAMP-CRP regulation, were analyzed in detail. QS and its associated regulatory pathways have been widely studied among several *Vibrio* sp., especially, the species involved in pathogenesis (Ng & Bassler, 2009, Seok et al., 2024, Simpson et al., 2024, Li et al., 2025, Morot et al., 2025). Using QS, bacteria are capable to adapt to their environment, regulating the gene expression depending on the cell density (Ng & Bassler, 2009). QS relies on the production of autoinducer molecules by the respective synthase, which are released in the surroundings. Accumulating autoinducers are detected by specific receptors located in the membrane or cytoplasm of the cells. At a certain threshold, gene expression is regulated in regard for community behavior (Figure 10, Rutherford & Bassler, 2012).

The regulation of QS relies under the control of the master QS regulators AphA, the low cell density regulator, initializing individual behavior, and HapR/LuxR, the high cell density regulator, initiating group behavior (Ball et al., 2017). On a molecular level, the AI binds to the respective receptor, activating the corresponding histidine kinase, which then acts as a phosphatase dephosphorylating LuxO, repressing the transcription of Qrr sRNAs, activating HapR (Figure 10, Rutherford & Bassler, 2012). In 2002 Miller *et al.* identified a novel QS system in *Vibrio cholerae,* which is exclusively encoded in the genomes of representatives of the genus *Vibrio,* the cholera autoinducer system (CAI), respectively (Miller et al., 2002). Regulatory pathways controlled by QS are involved in biofilm formation, secretion systems, proteases and virulence factors (Simpson et al., 2024).
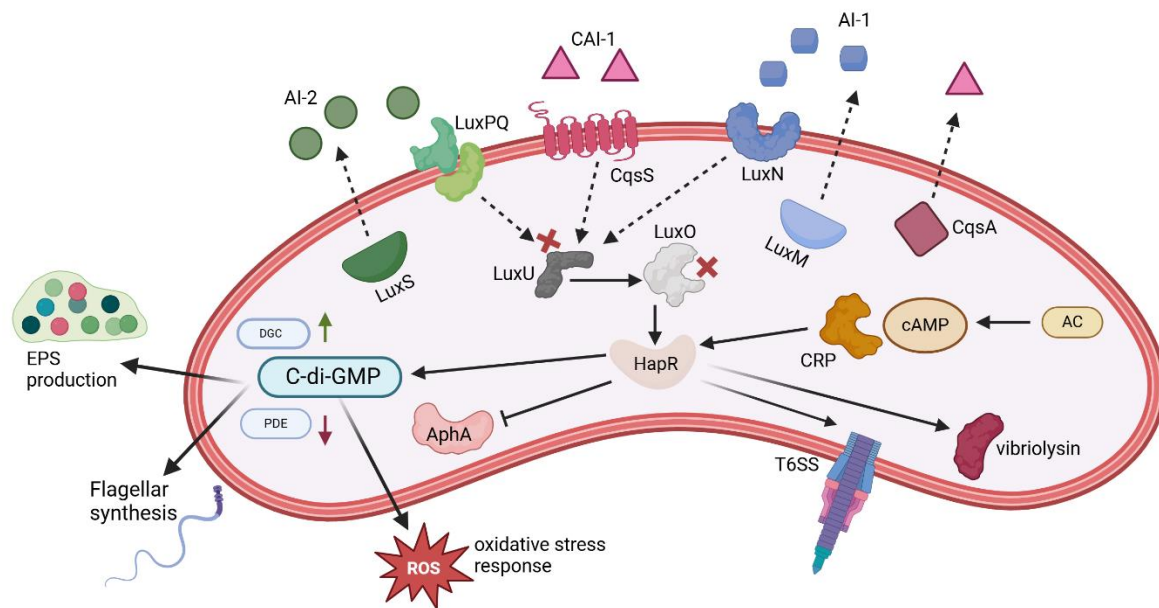
Figure 10: **Cellular model of regulation of global regulatory circuits including cyclic-di-GMP, cAMP-CRP and QS in DSM 21264**. DSM 21264 harbors three QS-systems, which initiate group behavior. The model shows gene regulation at high cell density. HapR, the master quorum sensing regulator, is upregulated at high density, and Apha, the master quorum sensing regulator at low cell density, is inhibited. CqsA, LuxS and LuxM are the autoinducer synthases, synthesizing CAI-1, AI-1 and AI-2. The autoinducers are bound by their corresponding response regulators CqsS, LuxN and LuxPQ, respectively. They thereupon dephosphorylate LuxU, inhibiting LuxO and therefore activate HapR. HapR, inter alia, induces the expression of T6SS and vibriolysin. HapR can additionally be activated by CRP-cAMP complex. The complex is formed by AC, synthesizing cAMP which binds to CRP. QS also regulates the c-di-GMP level in the cells by the induction of PDEs and DCGs. PDEs degrade c-di-GMP while DGCs synthesize the molecule. The c-di-GMP level inside the cell controls flagellar synthesis, EPS production or oxidative stress response, for example (Created with Biorender).

DSM 21264 harbors three QS systems, AI-1, including acyl-homoserine-lactone synthase LuxM and the corresponding histidine sensor kinase LuxN, *LuxS,* encodes autoinducer synthase responsible for AI-2 production. *LuxQ,* encodes the sensor kinase and along with the periplasmatic protein LuxP, detects AI-2. The Cholera autoinducer system (CAI) composes of the cholera autoinducer synthase (CqsA) and the response regulator (CqsS). The results of Chapter 1 have shown that biofilm formation is already altered at concentration of 0.5 mM BHET in the medium (Figure 9, Preuss et al., 2025). Regarding the RNAseq data of the different approaches in planktonic lifestyles as well as in biofilm status, we detect a highly distinct regulation of the QS systems. Autoinducer system 1 is strongly regulated in biofilm conditions and also in the presence of 30 mM BHET in planktonic cells. For lower concentrations of BHET and DSM 21264 grown in medium, supplemented with natural substrates, no particular changes in expression of the AI-1 system were observed. Regarding AI-2 system, strongest upregulation in DSM 21264 was observable in the presence of 5 mM

BHET, followed by 30 mM. Interestingly, in biofilm the AI-2 system was rather downregulated. The CAI system on the other hand was highly regulated under biofilm conditions, but no particular regulation was observed in the presence of BHET. The most intruding finding was detectable in the presence of 1 mM TPA, since the cholera autoinducer synthase (CqsA) was strongly downregulated (Preuss et al., 2025, FIGURE 5). Those findings indicate that DSM 21264 highly distinguishes between its surroundings and the organism adapts towards the environment, using different regulatory pathways, induced by the varying Quorum sensing systems. It is also assumable that DSM 21264 recognizes PET-degradation products as signal molecules influencing the transcription of the QS-systems. Research in *V. furnissii* have shown that AI-2 directly regulates the c-di-GMP level in the cells by the induction of phosphodiesterase activity, degrading c-di-GMP. The c-di-GMP level in the cell regulates the transcription of genes involved in stress response, enhancing oxidative stress tolerance and protection from DNA damage. Those genes include the universal stress proteins, namely UspA1, UspA2 and UspE (Zhang et al., 2025). The presence of 5 mM BHET induced the strongest upregulation of AI-2 in DSM 21264 and also UspB and UspE were upregulated by log2-foldchanges of 1 and 3, indicating that this regulatory circuit is equally induced in DSM 21264 (Preuss et al., 2025).

For the further understanding of the regulatory networks induced in the presence of BHET, genes associated with c-di-GMP were analyzed in detail. The ubiquitous bacterial second messenger controls a wide range of biological processes and is regulated by QS (Figure 10, Ball et al., 2017). Inter alia stress adaption, biofilm formation, virulence, motility or cell cycle progression are regulated by c-di-GMP (Jenal et al., 2017). The c-di-GMP synthesis is initiated from two guanosine-5'-triphosphate (GTP) molecules by diguanylate cyclases (DGCs) harboring a GGDEF domain. Phosphodiesterases (PDEs) containing an EAL or HD-GYP domain, which are c-di-GMP specific, thereupon degrade the c-di-GMP into GMP or 5'-phosphoguanylyl-(3', 5')-guanosine (pGpG) (Zhang et al., 2025). The level of cellular c-di-GMP is controlled by the expression of DGCs and PDEs synthesizing or degrading c-di-GMP, due to the response to internal or external signals. C-di-GMP concentration is an important regulator for the transition from motility to biofilm formation (Figure 10, Isenberg et al., 2024).

DSM 21264 codes for 14 DGCs and 10 PDEs in its genome, and many of them were differentially regulated either in biofilm status or in planktonic lifestyle supplemented with varying BHET concentrations (Preuss et al., 2025, FIGURE 4). For several pathogenic and few non-pathogenic *Vibrio* strains, the role of the individual c-di-GMP proteins are characterized in detail, revealing their role in biofilm matrix and extracellular polysaccharide production (EPS), and regulation of flagellar synthesis genes (Gong et al., 2023 Chen et al., 2024). For strains from the *Gazogenes*-clade, research within this field has not been yet conducted, so gene regulation in the presence of BHET remains unclear. Most of the flagellar-

associated genes were downregulated in DSM 21264 grown in medium supplemented with 30 mM BHET (Preuss et al., 2025, FIGURE 6). Downregulation of flagellar associated genes was also observed for *V. alginolyticus* with overexpressed VA4033, a diguanylate cyclase (Gong et al., 2023). Those finding indicates that homologues of this respective genes may as well be upregulated in DSM 21264, thus leading to similar phenotypes. Unfortunately, due to high sequence similarities between genes coding for DGCs, BLAST result showed high similarity to several DGCs. In our dataset, we were able to observe log2-foldchanges of 3.5 and 5 for *cdgG* and *acgB,* hypothesizing that they have a similar mode of action in DSM 21264 as VA4033 in *V. alginolyticus.*

Another important regulator for the switch from sessile to motile lifestyle is the cAMP receptor protein (CRP) (Manneh-Roussel et al., 2018). CRP binds to cAMP a second messenger which is synthesized by adenylate cyclases (ACs), forming the cAMP-CRP complex (Regmi et al., 2023). This conformational change enables the complex to bind to specific sequences, inducing or repressing the gene transcription of more than 100 promoters (Busby & Ebright, 1999). In *E. coli,* the mechanism of cAMP-CRP has originally been described to play a key role in utilization of non-preferred carbon sources. When glucose is absent in the medium, adenylate cyclase is upregulated producing cAMP (Figure 10, Saier et al., 1976). To date, six classes of ACs have been identified. *E. coli, Vibrio* sp and other Proteobacteria encode one AC gene belonging to the class AC-I (Linder, 2008). In the genome of DSM 21264, we only detected one gene (AAC977_15045), that can be assigned to class I adenylate cyclases. In the presence of 30 mM BHET, it was downregulated (log2-foldchange of -2) and slightly upregulated in the presence of 5 mM BHET (log2-foldchange of 0.8) Notably, in *V. parahaemolyticus* Δ*cyA* mutant strain an additional AC was identified, which is capable of cAMP synthesis. (Regmi et al., 2023). Therefore, transcriptional analysis of cyA in DSM 21264 may not be sufficient to determine intracellular cAMP concentrations, as the strain may express additional, yet unidentified, ACs. Further results revealed that deletion mutant Δ*crp* in *V. parahaemolyticus* formed significantly less biofilm than the wild-type strain, proving the relevance of CRP in biofilm formation (Regmi et al., 2023). This is in line with the finding that the regulation of master QS regulator HapR can further be controlled by cAMP receptor protein (CRP) (Silva & Benitez, 2004). Our RNAseq data revealed a strong downregulation of CRP and HapR in the presence of 30 mM BHET in DSM 21264 (log2-foldchange -2.8 and -1.8) and a reduced transcription in medium supplemented with 5 mM of BHET (log2-foldchange -1.2), respectively. Also, a slight decrease in transcription of *crp* was determined in the 0.5 mM BHET samples (log2-foldchange -0.3). This could indicate that BHET interferes with the transcription of *crp* explaining the decreased biofilm formation of DSM 21264, when it is present in the medium (Figure 9, Preuss et al., 2025, FIGURE 6).

Since those second messengers also have been determined to be essential for the formation of the plastisphere (Dey et al., 2022) the changes in transcription influenced by BHET might decrease bacterial attachment on PET surfaces in nature.

5.7 BHET induces oxidative stress in the DSM 21264

When exposed to 30 mM of BHET, DSM 21264 induced significantly differential expression of 20% of all its genes, indicating that the organism was highly challenged, and regulatory networks towards stress response were expressed. Differential gene response under varying stress environments have been documented for starvation, osmotic stress, phage induction, pH stress, DNA damage and also oxidative stress in bacteria (Durfee et al., 2007, Gunasekera et al., 2008, Wang et al., 2012). Those changes in expression patterns underly highly distinct regulatory networks, inducing up to hundreds of differentially expressed genes, resulting in varying phenotypes (Bhatia et al., 2022). OxyR has been identified as a major transcriptional regulator in response to oxidative stress in various bacterial species (Wang et al., 2012, Choudhary et al., 2024). The gene belongs to the LysR family, and is highly conserved among Gram-negative as well as Gram-positive bacteria. Besides oxidative stress, it also influences biofilm formation or virulence (Antelmann & Helmann, 2010). Interestingly, we detected a slight upregulation of OxyR in the presence of 5 mM BHET, but the gene was strongly upregulated at log2-foldchange above 3 in the presence of 30 mM BHET. Those regulation patterns indicate that increasing concentrations of this PET-degradation intermediate induce oxidative stress responses (Preuss et al., 2025, FIGURE 6). Oxidative stress can be caused by reactive oxygen species (ROS), a challenge for all living organisms, since it is responsible for major damage towards DNA, proteins and membranes (Wang et al., 2012). For PET nanoparticles, it has already been observed that the exposure towards *Chlorella vulgaris* resulted in reduced growth and also a significantly higher intracellular level of ROS (Vijayan et al., 2024). In *V. cholerae,* OxyR regulates the transcription of alkyl hydroxide peroxidases *ahpC* and *ahpF* (Wang et al., 2017). In DSM 21264, these genes have not only been upregulated in the presence of BHET, but interestingly they were also among the four significantly differentially expressed genes regarding the surface dependent RNAseq on PET compared to PE foil (Preuss et al., FIGURE 6, TABLE S2). Since we also detected BHET in the medium when DSM 21264 is incubated with PET, the gene regulation might also be induced by the degradation product BHET rather than the polymer itself. Additionally, Dps family protein and glutathione peroxidase were significantly upregulated during incubation on PET surface and supplemented with 30 mM BHET, which also have been characterized to be involved in oxidative stress response (Xia et al., 2017, Loterio et al., 2023).

Other regulatory pathways that were highly induced in the presence of BHET might also be related to oxidative stress, such as the increased transcription of all three prophages, encoded on the genome of DSM 21264. Medium supplemented with higher BHET concentrations increased transcription of VGPH01 and VGPH02 (Preuss et al., FIGURE 6, TABLE S3). Prophage induction is determined to be a reaction towards oxidative stress in the presence of ROS in other Gram-negative bacteria such as *Salmonella enterica* or *E. coli* (Filipiak et al., 2020, Uppalapati et al., 2024). Until now the information about prophages in *Vibrio* from the *Gazogenes*-clade is rare, thus deeper research has to be conducted to understand the regulatory pathways of prophage induction.

Overall, these findings indicate that not only PET, but also its intermediate BHET are highly toxic for the microplastic-associated community. Since DSM 21264 rapidly converts BHET into MEHT, it is likely that MHET also contributes to the observed toxicity towards the attached organisms. Furthermore, the oxidative stress due to ROS induced by PET and its intermediates, can negatively impact the aquaculture and its inhabitants and might be involved in the finding that PET is less colonized than other plastic polymers (Cai et al., 2019).

5.8 Prevention of biofouling due to surface adaption

Relevant aspects for surface attachment with focus on the plastisphere have already been discussed in detail. Not only plastic waste is colonized rapidly by the surrounding material, but also plastic surfaces, which are used in daily life, when they are exposed to biotic environment. Bacterial biofilms are considered a serious threat in processing facilities such as industrial sectors, food packaging or hospital settings, since bacteria also attach to medical devices or within the marine industry. This process is referred to as biofouling (Dobretsov et al., 2006, Muhammad et al., 2020). Especially, in water desalination for the supply of fresh water biofouling plays a threatening role. To obtain fresh-water from salt-water or other wastewater sources, reverse osmosis is predominantly used, filtering the water through thin-film composite polyamide membranes, which have a risk of microbiological fouling (Zamora et al., 2023, Wu et al., 2025). Discussing the plastisphere, the strong potential of bacteria to adapt to new ecological niches, and colonizing all kinds of surfaces with highly distinct biofilms, has already been clarified. Since the membrane bioreactors also comprise of plastic polymers, it can be assumed that comparable biofilms are formed on those polymers, harming the surface. For the prevention of biofouling, several studies focused on the adaption of the surface to decrease bacterial attachment (Kim et al., 2021, Burmeister et al., 2023[2], Burmeister et al., 2023[1] (Chapter 3), Zamora et al., 2023, Wu et al., 2025). Within Chapter 3, PE, the most produced plastic polymer, was used as a base material, and polymeric *N*-oxides were grafted on the substrate. Three different polymeric *N*-oxides were grafted on the PE surface, namely PE-poly-

(VBNOx), PE-poly-(MAANOx) and PE-poly-(MANOx) (Burmeister et al., 2023[1]). To evaluate the changes in bacterial adhesion, marine *Vibrio campelli* was incubated on treated compared to untreated PE, and observed at the Laser Scanning Microscope. The images revealed a significant decrease of attaching cells (Burmeister et al., 2023[1], FIGURE 4). *V. campbelli* is ubiquitously occurring in marine systems, and has also been reported to be abundant in the plastisphere. Additionally, it is classified as an emerging pathogen towards the aquaculture, and harbors numerous antibiotic resistant genes (Defoirdt et al., 2006, Lacerda et al., 2024, Zhang et al., 2024).

Recently, poly (amine oxide) (PAO) was introduced as an alternative to polyethylene glycol (PEG), which is widely used in stealth material in numerous medical products, but is often affected by biofouling. PAO is also based on grafting zwitterionic *N*-oxides on the surface. Modified surfaces also led to decreased bacterial attachment (Luc et al., 2023). The prevention of attachment and biofouling due to zwitterions has already been studied in recent years. They contain an equal number of oppositely charged ions, zwitterions, which are characterized as hydrophilic biomaterials binding water molecules via electrostatically induced hydration (Li et al., 2019). Within Chapter 3, poly *N*-oxides were used as zwitterions, which have to that time not been described for their antibacterial activity. The expected antimicrobial mechanism of the poly *N*-oxide grafted surfaces relies on the release of ROS in the presence of microorganisms, which has been determined by paramagnetic resonance (EPR)-spectroscopy for all three grafted surfaces (Burmeister et al., 2023[1]). The release of ROS triggers oxidative stress within the bacterial cell, leading to the damage of DNA, membranes and proteins. Bacteria possess several oxidative defense related genes, which were already detailed characterized (Wang et al., 2012). Nevertheless, if ROS concentration is too high, bacterial defense mechanisms are not sufficient to maintain survival of the cells, as described in Chapter 3 on adapted PE-surfaces (Burmeister et al., 2023[1]). Other studies also generated surface coatings, using different chemical compounds, which showed antibiofouling due to the release of ROS (Natarajan et al., 2016, Ma et al., 2020) Despite the advantages of low-fouling, induced by ROS, it also presents risks by harming the aquaculture (Braz-Mota et al., 2018). Since the release of ROS by poly *N*-oxides is only triggered in the presence of bacteria, no toxic effects originating from the surface can be assumed. Yet, to confirm this assumption further research needs to be conducted.

Interestingly, our study revealed an equal effect of BHET like the adapted surfaces, where no bacterial attachment was observed. Since studies have shown that PET is less colonized than other plastic polymers it is likely that this observation is due to BHET release in the surface and thereupon the release of ROS decreasing potential biodegradation.

The mechanism of grafting different poly *N*-oxides can be used for other plastics than PE as a base material, offering novel possibilities to prevent biofouling (Burmeister et al., 2023[1]). Additional advantages of the reduction of biofouling is an exceeding durability of the plastics used in varying industries, since they don't have to be exchanged due to occurring biodegradation or contamination with potential pathogens. Extending the durability might decreases plastic waste, and thereupon contributes to less environmental pollution by the polymers.

Regarding the emerging plastic pollution, the question, if the adapted or coated materials change bacterial colonization in the marine ecosystem on the respective polymer, occurs inevitably. It might be assumed that those polymers are less colonized in the aquatic system. This might further reduce the capabilities of biodegradation by the attaching microorganisms, but it can also be classified as an advantage, since the risk of accumulating pathogens and also of alien species, invading new environments, is significantly reduced. Further this might protect the aquaculture and eventually also human well-being.

6   Conclusion & Outlook

The present study addresses major concerns occurring with the increasing plastic production and the accompanying global plastic pollution. Within this framework three target problems were addressed, contributing to a better understanding of the bacterial gene expression in the plastisphere and also the influence of PET breakdown products (I), degradation of PET polymer under laboratory conditions and in the native host (II). Further the prevention of biofouling was investigated (III).

(I)   The first part of this study focused on a more detailed understanding of the gene regulation during initial attachment, using model organism DSM 21264 with respect to the expression of the PET esterase, PET6. The results revealed that potential PET-degrading DSM 21264 does not distinguish significantly between PET and PE surface during initial attachment. However, transcriptome analyses identified genes, which are important for the initial attachment, and might also play a role in the plastisphere, respectively. Among those genes were *ompU, secY, hapR* and other relevant virulence factors.

While PET-film does not appear to have a major impact on the gene transcription of DSM 21264 during first attachment, the PET degradation products BHET and TPA lead to strong changes in several metabolic pathways, including cyclic-di-GMP production, Quroum-sensing and cAMP-CRP circuit. RNAseq further revealed upregulation of *oxyR*, transcriptional regulator towards oxidative stress response, indicating for the first time that PET breakdown products induce oxidative stress maybe due to ROS in bacteria, identifying a possible threat for bacteria in the plastisphere.

(II)   Within in the second Chapter, the first PET degrading enzymes from the phylum Bacteroidetes were identified, which is among the most abundant phyla within the plastisphere. Characterization of those enzymes gives a more detailed understanding of the molecular mechanism, and contributes to the finding of novel PETases. Additionally, biofilm analysis has shown that *K. jeonii* attaches to PET surface and along with the identified signal peptides of PET27 and PET30, it is very likely that species from the phylum Bacteroidetes also contribute to the degradation of PET in nature.

(III)   The third Chapter of the study aimed to prevent attachment to plastic surfaces, using model organism from *Vibrio* sp., determining the decrease in colonization. The process of preventing biofouling was forwarded by adapting PE surface by grafting the polymer with zwitterionic poly-*N*-oxides. Results have shown that less

bacteria are able to form biofilms on the adapted surfaces. Since the surface adaption can be integrated also on other plastic polymers as base material, biofouling can be prevented, enhancing the durability of these plastics, and therefore plastic waste might further be reduced to a respective level. Additionally, if those adapted polymers end up in the environment, the risk of the accumulation of pathogenic bacteria might decrease.

Overall, this study provides valuable insights into plastic colonization and forwards its better understanding. Additionally, potential degradation as well as strategies for the prevention of biofouling were analyzed. This contributes to improved recycling and may also reduce plastic waste, by expanding the lifetime duration of the materials. Approaches targeting different points accompanying with the emerging threat due to plastic pollution were made, outlining perspectives for an improved management towards plastic waste. Notably, this study identified, for the first time, PET-degradation products as risk factors for bacterial systems, highlighting their potential, negative, impact on both, microbial communities and the marine environment. The obtained results provide a promising basis for future investigations and offer new perspectives for the scientific research in the field of plastic colonization and biodegradation.

.

7   References

Ahmad, M., Ahmad, J., Usama, M., Al-Swadi, H. A., Mousa, M. A., Rafique, M. I., Al-Wabel, M. I., & Al-Farraj, A. S. F. (2025). Microplastic contamination in commercial food and drink products and associated risk of potential human intake in Riyadh, Saudi Arabia. *Environmental Monitoring and Assessment*, *197*(3). https://doi.org/10.1007/s10661-025-13680-9

Ahmad, M., Li, J. L., Wang, P. D., Hozzein, W. N., & Li, W. J. (2020). Environmental perspectives of microplastic pollution in the aquatic environment: a review. In *Marine Life Science and Technology* (Vol. 2, Issue 4, pp. 414–430). Springer. https://doi.org/10.1007/s42995-020-00056-w

Ali, M. I., Ahmed, S., Robson, G., Javed, I., Ali, N., Atiq, N., & Hameed, A. (2014). Isolation and molecular characterization of polyvinyl chloride (PVC) plastic degrading fungal isolates. *Journal of Basic Microbiology*, *54*(1), 18–27. https://doi.org/10.1002/jobm.201200496

Alencar, M. V., Gimenez, B. G., Sasahara, C., Elliff, C. I., Rodrigues, L. S., Conti, L. A., Gonçalves Dias, S. L. F., Cetrulo, T. B., Scrich, V. M., & Turra, A. (2022). How far are we from robust estimates of plastic litter leakage to the environment? *Journal of Environmental Management*, *323*. https://doi.org/10.1016/j.jenvman.2022.116195

Allen, G. R., Reichelt, J. L., Grayv, P. P., & Wales, S. (1983). Influence of Environmental Factors and Medium Composition on Vibrio gazogenes Growth and Prodigiosin Production. In *APPLIED AND ENVIRONMENTAL MICROBIOLOGY* (Vol. 45, Issue 6).

Almeida, E. L., Rincón, A. F. C., Jackson, S. A., & Dobson, A. D. W. (2019). In silico Screening and Heterologous Expression of a Polyethylene Terephthalate Hydrolase (PETase)-Like Enzyme (SM14est) With Polycaprolactone (PCL)-Degrading Activity, From the Marine Sponge-Derived Strain Streptomyces sp. SM14. *Frontiers in Microbiology*, *10*. https://doi.org/10.3389/fmicb.2019.02187

Amaral-Zettler, L. A., Zettler, E. R., & Mincer, T. J. (2020). Ecology of the plastisphere. In *Nature Reviews Microbiology* (Vol. 18, Issue 3, pp. 139–151). Nature Research. https://doi.org/10.1038/s41579-019-0308-0

Amaral-Zettler, L. A., Zettler, E. R., Slikas, B., Boyd, G. D., Melvin, D. W., Morrall, C. E., Proskurowski, G., & Mincer, T. J. (2015). The biogeography of the Plastisphere: Implications for policy. *Frontiers in Ecology and the Environment*, *13*(10), 541–546. https://doi.org/10.1890/150017

Andrady, A. L. (2011). Microplastics in the marine environment. In *Marine Pollution Bulletin* (Vol. 62, Issue 8, pp. 1596–1605). https://doi.org/10.1016/j.marpolbul.2011.05.030

Antelmann, H., & Helmann, J. D. (n.d.-a). Thiol-Based Redox Switches and Gene Regulation. In *Antioxid. Redox Signal* (Vol. 14).

Anuar Sharuddin, S. D., Abnisa, F., Wan Daud, W. M. A., & Aroua, M. K. (2016). A review on pyrolysis of plastic wastes. In *Energy Conversion and Management* (Vol. 115, pp. 308–326). Elsevier Ltd. https://doi.org/10.1016/j.enconman.2016.02.037

Arnal, G., Anglade, J., Gavalda, S., Tournier, V., Chabot, N., Bornscheuer, U. T., Weber, G., & Marty, A. (2023). Assessment of Four Engineered PET Degrading Enzymes Considering Large-Scale Industrial Applications. *ACS Catalysis*, *13*(20), 13156–13166. https://doi.org/10.1021/acscatal.3c02922

References

Auta, H. S., Emenike, C. U., & Fauziah, S. H. (2017). Screening of Bacillus strains isolated from mangrove ecosystems in Peninsular Malaysia for microplastic degradation. *Environmental Pollution*, *231*, 1552–1559. https://doi.org/10.1016/j.envpol.2017.09.043

Baker-Austin, C., Oliver, J. D., Alam, M., Ali, A., Waldor, M. K., Qadri, F., & Martinez-Urtaza, J. (2018). Vibrio spp. infections. *Nature Reviews Disease Primers*, *4*(1). https://doi.org/10.1038/s41572-018-0005-8

Ball, A. S., Chaparian, R. R., & van Kessel, J. C. (2017). *Quorum Sensing Gene Regulation by LuxR/HapR Master Regulators in Vibrios.* https://doi.org/10.1128/jb.00105-17

Baumann, P., Baumann, L., Bang, S. S., & Woolkalis, M. J. (n.d.-a). Reevaluation of the Taxonomy of Vibrio, Beneckea, and Photobacterium: Abolition of the Genus Beneckea. In *NI M[c~ROBIOLOOY* (Vol. 4).

Bhagwat, G., Zhu, Q., O'Connor, W., Subashchandrabose, S., Grainge, I., Knight, R., & Palanisami, T. (2021). Exploring the Composition and Functions of Plastic Microbiome Using Whole-Genome Sequencing. *Environmental Science and Technology*, *55*(8), 4899–4913. https://doi.org/10.1021/acs.est.0c07952

Bhatia, R. P., Kirit, H. A., Predeus, A. v., & Bollback, J. P. (2022). Transcriptomic profiling of Escherichia coli K-12 in response to a compendium of stressors. *Scientific Reports*, *12*(1). https://doi.org/10.1038/s41598-022-12463-3

Braz-Mota, S., Campos, D. F., MacCormack, T. J., Duarte, R. M., Val, A. L., & Almeida-Val, V. M. F. (2018). Mechanisms of toxic action of copper and copper nanoparticles in two Amazon fish species: Dwarf cichlid (Apistogramma agassizii) and cardinal tetra (Paracheirodon axelrodi). *Science of the Total Environment*, *630*, 1168–1180. https://doi.org/10.1016/j.scitotenv.2018.02.216

Buchholz, P. C. F., Feuerriegel, G., Zhang, H., Perez-Garcia, P., Nover, L. L., Chow, J., Streit, W. R., & Pleiss, J. (2022). Plastics degradation by hydrolytic enzymes: The plastics-active enzymes database—PAZy. *Proteins: Structure, Function and Bioinformatics*, *90*(7), 1443–1456. https://doi.org/10.1002/prot.26325

Buhari, S. B., Ghahremani Nezhad, N., Normi, Y. M., Mohd Shariff, F., & Leow, T. C. (2025). Homology modeling and thermostability enhancement of Vibrio palustris PETase via hydrophobic interactions. *Journal of Biomolecular Structure and Dynamics*. https://doi.org/10.1080/07391102.2024.2440646

Burmeister[1], N., Zorn, E., Farooq, A., Preuss, L., Vollstedt, C., Friedrich, T., Mantel, T., Scharnagl, N., Rohnke, M., Ernst, M., Wicha, S. G., Streit, W. R., & Maison, W. (2023). Surface Grafted N-Oxides have Low-Fouling and Antibacterial Properties. *Advanced Materials Interfaces*, *10*(35). https://doi.org/10.1002/admi.202300505

Burmeister[2], N., Zorn, E., Preuss, L., Timm, D., Scharnagl, N., Rohnke, M., Wicha, S. G., Streit, W. R., & Maison, W. (2023). Low-Fouling and Antibacterial Polymer Brushes via Surface-Initiated Polymerization of a Mixed Zwitterionic and Cationic Monomer. *Langmuir*, *39*(49), 17959–17971. https://doi.org/10.1021/acs.langmuir.3c02657

Burmeister[3], N., Vollstedt, C., Kröger, C., Friedrich, T., Scharnagl, N., Rohnke, M., Zorn, E., Wicha, S. G., Streit, W. R., & Maison, W. (2023). Zwitterionic surface modification of polyethylene via atmospheric plasma-induced polymerization of (vinylbenzyl-)sulfobetaine and evaluation of antifouling properties. *Colloids and Surfaces B: Biointerfaces*, *224*. https://doi.org/10.1016/j.colsurfb.2023.113195

References

Busby, S., & Ebright, R. H. (n.d.-a). *Transcription Activation by Catabolite Activator Protein (CAP)*. http://www.idealibrary.com

Cai, L., Wu, D., Xia, J., Shi, H., & Kim, H. (2019). Influence of physicochemical surface properties on the adhesion of bacteria onto four types of plastics. *Science of the Total Environment*, *671*, 1101–1107. https://doi.org/10.1016/j.scitotenv.2019.03.434

Carpenter, E. J., & Smith, K. L. JR. (1972). *Plastics on the Sargasso Sea Surface*. https://www.science.org

Carter, L. M., MacFarlane, C. E., Karlock, S. P., Sen, T., Kaar, J. L., Berberich, J. A., & Boock, J. T. (2024). Increased cytoplasmic expression of PETase enzymes in E. coli. *Microbial Cell Factories*, *23*(1). https://doi.org/10.1186/s12934-024-02585-w

Castro, A. J. (1967).Antimicrobial Activity of Prodigiosin *213903a0, Nature portfolio*.

Che, J., Liu, B., Fang, Q., Nissa, M. un, Luo, T., Wang, L., & Bao, B. (2025). Biological studies reveal the role of trpA gene in biofilm formation, motility, hemolysis and virulence in Vibrio anguillarum. *Microbial Pathogenesis*, *200*. https://doi.org/10.1016/j.micpath.2025.107331

Chen, X. Q., Rao, D. M., Zhu, X. Y., Zhao, X. M., Huang, Q. S., Wu, J., & Yan, Z. F. (2025). Current state and sustainable management of waste polyethylene terephthalate bio-disposal: enzymatic degradation to upcycling. In *Bioresource Technology* (Vol. 429). Elsevier Ltd. https://doi.org/10.1016/j.biortech.2025.132492

Chen, Y. W., Tseng, T. S., Chen, K. T., & Lai, S. J. (2024). A novel Diguanylate cyclase VdcR has multifaceted regulatory functions in the pathogenicity of Vibrio vulnificus. *Journal of Microbiology, Immunology and Infection*. https://doi.org/10.1016/j.jmii.2024.11.013

Choudhary, D., Foster, K. R., & Uphoff, S. (2024). The master regulator OxyR orchestrates bacterial oxidative stress response genes in space and time. *Cell Systems*, *15*(11), 1033-1045.e6. https://doi.org/10.1016/j.cels.2024.10.003

Chow, J., Perez-Garcia, P., Dierkes, R., & Streit, W. R. (2023). Microbial enzymes will offer limited solutions to the global plastic pollution crisis. In *Microbial Biotechnology* (Vol. 16, Issue 2, pp. 195–217). John Wiley and Sons Ltd. https://doi.org/10.1111/1751-7915.14135

Clayman, H. M. (n.d.). *Polypropylene*.

Conkle, J. L., Báez Del Valle, C. D., & Turner, J. W. (2018). Are We Underestimating Microplastic Contamination in Aquatic Environments? *Environmental Management*, *61*(1), 1–8. https://doi.org/10.1007/s00267-017-0947-8

Danso, D., Chow, J., & Streit, W. R. (2019). Plastics: Environmental and biotechnological perspectives on microbial degradation. In *Applied and Environmental Microbiology* (Vol. 85, Issue 19). American Society for Microbiology. https://doi.org/10.1128/AEM.01095-19

Danso, D., Schmeisser, C., Chow, J., Zimmermann, W., Wei, R., Leggewie, C., Li, X., Hazen, T., Streit, W. R., & Danso, C. D. (2018). *New Insights into the Function and Global Distribution of Polyethylene Terephthalate (PET)-Degrading Bacteria and Enzymes in Marine and Terrestrial Metagenomes*. https://doi.org/10.1128/AEM

Davidov, K., Iankelevich-Kounio, E., Yakovenko, I., Koucherov, Y., Rubin-Blum, M., & Oren, M. (2020). Identification of plastic-associated species in the Mediterranean Sea using DNA metabarcoding with Nanopore MinION. *Scientific Reports*, *10*(1). https://doi.org/10.1038/s41598-020-74180-z

References

Davidov, K., Marsay, K. S., Itzahri, S., Rubin-Blum, M., Sobral, P., Kranzler, C. F., & Oren, M. (2024). Community composition and seasonal dynamics of microplastic biota in the Eastern Mediterranean Sea. *Scientific Reports*, *14*(1), 26131. https://doi.org/10.1038/s41598-024-73281-3

de Oliveira, M. V. D., Calandrini, G., da Costa, C. H. S., da Silva de Souza, C. G., Alves, C. N., Silva, J. R. A., Lima, A. H., & Lameira, J. (2025). Evaluating cutinase from Fusarium oxysporum as a biocatalyst for the degradation of nine synthetic polymer. *Scientific Reports*, *15*(1), 2887. https://doi.org/10.1038/s41598-024-84718-0

Defoirdt, T., Halet, D., Vervaeren, H., Boon, N., van de Wiele, T., Sorgeloos, P., Bossier, P., & Verstraete, W. (2007). The bacterial storage compound poly-β-hydroxybutyrate protects Artemia franciscana from pathogenic Vibrio campbellii. *Environmental Microbiology*, *9*(2), 445–452. https://doi.org/10.1111/j.1462-2920.2006.01161.x

Delacuvellerie, A., Ballerini, T., Frère, L., Matallana-Surget, S., Dumontet, B., & Wattiez, R. (2022). From rivers to marine environments: A constantly evolving microbial community within the plastisphere. *Marine Pollution Bulletin*, *179*. https://doi.org/10.1016/j.marpolbul.2022.113660

Delacuvellerie, A., Benali, S., Cyriaque, V., Moins, S., Raquez, J. M., Gobert, S., & Wattiez, R. (2021). Microbial biofilm composition and polymer degradation of compostable and non-compostable plastics immersed in the marine environment. *Journal of Hazardous Materials*, *419*. https://doi.org/10.1016/j.jhazmat.2021.126526

Deng, J. J., Zhang, J. R., Mao, H. H., Zhang, M. S., Lu, Y. S., & Luo, X. C. (2025). Chitinases are important virulence factors in Vibrio for degrading the chitin-rich barrier of shrimp. *International Journal of Biological Macromolecules*, *293*. https://doi.org/10.1016/j.ijbiomac.2024.139215

Derraik, B. (n.d.-a). *The pollution of the marine environment by plastic debris: a review Jos e e G*. www.elsevier.com/locate/marpolbul

Dey, S., Rout, A. K., Behera, B. K., & Ghosh, K. (2022). Plastisphere community assemblage of aquatic environment: plastic-microbe interaction, role in degradation and characterization technologies. In *Environmental Microbiomes* (Vol. 17, Issue 1). BioMed Central Ltd. https://doi.org/10.1186/s40793-022-00430-4

Dierkes, R. F., Wypych, A., Pérez-García, P., Danso, D., Chow, J., & Streit, W. R. (2023). An Ultra-Sensitive Comamonas thiooxidans Biosensor for the Rapid Detection of Enzymatic Polyethylene Terephthalate (PET) Degradation. *Applied and Environmental Microbiology*, *89*(1). https://doi.org/10.1128/aem.01603-22

Dileepan, A. G. B., Jeyaram, S., Arumugam, N., Almansour, A. I., & Santhamoorthy, M. (2025). Identification and occurrence of microplastics in drinking water bottles and milk packaging consumed by humans daily. *Environmental Monitoring and Assessment*, *197*(3). https://doi.org/10.1007/s10661-025-13721-3

Dobretsov, S., Dahms, H. U., & Qian, P. Y. (2006). Inhibition of biofouling by marine microorganisms and their metabolites. In *Biofouling* (Vol. 22, Issue 1, pp. 43–54). https://doi.org/10.1080/08927010500504784

References

Duan, S., Zhang, N., Chao, T., Wu, Y., & Wang, M. (2023). The structural and molecular mechanisms of type II PETases: a mini review. In *Biotechnology Letters* (Vol. 45, Issue 10, pp. 1249–1263). Springer Science and Business Media B.V. https://doi.org/10.1007/s10529-023-03418-3

Durfee, T., Hansen, A. M., Zhi, H., Blattner, F. R., & Ding, J. J. (2008). Transcription profiling of the stringent response in Escherichia coli. *Journal of Bacteriology*, *190*(3), 1084–1096. https://doi.org/10.1128/JB.01092-07

Economou, A. (1998). Bacterial preprotein translocase: Mechanism and conformational dynamics of a processive enzyme. In *Molecular Microbiology* (Vol. 27, Issue 3, pp. 511–518). https://doi.org/10.1046/j.1365-2958.1998.00713.x

Filipiak, M., Łoś, J. M., & Łoś, M. (2020). Efficiency of induction of Shiga-toxin lambdoid prophages in Escherichia coli due to oxidative and antibiotic stress depends on the combination of prophage and the bacterial strain. *Journal of Applied Genetics*, *61*(1), 131–140. https://doi.org/10.1007/s13353-019-00525-8

Franden, M. A., Jayakody, L. N., Li, W. J., Wagner, N. J., Cleveland, N. S., Michener, W. E., Hauer, B., Blank, L. M., Wierckx, N., Klebensberger, J., & Beckham, G. T. (2018). Engineering Pseudomonas putida KT2440 for efficient ethylene glycol utilization. *Metabolic Engineering*, *48*, 197–207. https://doi.org/10.1016/j.ymben.2018.06.003

Frère, L., Maignien, L., Chalopin, M., Huvet, A., Rinnert, E., Morrison, H., Kerninon, S., Cassone, A. L., Lambert, C., Reveillaud, J., & Paul-Pont, I. (2018). Microplastic bacterial communities in the Bay of Brest: Influence of polymer type and size. *Environmental Pollution*, *242*, 614–625. https://doi.org/10.1016/j.envpol.2018.07.023

Fritzsche, S., Popp, M., Spälter, L., Bonakdar, N., Vogel, N., & Castiglione, K. (2025). Recycling the recyclers: strategies for the immobilisation of a PET-degrading cutinase. *Bioprocess and Biosystems Engineering*. https://doi.org/10.1007/s00449-025-03131-7

Fung, B. L., & Visick, K. L. (2025). LitR and its quorum-sensing regulators modulate biofilm formation by Vibrio fischeri. *Journal of Bacteriology*, *207*(2). https://doi.org/10.1128/jb.00476-24

Garces, F., Fernández, F. J., Montellà, C., Penya-Soler, E., Prohens, R., Aguilar, J., Baldomà, L., Coll, M., Badia, J., & Vega, M. C. (2010). Molecular architecture of the Mn2+-dependent lactonase UlaG reveals an RNase-like metallo-β-lactamase fold and a novel quaternary structure. *Journal of Molecular Biology*, *398*(5), 715–729. https://doi.org/10.1016/j.jmb.2010.03.041

Garces, F., Fernández, F. J., Pérez-Luque, R., Aguilar, J., Baldomà, L., Coll, M., Badía, J., & Vega, M. C. (2008). Overproduction, crystallization and preliminary X-ray analysis of the putative L-ascorbate-6-phosphate lactonase UlaG from Escherichia coli. *Acta Crystallographica Section F: Structural Biology and Crystallization Communications*, *64*(1), 36–38. https://doi.org/10.1107/S1744309107065256

Garcés-Ordóñez, O., Córdoba-Meza, T., Sáenz-Arias, S., Blandón, L., Espinosa-Díaz, L. F., Pérez-Duque, A., Thiel, M., & Canals, M. (2024). Potentially pathogenic bacteria in the plastisphere from water, sediments, and commercial fish in a tropical coastal lagoon: An assessment and management proposal. *Journal of Hazardous Materials*, *479*. https://doi.org/10.1016/j.jhazmat.2024.135638

Geyer, R., Jambeck, J. R., & Law, K. L. (2017). *Production, use, and fate of all plastics ever made*. https://www.science.org

References

Ghatge, S., Yang, Y., Ahn, J. H., & Hur, H. G. (2020). Biodegradation of polyethylene: a brief review. In *Applied Biological Chemistry* (Vol. 63, Issue 1). Springer Science and Business Media B.V. https://doi.org/10.1186/s13765-020-00511-3

Gong, X. X., Zeng, Y. H., Chen, H. M., Zhang, N., Han, Y., Long, H., & Xie, Z. Y. (2023). Bioinformatic and functional characterization of cyclic-di-GMP metabolic proteins in Vibrio alginolyticus unveils key diguanylate cyclases controlling multiple biofilm-associated phenotypes. *Frontiers in Microbiology*, *14*. https://doi.org/10.3389/fmicb.2023.1258415

Grant, T. A., López-Pérez, M., Haro-Moreno, J. M., & Almagro-Moreno, S. (2023). Allelic diversity uncovers protein domains contributing to the emergence of antimicrobial resistance. *PLoS Genetics*, *19*(3). https://doi.org/10.1371/journal.pgen.1010490

Gregory, M. R. (1996). Plastic "Scrubbers" in Hand Cleansers: a Further (and Minor) Source for Marine Pollution Identified. In *Marine Pollution Bulletin* (Vol. 32, Issue 12).

Gulizia, A. M., Bell, S. C., Kuek, F., Santana, M. M. F., Edmunds, R. C., Yeoh, Y. K., Sato, Y., Haikola, P., van Herwerden, L., Motti, C. A., Bourne, D. G., & Vamvounis, G. (2025). Biofilm development as a factor driving the degradation of plasticised marine microplastics. *Journal of Hazardous Materials*, *487*. https://doi.org/10.1016/j.jhazmat.2024.136975

Gunasekera, T. S., Csonka, L. N., & Paliy, O. (2008). Genome-wide transcriptional responses of Escherichia coli K-12 to continuous osmotic and heat stresses. *Journal of Bacteriology*, *190*(10), 3712–3720. https://doi.org/10.1128/JB.01990-07

Hachisuka, S. ichi, Chong, J. F., Fujiwara, T., Takayama, A., Kawakami, Y., & Yoshida, S. (2022). Ethylene glycol metabolism in the poly(ethylene terephthalate)-degrading bacterium Ideonella sakaiensis. *Applied Microbiology and Biotechnology*, *106*(23), 7867–7878. https://doi.org/10.1007/s00253-022-12244-y

Hammer, B. K., & Bassler, B. L. (2003). Quorum sensing controls biofilm formation in Vibrio cholerae. *Molecular Microbiology*, *50*(1), 101–104. https://doi.org/10.1046/j.1365-2958.2003.03688.x

Hansen, J., Melchiorsen, J., Ciacotich, N., Gram, L., & Sonnenschein, E. C. (2021). Effect of polymer type on the colonization of plastic pellets by marine bacteria. *FEMS Microbiology Letters*, *368*(5). https://doi.org/10.1093/femsle/fnab026

Hanževački, M., Croft, A. K., & Jäger, C. M. (2022). Activation of Glycyl Radical Enzymes—Multiscale Modeling Insights into Catalysis and Radical Control in a Pyruvate Formate-Lyase-Activating Enzyme. *Journal of Chemical Information and Modeling*, *62*(14), 3401–3414. https://doi.org/10.1021/acs.jcim.2c0036

Harwood, C. S. (1978). *Beneckea gazogenes* sp. nov., a red facultatively anaerobic, marine bacterium, Current Microbiology. In *Current Microbiology*

Hay, I. D., Belousoff, M. J., & Lithgow, T. (2017). Structural basis of type 2 secretion system engagement between the inner and outer bacterial membranes. *MBio*, *8*(5). https://doi.org/10.1128/mBio.01344-17

He, X., Zhang, Y., Wang, X., Zhu, X., Chen, L., Liu, W., Lyu, Q., Ran, L., Cheng, H., & Zhang, X. H. (2022). Characterization of Multiple Alginate Lyases in a Highly Efficient Alginate-Degrading Vibrio Strain and Its Degradation Strategy. *Applied and Environmental Microbiology*, *88*(23). https://doi.org/10.1128/aem.01389-22

References

Hodkovicova, N., Hollerova, A., Svobodova, Z., Faldyna, M., & Faggio, C. (2022). Effects of plastic particles on aquatic invertebrates and fish – A review. In *Environmental Toxicology and Pharmacology* (Vol. 96). Elsevier B.V. https://doi.org/10.1016/j.etap.2022.104013

Hong, H., Deng, A., Tang, Y., & Liu, Z. (2024). How to identify biofouling species in marine and freshwater. In *Biofouling* (Vol. 40, Issue 2, pp. 130–152). Taylor and Francis Ltd. https://doi.org/10.1080/08927014.2024.2324008

Huang, J. F., Zeng, B. Q., Liu, D., Wu, R. B., Zhang, J., Liao, B. Q., He, H. L., & Bian, F. (2018). Classification and structural insight into vibriolysin-like proteases of Vibrio pathogenicity. *Microbial Pathogenesis*, *117*, 335–340. https://doi.org/10.1016/j.micpath.2018.03.002

Iqbal, A., Azim, M. K., Hashmi, N., Ali, S. A., & Ghulam Musharraf, S. (2011). Structural Characterization of Metalloprotease Vibriolysin of Cholera Pathogen Vibrio cholerae. In *Protein & Peptide Letters* (Vol. 18).

Isenberg, R. Y., Holschbach, C. S., Gao, J., & Mandel, M. J. (2024). Functional analysis of cyclic diguanylate-modulating proteins in *Vibrio fischeri*. *MSystems*, *9*(11). https://doi.org/10.1128/msystems.00956-24

Jahanshahi, D. A., Barzani, M. R. R., Bahram, M., Ariaeenejad, S., & Kavousi, K. (2025). Metagenomic exploration and computational prediction of novel enzymes for polyethylene terephthalate degradation. *Ecotoxicology and Environmental Safety*, *289*. https://doi.org/10.1016/j.ecoenv.2024.117640

Jenal, U., Reinders, A., & Lori, C. (2017). Cyclic di-GMP: Second messenger extraordinaire. In *Nature Reviews Microbiology* (Vol. 15, Issue 5, pp. 271–284). Nature Publishing Group. https://doi.org/10.1038/nrmicro.2016.190

Ji, Y., Mao, G., Wang, Y., & Bartlam, M. (2013). Structural insights into diversity and n-alkane biodegradation mechanisms of alkane hydroxylases. *Frontiers in Microbiology*, *4*. https://doi.org/10.3389/fmicb.2013.00058

Joshi, G., Goswami, P., Verma, P., Prakash, G., Simon, P., Vinithkumar, N. V., & Dharani, G. (2022). Unraveling the plastic degradation potentials of the plastisphere-associated marine bacterial consortium as a key player for the low-density polyethylene degradation. *Journal of Hazardous Materials*, *425*. https://doi.org/10.1016/j.jhazmat.2021.128005

Junaid, M., Siddiqui, J. A., Sadaf, M., Liu, S., & Wang, J. (2022). Enrichment and dissemination of bacterial pathogens by microplastics in the aquatic environment. In *Science of the Total Environment* (Vol. 830). Elsevier B.V. https://doi.org/10.1016/j.scitotenv.2022.154720

Katnic, S. P., & Gupta, R. K. (2025). From biofilms to biocatalysts: Innovations in plastic biodegradation for environmental sustainability. In *Journal of Environmental Management* (Vol. 374). Academic Press. https://doi.org/10.1016/j.jenvman.2025.124192

Kauffman, G. B., & Seymour1, R. B. (n.d.-a). *Polyurethanes: A Class of Modern Versatile Materials*. https://pubs.acs.org/sharingguidelines

Khan, M. T., Hong, P. Y., Nada, N., & Croue, J. P. (2015). Does chlorination of seawater reverse osmosis membranes control biofouling? *Water Research*, *78*, 84–97. https://doi.org/10.1016/j.watres.2015.03.029

References

Khusnutdinova, A. N., Batyrova, K. A., Wang, P. H., Flick, R., Edwards, E. A., & Yakunin, A. F. (2024). Enzyme cascades for in vitro and in vivo FMN prenylation and UbiD (de)carboxylase activation under aerobic conditions. In *Methods in Enzymology*. Academic Press Inc. https://doi.org/10.1016/bs.mie.2024.10.015

Kim, H. J., Park, J. S., Lee, T. K., Kang, D., Kang, J. H., Shin, K., & Jung, S. W. (2021). Dynamics of marine bacterial biofouling communities after initial Alteromonas genovensis biofilm attachment to anti-fouling paint substrates. *Marine Pollution Bulletin*, *172*. https://doi.org/10.1016/j.marpolbul.2021.112895

Kirstein, I. v., Kirmizi, S., Wichels, A., Garin-Fernandez, A., Erler, R., Löder, M., & Gerdts, G. (2016). Dangerous hitchhikers? Evidence for potentially pathogenic Vibrio spp. on microplastic particles. *Marine Environmental Research*, *120*, 1–8. https://doi.org/10.1016/j.marenvres.2016.07.004

Kirstein, I. v., Wichels, A., Krohne, G., & Gerdts, G. (2018). Mature biofilm communities on synthetic polymers in seawater - Specific or general? *Marine Environmental Research*, 147–154. https://doi.org/10.1016/j.marenvres.2018.09.028

Korotkov, K. v., Sandkvist, M., & Hol, W. G. J. (2012). The type II secretion system: Biogenesis, molecular architecture and mechanism. In *Nature Reviews Microbiology* (Vol. 10, Issue 5, pp. 336–351). https://doi.org/10.1038/nrmicro2762

Kumar, M., Kumar, R., Chaudhary, D. R., & Jha, B. (2022). An appraisal of early stage biofilm-forming bacterial community assemblage and diversity in the Arabian Sea, India. *Marine Pollution Bulletin*, *180*. https://doi.org/10.1016/j.marpolbul.2022.113732

Lacerda, A. L. d. F., Taylor, J. D., Rodrigues, L. d. S., Kessler, F., Secchi, E., & Proietti, M. C. (2022). Floating plastics and their associated biota in the Western South Atlantic. *Science of the Total Environment*, *805*. https://doi.org/10.1016/j.scitotenv.2021.150186

Landrigan, P. J., Raps, H., Cropper, M., Bald, C., Brunner, M., Canonizado, E. M., Charles, D., Chiles, T. C., Donohue, M. J., Enck, J., Fenichel, P., Fleming, L. E., Ferrier-Pages, C., Fordham, R., Gozt, A., Griffin, C., Hahn, M. E., Haryanto, B., Hixson, R., Dunlop, S. (2023). The Minderoo-Monaco Commission on Plastics and Human Health. *Annals of Global Health*, *89*(1). https://doi.org/10.5334/aogh.4056

Latva, M., Dedman, C. J., Wright, R. J., Polin, M., & Christie-Oleza, J. A. (2022). Microbial pioneers of plastic colonisation in coastal seawaters. *Marine Pollution Bulletin*, *179*. https://doi.org/10.1016/j.marpolbul.2022.113701

Lee, Y., Cho, J., Sohn, J., & Kim, C. (2023). Health Effects of Microplastic Exposures: Current Issues and Perspectives in South Korea. In *Yonsei Medical Journal* (Vol. 64, Issue 5, pp. 301–308). Yonsei University College of Medicine. https://doi.org/10.3349/ymj.2023.0048

Li, B., Jain, P., Ma, J., Smith, J. K., Yuan, Z., Hung, H.-C., He, Y., Lin, X., Wu, K., Pfaendtner, J., & Jiang, S. (2019). Trimethylamine N-oxide-derived zwitterionic polymers: A new class of ultralow fouling bioinspired materials. In *Sci. Adv* (Vol. 5).

Li, X., Liu, X., Ma, T., Su, H., Sui, B., Wang, L., Murtaza, B., Xu, Y., Li, N., & Tan, D. (2025). Understanding phage BX-1 resistance in Vibrio alginolyticus AP-1 and the role of quorum-sensing regulation. *Microbiology Spectrum*, e0243524. https://doi.org/10.1128/spectrum.02435-24

References

Lichtstein, H. C. and Van de Sand, V. F. (1946). The antibiotic activity of violacein, prodigiosin, and phthiocol. *Journal of Bacteriology*

Linder, J. U. (2008). Structure-function relationships in Escherichia coli adenylate cyclase. *Biochemical Journal*, *415*(3), 449–454. https://doi.org/10.1042/BJ20080350

Liu, D. R., Yan, Q. X., Zou, Z. B., Xie, C. L., Yang, X. W., & Jia, A. Q. (2023). Cladosporium sphaerospermum extract inhibits quorum sensing associated virulence factors of Serratia marcescens. *Biofilm*, *6.* https://doi.org/10.1016/j.bioflm.2023.100146

Liu, R., Xu, H., Zhao, S., Dong, C., Li, J., Wei, G., Li, G., Gong, L., Yan, P., & Shao, Z. (2024). Polyethylene terephthalate (PET)-degrading bacteria in the pelagic deep-sea sediments of the Pacific Ocean. *Environmental Pollution*, *352.* https://doi.org/10.1016/j.envpol.2024.124131

Loterio, R. K., Thomas, D. R., Andrade, W., Lee, Y. W., Santos, L. L., Mascarenhas, D. P. A., Steiner, T. M., Chiaratto, J., Fielden, L. F., Lopes, L., Bird, L. E., Goldman, G. H., Stojanovski, D., Scott, N. E., Zamboni, D. S., & Newton, H. J. (2023). Coxiella co-opts the Glutathione Peroxidase 4 to protect the host cell from oxidative stress–induced cell death. *Proceedings of the National Academy of Sciences of the United States of America*, *120*(36). https://doi.org/10.1073/pnas.2308752120

Luc, V. S., Lin, C. C., Wang, S. Y., Lin, H. P., Li, B. R., Chou, Y. N., & Chang, C. C. (2023). Antifouling Properties of Amine-Oxide-Containing Zwitterionic Polymers. *Biomacromolecules*, *24*(11), 5467–5477. https://doi.org/10.1021/acs.biomac.3c00948

Lydick, V. N., Mass, S., Pepin, R., Podicheti, R., Klempic, E., Rusch, D. B., Ushijima, B., Brown, L. C., Salomon, D., & van Kessel, J. C. (2025). Quorum sensing regulates virulence factors in the coral pathogen Vibrio coralliilyticus. *Applied and Environmental Microbiology*, *91*(2). https://doi.org/10.1128/aem.01143-24

Ma, Y., Zhang, Z., Nitin, N., & Sun, G. (2020). Integration of photo-induced biocidal and hydrophilic antifouling functions on nanofibrous membranes with demonstrated reduction of biofilm formation. *Journal of Colloid and Interface Science*, *578*, 779–787. https://doi.org/10.1016/j.jcis.2020.06.037

Maity, W., Maity, S., Bera, S., & Roy, A. (2021). Emerging Roles of PETase and MHETase in the Biodegradation of Plastic Wastes. In *Applied Biochemistry and Biotechnology* (Vol. 193, Issue 8, pp. 2699–2716). Springer. https://doi.org/10.1007/s12010-021-03562-4

Malla, M. A., Nomalihle, M., Featherston, J., Kumar, A., Amoah, I. D., Ismail, A., Bux, F., & Kumari, S. (2025). Comprehensive profiling and risk assessment of antibiotic resistomes in surface water and plastisphere by integrated shotgun metagenomics. *Journal of Hazardous Materials*, *487*. https://doi.org/10.1016/j.jhazmat.2025.137180

Manneh-Roussel, J., Haycocks, J. R. J., Magán, A., Perez-Soto, N., Voelz, K., Camilli, A., Krachler, A. M., & Grainger, D. C. (2018). Camp receptor protein controls Vibrio cholerae gene expression in response to host colonization. *MBio*, *9*(4). https://doi.org/10.1128/mBio.00966-18

McBride, M., & Zhu, Y. (2013). Gliding motility and por secretion system genes are widespread among members of the phylum bacteroidetes. *Journal of Bacteriology*, *195*(2), 270–278. https://doi.org/10.1128/JB.01962-12

References

Matsuoka, J. I., Ishizuna, F., Kurumisawa, K., Morohashi, K., Ogawa, T., Hidaka, M., Saito, K., Ezawa, T., & Aono, T. (2017). Stringent expression control of pathogenic R-body production in legume symbiont Azorhizobium caulinodans. *MBio*, *8*(4). https://doi.org/10.1128/mBio.00715-17

McCormick, A., Hoellein, T. J., Mason, S. A., Schluep, J., & Kelly, J. J. (2014). Microplastic is an abundant and distinct microbial habitat in an urban river. *Environmental Science and Technology*, *48*(20), 11863–11871. https://doi.org/10.1021/es503610r

Messer, L. F., Lee, C. E., Wattiez, R., & Matallana-Surget, S. (2024). Novel functional insights into the microbiome inhabiting marine plastic debris: critical considerations to counteract the challenges of thin biofilms using multi-omics and comparative metaproteomics. *Microbiome*, *12*(1). https://doi.org/10.1186/s40168-024-01751-x

Miller, M. B., Skorupski, K., Lenz, D. H., Taylor, R. K., & Bassler, B. L. (2002). *Parallel Quorum Sensing Systems Converge to Regulate Virulence in Vibrio cholerae*.

Mizgalska, D., Rodríguez-Banqueri, A., Veillard, F., Książek, M., Goulas, T., Guevara, T., Eckhard, U., Potempa, J., & Gomis-Rüth, F. X. (2024). Structural and functional insights into the C-terminal signal domain of the Bacteroidetes type-IX secretion system. *Open Biology*, *14*(6). https://doi.org/10.1098/rsob.230448

Morot, A., Lambert, C., Bidault, A., Dufour, A., Rodrigues, S., Delavat, F., & Paillard, C. (2025). Vibrio harveyi uses both type III secretion system and quorum sensing for the colonization of the European abalone. *Fish and Shellfish Immunology*, *157*. https://doi.org/10.1016/j.fsi.2024.110103

Mphasa, M., Ormsby, M. J., Mwapasa, T., Nambala, P., Chidziwisano, K., Morse, T., Feasey, N., & Quilliam, R. S. (2025). Urban waste piles are reservoirs for human pathogenic bacteria with high levels of multidrug resistance against last resort antibiotics: A comprehensive temporal and geographic field analysis. *Journal of Hazardous Materials*, *484*. https://doi.org/10.1016/j.jhazmat.2024.136639

Muhammad, T., Li, L., Xiao, Y., Zhou, Y., Liu, Z., He, X., Bazai, N. A., & Li, Y. (2022). Multiple fouling dynamics, interactions and synergistic effects in brackish surface water distribution systems. *Chemosphere*, *287*. https://doi.org/10.1016/j.chemosphere.2021.132268

Musik, J. E., Zalucki, Y. M., Day, C. J., & Jennings, M. P. (2019). Efficient function of signal peptidase 1 of Escherichia coli is partly determined by residues in the mature N-terminus of exported proteins. *Biochimica et Biophysica Acta - Biomembranes*, *1861*(5), 1018–1022. https://doi.org/10.1016/j.bbamem.2019.03.001

Naser, I. bin, Shishir, T. A., Faruque, S. N., Mozammel Hoque, M., Hasan, A., & Faruque, S. M. (2021). Environmental prevalence of toxigenic Vibrio cholerae O1 in Bangladesh coincides with V. cholerae non-O1 non-O139 genetic variants which overproduce autoinducer-2. *PLoS ONE*, *16*(7 July). https://doi.org/10.1371/journal.pone.0254068

Natarajan, S., Bhuvaneshwari, M., Lakshmi, D. S., Mrudula, P., Chandrasekaran, N., & Mukherjee, A. (2016). Antibacterial and antifouling activities of chitosan/TiO2/Ag NPs nanocomposite films against packaged drinking water bacterial isolates. *Environmental Science and Pollution Research*, *23*(19), 19529–19540. https://doi.org/10.1007/s11356-016-7102-6

Ng, W. L., & Bassler, B. L. (2009). Bacterial quorum-sensing network architectures. In *Annual Review of Genetics* (Vol. 43, pp. 197–222). https://doi.org/10.1146/annurev-genet-102108-134304

References

Nisticò, R. (2020). Polyethylene terephthalate (PET) in the packaging industry. In *Polymer Testing* (Vol. 90). Elsevier Ltd. https://doi.org/10.1016/j.polymertesting.2020.106707

Oberbeckmann, S., Loeder, M. G. J., Gerdts, G., & Osborn, M. A. (2014). Spatial and seasonal variation in diversity and structure of microbial biofilms on marine plastics in Northern European waters. *FEMS Microbiology Ecology*, *90*(2), 478–492. https://doi.org/10.1111/1574-6941.12409

Ogonowski, M., Motiei, A., Ininbergs, K., Hell, E., Gerdes, Z., Udekwu, K. I., Bacsik, Z., & Gorokhova, E. (2018). Evidence for selective bacterial community structuring on microplastics. *Environmental Microbiology*, *20*(8), 2796–2808. https://doi.org/10.1111/1462-2920.14120

Owji, H., Nezafat, N., Negahdaripour, M., Hajiebrahimi, A., & Ghasemi, Y. (2018). A comprehensive review of signal peptides: Structure, roles, and applications. In *European Journal of Cell Biology* (Vol. 97, Issue 6, pp. 422–441). Elsevier GmbH. https://doi.org/10.1016/j.ejcb.2018.06.003

Oliver, D. M., Metcalf, R., Jones, D. L., Matallana-Surget, S., Thomas, D. N., Robins, P., Tulloch, C. L., Cotterell, B. M., Williams, G., Christie-Oleza, J. A., & Quilliam, R. S. (2024). Plastic pollution and human pathogens: Towards a conceptual shift in risk management at bathing water and beach environments. In *Water Research* (Vol. 261). Elsevier Ltd. https://doi.org/10.1016/j.watres.2024.122028

Ormsby, M. J., Woodford, L., White, H. L., Fellows, R., Oliver, D. M., & Quilliam, R. S. (2024). Toxigenic Vibrio cholerae can cycle between environmental plastic waste and floodwater: Implications for environmental management of cholera. *Journal of Hazardous Materials*, *461*. https://doi.org/10.1016/j.jhazmat.2023.132492

Paetzel, M. (2019). Bacterial Signal Peptidases. In *Subcellular Biochemistry* (Vol. 92, pp. 187–219). Springer New York. https://doi.org/10.1007/978-3-030-18768-2_7

Pan, J., Ai, X., Ma, C., & Zhang, G. (2022). Degradable Vinyl Polymers for Combating Marine Biofouling. *Accounts of Chemical Research*, *55*(11), 1586–1598. https://doi.org/10.1021/acs.accounts.2c00187

Pena, R. T., Blasco, L., Ambroa, A., González-Pedrajo, B., Fernández-García, L., López, M., Bleriot, I., Bou, G., García-Contreras, R., Wood, T. K., & Tomás, M. (2019). Relationship between quorum sensing and secretion systems. In *Frontiers in Microbiology* (Vol. 10, Issue JUN). Frontiers Media S.A. https://doi.org/10.3389/fmicb.2019.01100

Perez-Garcia, P., Kobus, S., Gertzen, C. G. W., Hoeppner, A., Holzscheck, N., Strunk, C. H., Huber, H., Jaeger, K. E., Gohlke, H., Kovacic, F., Smits, S. H. J., Streit, W. R., & Chow, J. (2021). A promiscuous ancestral enzyme´s structure unveils protein variable regions of the highly diverse metallo-β-lactamase family. *Communications Biology*, *4*(1). https://doi.org/10.1038/s42003-021-01671-8

Pinto, M., Langer, T. M., Hüffer, T., Hofmann, T., & Herndl, G. J. (2019). The composition of bacterial communities associated with plastic biofilms differs between different polymers and stages of biofilm succession. *PLoS ONE*, *14*(6). https://doi.org/10.1371/journal.pone.0217165

Plastics Europe 2024; https://plasticseurope.org/knowledge-hub/plastics-the-fast-facts-2024/.

Potapova, A., Garvey, W., Dahl, P., Guo, S., Chang, Y., Schwechheimer, C., Trebino, M. A., Floyd, K. A., Phinney, B. S., Liu, J., Malvankar, N. S., & Yildiz, F. H. (2024). Outer membrane vesicles and the outer membrane protein OmpU govern Vibrio cholerae biofilm matrix assembly. *MBio*, *15*(2). https://doi.org/10.1128/mbio.03304-23

References

Prince, R. C., Gramain, A., & McGenity, T. J. (2010). Prokaryotic Hydrocarbon Degraders. In *Handbook of Hydrocarbon and Lipid Microbiology* (pp. 1669–1692). Springer Berlin Heidelberg. https://doi.org/10.1007/978-3-540-77587-4_118

Qian, P. Y., Cheng, A., Wang, R., & Zhang, R. (2022). Marine biofilms: diversity, interactions and biofouling. In *Nature Reviews Microbiology* (Vol. 20, Issue 11, pp. 671–684). Nature Research. https://doi.org/10.1038/s41579-022-00744-7

Quero, G. M., & Luna, G. M. (2017). Surfing and dining on the "plastisphere": Microbial life on plastic marine debris. In *Advances in Oceanography and Limnology* (Vol. 8, Issue 2, pp. 199–207). Page Press Publications. https://doi.org/10.4081/aiol.2017.7211

Raczyńska, A., Góra, A., & André, I. (2024). An overview on polyurethane-degrading enzymes. In *Biotechnology Advances* (Vol. 77). Elsevier Inc. https://doi.org/10.1016/j.biotechadv.2024.108439

Raghul, S. S., Bhat, S. G., Chandrasekaran, M., Francis, V., & Thachil, E. T. (2014). Biodegradation of polyvinyl alcohol-low linear density polyethylene-blended plastic film by consortium of marine benthic vibrios. *International Journal of Environmental Science and Technology*, *11*(7), 1827–1834. https://doi.org/10.1007/s13762-013-0335-8

Regmi, A., Tague, J. G., Lichty, K. E. B., & Boyd, E. F. (2023). A Class IV Adenylate Cyclase, CyaB, Is Required for Capsule Polysaccharide Production and Biofilm Formation in Vibrio parahaemolyticus. *Applied and Environmental Microbiology*, *89*(1). https://doi.org/10.1128/aem.01874-22

Roager, L., & Sonnenschein, E. C. (2019). Bacterial Candidates for Colonization and Degradation of Marine Plastic Debris. In *Environmental Science and Technology* (Vol. 53, Issue 20, pp. 11636–11643). American Chemical Society. https://doi.org/10.1021/acs.est.9b02212

Rodrigues, A., Oliver, D. M., McCarron, A., & Quilliam, R. S. (2019). Colonisation of plastic pellets (nurdles) by E. coli at public bathing beaches. *Marine Pollution Bulletin*, *139*, 376–380. https://doi.org/10.1016/j.marpolbul.2019.01.011

Rutherford, S. T., & Bassler, B. L. (2012). Bacterial quorum sensing: Its role in virulence and possibilities for its control. In *Cold Spring Harbor Perspectives in Medicine* (Vol. 2, Issue 11). Cold Spring Harbor Laboratory Press. https://doi.org/10.1101/cshperspect.a012427

Saier, M. H., Feucht, B. U., & Hofstadter, L. J. (1976). Regulation of Carbohydrate Uptake and Adenylate Cyclase Activity Mediated by the Enzymes II of the Phosphoenolpyruvate:Sugar Phosphotransferase System in Escherichia coli*. In *THE ~JOURNAL OF BIOLOGICAL CHEMISTRY* (Vol. 251, Issue 3)

Sathiyamoorthi, E., Boya, B. R., Lee, J. H., & Lee, J. (2025). Antimicrobial Efficacy of Trifluoro-Anilines Against Vibrio Species. *International Journal of Molecular Sciences*, *26*(2). https://doi.org/10.3390/ijms26020623

Schrallhammer, M., Galati, S., Altenbuchner, J., Schweikert, M., Görtz, H. D., & Petroni, G. (2012). Tracing the role of R-bodies in the killer trait: Absence of toxicity of R-body producing recombinant E. coli on paramecia. *European Journal of Protistology*, *48*(4), 290–296. https://doi.org/10.1016/j.ejop.2012.01.008

Seok, B., Kim, M. S., & Kim, B. S. (2024). Genome-wide analysis of quorum sensing regulon in marine fish pathogen Vibrio scophthalmi. *Scientific Reports*, *14*(1). https://doi.org/10.1038/s41598-024-78803-7

References

Shao, Y., & Bassler, B. L. (2014). Quorum regulatory small RNAs repress type VI secretion in vibrio cholerae. *Molecular Microbiology*, *92*(5), 921–930. https://doi.org/10.1111/mmi.12599

Shen, M., Zhu, Y., Zhang, Y., Zeng, G., Wen, X., Yi, H., Ye, S., Ren, X., & Song, B. (2019). Micro(nano)plastics: Unignorable vectors for organisms. *Marine Pollution Bulletin*, *139*, 328–331. https://doi.org/10.1016/j.marpolbul.2019.01.004

Silva, A. J., & Benitez, J. A. (2004). Transcriptional regulation of Vibrio cholerae hemagglutinin/protease by the cyclic AMP receptor protein and RpoS. *Journal of Bacteriology*, *186*(19), 6374–6382. https://doi.org/10.1128/JB.186.19.6374-6382.2004

Simpson, C. A., Celentano, Z. R., Haas, N. W., McKinlay, J. B., Nadell, C. D., & van Kessel, J. C. (2024). Quorum sensing in Vibrio controls carbon metabolism to optimize growth in changing environmental conditions. *PLOS Biology*, *22*(11), e3002891. https://doi.org/10.1371/journal.pbio.3002891

Son, J. S., Lee, S., Hwang, S., Jeong, J., Jang, S., Gong, J., Choi, J. Y., Je, Y. H., & Ryu, C. M. (2024). Enzymatic oxidation of polyethylene by Galleria mellonella intestinal cytochrome P450s. *Journal of Hazardous Materials*, *480*. https://doi.org/10.1016/j.jhazmat.2024.136264

Stepnov, A. A., Lopez-Tavera, E., Klauer, R., Lincoln, C. L., Chowreddy, R. R., Beckham, G. T., Eijsink, V. G. H., Solomon, K., Blenner, M., & Vaaje-Kolstad, G. (2024). Revisiting the activity of two poly(vinyl chloride)- and polyethylene-degrading enzymes. *Nature Communications*, *15*(1), 8501. https://doi.org/10.1038/s41467-024-52665-z

Su, Y., Zhang, Z., Wu, D., Zhan, L., Shi, H., & Xie, B. (2019). Occurrence of microplastics in landfill systems and their fate with landfill age. *Water Research*, *164*. https://doi.org/10.1016/j.watres.2019.114968

Sudhakar, M., Doble, M., Murthy, P. S., & Venkatesan, R. (2008). Marine microbe-mediated biodegradation of low- and high-density polyethylenes. *International Biodeterioration and Biodegradation*, *61*(3), 203–213. https://doi.org/10.1016/j.ibiod.2007.07.011

Sugathapala, T. M., Capuano, T., Brandt, L., Iudicone, D., & Sardina, G. (2025). Vertical transport of buoyant microplastic particles in the ocean: The role of turbulence and biofouling. *Environmental Pollution*, *369*. https://doi.org/10.1016/j.envpol.2025.125819

Sulaiman, S., Yamato, S., Kanaya, E., Kim, J. J., Koga, Y., Takano, K., & Kanaya, S. (2012). Isolation of a novel cutinase homolog with polyethylene terephthalate-degrading activity from leaf-branch compost by using a metagenomic approach. *Applied and Environmental Microbiology*, *78*(5), 1556–1562. https://doi.org/10.1128/AEM.06725-11

Tirkey, A., & Upadhyay, L. S. B. (2021). Microplastics: An overview on separation, identification and characterization of microplastics. In *Marine Pollution Bulletin* (Vol. 170). Elsevier Ltd. https://doi.org/10.1016/j.marpolbul.2021.112604

Tournier, V., Topham, C. M., Gilles, A., David, B., Folgoas, C., Moya-Leclair, E., Kamionka, E., Desrousseaux, M. L., Texier, H., Gavalda, S., Cot, M., Guémard, E., Dalibey, M., Nomme, J., Cioci, G., Barbe, S., Chateau, M., André, I., Duquesne, S., & Marty, A. (2020). An engineered PET depolymerase to break down and recycle plastic bottles. *Nature*, *580*(7802), 216–219. https://doi.org/10.1038/s41586-020-2149-4

Uppalapati, S., Kant, S., Liu, L., Kim, J. S., Orlicky, D., McClelland, M., & Vazquez-Torres, A. (2024). Prophage terminase with tRNase activity sensitizes Salmonella enterica to oxidative stress. *Science*, *384*(6691), 100–105. https://doi.org/10.1126/science.adl3222

References

Urbelienė, N., Gasparavičiūtė, R., Vaitekūnas, J., Meškienė, R., Valantinaitė, U., Kruopis, P., Gudiukaitė, R., & Meškys, R. (2025). A screening method for polyester films-degrading microorganisms and enzymes. *Journal of Hazardous Materials*, *487*. https://doi.org/10.1016/j.jhazmat.2025.137177

van Kessel, J. C., & Camilli, A. (2024). Vibrio cholerae: a fundamental model system for bacterial genetics and pathogenesis research. In *Journal of bacteriology* (Vol. 206, Issue 11, p. e0024824). https://doi.org/10.1128/jb.00248-24

Vijay, D., Alshamsi, N. S., Moussa, Z., & Akhtar, M. K. (2022). Extraction of the Anticancer and Antimicrobial Agent, Prodigiosin, from Vibrio gazogenes PB1 and Its Identification by 1D and 2D NMR. *Molecules*, *27*(18). https://doi.org/10.3390/molecules27186030

Vijayan, S., Liu, R., George, S., & Bhaskaran, S. (2024). Polyethylene terephthalate nanoparticles induce oxidative damage in Chlorella vulgaris. *Plant Physiology and Biochemistry*, *215*. https://doi.org/10.1016/j.plaphy.2024.108987

Vural, C., & Ettadili, H. (2024). Biodegradation of phthalic acid and terephthalic acid by Comamonas testosteroni strains. *Folia Microbiologica*. https://doi.org/10.1007/s12223-024-01176-x

Walker, S., & Rothman, R. (2020). Life cycle assessment of bio-based and fossil-based plastic: A review. In *Journal of Cleaner Production* (Vol. 261). Elsevier Ltd. https://doi.org/10.1016/j.jclepro.2020.121158

Wang, H., Chen, S., Zhang, J., Rothenbacher, F. P., Jiang, T., Kan, B., Zhong, Z., & Zhu, J. (2012). Catalases Promote Resistance of Oxidative Stress in Vibrio cholerae. *PLoS ONE*, *7*(12). https://doi.org/10.1371/journal.pone.0053383

Wang, H., Naseer, N., Chen, Y., Zhu, A. Y., Kuai, X., Galagedera, N., Liu, Z., & Zhu, J. (2017). OxyR2 modulates OxyR1 activity and Vibrio cholerae oxidative stress response. *Infection and Immunity*, *85*(4). https://doi.org/10.1128/IAI.00929-16

Wang, L., Zhang, T. L., Xiang, Q., Fu, C. X., Qiao, M., Ding, L. J., & Zhu, D. (2024). Selective enrichment of virulence factor genes in the plastisphere under antibiotic and heavy metal pressures. *Journal of Hazardous Materials*, *465*. https://doi.org/10.1016/j.jhazmat.2023.133319

Wang, Q., Sha, C., Wang, H., Ma, K., Wiegle, J., Abomohra, A. E. F., & Shao, W. (2021). A novel bifunctional aldehyde/alcohol dehydrogenase catalyzing reduction of acetyl-CoA to ethanol at temperatures up to 95 °C. *Scientific Reports*, *11*(1). https://doi.org/10.1038/s41598-020-80159-7

Wang, T., Lu, F., Yang, C., Wang, C., Liao, Y., Mkuye, R., & Deng, Y. (2024). Exploring changes in microplastic-associated bacterial communities with time, location, and polymer type in Liusha Bay, China. *Marine Environmental Research*, *198*. https://doi.org/10.1016/j.marenvres.2024.106525

Wang, Z., Gao, J., Zhao, Y., Dai, H., Jia, J., & Zhang, D. (2021). Plastisphere enrich antibiotic resistance genes and potential pathogenic bacteria in sewage with pharmaceuticals. *Science of the Total Environment*, *768*. https://doi.org/10.1016/j.scitotenv.2020.144663

Weber, F., & Esmaeili, N. (2023). Marine biofouling and the role of biocidal coatings in balancing environmental impacts. In *Biofouling* (Vol. 39, Issue 6, pp. 661–681). Taylor and Francis Ltd. https://doi.org/10.1080/08927014.2023.2246906

References

Wei, R., & Zimmermann, W. (2017). Microbial enzymes for the recycling of recalcitrant petroleum-based plastics: how far are we? In *Microbial Biotechnology* (Vol. 10, Issue 6, pp. 1308–1322). John Wiley and Sons Ltd. https://doi.org/10.1111/1751-7915.12710

Weigert, S., Perez-Garcia, P., Gisdon, F. J., Gagsteiger, A., Schweinshaut, K., Ullmann, G. M., Chow, J., Streit, W. R., & Höcker, B. (2022). Investigation of the halophilic PET hydrolase PET6 from Vibrio gazogenes. *Protein Science*, *31*(12). https://doi.org/10.1002/pro.4500

Wright, R. J., Erni-Cassola, G., Zadjelovic, V., Latva, M., & Christie-Oleza, J. A. (2020). Marine Plastic Debris: A New Surface for Microbial Colonization. *Environmental Science and Technology*, *54*(19), 11657–11672. https://doi.org/10.1021/acs.est.0c02305

Wright, R. J., Langille, M. G. I., & Walker, T. R. (2021). Food or just a free ride? A meta-analysis reveals the global diversity of the Plastisphere. *ISME Journal*, *15*(3), 789–806. https://doi.org/10.1038/s41396-020-00814-9

Wu, F., Li, Q., Zhang, Z., Zhou, X., & Pang, R. (2025). A review on antifouling polyamide reverse osmosis membrane for seawater desalination. In *Environmental Research* (Vol. 274). Academic Press Inc. https://doi.org/10.1016/j.envres.2025.121305

Xia, X., Larios-Valencia, J., Liu, Z., Xiang, F., Kan, B., Wang, H., & Zhu, J. (2017). OxyR-Activated expression of Dps is important for Vibrio cholerae oxidative stress resistance and pathogenesis. *PLoS ONE*, *12*(2). https://doi.org/10.1371/journal.pone.0171201

Xiang, T., Zhou, W., Xu, C., Xu, J., Liu, R., Wang, N., Xu, L., Zhao, Y., Luo, M., Mo, X., Mao, Z., & Wan, Y. (2022). Transcriptomic Analysis Reveals Competitive Growth Advantage of Non-pigmented Serratia marcescens Mutants. *Frontiers in Microbiology*, *12*. https://doi.org/10.3389/fmicb.2021.793202

Xu, J. L., Lin, X., Wang, J. J., & Gowen, A. A. (2022). A review of potential human health impacts of micro- and nanoplastics exposure. In *Science of the Total Environment* (Vol. 851). Elsevier B.V. https://doi.org/10.1016/j.scitotenv.2022.158111

Yadav, D. S., & Mantri, V. A. (2025). The microplastic menace: a critical review of its impact on marine photoautotrophs and their environment. In *Environmental Science and Pollution Research*. Springer. https://doi.org/10.1007/s11356-025-35981-9

Yang, W. K., Gong, Z., Wang, B. T., Hu, S., Zhuo, Y., Jin, C. Z., Jin, L., Lee, H. G., & Jin, F. J. (2024). Biodegradation of low-density polyethylene by mixed fungi composed of Alternaria sp. and Trametes sp. isolated from landfill sites. *BMC Microbiology*, *24*(1). https://doi.org/10.1186/s12866-024-03477-0

Yee, M. S. L., Hii, L. W., Looi, C. K., Lim, W. M., Wong, S. F., Kok, Y. Y., Tan, B. K., Wong, C. Y., & Leong, C. O. (2021). Impact of microplastics and nanoplastics on human health. In *Nanomaterials* (Vol. 11, Issue 2, pp. 1–23). MDPI AG. https://doi.org/10.3390/nano11020496

Yoo, W., Shealy, N. G., Zieba, J. K., Torres, T. P., Baltagulov, M., Thomas, J. D., Shelton, C. D., McGovern, A. G., Foegeding, N. J., Olsan, E. E., & Byndloss, M. X. (2024). Salmonella Typhimurium expansion in the inflamed murine gut is dependent on aspartate derived from ROS-mediated microbiota lysis. *Cell Host and Microbe*, *32*(6), 887-899.e6. https://doi.org/10.1016/j.chom.2024.05.001

Yoshida, S., Hiraga, K., Takehana, T., Taniguchi, I., Yamaji, H., Maeda, Y., Toyohara, K., Miyamoto, K., Kimura, Y., & Oda, K. (n.d.-a). *A bacterium that degrades and assimilates poly(ethylene terephthalate)*. https://www.science.org

References

Yu, Y., Miao, L., Adyel, T. M., Waldschläger, K., Wu, J., & Hou, J. (2023). Aquatic plastisphere: Interactions between plastics and biofilms. In *Environmental Pollution* (Vol. 322). Elsevier Ltd. https://doi.org/10.1016/j.envpol.2023.121196

Zamora, R., McEvoy, J., Colbert, C., Chacana Olivares, J., Kaewlom, P., & Khan, E. (2023). Blocking bacterial appendage attachment to wastewater treatment membranes using anti-adhesins. *Chemosphere*, *323*. https://doi.org/10.1016/j.chemosphere.2023.138246

Zettler, E. R., Mincer, T. J., & Amaral-Zettler, L. A. (2013). Life in the "plastisphere": Microbial communities on plastic marine debris. *Environmental Science and Technology*, *47*(13), 7137–7146. https://doi.org/10.1021/es401288x

Zimmermann, W., & Billig, S. (2011). Enzymes for the biofunctionaliza-tion of poly(ethylene terephthalate). Advances in BiochemicalEngineering/Biotechnology, 125, 97–120.JOURNAL OF BIOMOLECULAR STRUCTURE AND DYNAMICS 6849. https://doi.org/10.1007/10_2010_87

Zhai, X., Zhang, X. H., & Yu, M. (2023). Microbial colonization and degradation of marine microplastics in the plastisphere: A review. In *Frontiers in Microbiology* (Vol. 14). Frontiers Media S.A. https://doi.org/10.3389/fmicb.2023.1127308

Zhang, F., Zhao, Y., Wang, D., Yan, M., Zhang, J., Zhang, P., Ding, T., Chen, L., & Chen, C. (2021). Current technologies for plastic waste treatment: A review. In *Journal of Cleaner Production* (Vol. 282). Elsevier Ltd. https://doi.org/10.1016/j.jclepro.2020.124523

Zhang, H., Perez-Garcia, P., Dierkes, R. F., Applegate, V., Schumacher, J., Chibani, C. M., Sternagel, S., Preuss, L., Weigert, S., Schmeisser, C., Danso, D., Pleiss, J., Almeida, A., Höcker, B., Hallam, S. J., Schmitz, R. A., Smits, S. H. J., Chow, J., & Streit, W. R. (2022). The Bacteroidetes Aequorivita sp. and Kaistella jeonii Produce Promiscuous Esterases With PET-Hydrolyzing Activity. *Frontiers in Microbiology*, *12*. https://doi.org/10.3389/fmicb.2021.803896

Zhang, H., Pap, S., Taggart, M. A., Boyd, K. G., James, N. A., & Gibb, S. W. (2020). A review of the potential utilisation of plastic waste as adsorbent for removal of hazardous priority contaminants from aqueous environments. In *Environmental Pollution* (Vol. 258). Elsevier Ltd. https://doi.org/10.1016/j.envpol.2019.113698

Zhang, H., Zhao, W., Yang, W., Zhang, H., Qian, X., Sun, K., Yang, Q., Shen, X., & Zhang, L. (2025). Autoinducer-2 enhances the defense of Vibrio furnissii against oxidative stress and DNA damage by modulation of c-di-GMP signaling via a two-component system. *MBio*, *16*(2). https://doi.org/10.1128/mbio.02922-24

Zhang, Q., He, Y., Cheng, R., Li, Q., Qian, Z., & Lin, X. (2022). Recent advances in toxicological research and potential health impact of microplastics and nanoplastics in vivo. In *Environmental Science and Pollution Research* (Vol. 29, Issue 27, pp. 40415–40448). Springer Science and Business Media Deutschland GmbH. https://doi.org/10.1007/s11356-022-19745-3

Zhang, S. J., Zeng, Y. H., Zhu, J. M., Cai, Z. H., & Zhou, J. (2022). The structure and assembly mechanisms of plastisphere microbial community in natural marine environment. *Journal of Hazardous Materials*, *421*. https://doi.org/10.1016/j.jhazmat.2021.126780

Zhang, W., Geng, J., Sun, M., Jiang, C., Lin, H., Chen, H., & Yang, Y. (2024). Distinct species turnover patterns shaped the richness of antibiotic resistance genes on eight different microplastic polymers. *Environmental Research*, *259*. https://doi.org/10.1016/j.envres.2024.119562

References

Zhong, X., Zhao, X., Qian, Y., & Zou, Y. (2017). *Polyethylene plastic production process.*

Zurier, H. S., & Goddard, J. M. (2023). A high-throughput expression and screening platform for applications-driven PETase engineering. *Biotechnology and Bioengineering*, *120*(4), 1000–1014. https://doi.org/10.1002/bit.28319

8   Appendix

8.1   Polyethylene terephthalate (PET) primary degradation products affect c-di-GMP-, cAMP-signaling and quorum sensing (QS) in *Vibrio gazogenes* DSM 21264

The transcriptomic data can be accessed online via under accession PRJEB80907 at European Nucleotide Archive (ENA). Additional supplementary material is temporary available at: Polyethylene terephthalate (PET) primary degradation products affect c-di-GMP-, signaling and quorum sensing (QS) in Vibrio gazogenes DSM 21264 | bioRxiv

TABLE S2: *V. gazogenes* DSM 241264 transcriptomes established and analyzed in this study.

Lifestyle	Average read number (mio. *reads*)	Reads mapped (%)	Reads mapped to *rpoD* (# *reads*)	Reads mapped to *pet6* (# *reads*) (% of *rpoD*)
Biofilm				
PET foil	11.0	96.3	11.879	50.0 (0.4)
PE foil	10.1	95.9	11.772	50.0 (0.4)
PET foil plasma	11.0	95.9	14.107	48.0 (0.3)
PE foil plasma	10.9	96.1	17.522	39.0 (0.2)
Planktonic				
CMC (1% w/v)	64.4	99.6	3.998	64 (1.6)
Alginate (1% w/v)	15.3	75.6	2.450	32 (1.3)
Chitin (1% w/v)	138.4	99.59	5.276	52 (1.0)
PET powder (1% w/v)	153.4	99.8	5.159	69 (1.3)
BHET (30 mM)	20.6	94.6	3.396	140 (4.1)
BHET (5.0 mM)	14.6	875	7.680	1.289 (16.8)
BHET (0.5 mM)	15.9	90.2	11.850	69.0 (0.6)
TPA (1mM)	16.4	91.2	10.968	110.0 (1.0)
DMSO	17.1	86.8	8.434	44.0 (0.5)
No additional carbon source added	127.9	99.9	6.017	44.0 (0.8)

Cells were grown in artificial sweater medium (ASWM) and in part supplemented with various listed carbon sources. Biofilm cultures were grown in ASWM and planktonic cultures in 1:10 diluted ASWM. PE and PET plasma indicate plasma-treated foil. Data are mean values of three independent biological experiments. Transcriptome data analysis results are available in the supplementary table S1.

TABLE S3: Significantly differentially expressed genes in PET vs. PE grown biofilms of DSM 21264

Locus tag	Predicted Function	Log2-foldchange
AAC977_01250	predicted glutathione peroxidase, *gene*	2.73
AAC977_19780	alkyl hydroperoxide reductase subunit F, *aphF*	2.41
AAC977_19785	alkyl hydroperoxide reductase subunit C, *aphC*	2.33
AAC977_14955	Dps family protein	2.02

TABLE S4: Log2-foldchanges of known prophage genes in the genome of DSM 21264 grown in the presence of BHET (30, 5.0 and 0.5 mM) in planktonic cultures.

Locus tag	Predicted function	0.5 mM BHET	5 mM BHET	30 mM BHET
	VGPH01			
AAC977_19445	hypothetical protein	0.25	0.29	-2.12
AAC977_19450	hypothetical protein	0.16	0.46	-2.07
AAC977_19455	putative phage tail protein	0.33	0.44	1.02
AAC977_19460	baseplate J/gp47 family protein	1.12	1.11	2.78
AAC977_19465	phage GP46 family protein	-0.21	0.93	3.85
AAC977_19470	phage baseplate assembly protein V	0.36	0.40	2.85
AAC977_19475	phage baseplate assembly protein	0.18	0.50	3.03
AAC977_19480	DNA circularization N-terminal domain-containing protein	0.33	1.60	3.65
AAC977_19485	phage tail tape measure protein	0.29	0.85	2.56
AAC977_19490	phage tail assembly protein	0.69	1.67	4.09
AAC977_19495	phage tail tube protein	1.40	1.99	2.49
AAC977_19500	phage tail sheath subtilisin-like domain-containing protein	0.72	0.09	2.33
AAC977_19505	DUF2635 domain-containing protein	-0.11	0.60	2.85
AAC977_19510	hypothetical protein	-0.27	1.07	2.61
AAC977_19515	phage virion morphogenesis protein	1.73	0.79	4.90
AAC977_19520	DUF1320 domain-containing protein	-0.17	-1.28	0.31
AAC977_19525	hypothetical protein	-0.12	0.28	2.41
AAC977_19530	hypothetical protein	-0.02	0.19	3.48
AAC977_19535	hypothetical protein	2.93	3.36	4.36
AAC977_19540	Mu-like prophage major head subunit gpT family protein	0.47	1.88	3.29
AAC977_19545	phage protease	-0.17	1.86	5.22
AAC977_19550	phage minor head protein	-0.04	0.06	2.75
AAC977_19555	DUF935 domain-containing protein	0.25	1.18	3.72
AAC977_19560	terminase family protein	0.95	1.91	3.93
AAC977_19565	hypothetical protein	-2.21	-1.45	4.18
AAC977_19570	DUF3486 family protein	3.54	3.48	3.71

AAC977_19575	ArsR family transcriptional regulator	NA	NA	5.10
AAC977_19580	DUF2730 family protein	-0.73	-0.14	6.07
AAC977_19585	TraR/DksA C4-type zinc finger protein	0.00	2.48	0.00
AAC977_19590	hypothetical protein	1.14	1.62	4.14
AAC977_19595	hypothetical protein	0.00	3.81	7.56
AAC977_19600	DUF5675 family protein	2.22	-0.34	6.02
AAC977_19605	hypothetical protein	-0.17	-0.37	0.80
AAC977_19610	Mor transcription activator family protein	-2.49	-1.25	3.43
AAC977_19615	hypothetical protein	-0.72	-0.64	-0.44
AAC977_19620	regulatory protein GemA	0.07	0.26	-1.08
AAC977_19625	hypothetical protein	-2.40	0.82	2.18
AAC977_19630	hypothetical protein	-0.35	1.25	1.05
AAC977_19635		NA	NA	NA
AAC977_19640	hypothetical protein	-0.09	-1.14	1.88
AAC977_19645	DUF2786 domain-containing protein	0.08	1.04	2.32
AAC977_19650	hypothetical protein	1.86	1.45	3.22
AAC977_19655	DUF3164 family protein	-1.35	1.14	2.46
AAC977_19660	hypothetical protein	0.00	3.01	3.73
AAC977_19665	hypothetical protein	-1.95	-1.19	2.18
AAC977_19670	hypothetical protein	0.82	2.51	4.09
AAC977_19675	hypothetical protein	-0.14	2.83	4.26
AAC977_19680	hypothetical protein	-2.75	-2.00	4.73
AAC977_19685	AAA family ATPase	-0.26	0.45	3.30
AAC977_19690	transposase domain-containing protein	0.39	1.68	3.43
AAC977_19695	helix-turn-helix domain-containing protein	0.00	3.38	3.60
AAC977_19700	S24 family peptidase	-0.04	-0.42	-0.46
VGPH02				
AAC977_20360	hypothetical protein	0.43	1.99	1.15
AAC977_20365	helix-turn-helix transcriptional regulator	-0.18	1.31	4.03
AAC977_20370	hypothetical protein	-0.90	0.45	3.77
AAC977_20375	hypothetical protein	-0.28	0.95	5.06
AAC977_20380	DNA-binding protein	-0.24	0.53	5.25
AAC977_20385	hypothetical protein	0.40	1.35	6.31
AAC977_20390	hypothetical protein	0.38	1.55	4.96
AAC977_20395	phage tail protein	0.27	1.34	4.52
AAC977_20400	hypothetical protein	0.09	0.53	5.79
AAC977_20405	phage tail protein	0.31	1.14	5.43
AAC977_20410	phage tail protein	-0.83	1.21	5.85
AAC977_20415	baseplate J/gp47 family protein	0.20	1.21	6.81
AAC977_20420	DUF2590 family protein	-4.26	-1.30	6.56
AAC977_20425	hypothetical protein	0.46	1.52	4.07
AAC977_20430	hypothetical protein	0.82	3.02	8.18
AAC977_20435	putative phage tail assembly chaperone	-0.88	2.98	6.89
AAC977_20440	phage protein	0.18	2.67	6.02
AAC977_20445	DUF2586 domain-containing protein	0.84	3.03	5.93
AAC977_20450	phage tail protein	1.48	2.07	3.70

AAC977_20455	ogr/Delta-like zinc finger family protein	0.03	-0.20	-0.25
AAC977_20460	hypothetical protein	3.47	3.83	5.85
AAC977_20465	hypothetical protein	0.46	-0.64	4.16
AAC977_20470	lysozyme	-0.61	-0.43	2.82
AAC977_20475	hypothetical protein	2.47	2.32	1.43
AAC977_20480	hypothetical protein	0.16	0.82	4.24
AAC977_20485	S24 family peptidase	-0.29	-1.19	0.23
AAC977_20490	anaerobic C4-dicarboxylate transporter	0.29	0.73	4.42
VGPH03				
AAC977_09080	contractile injection system protein%2C VgrG/Pvc8 family	0.21	0.57	0.29
AAC977_09085	tail protein X	0.94	1.01	0.91
AAC977_09090	phage tail protein	0.92	1.23	0.35
AAC977_09095	phage tail tape measure protein	0.16	-0.14	0.39
AAC977_09100	phage tail assembly protein	0.47	-0.98	0.81
AAC977_09105	phage major tail tube protein	0.15	1.36	-2.13
AAC977_09110	phage tail protein	0.28	-0.37	-1.41
AAC977_09115	hypothetical protein	-0.04	-0.56	-0.57
AAC977_09120	hypothetical protein	0.57	0.24	-0.20
AAC977_09125	phage tail protein	-0.14	-0.52	0.34
AAC977_09130	hypothetical protein	-0.14	-0.71	2.20
AAC977_09135	hypothetical protein	0.35	-0.10	2.04
AAC977_09140	tail fiber assembly protein	0.29	0.18	-0.44
AAC977_09145	hypothetical protein	0.16	-0.18	0.35
AAC977_09150	hypothetical protein	-0.04	-0.21	0.40
AAC977_09155	hypothetical protein	0.49	0.04	0.05
AAC977_09160	hypothetical protein	-0.07	0.21	1.09
AAC977_09165	SUMF1/EgtB/PvdO family nonheme iron enzyme	0.37	1.54	0.75
AAC977_09170	phage tail protein	0.15	1.60	0.00
AAC977_09175	phage tail protein I	0.55	0.12	1.12
AAC977_09180	baseplate J/gp47 family protein	0.45	0.09	-0.34
AAC977_09185	phage baseplate protein	0.15	-0.64	0.72
AAC977_09190	hypothetical protein	1.47	2.24	2.86
AAC977_09195	phage baseplate assembly protein V	0.80	0.51	0.92
AAC977_09200	hypothetical protein	-0.26	-0.29	2.01
AAC977_09205	hypothetical protein	-0.08	-0.50	3.44
AAC977_09210	S24 family peptidase	-0.43	0.02	1.04

Table S5:   **Confocal microscope settings.**

Physical parameter	Settings	
	Propidium iodide	SYTO 9
Gamma value	1.0	
Pinhole	46 µm	
Detector digital	1.0	
Laser intensity	0.2%	
Laser wavelength	561 nm	488 nm
Detection wavelength	560-700 nm	410-560 nm
Detector gain	663 V	685 V
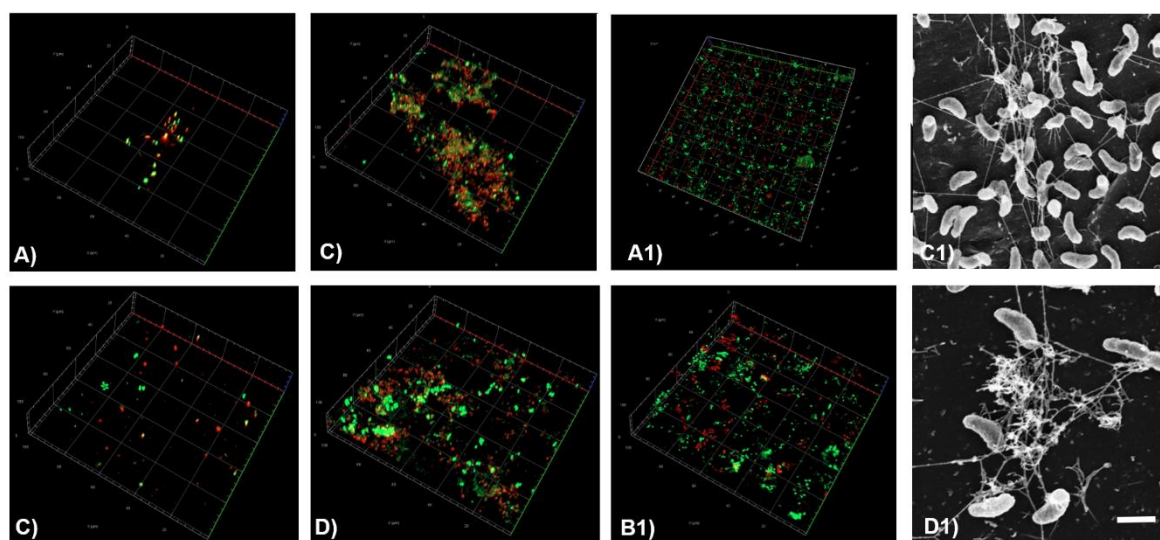
FIGURE S1: Confocal laser scanning microscope (CLSM) images of *V. gazogenes* DSM 21246 grown on PET and PE. CLSM images show DSM 21246 grown on PET **A)**, **C)** and PE **B)**, **D)** in ASW salt solution with additional trace elements after 10 days **A)**; **B)** and 180 days **C)**; **D)** of incubation at 22 °C. Figures **A1)-D1)** show PE and PET foil previously plasma activated. **A1)** and **B1)** show PE foil, biofilm is evaluated using CLSM and SEM, while **C1)** and **D1)** is DSM 21264 incubated on PET foil.
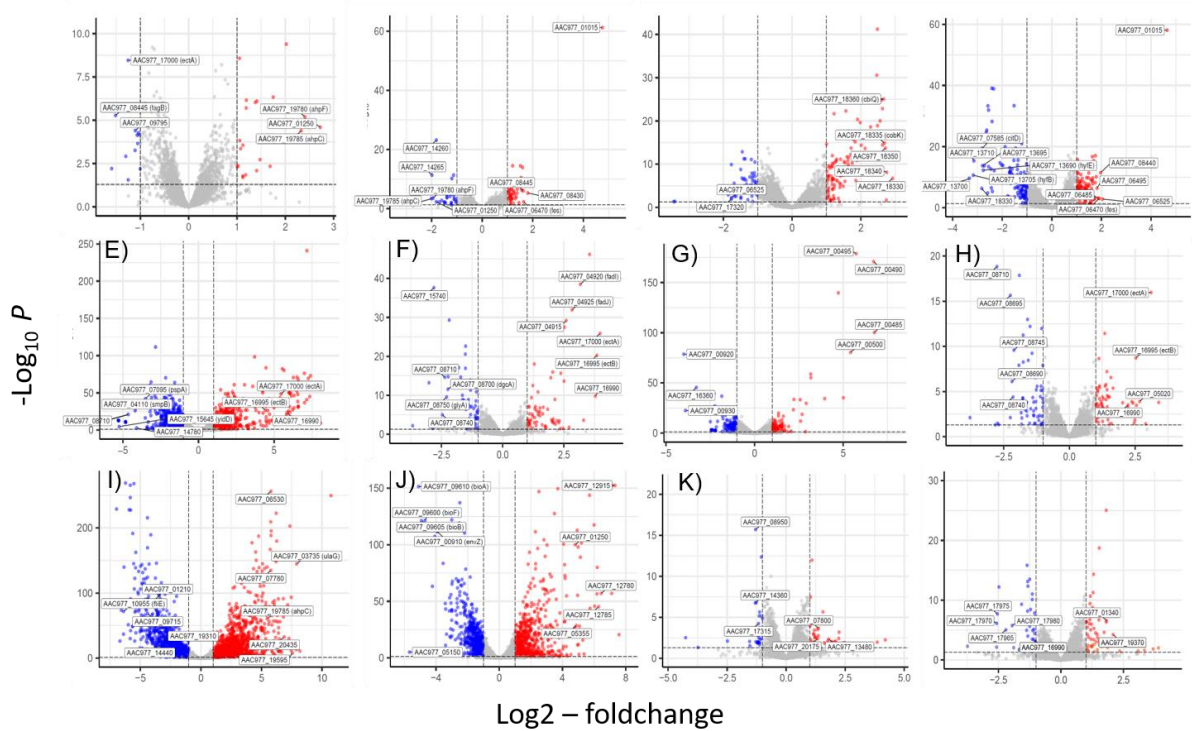
FIGURE S2: Volcano plots of *V. gazogenes* DSM 21264 transcriptomes and cells grown under different conditions and surfaces. X-axis show log2-foldchange, y-axis show false discovery rate, meaning the significance of the transcripts. Blue dots indicate significantly downregulated genes and red dots significantly upregulated genes. Grey dots indicate not significantly differentially expressed genes. **A)-D)** cells grown in biofilm on plastic surfaces **A)** PET foil vs. PE foil, **B)** PETplasma_PET, **C)** PETplasma_PEplasma, **D)** PEplasma_PE; **E)-L)** transcriptomes of liquid cultures grown with different carbon sources grown in batch cultures in artificial seawater medium at 28°C und under constant shaking at 130 rpM. Biofilms cultures were cultivated as described in 9 tested **E)** alginate, **F)** chitin, **G)** CMC and **H)** PET powder; **I)**, 30 mM BHET; **J)**, 5 mM BHET; **K)**, 0.5 mM BHET and **L)** 1mM TPA. The mRNAs were extracted after 8 hours of growth. The data represent mean values of three individual biological replicates for each carbon source or surface.

Locus/ORF tags of most strongly differentiated genes are indicated in the various plots.
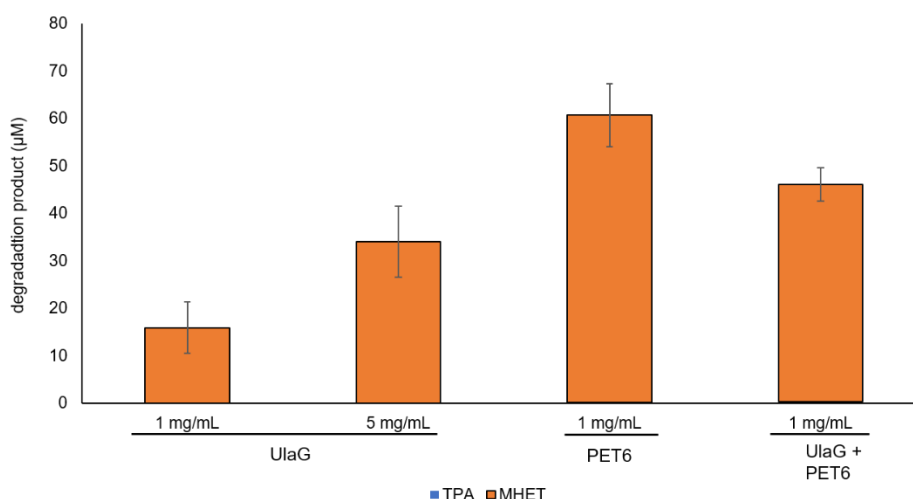
FIGURE S3: **BHET degradation assay of recombinant and purified UlaG and PET6**. Samples were measured using UHPLC ad as outlined in the Materials and Methods section. For detection of degradation products MHET and TPA. BHET was added at 300 µM. Bars indicate production of MHET. Data are mean values of three measurements and the simple SD is given. Data were recorded after 24 hours of incubation.
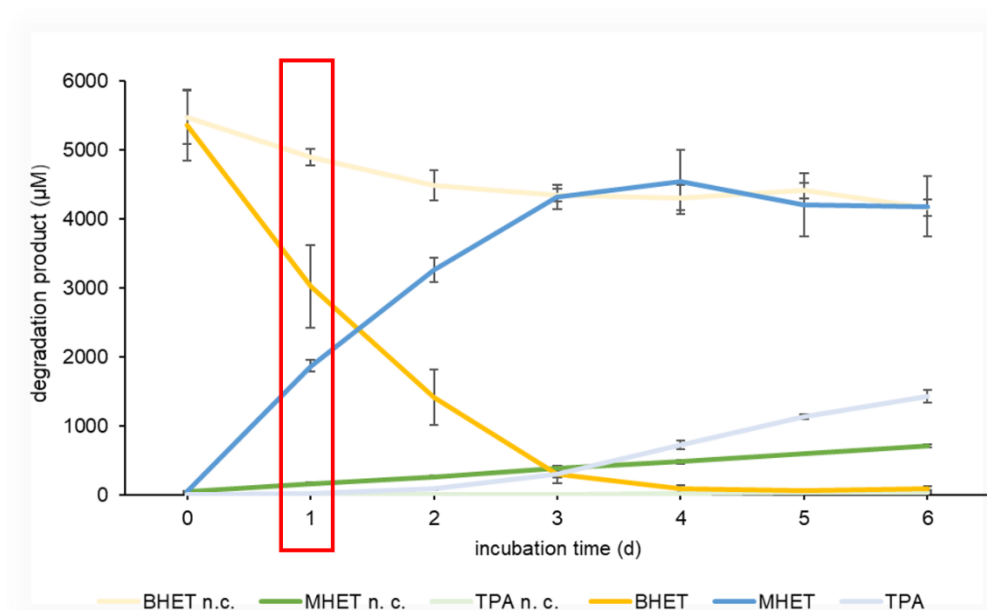
FIGURE S4: DSM 21264 incubated with 5 mM BHET in artificial seawater salt solution and incubated with 5 mM of glucose for 6 days at 28 °C at 130 rpm shaking. Graphic shows BHET degradation and its degradation products over time. The red box indicated the timepoint when RNAseq samples were taken. After 3 days BHET is completely degraded into MHET and TPA concentration is increasing. N.c., negative control was E. coli DH5α grown at the same OD and under the same conditions.

Data are mean values of five independent measurements and error bars indicate the simple standard deviation.
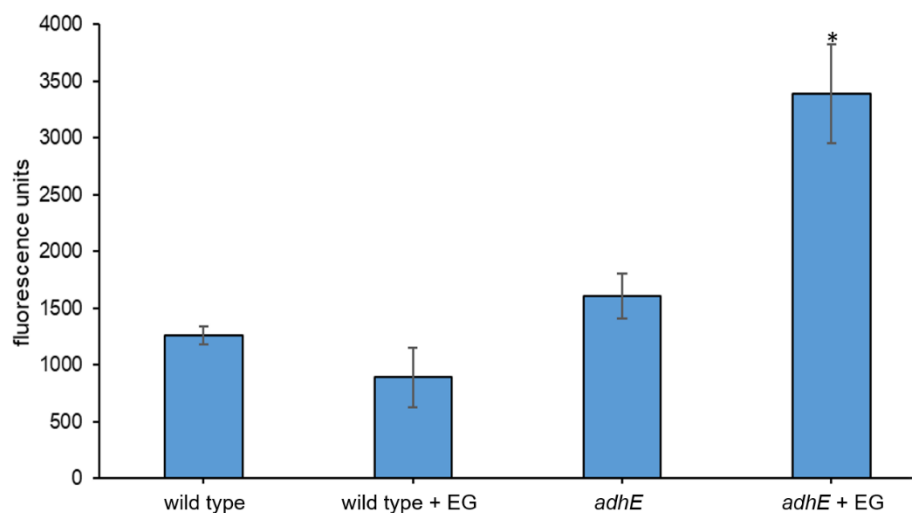
FIGURE S5: Incubation of DSM 21264 carrying pBBR1-MCS-1_adhE_amcyan in M9 medium (30 g/L NaCl) with 5 mM glucose for 24 h shaking. The promoter fusion of the alcohol dehydrogenase gene *adhE* was induced with 5 mM ethylene glycol. As controls wild type with and without ethylene glycol as well as the promoter fusion without ethylene glycol were used. The promoter fusion constructs induced with ethylene glycol had significantly higher fluorescence values than all used controls at P<0.01 and are marked with an asterisk.

Data are mean values of four independent measurements and error bars indicate the simple standard deviation.

FIGURE S6: Phenotypical changes of DSM 21264 influenced by BHET and TPA Confocal laser scanning microscope (CLSM) images **(A-J)** of V. gazogenes DSM 21246 biofilms grown in the presence of increasing concentrations of BHET **(B-E)** and TPA **(G-J)** for 24 h of incubation at 28 °C. BHET concentrations ranged from 0.5 mM **B)**, 5 mM **C)**, 10 mM **D)**, 30 mM **E)**. Used TPA concentrations were 1 mM**(G)**, 5 mM **H)**, 10 mM **I)** and 20 mM **J)**. As controls DSM 21264 was inoculated with DMSO **F)** and also without any added substrates **A)**. Cells were stained using LIVE/DEAD stain.

K) Changing colony morphology of DSM 21246 in the presence of increasing BHET concentrations in LB agar plates at 28 °C after 24h of incubation.

A)

B)

FIGURE S7: VENN diagrams of differentially transcribed genes with log2-foldchange above 2. **A)** shows upregulated genes and **B)** downregulated genes regarding the respective condition. Files were evaluated using https://bioinformatics.psb.ugent.be/webtools/Venn/ website
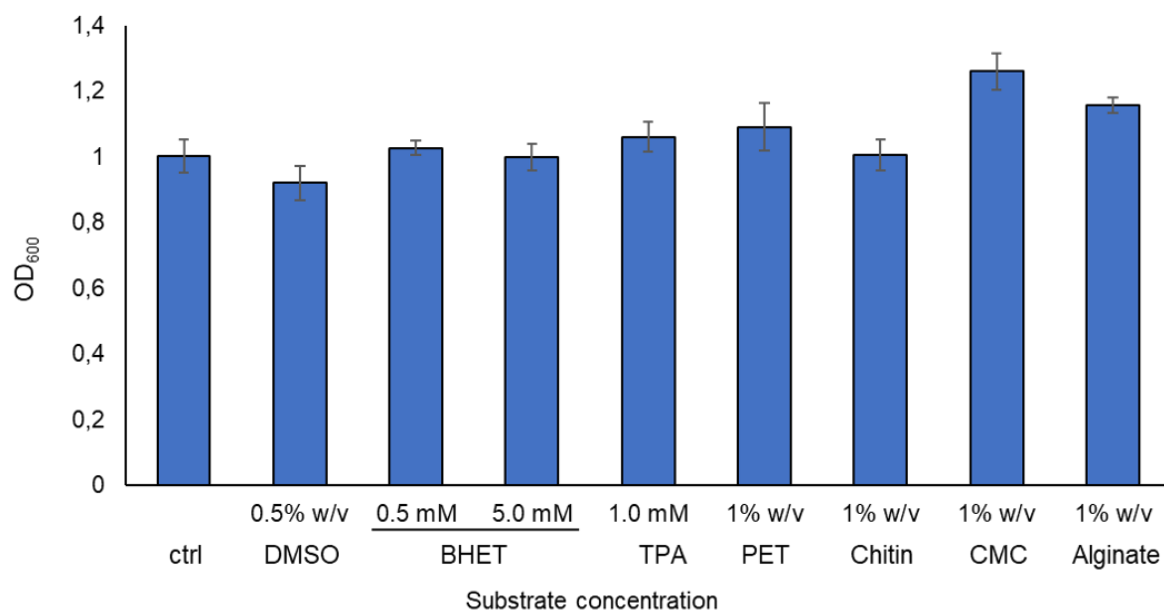
FIGURE S8: Optical density of DSM 21264 incubated for 24 h in Artificial Seawater with reduced carbon source (see Material and Methods) and supplemented with natural substrates, PET, TPA and varying concentrations of BHET. OD measurements were performed before harvesting cells of respective samples for RNAseq analysis. Results show that supplementing DSM 21264 with additional carbon sources doesn't affect the growth of the strain significantly.

Acceptance letter of the manuscript Polyethylene terephthalate (PET) primary degradation products affect c-di-GMP-, cAMP-signaling and quorum sensing (QS) in *Vibrio gazogenes* DSM 21264 in Microbiology Spectrum

Date: 2025-05-04 04:45:43
Last Sent: 2025-05-04 04:45:43
Triggered By: Redacted
BCC: Redacted
Subject: Spectrum00181-25R1 Decision Letter
Message: Re: Spectrum00181-25R1 (Polyethylene terephthalate (PET) primary degradation products affect c-di-GMP-, cAMP-signaling and quorum sensing (QS) in Vibrio gazogenes DSM 21264)

Dear Prof. Wolfgang R. Streit:

Your manuscript has been accepted, and I am forwarding it to the ASM production staff for publication. Your paper will first be checked to make sure all elements meet the technical requirements. ASM staff will contact you if anything needs to be revised before copyediting and production can begin. Otherwise, you will be notified when your proofs are ready to be viewed.

Data Availability: ASM policy requires that data be available to the public upon online posting of the article, so please verify all links to sequence records, if present, and make sure that each number retrieves the full record of the data. If a new accession number is not linked or a link is broken, provide production staff with the correct URL for the record. If the accession numbers for new data are not publicly accessible before the expected online posting of the article, publication may be delayed; please contact ASM production staff immediately with the expected release date.

Publication Fees: For information on publication fees and which article types have charges, please visit our website. We have partnered with Copyright Clearance Center (CCC) to collect author charges. If fees apply to your paper, you will receive a message from no-reply@copyright.com with further instructions. For questions related to paying charges through RightsLink, please contact CCC at ASM_Support@copyright.com or toll free at +1-877-622-5543. CCC makes every attempt to respond to all emails within 24 hours.

ASM Membership: Corresponding authors may join or renew ASM membership to obtain discounts on publication fees. Need to upgrade your membership level? Please contact Customer Service at Service@asmusa.org.

PubMed Central: ASM deposits all Spectrum articles in PubMed Central and international PubMed Central-like repositories immediately after publication. Thus, your article is automatically in compliance with the NIH access mandate. If your work was supported by a funding agency that has public access requirements like those of the NIH (e.g., the Wellcome Trust), you may post your article in a similar public access site, but we ask that you specify that the release date be no earlier than the date of publication on the Spectrum website.

Embargo Policy: A press release may be issued as soon as the manuscript is posted on the Spectrum Latest Articles webpage. The corresponding author will receive an email with the subject line "ASM Journals Author Services Notification" when the article is available online.

The ASM Journals program strives for constant improvement in our submission and publication process. Please tell us how we can improve your experience by taking this quick Author Survey.

Thank you for submitting your paper to Spectrum.

Sincerely,
Livnat Afriat-Jurnou
Editor
Microbiology Spectrum

Reviewer #1 (Comments for the Author):

the new version is improved. no need for further modifications. it is an interesting plastisphere story.


Reviewer #2 (Comments for the Author):

The comments and suggestions are followed carefully and I am happy with the revised version of the manuscript based on insightful work.

8.2   The Bacteroidetes *Aequorivita* sp. and *Kaistella jeonii* produce promiscuous esterases with PET-hydrolyzing activity
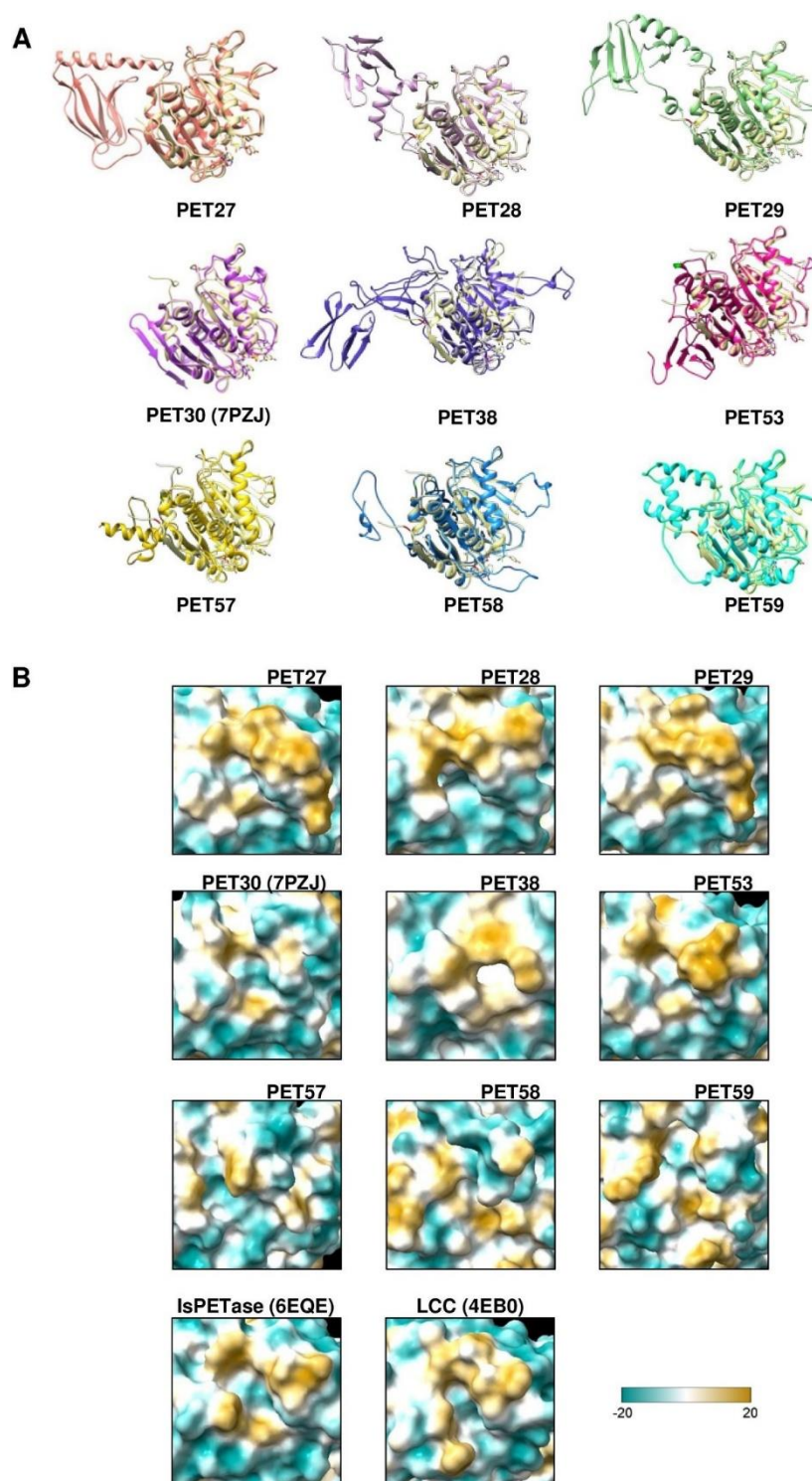
All Supplementary Material is available online at: https://www.frontiersin.org/articles/10.3389/fmicb.2021.803896/full#supplementary-material
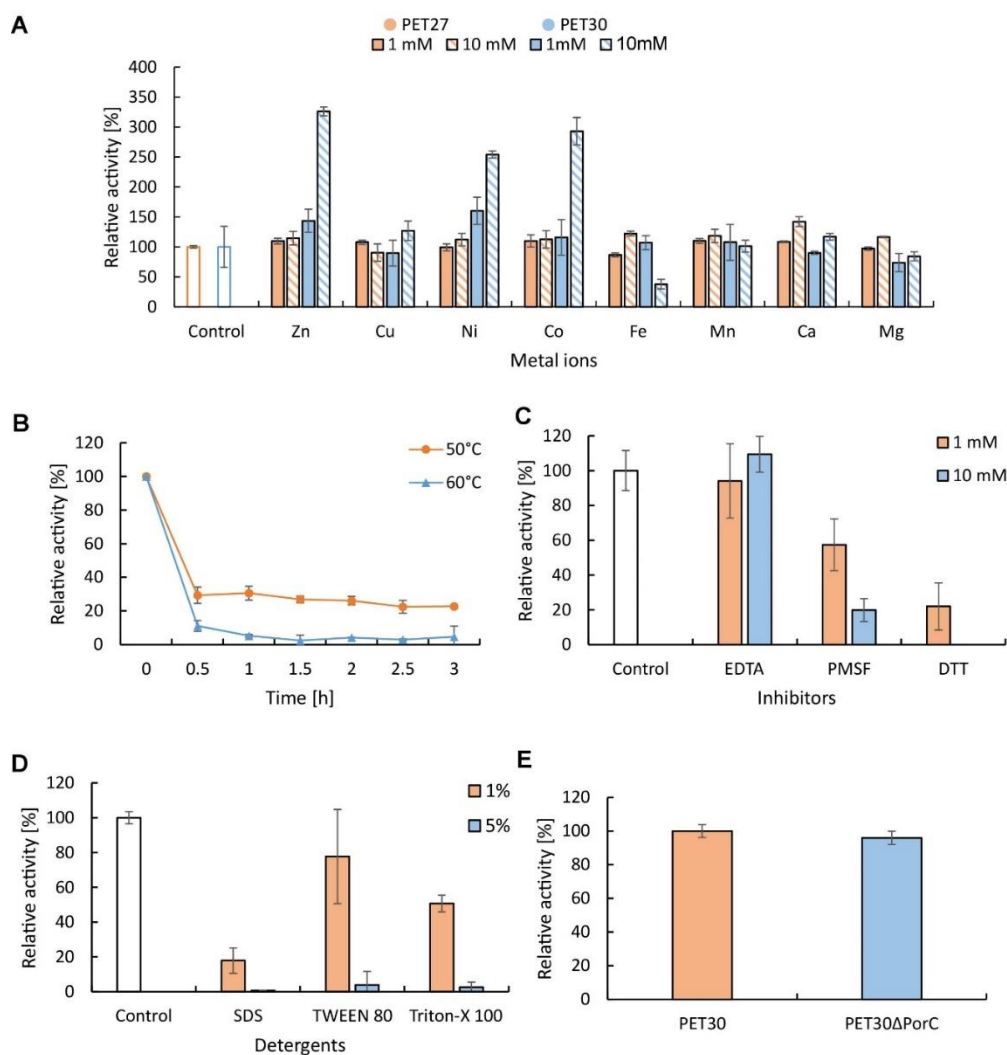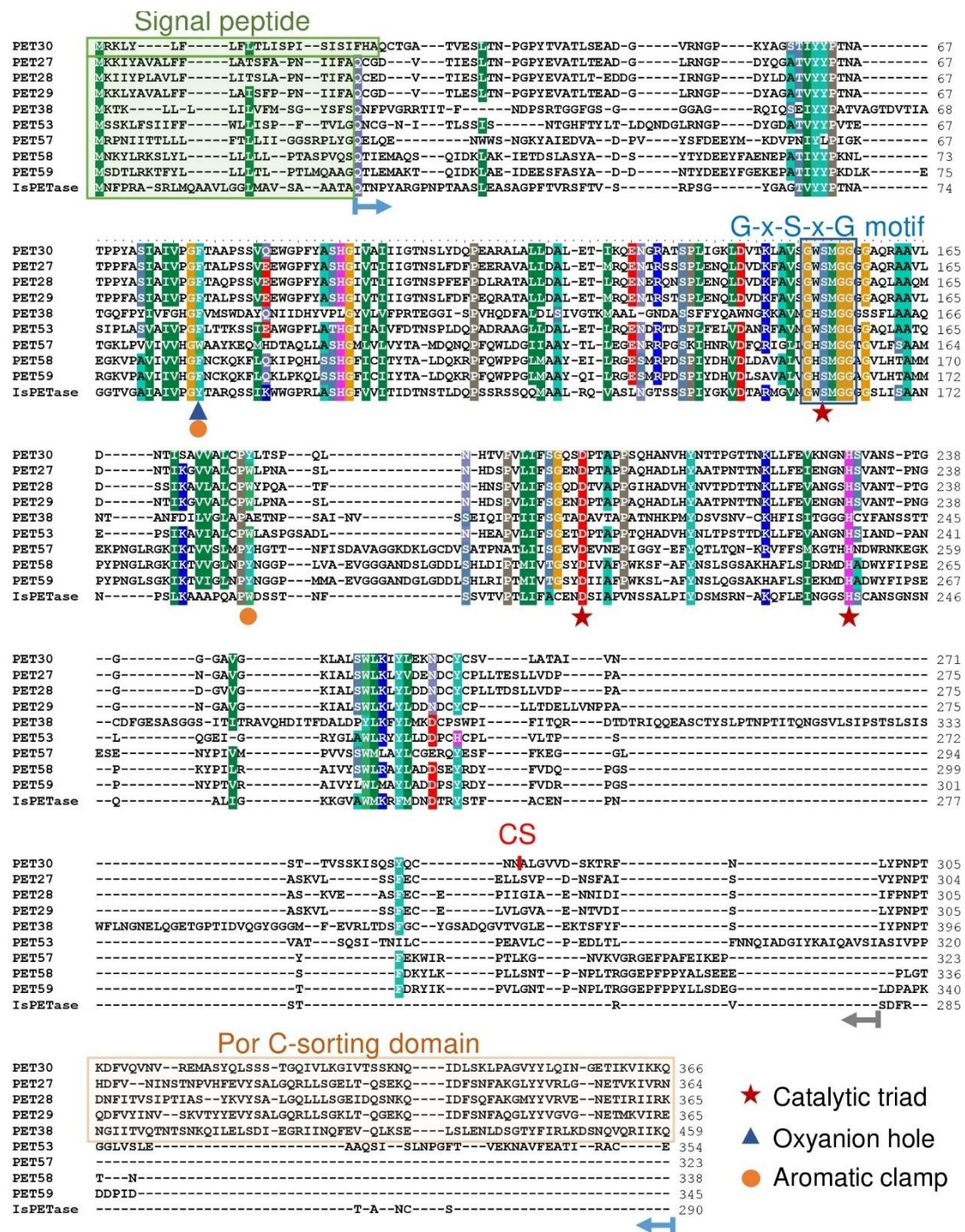

Supplementary Figure 1 | Further biochemical characterization of PET27 and PET30 using *p*NP-substrates. Cofactor requirements were tested for PET27 with *p*NP-C8 at 40°C and for PET30 with *p*NP-C6 at 30°C **(A)**. For PET30, all other tests were carried out with *p*NP-C6 and all assays except **(B)** were conducted at 30°C. Thermostability of PET30 was assessed at 50 and 60°C over 3 h with *p*NP-C6 **(B)**. Inhibitors **(C)** and detergents **(D)** generally decrease the activity of PET30, particularly with higher concentrations. Activity of PET30 and PET30ΔPorC were compared under the same conditions using *p*NP-C6 **(E)**. Data represent mean values of at least three independent measurements.
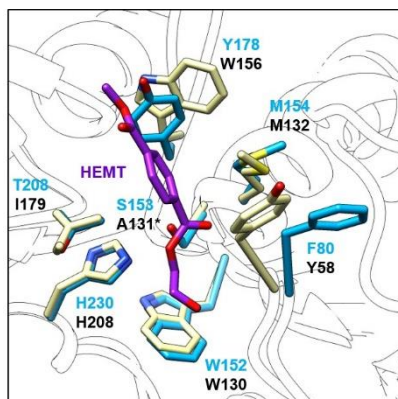
Supplementary Figure 2 | Zoom into the active site of PET30ΔPorC. Overlaid are the structures of PET30ΔPorC (blue) with the PETase from *I. sakaiensis* (light yellow, black labeling) in complex with HEMT (purple; PDB code 5XH3). The residues involved in binding are highlighted and numbered according to their structure. *The structure 5XH3 is a mutant where the catalytic Serine was mutated to an Alanine.

Supplementary Figure 3 | Structure prediction models of verified and predicted PETases affiliated with the phylum of the Bacteroidetes. **(A)** 3D structures were modeled using the Robetta server using the *Is*PETase crystal structure (light yellow, 6EQE) as a backbone. For PET30, the crystal structure was shown. **(B)** Surface hydrophobicity around the tunnel leading to the active site of putative bacteroidetal PETases and functionally verified PET-degrading enzymes. Hydrophilic regions are displayed in turquoise and hydrophobic in gold.

Supplementary Figure 4 | Amino acid alignment of 9 potential PETases affiliated with the Bacteroidetes phylum. The original sequences were used for the structural alignment and the alignment was constructed with T-Coffee. Alignment was visualized with Bioedit version 7.0.5. The *Is*PETase was included for reasons of benchmarking. Blue arrows indicate the start and the end of the active PET27 and PET30 clones. We introduced a methionine as the first aa of the protein sequences. The signal peptide deleted version of the enzymes was functionally verified. The red arrow labeled with CS indicates the predicted cleavage site of C-terminal PorC domain (Lasica et al., 2017). The gray arrow indicates the C-terminus of the truncated

version of PET30 (PET30Δ300-366), number indicates the position of amino acid). PET30Δ300-366 was active on PCL and BHET.

Supplementary Figure 5 | Confocal microscopic pictures of *K. jeonii* colonizing PET foil. The pictures were taken after 5–7 days of incubation of *K. jeonii* in R2A medium. Cells are dyed with LIVE/DEAD™ stain. Green fluorescence shows living cells, red fluorescence indicates dead cells. 2D front pictures were taken with Axio Observer Z1/7, LSM 800 (Carl Zeiss, Jena, Germany) of a 3D Z-stack image.

TABLE S1: Bacterial strains and plasmids used in this work.

Strain	Properties	Reference/source
E. coli DH5α	*supE*44 Δ*lacU*169 (Φ80 lac*Z* ΔM15) *hsdR*17 *recA*1 *endA*1 *gyrA*96 *thi*-1 *relA*1	Invitrogen (Karlsruhe, Germany)
E. coli BL21 (DE3)	F⁻, *ompT*, *hsdS* B (r_B⁻ m_B⁻) *gal*, *dcm*, λDE3	Novagen/Merck (Darmstadt, Germany)
E. coli SHuffle® T7	*huA2 lacZ*::T7 gene1 [lon] *ompT ahpC gal* λatt::pNEB3-r1-cDsbC (SpecR, lacIq) Δ*trxB sulA*11 R(mcr-73::miniTn10--TetS)2 [dcm] R(zgb-210::Tn10 --TetS) *endA*1 Δ*gor* Δ(*mcrC-mrr*)114::IS10	NEB (Frankfurt am Main, Germany)

Vector	Properties	Reference/source
pET21a(+)	Expression vector, *lacI*, Amp^R, T7-*lac*- promoter, C-terminal His_6-tag coding sequence	Novagen/Merck (Darmstadt, Germany)
pET21a(+)::PET27	1026 bp insert in pET21a(+) coding for PET27	This work
pET21a(+)::PET28	1029 bp insert in pET21a(+) coding for PET28	This work
pET21a(+)::PET29	1029 bp insert in pET21a(+) coding for PET29	This work
pET21a(+)::PET30	1032 bp insert in pET21a(+) coding for PET30	This work
pET21a(+)::PET30_Δ300-366	831 bp insert in pET21a(+) coding for PET30, truncated protein lacking PorC	This work
pET21a(+)::PET38	1341 bp insert in pET21a(+) coding for PET38	This work
pET21a(+)::PET53	1072 bp insert in pET21a(+) coding for PET53	This work
pET21a(+)::PET57	969 bp insert in pET21a(+) coding for PET57	This work
pET21a(+)::PET58	1014 bp insert in pET21a(+) coding for PET58	This work
pET21a(+)::PET59	1035 bp insert in pET21a(+) coding for PET59	This work
pMAL-p4x::IsPETase	795 bp insert in pMAL-p4x coding for the wildtype *Is*PETase from *Ideonella sakaiensis*	This work

TABLE S2: Primers used in this work.

Primer	Sequence (5' → 3')	Length (bp)	Tm (°C)	Source
T7_prom	TAATACGACTCACTATAGGG	20	53	Eurofins MWG (Elsberg, Germany)
T7_term	CTAGTTATTGCTCAGCGGT	19	54	Eurofins MWG (Elsberg, Germany)
PET_for	ATATAGGCGCCAGCAACC	18	59	Novagen/Merck (Darmstadt, Germany)
PET_rev	TCCGGATATAGTTCCTC	17	52	Novagen/Merck (Darmstadt, Germany)

TABLE S3: Identifiers and GenBank entries employed in the phylogenetic clustering of PET active enzymes in FIGURE 4.

Name	GenBank or PDB entry	Phylogenetic Affiliation	Reference
BsEstB	ADH43200.1	*Bacillus subtilis* 4P3-11	Herrero Acero *et al.* 2011
CalB	4K6G_A	*Candida antarctica*	Andersen *et al.* 1999; Xie *et al.* 2014
Cut190	BAO42836.1	*Saccharomonospora viridis* AHK190	Kawai *et al.* 2014
FsC	1CEX	*Fusarium solani* pisi	Silva *et al.* 2005
HiC	4OYY	*Humicola insolens*	Ronkvist *et al.* 2009
*Is*PETase	GAP38373.1	*Ideonella sakaiensis* 201-F6	Yoshida *et al.* 2016
LCC	AEV21261.1	uncultured bacterial species (leaf-branch compost)	Sulaiman *et al.* 2012
PE-H	A0A1H6AD45	*Pseudomonas aestusnigri* VGXO14T	Bollinger *et al.* 2020
PET2	C3RYL0	uncultured bacterium	
PET5	R4YKL9	*Oleispira antarctica* RB-8	Danso *et al.* 2018
PET6	A0A1Z2SIQ1	*Vibrio gazogenes*	
PET12	A0A0G3BI90	*Polyangium brachysporum*	
Tcur0390	WP_012850775.1	*Thermomonospora curvata* DSM43183	Wei *et al.* 2014
Tcur1278	WP_012851645.1	*Thermomonospora curvata* DSM43183	Chertkov *et al.* 2011
TfH	WP_011291330.1	*Thermobifida fusca* DSM43793	Müller *et al.* 2005
Thc_Cut1	ADV92526.1	*Thermobifida cellulosilytica* DSM44535	
Thc_Cut2	ADV92527.1	*Thermobifida cellulosilytica* DSM44535	Herrero Acero *et al.* 2011
Thf42_Cut1	ADV92528.1	*Thermobifida fusca* DSM44342	
Tha_Cut1	ADV92525.1	*Thermobifida alba* DSM43185	Ribitsch *et al.* 2012
Thh_Est	AFA45122.1	*Thermobifida halotolerans* DSM44931	

TABLE S4: Data collection and refinement statistics for PET30

	PET30
Wavelength	0.9795
Resolution range	38.8 - 2.1 (2.175 - 2.1)
Space group	P 43 21 2
Unit cell	109.755 109.755 41.803 90 90 90
Total reflections	267429 (24691)
Unique reflections	15447 (1505)
Multiplicity	17.3 (16.4)
Completeness (%)	99.95 (100.00)
Mean I/sigma(I)	13.95 (5.38)
Wilson B-factor	24.09
R-merge	0.1746 (0.7031)
R-meas	0.1799 (0.7255)
R-pim	0.04277 (0.1772)
CC1/2	0.997 (0.945)
CC*	0.999 (0.986)
Reflections used in refinement	15443 (1507)
Reflections used for R-free	716 (78)
R-work	0.1619 (0.1655)
R-free	0.2187 (0.2460)
CC(work)	0.962 (0.901)
CC(free)	0.932 (0.840)
Number of non-hydrogen atoms	2208
macromolecules	2006
solvent	202
Protein residues	273
RMS(bonds)	0.011
RMS(angles)	1.21
Ramachandran favored (%)	95.57
Ramachandran allowed (%)	3.69
Ramachandran outliers (%)	0.74
Rotamer outliers (%)	0.00
Clashscore	5.01
Average B-factor	27.12
macromolecules	26.45
solvent	33.82

Statistics for the highest-resolution shell are shown in parentheses.

TABLE S5: Homologs of bacteroidetal PET27 and PET30 hydrolases in metagenomes.

Locus Tag	Gene ID	Genome Name (GREEN=Bacteroidetes; YELLOW=FCB)	NCBI Biosample Accession	Pubmed ID /GenBank entry
Ga0266410_112824	2790477168	*Aequorivita sp.* CPC67	SAMEA2621812	25999513
Ga0267287_12740	2786516536	*Marinimicrobia bacterium* SP4388	SAMEA2621812	25999513
Ga0214074_111348	2758370761	*Psychroflexus torquis* ATCC 700755	SAMN02603919	24391155 , 32431677
Ga0441744_095_43538_44635	2893010289	*Psychroflexus gondwanensis* ACAM 365	SAMN10790446	24391155, 32431677
Ga0452869_05_68007_69104	2890419200	*Brumimicrobium glaciale* IC156	SAMN10779751	24391155, 32431677
Ga0125537_104199	2776033716	*Altibacter lentus* JL2010	SAMN02988278	25342673
Ga0101260_1142	2663974789	*Bacteroidetes bacterium* SCGC AD-308-D03 - v2	SAMN06314724	373136
Ga0266415_110121	2790487960	*Aequorivita sp.* SAT106	SAMEA2620929	25999513
Ga0266677_12858	2778555477	*Flavobacteriaceae bacterium* SAT1509	SAMEA2620929	25999513
Ga0267170_100812	2814895288	*Gemmatimonadetes bacterium* RS373	SAMEA2620929	25999513
Ga0267250_100918	2786410539	*Marinimicrobia bacterium* RS418	SAMEA2620929	25999513
Ga0267252_10536	2786413511	*Marinimicrobia bacterium* RS816	SAMEA2620929	25999513
Ga0267252_10542	2786413517	*Marinimicrobia bacterium* RS816	SAMEA2620929	25999513
Ga0266410_112825	2769034576	*Aequorivita sp.* CPC68	SAMEA2621812	25999513
Ga0267287_12741	2767134878	*Marinimicrobia bacterium* SP4389	SAMEA2621812	25999513
Ga0214074_111349	2765235181	*Psychroflexus torquis* ATCC 700756	SAMN02603919	24391155 , 32431678
Ga0441744_095_43538_44636	2763335483	*Psychroflexus gondwanensis* ACAM 366	SAMN10790446	24391155, 32431677
Ga0452869_05_68007_69105	2761435786	*Brumimicrobium glaciale* IC157	SAMN10779751	24391155, 32431677
Ga0267200_1431	2786528832	*Marinimicrobia bacterium* EAC25	SAMEA2620855	25999513, 29337314
Ga0267200_1544	2786528992	*Marinimicrobia bacterium* EAC25	SAMEA2620855	25999513, 29337314
Ga0416765_13_4825_5925	2860314059	*Chryseobacterium sp.* 16F	SAMN14915977	25824943
PI23P_05397	639004873	*Polaribacter irgensii* 23-P	SAMN02436114	9542092 /NZ_CH724148.1
Aeqsu_2514	2509583556	*Aequorivita sublithincola* QSSC9-3, DSM 14238	SAMN02232006	28604660
Ga0266584_11073	2788314349	*Cryomorphaceae bacterium* CPC63	SAMEA2622923	25999513
Ga0266589_10312	2787698016	*Cytophagia bacterium* NAT375	SAMEA2622923	25999513
Ga0267262_14611	2786499724	*Marinimicrobia bacterium* SAT24	SAMEA2622923	25999513
Ga0267263_11113	2786500508	*Marinimicrobia bacterium* SAT2619	SAMEA2622923	25999513
Ga0267267_12326	2786498443	*Marinimicrobia bacterium* SP108	SAMEA2622923	25999513
Ga0267268_10328	2786441642	*Marinimicrobia bacterium* SP173	SAMEA2622923	25999513
Ga0267268_1112	2786442127	*Marinimicrobia bacterium* SP173	SAMEA2622923	25999513
Ga0267270_13120	2786484524	*Marinimicrobia bacterium* SP276	SAMEA2622923	25999513
Ga0267272_1173	2786478779	*Marinimicrobia bacterium* SP3060	SAMEA2622923	25999513
Ga0267273_13417	2786477564	*Marinimicrobia bacterium* SP3097	SAMEA2622923	25999513
Ga0267276_13625	2786480397	*Marinimicrobia bacterium* SP3117	SAMEA2622923	25999513
Ga0267279_10440	2786489803	*Marinimicrobia bacterium* SP328	SAMEA2622923	25999513
Ga0267280_12433	2786520859	*Marinimicrobia bacterium* SP359	SAMEA2622923	25999513
Ga0267282_10178	2786519018	*Marinimicrobia bacterium* SP4039	SAMEA2622923	25999513
Ga0063505_10623	2606052547	*Roseivirga seohaensis aquiponti* D-25	SAMN03145748	27107724/ JSVA01000000

Ga0267161_105313	2814952585	Gemmatimonadetes bacterium EAC635	SAMEA2623295	25999513
Ga0267164_1577	2814955360	Gemmatimonadetes bacterium NAT196	SAMEA2623295	25999513
Ga0267234_12226	2786460090	Marinimicrobia bacterium NAT495	SAMEA2623295	25999513
Ga0267237_1518	2786446587	Marinimicrobia bacterium NAT62	SAMEA2623295	25999513
Ga0267238_1416	2786464404	Marinimicrobia bacterium NAT74	SAMEA2623295	25999513
Ga0267239_13724	2786462435	Marinimicrobia bacterium NP104	SAMEA2623295	25999513
Ga0215720_101116	2756777030	Marinirhabdus gelatinilytica DSM 101478	SAMN08776299	QRAO00000000
Ga0266586_11614	2788308996	Cryomorphaceae bacterium SP53	SAMEA2619927	25999513
Ga0267165_10476	2814943193	Gemmatimonadetes bacterium NP105	SAMEA2619818	25999513
SCB49_04680	641143976	Ulvibacter sp. SCB49	SAMN02981237	ABCO00000000
G440DRAFT_00359	2524126300	Aequorivita capsosiphonis DSM 23843	SAMN02440880	AUBG00000000
Ga0266370_16423	2789796087	Altibacter sp. EAC109	SAMEA2619376	25999513
Ga0266560_154	2825980380	Crocinitomicaceae bacterium NAT165	SAMEA2619376	25999513
Ga0267217_1484	2786425266	Marinimicrobia bacterium MED806	SAMEA2619376	25999513
Ga0267217_16831	2786425767	Marinimicrobia bacterium MED806	SAMEA2619376	25999513
Ga0267218_1219	2786426885	Marinimicrobia bacterium MED808	SAMEA2619376	25999513
Ga0267219_10943	2786427199	Marinimicrobia bacterium MED812	SAMEA2619376	25999513
Ga0267220_10096	2786428744	Marinimicrobia bacterium MED829	SAMEA2619376	25999513
Ga0267220_10106	2786428754	Marinimicrobia bacterium MED829	SAMEA2619376	25999513
Ga0267224_14310	2786401069	Marinimicrobia bacterium NAT217	SAMEA2619376	25999513
Ga0267226_12918	2786404156	Marinimicrobia bacterium NAT220	SAMEA2619376	25999513
Ga0267227_13041	2786403315	Marinimicrobia bacterium NAT224	SAMEA2619376	25999513
Ga0267228_1422	2786399119	Marinimicrobia bacterium NAT230	SAMEA2619376	25999513
Ga0267208_10372	2786507568	Marinimicrobia bacterium MED586	SAMEA2619667	25999513
Ga0267208_10412	2786507636	Marinimicrobia bacterium MED586	SAMEA2619667	25999513
Ga0267209_1018	2786508441	Marinimicrobia bacterium MED589	SAMEA2619667	25999513
Ga0267212_106014	2786417419	Marinimicrobia bacterium MED648	SAMEA2619667	25999513
Ga0267212_10712	2786417608	Marinimicrobia bacterium MED648	SAMEA2619667	25999513
Ga0267212_110812	2786418228	Marinimicrobia bacterium MED648	SAMEA2619667	25999513
Ga0267213_15817	2786422578	Marinimicrobia bacterium MED757	SAMEA2619667	25999513
Ga0267214_1214	2786420423	Marinimicrobia bacterium MED764	SAMEA2619667	25999513
Ga0267214_12210	2786420472	Marinimicrobia bacterium MED764	SAMEA2619667	25999513
Ga0267214_1225	2786420467	Marinimicrobia bacterium MED764	SAMEA2619667	25999513
Ga0267214_14025	2786421083	Marinimicrobia bacterium MED764	SAMEA2619667	25999513
Ga0344934_2405	2839770976	Dokdonia sinensis SH27	SAMN10250232	32228747
Ga0441973_01_775875_776969	2890600833	Ulvibacter sp. KK4	SAMD00166796	32539909
LY87DRAFT_1302	2597312806	Dokdonia sp. Hel_I_5	SAMN05661066	32539909
Ga0267202_1226	2786524372	Marinimicrobia bacterium EAC649	SAMEA2620230	25999513
Ga0267202_13210	2786524561	Marinimicrobia bacterium EAC649	SAMEA2620230	25999513
Ga0267202_13216	2786524567	Marinimicrobia bacterium EAC649	SAMEA2620230	25999513
Ga0350409_3222	2848310855	Psychroflexus sp. MES1-P1E	SAMN08125772	PJBS00000000, CM009131
Ga0066802_10753	2623289129	Aequorivita viscosa DSM 26349	SAMN04487908	FQYV00000000
Ga0077144_1092	2641186029	Chryseobacterium jeonii DSM 17048	SAMN03145167	JSYL00000000
Ga0079842_10854	2668214597	Aequorivita viscosa CGMCC 1.11023	SAMN05216556	FNNS00000000

Ga0104531_1111	2676887423	*Chryseobacterium jeonii* DSM 17048	SAMN05421876	FOLA00000000
Ga0114183_10545	2656209723	*Roseivirga seohaensis* SW-152	SAMN04423148	28077207
Ga0170448_3258	2729662814	*Ulvibacter antarcticus* DSM 23424	SAMN06264851	REFC00000000
Ga0310487_0626	2799156613	*Roseivirga ehrenbergii* DSM 102268	SAMN10864729	SMGS00000000
Ga0336340_1074	2835308220	*Winogradskyella sp.* KYW1333	SAMN09667312	QPHL00000000
Ga0336670_2825	2837407865	*Aequorivita lipolytica* CIP 107455	SAMEA4644770	30225207
Ga0336672_3534	2835103747	*Aequorivita antarctica* CIP 107457	SAMEA4644771	PMC6139392
Ga0443045_01_3096381_3097484	2884436497	*Nonlabens sp.* Ci31	SAMN12697551	CP043633
pgond44_05165	2533771942	*Psychroflexus gondwanensis* ACAM 44	SAMN02471957	24391155
Ga0077372_102327	2628626758	*Aequorivita vladivostokensis* KMM 3516	SAMN03084320	JSVU00000000
Ga0114184_10616	2654412999	*Roseivirga echinicomitans* KMM 6058	SAMN04382068	LRDB00000000.1
Ga0248413_145580	2812952679	*Roseivirga ehrenbergii* KMM 6017	SAMN03084331	LQZQ00000000
Ga0373279_1152	2830035069	*Lewinella antarctica* DSM 105096	SAMN13172327	PMC6139392
Ga0336671_791	2835108492	*Aequorivita sp.* CIP 111184	SAMEA4704834	UEFQ00000000
Ga0399719_270	2836794304	*Aequorivita sp.* H23M31	SAMN10518960	CP034951
Ga0441974_01_521424_522518	2890652824	*Ulvibacter marinus* KCTC 32322T	SAMD00166797	BKCG00000000.1

8.3 Surface Grafted *N*-Oxides have Low-Fouling and Antibacterial Properties

All Supplementary Material is available online at: downloadSupplement

WILEY-VCH

Figure S1. ATR-FTIR-spectra of PE-poly (MANOx) and PE-poly (MAANOx)
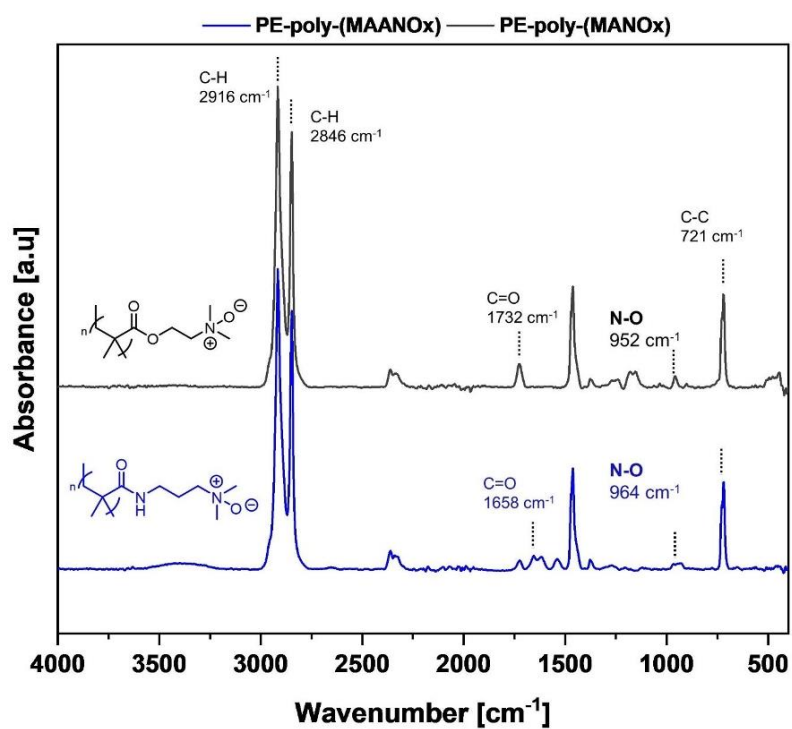
Figure S2. XPS survey spectra of pristine PE
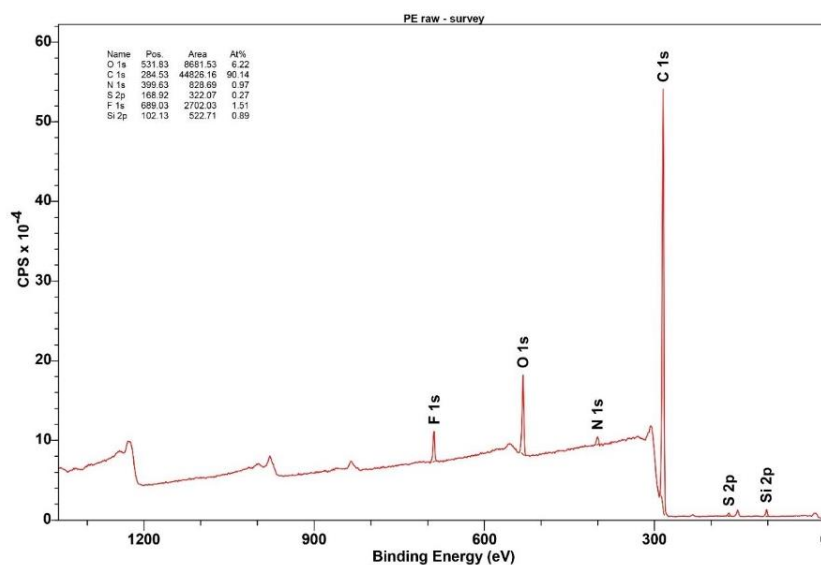
Figure S3. XPS survey spectra of plasma-activated PE.
Spectra were recorded 72 h after plasma activation.

WILEY-VCH
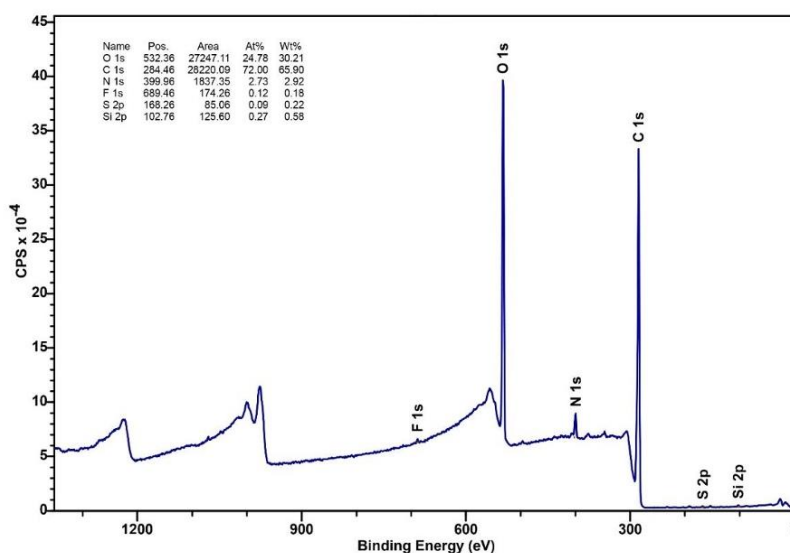
Figure S4. Deconvoluted XPS spectra of plasma-activated PE.

a) Deconvoluted N1s region of plasma-activated PE and b) Deconvoluted XPS region of the O1s region of plasma-activated PE. Plasma activation was carried out as described in the experimental section. Spectra were recorded 72 h after plasma activation. Plasma-activated PE samples were stored under nitrogen atmosphere prior XPS measurements.

WILEY-VCH
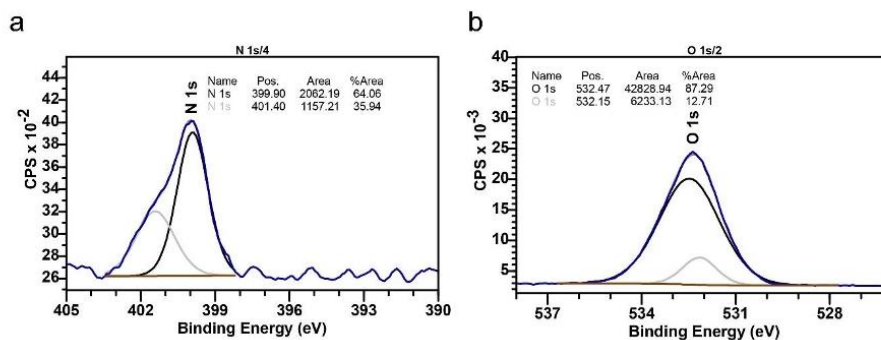
Figure S5. XPS survey spectra of PE-poly-(VBNOx).

Synthesis and polymerization protocols were carried out as described in the experimental section. Atomic ratio for N/C is similar to the theoretical ratio. The deviation of the N/O and C/O ratio were assigned to non-identified impurities, most likely absorbed CO. Residues of sodium hydroxide species from the decomposition process of the material as well as artifacts of the synthetic procedure and packaging material (Si 2p, S 2p, Ca 1s, F 1s) are visible.
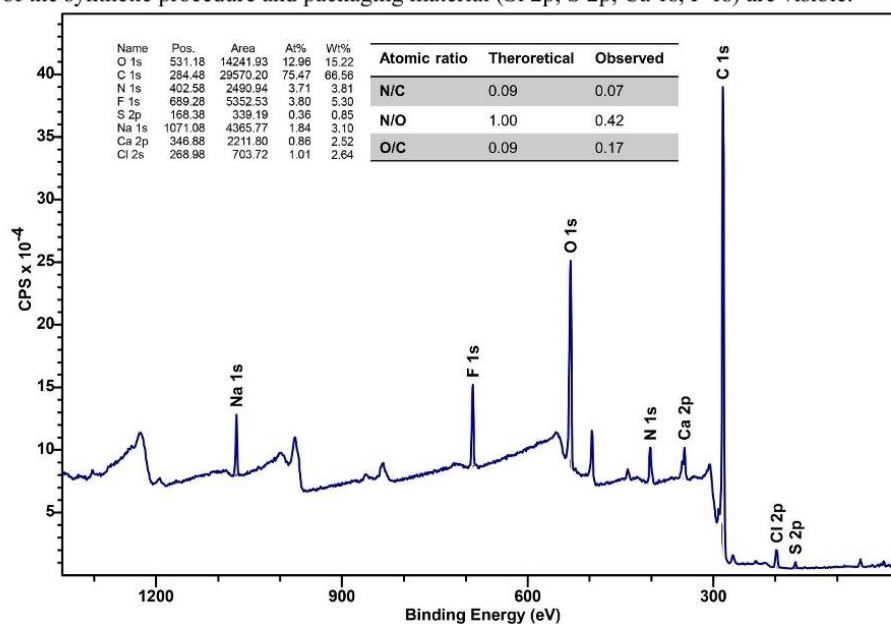
Figure S6. Deconvoluted XPS spectra: N1s region of PE-poly-(VBNOx).
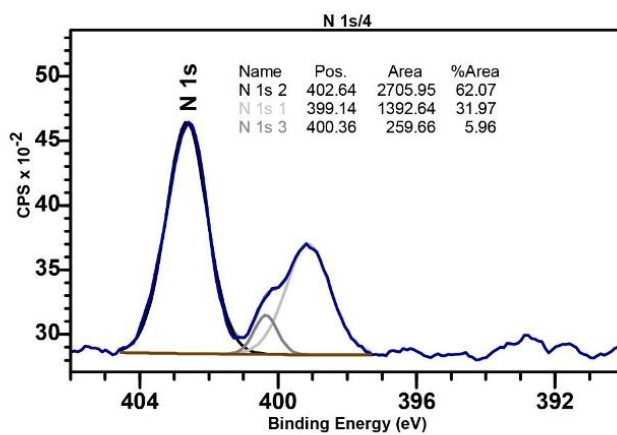
Table S1. MIC-Tests of *N*-oxide derivatives.

Molecule	MIC, *E. coli* ATCC 25922	MIC, *S. aureus* ATCC 29213
VBNOx	>1024 µg/mL	>1024 µg/mL
MANOx	>1024 µg/mL	>1024 µg/mL
MAANOx	>1024 µg/mL	>1024 µg/mL
Benzalkoniumchloride	<16 µg/mL	<16 µg/mL

WILEY-VCH

Figure S7. Agar plate diffusion test (DIN EN ISO 20645:2002-02).

Examplary images of the agar plate diffusion test (DIN EN ISO 20645:2002-02) a) PE-poly-(VBNOx) sample and b) pristine PE after 20 hours at 37°C incubation against *S. aureus* ATC29213.

$$IZ = \frac{D - d}{2} \ (1)$$

IZ: Inhibition zone [mm]
D: Diameter of sample and inhibition zone [mm]
d: Diameter of sample [mm]

material	IZ [mm], *E. coli* ATCC 25922	IZ [mm], *S. aureus* ATCC 29213
PE-poly-(VBNOx)	11.8 ± 2.2	14.1 ± 1.6
PE Ctrl	No inhibition zone	No inhibition zone

IZ-values were determined using equation (1) and are given as mean value ± SD of three independent measurements.
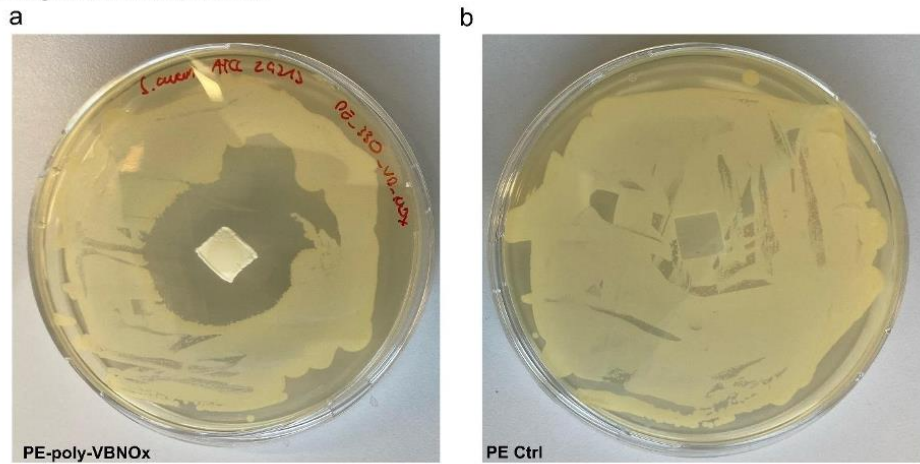
Figure S8. Bacterial adhesion assay of poly-N-Oxide materials.

Bacterial adhesion assay of PE-poly-(VBNOx) compared to PE-poly-(MANOx) and PE-poly-(MAANOx). To all experiments, positive controls of pristine PE were added (PE Ctrl) as well as negative controls of pure MHB. Bars are represented as mean values ± SD of three independent measurements. Statistical significance was determined using the Tukey test *via* pairwise comparison $p \leq 0.001$ (***).

WILEY-VCH
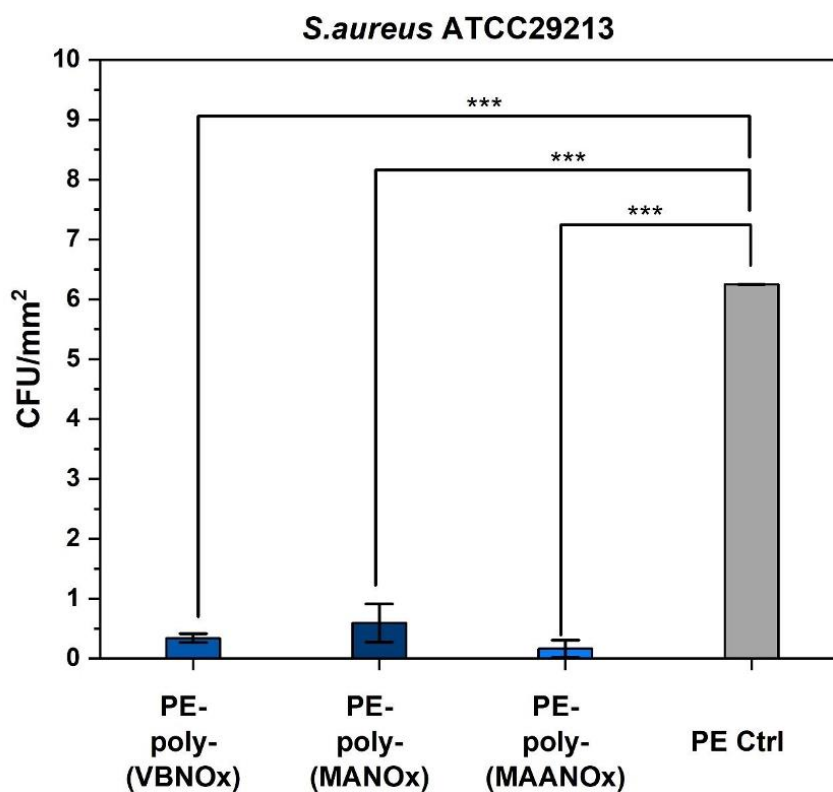
Figure S9. Bacterial adhesion assay – growth controls.

Growth control experiments of the bacterial adhesion assay of PE-poly-(VBNOx), PE-poly-(MANOx), PE-poly-(MAANOx) and the pristine PE (PE Ctrl) incubated media. All growth controls were validated against one negative control of pure MHB (Ctrl -). Colony counts above 250 were set as too numerous to count (TNTC) (a). Statistical significance was determined using the Tukey test *via* pairwise comparison. A p-value above 0.05 (*) was considered non-significant (ns).
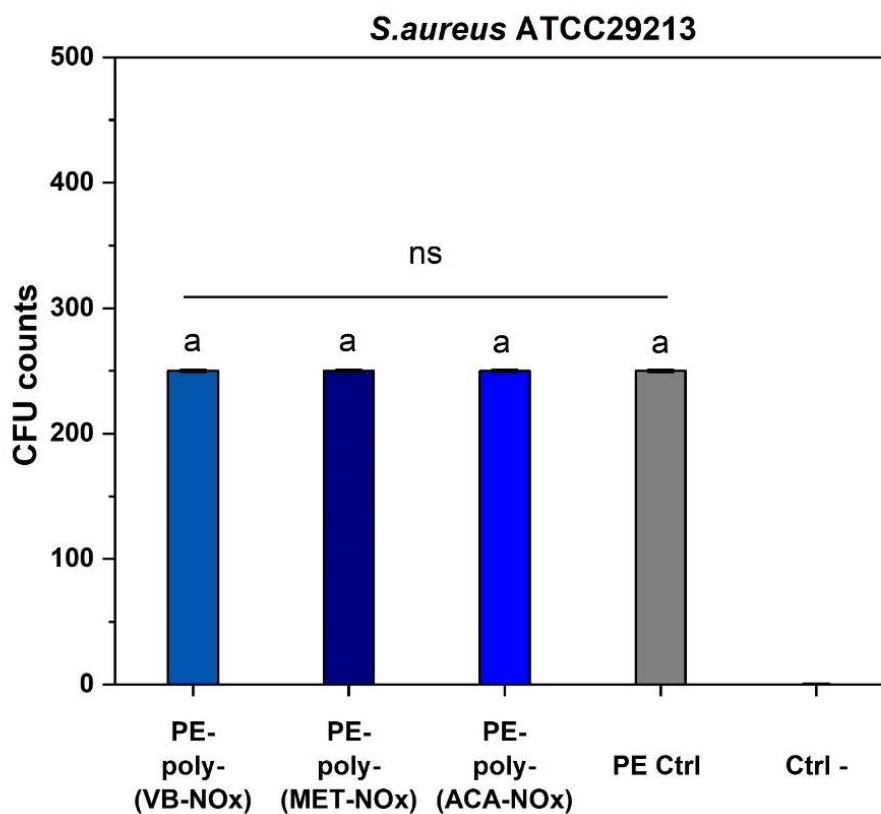
Figure S10. HRP assay of PE-poly-(VBNOx).

Horseradish-peroxidase assay: A) Scheme of horseradish peroxidase (HRP) catalyzed dimerization of pyrogallol in presence of H_2O_2 and its detection via UV/vis measurements at 420 nm. B) Results of the HRP assay: Assay was carried out and HRP relative was calculated as described in the experimental section. For comparison, an H_2O_2 containing positive control (Ctrl H_2O_2 +) with a final H_2O_2 concentration of 0.1 mM was added. Furthermore, a negative control without H_2O_2 (Ctrl H_2O_2 -) was added. Bars are represented as mean values ± SD of at least three independent measurements. Statistical significance was determined using the Tukey test *via* pairwise comparison $p \leq 0.001$ (***) and a p-value above 0.05 (*) was considered as non-significant (ns).

WILEY-VCH
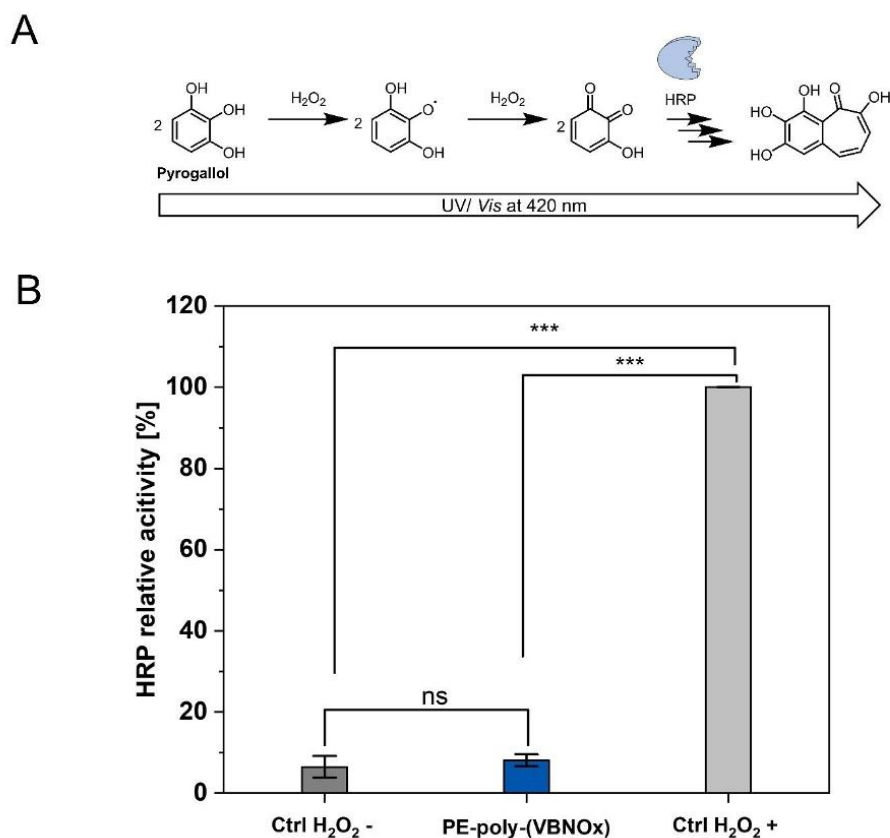
Figure S11. DPPH assay: Overview of DPPH-assay at 70°C in benzene for 24 hours of incubation.

The assay was carried out as described in the experimental section. As control experiments pristine PE (PE Ctrl), plasma-activated PE and grafted poly-vinylbenzyltrimethylammonium-chloride PE-poly-(VBTAC) were added. Bars are represented as mean values ± SD of at least three independent measurements. Statistical significance was determined using the Tukey test *via* pairwise comparison $p \leq 0.001$ (***).
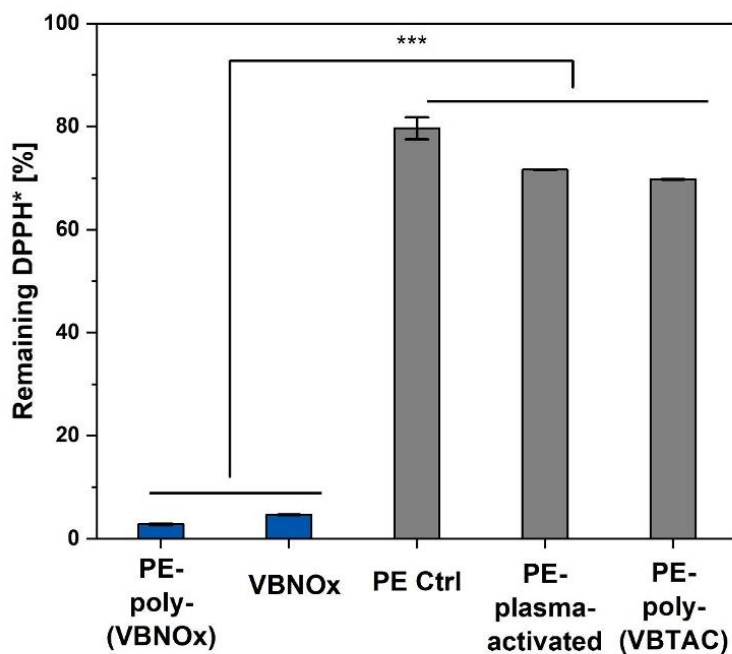
Figure S12. Control experiments of the EPR spectroscopy.
a) pristine PE incubated with spin trapping DMPO (PE-Ctrl) showing no radical formation. b)
PE-poly-(VBNOx) incubated without spin trapping DMPO (DMPO Ctrl -).
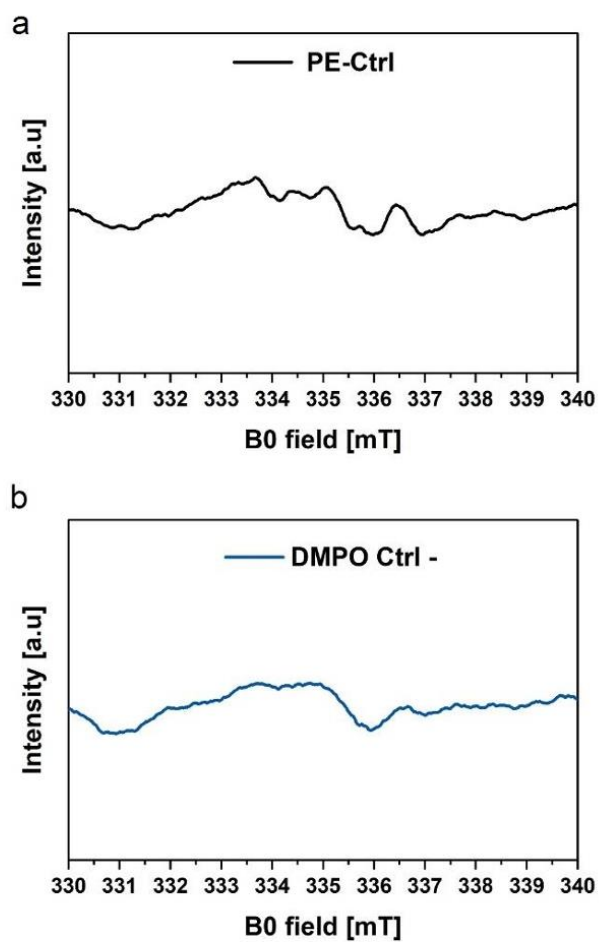
Figure S13. Water contact angles, Zeta potential and ATR-FTIR spectra after repeated ASTM E2149-13a (three times).

A) Zeta potential measurements of PE-poly-(VBNOx) before and after the antibacterial activity test (ASTM e2149-13a), for further comparison the precursor tertiary amine containing material PE-poly(VBDMA) was added. B) ATR-FTIR spectra after the 3rd ASTM e2149-13a repetition with subsequent cleaning in water/iPrOH and drying at room temperature. C) Advancing water contact angles (WCAs) of PE-poly-(VBNOx) before (virgin) and after the 3rd ASTM E2149-13a repetition (used). Pristine PE was used for comparison.
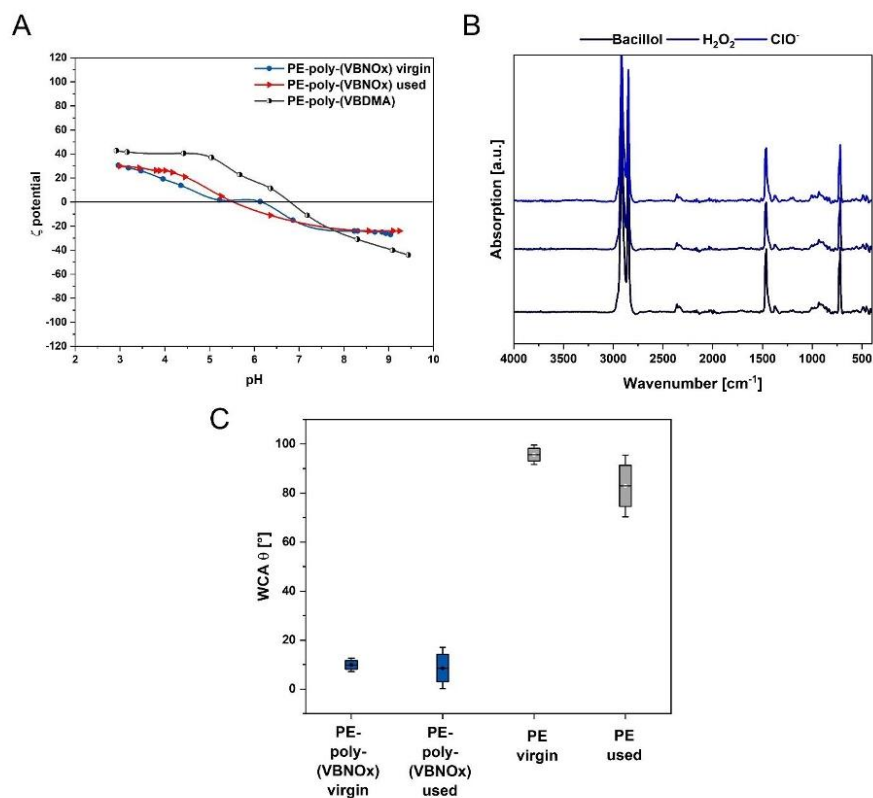
Estimated grafting yield of PE-poly-(VBNOx)

The grafting yield σ of PE-poly-(VBNOx) was calculated to be 10.5 µg*cm^{-2} using the following equation:

$$\sigma(poly-VBNOx) = d * 1\ cm^2 * \rho$$

σ (poly-VBNOx): Grafting yield of poly-VBNOx [µg*cm^{-2}]
d: Layer thickness calculated by ToF-SIMS-SPM analysis was 100 nmρ: Density of a styrene-based-polymer = 1.05 g*cm^{-3}

Synthetic procedures

PE-poly-(VBTAC) was prepared according to a previously reported method.[1]

N,N-Dimethyl-1-(4-vinylbenzylamine-*N*-oxide) (VBNOx): *N,N*-Dimethyl-1-(4-vinylbenzylamine) VBDMA (1eq, 12.40 mmol, 2.00 g) was added dropwise at 0°C to a solution of aqueous hydrogen peroxide (30% w/w) (8 eq, 99.23 mmol, 10.14 mL). The reaction mixture was stirred for 10 hours at room temperature. Activated carbon was added to the solution at 0°C for decomposition of excess hydrogen peroxide. The decomposition of hydrogen peroxide was tracked using peroxide test stripes. After completed decomposition, the reaction mixture was filtered and all volatile compounds were removed under reduced pressure. Freeze drying of the crude product gave 2.15 g (12.13 mmol, 98%) of the title compound VBNOx as a colorless powder. ^{1}H NMR (400 MHz, D_2O): [δ ppm] = 7.59 (d, $^3J_{HH}$ = 8.3 Hz, 2H, 4-H, 7-H), 7.52 (d, $^3J_{HH}$ = 8.3 Hz, 2H, 5-H, 6-H), 6.85 (dd, $^3J_{HH}$ = 11.0, 17.8 Hz, 1H, 9-H), 5.94 (dd, $^2J_{HH}$ = 0.9, 17.7 Hz, 1H, 10a-H), 5.40 (dd, $^2J_{HH}$ = 0.9, 17.7 Hz, 1H, 10b-H), 4.44 (s, 2H, 2-H), 3.16 (s, 6H, 1-H). ^{13}C NMR (150 MHz, D_2O): [δ ppm] = 138.9 (C9), 135.9 (C8), 132.9 (C, C7), 128.9 (C3), 126.3 (C5, C6), 115.6 (C10) 73.5 (C2), 56.7 (C1). HRMS (ESI): m/z calculated for $C_{11}H_{15}NO$: 178.1226, found 178.1227 [M-H]$^+$.

3-Methacrylamido-*N,N*-dimethylpropan-1-amine oxide (MAANOx): *N*-[3-(Dimethylamino)-propyl]methacrylamide (1 eq, 11.63 mmol, 2.00 g) was dissolved in 5 mL demineralized water and was added dropwise at 0°C to a solution of aqueous hydrogen peroxide (30% w/w) (8 eq, 93.04 mmol, 9.50 mL). The reaction mixture was stirred for 6 hours at 0°C. Activated carbon was added to the solution at 0°C for decomposition of excess hydrogen peroxide. The decomposition of hydrogen peroxide was confirmed with peroxide test stripes. After completed decomposition, the reaction mixture was filtered and all volatile compounds were removed under reduced pressure. The final lyophilization of the crude product gave 1.98 g (10.63 mmol, 91 %) of the title compound MAANOx as a colorless viscous liquid. ^{1}H NMR (400 MHz, D_2O): [δ ppm] = 5.73-5.71 (m, 1H, 7a-H), 5.49-5.46 (m, 1H, 7b-H), 3.41-3.35 (m, 4H, 4-H, 6-H), 3.04 (s, 6H, 9-H), 2.13-2.04 (m, 2H, 5-H), 1.78 (t, $^3J_{HH}$ = 2.6 Hz, 8-H). ^{13}C NMR (100 MHz, D_2O): [δ ppm] = 171.9 (C2), 138.9 (C1), 121.5 (C7), 67.9 (C6), 57.3 (C9), 36.6 (C4), 23.0 (C5), 17.6 (C8). HRMS (ESI): m/z calculated for $C_9H_{18}N_2O_2$: 187.1441, found 187.1431 [M-H]$^+$.
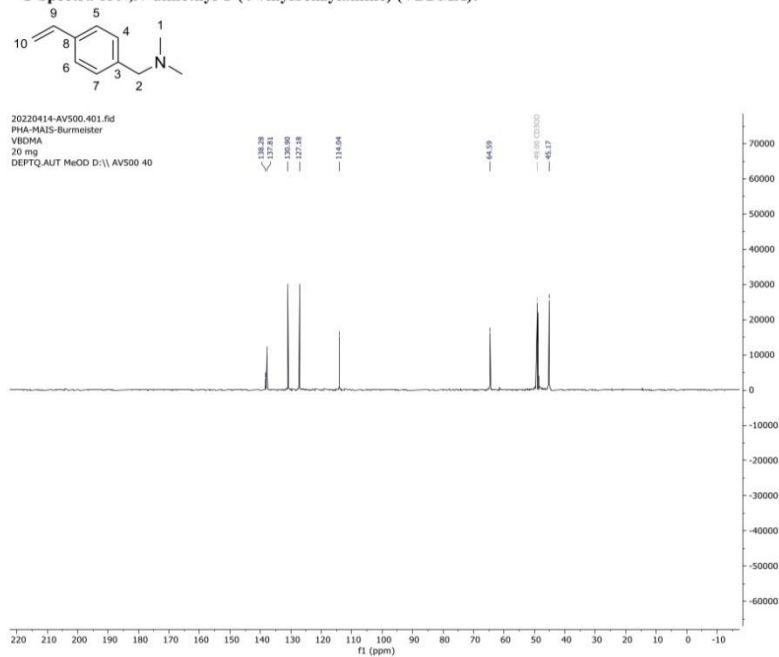
2-(Methacryloyloxy)-*N,N*-dimethylethan-1-amine oxide (MANOx): 2-(Dimethylamino)ethyl methacrylate (1eq, 12.59 mmol, 2.00 g) was dissolved in 5 mL demineralized water and was added dropwise at 0°C to a solution of aqueous hydrogen peroxide (30% w/w) (8 eq, 100.76 mmol, 10.29 mL). The reaction mixture was stirred for 10 hours at 0°C. Activated carbon was added to the solution at 0°C to decompose excess hydrogen peroxide. The decomposition of hydrogen peroxide was confirmed with peroxide test stripes. After completed decomposition, the reaction mixture was filtered and all volatile compounds were removed under reduced pressure. The crude product was dissolved in 10 mL of demineralized water. The pH was adjusted with 0.1M NaOH to 12 and 10 mL of Et_2O were added. Layers were separated and the aqueous layer was extracted 3 times with each 10 mL of Et_2O. Freeze drying of the aqueous phase gave 2.01 g (11.60 mmol, 92 %) of the title compound MANOx as a colorless viscous liquid. ^{1}H NMR (500 MHz, D_2O): [δ ppm] = 5.60-5.58 (m, 1H, 7a-H), 5.29-5.27 (m, 1H, 7b-H), 3.94 (t, $^3J^{HH}$ = 5.1 Hz, 2H, 4-H), 3.40 (t, $^3J^{HH}$ = 5.1 Hz, 2H, 3-H), 3.18 (s, 6H, 5-H), 1.82 (t, $^3J^{HH}$ = 1.2 Hz, 3H, 7-H). ^{13}C NMR (126 MHz, D_2O): [δ ppm] =142.3 (C2), 120.3 (C7), 71.6 (C4), 58.1 (C5), 56.0 (C3), 18.9 (C6). HRMS (ESI): m/z calculated for $C_8H_{15}NO_3$: 174.1124, found 174.1104 [M-H]$^+$.
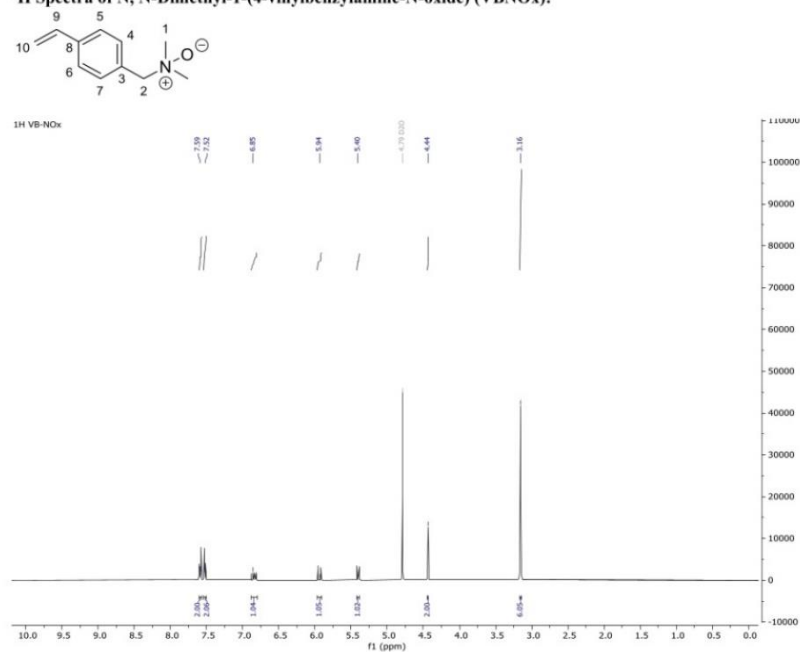
WILEY-VCH

NMR-spectra

^{1}H Spectra of *N*,*N*-dimethyl-1-(4-vinylbenzylamine) (VBDMA):

20220701-AVIII400.70.fid
PHA-MAIS-Burmeister
VBDMA 27mg
PROTON.AUT MeOD F:\\ AVIII400 7

WILEY-VCH

^{13}C Spectra of *N*,*N*-dimethyl-1-(4-vinylbenzylamine) (VBDMA):

20220414-AV500.401.fid
PHA-MAIS-Burmeister
VBDMA
20 mg
DEPTQ.AUT MeOD D:\\ AV500 40
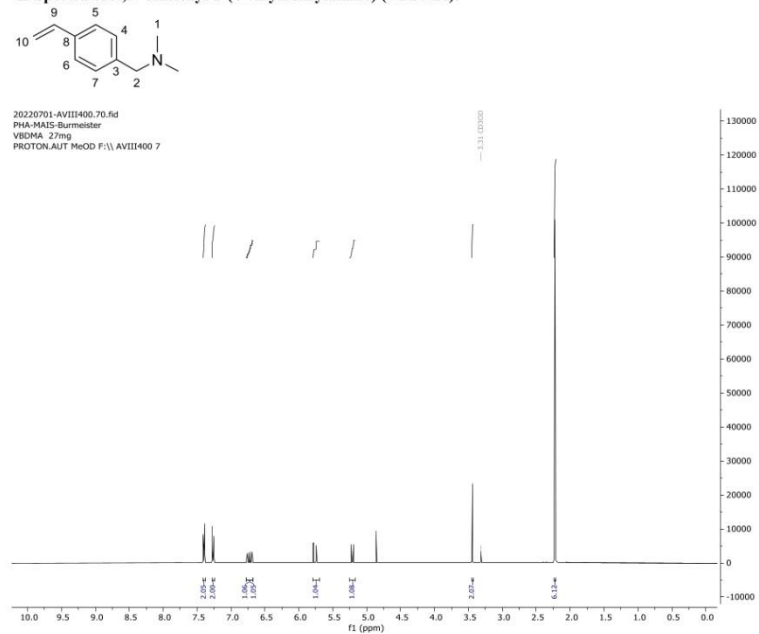
WILEY-VCH

¹H Spectra of N, N-Dimethyl-1-(4-vinylbenzylamine-N-oxide) (VBNOx):

WILEY-VCH

¹³C Spectra of N, N-Dimethyl-1-(4-vinylbenzylamine-N-oxide) (VBNOx):
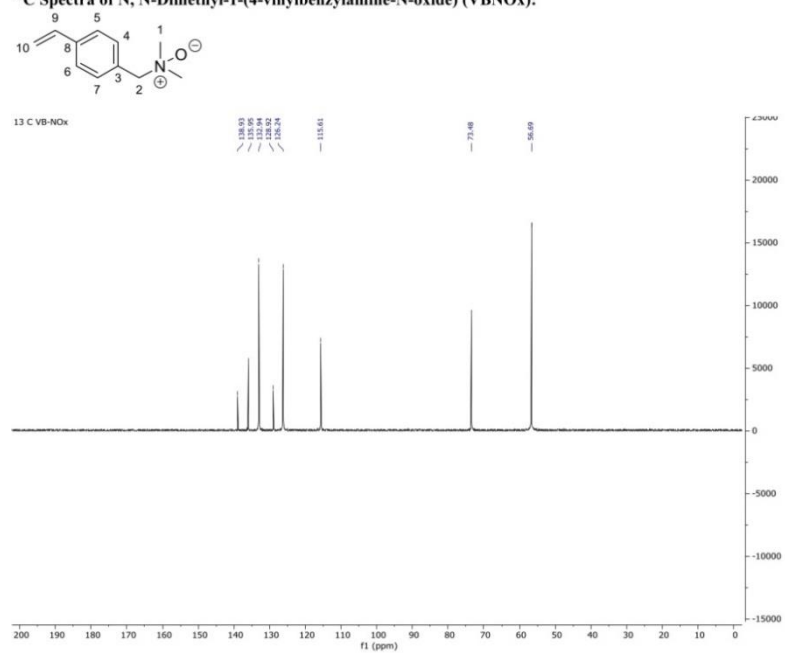
¹H Spectra of 3-methacrylamido-*N,N*-dimethylpropan-1-amine oxide (MAANOx):
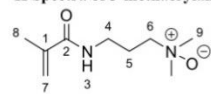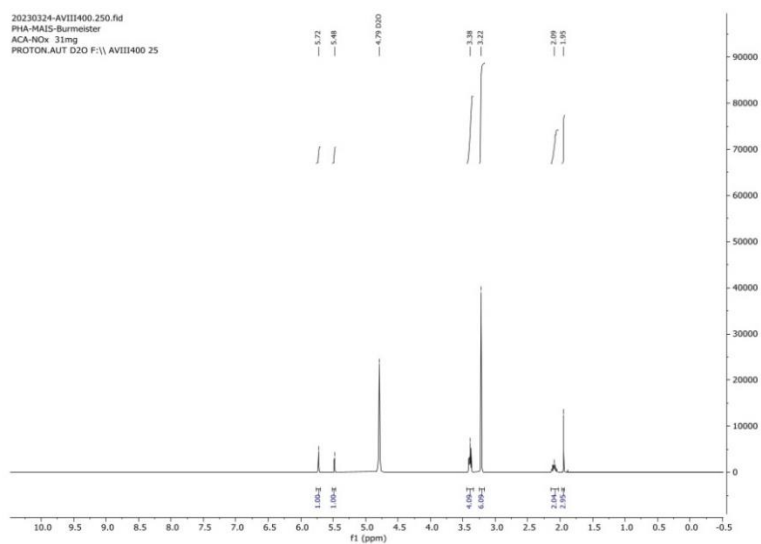
¹³C Spectra of 3-methacrylamido-*N,N*-dimethylpropan-1-amine oxide (MAANOx):
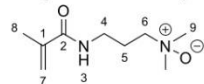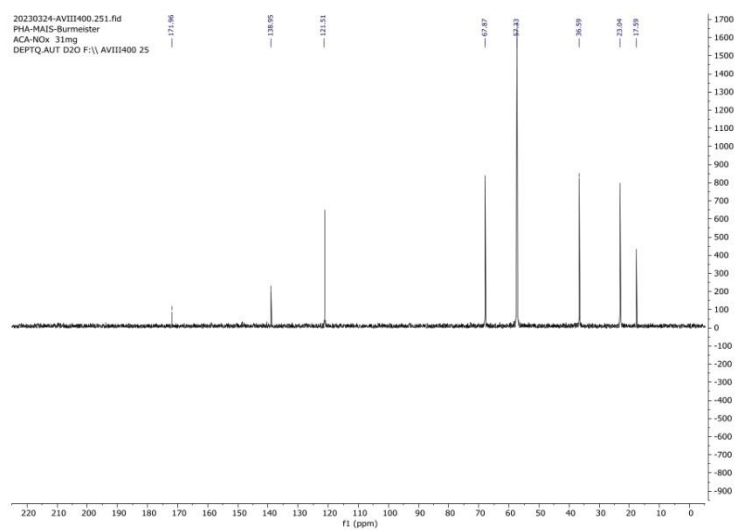
WILEY-VCH

¹H Spectra of 2-(methacryloyloxy)-*N*,*N*-dimethylethan-1-amine oxide (MAOx):
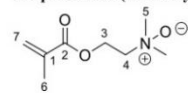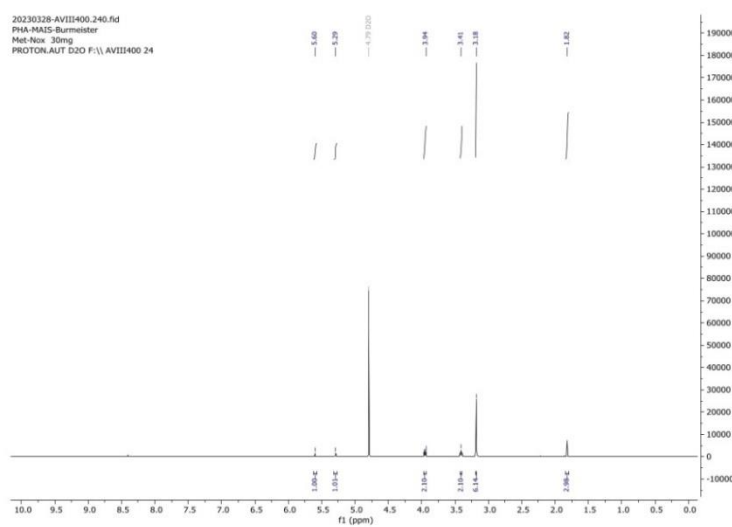
WILEY-VCH

¹³C Spectra of 2-(methacryloyloxy)-*N*,*N*-dimethylethan-1-amine oxide (MANOx):
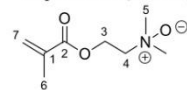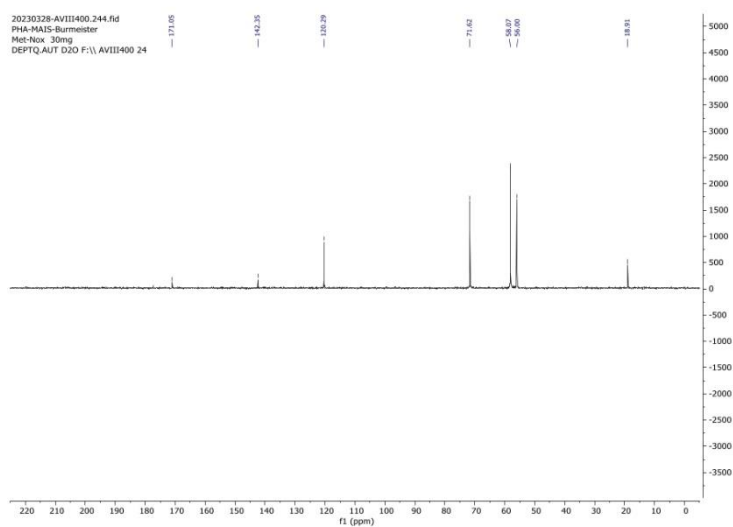
[1]   S. Kliewer, S. G. Wicha, A. Broker, T. Naundorf, T. Catmadim, E. K. Oellingrath, M. Rohnke, W. R. Streit, C. Vollstedt, H. Kipphardt, W. Maison, *Colloids Surf., B* **2020**, *186*, 110679.

9   Acknowledgements

First of all, I am very grateful that Prof. Dr. Wolfgang R. Streit gave me the opportunity, to conduct my doctoral research in his department. I am very thankful for his continuous support, the numerous advices, and guidance during almost four years of my PhD thesis.

I would also like to thank Prof. Dipl.-Ing. Dr. Agnes Weiß for reviewing my thesis, and always taking the time to answer my questions.

Additionally, I am thankful for the FuturEnzyme project for funding my research and making it possible for me to work on this topic.

A very special thanks goes to Dr. Christel Vollstedt for her countless hours of support, the many meetings, and her encouragement during my PhD. It meant a lot to me, to have someone by my side, who was always willing to listen, and help me overcome any issues along the way.

Further, I want to thank Dr. Pablo Pérez-García for his assistance with enzymatic topics, and for taking the time to proofread my work.

Also, I would like to thank all my colleagues in the Department of Microbiology and Biotechnology. A special thanks to Tim, Calvin, and Raphael for fun days in the office even during difficult times.

Finally, I would like to thank my parents for their unconditional support through my academic journey and for making this entire experience possible. Also, I'm so thankful for my friends, who were always there for me and supported me during the more exhausting phases.

Last but not least, I want to thank my boyfriend, Robin, who stood by my side through every step of this journey.